ISSN 2095-8137 CN 53-1229/Q

ZR

Volume 40 Issue 4
18 July 2019

Zoological Research

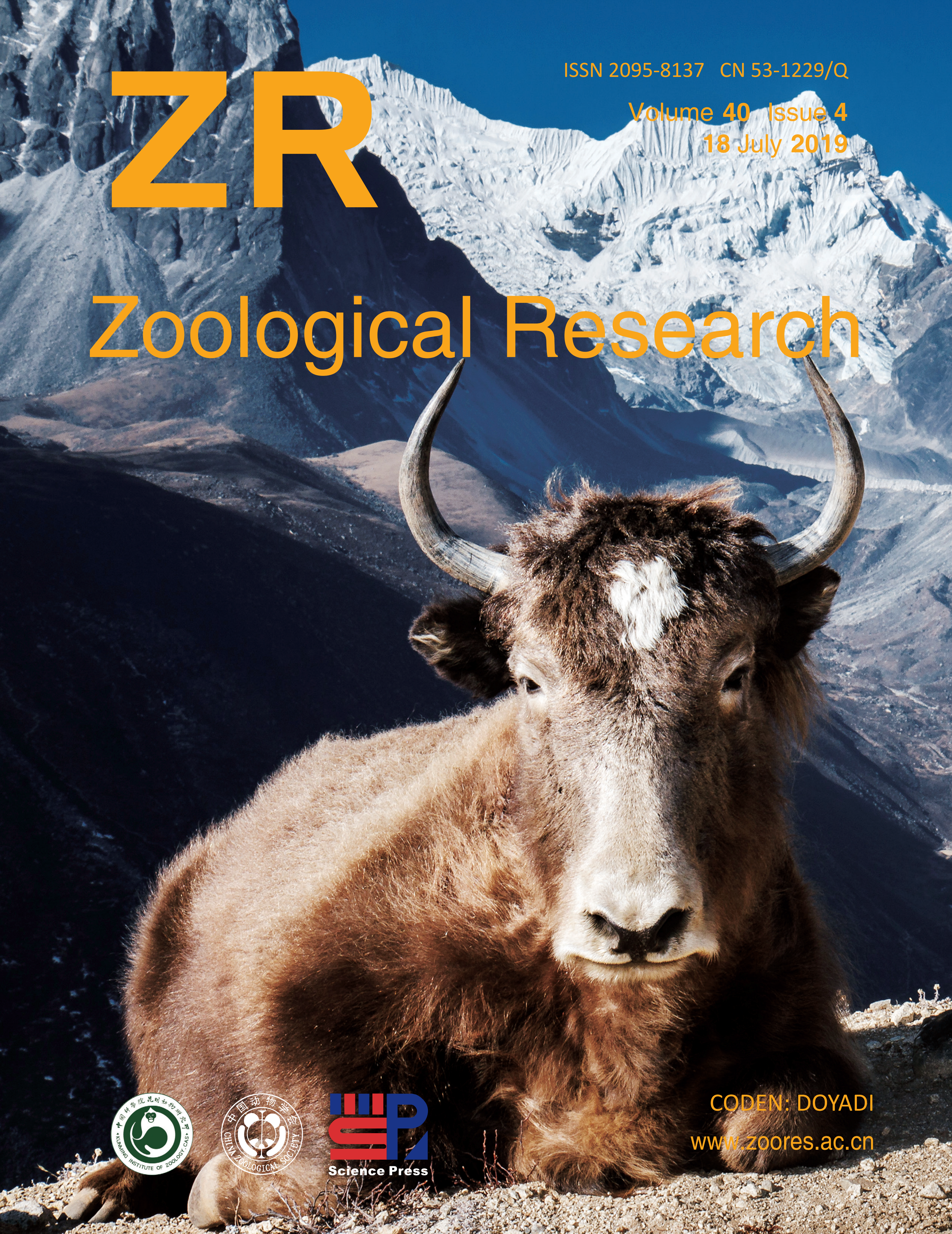

Science Press

CODEN: DOYADI
www.zoores.ac.cn

ZOOLOGICAL RESEARCH

Volume 40, Issue 4 18 July 2019

CONTENTS

Editorial

Research highlight

Articles

Reports

Letters to the editor

Cover image: Dzo (*Bos taurus*×*Bos grunniens*). Photo by Petr Meissner

Cover design: Li-Bin Wu

Zoological Research Website: http://www.zoores.ac.cn/

An “impact” in publishing

On 20 June 2019, Clarivate Analytics (2019) announced its Journal Citation Reports of 2018. From this, *Zoological Research* (*ZR*) received its first impact factor based on citations in 2018 for indexed papers published during 2016 to 2017. Although the new impact factor (1.556) is modest, it ranks *ZR* at 52 among the 170 SCI journals (quartile 2) in the Zoology category. This excellent result is not only a reflection of your enduring support, but also in recognition of our efforts to boost *ZR* from a Chinese-language only journal in 1980 to an English-language only journal of international standing by 2014.

From its original founding by a group of first-generation zoologists in "New China", *ZR* has aimed to publish the latest advances and scientific findings in the field of zoology. This goal has remained unchanged for the past four decades and has allowed *ZR* to become a respected platform that encourages fair and open scientific discussion. We hope that the rigorous and meaningful science published in *ZR* will reach ever wider audiences as such outstanding research deserves international recognition. It is for this reason that we continue to publish via open access.

With the official announcement of our latest impact factor, we have witnessed a boost in submissions from researchers across the world within the zoological field. In addition to the recently announced impact factor, we also believe this increase to be a reflection of our reputation as a prompt and well-respected platform for the dissemination of cutting-edge and high-quality research. As such, we wish to emphasize the journal's unique areas of interest and warmly welcome submissions with a research focus on: (1) Primates and Animal Models; (2) Conservation and Utilization of Animal Resources, and (3) Animal Diversity and Evolution.

ZR also continues to maintain its academic publishing integrity and reinforce its publishing policies (Editorial Office of Zoological Research, 2016; Liu, 2016; Yao & Jiang, 2018). Most recently, *ZR* amended the ethics requirements regarding submissions involving field animal surveys and sample collection, as well as animal material import and export, which applies to all submissions since 01 June 2019. From that date, all submissions must clearly state whether "*all applicable international, national, and/or institutional guidelines for the care and use of animals were strictly followed; all animal sample collection protocols complied with the current laws of XX (country name) …* " or not; and "*permission/document/series numbers for conducting scientific field surveys and/or material transfer agreements*" must be provided (Editorial Office of Zoological Research, 2019).

In addition, for papers that have encountered problems with previous peer review, *ZR* offers a chance for successful and fast publication for those authors whose work is of a suitably high standard. Authors can submit their manuscript along with a point-by-point reply to the issues and comments raised by the reviewers. Such submissions will be fairly and promptly evaluated by *ZR* editorial board members and experts in the field, and, if accepted, be guaranteed fast-track publication.

Peer review is an effective and vital measure to ensure the academic quality of publications. However, the improper handling of conflicts of interest (COIs) during manuscript review can introduce bias in evaluating research findings. Thus, *ZR* authors must disclose all potential COIs and all reviewers and editors must follow the recommendations of the International Committee of Medical Journal Editors (ICMJE) in handling potential COIs. Reviewers and editors must declare all COIs relevant to the work under consideration (i. e., relationships, both financial and personal, that may interfere with the interpretation of the work) to avoid potential bias and, furthermore, must not use knowledge of the work they are reviewing before its publication in furtherance of their own interests (International Committee of Medical Journal Editors, 2017, 2018).

Receiving its first impact factor is another stepping-stone along the evolutionary path of *ZR*. With strong support from our editors, reviewers, authors, and readers, *ZR* will continue to progress and improve. We hope that the pride we feel in publishing your excellent research is shared in return. Should you have any exciting work or constructive suggestions you would like to share, please do not hesitate to contact us.

Sincerely yours,

Yong-Gang Yao, Editor-in-Chief

Kunming Institute of Zoology, *Chinese Academy of Sciences*, *Kunming Yunnan* 650223, *China*

Yun Zhang, Executive Editor-in-Chief

Kunming Institute of Zoology, *Chinese Academy of Sciences*, *Kunming Yunnan* 650223, *China*

DOI: 10.24272/j.issn.2095-8137.2019.040

Yongtang Zheng

Yong-Tang Zheng, Associate Editor-in-Chief

Kunming Institute of Zoology, *Chinese Academy of Sciences*,
Kunming Yunnan 650223, *China*

REFERENCES

Clarivate Analytics. 2019. Journal Citation Reports 2018. https://clarivate.com/blog/science-research-connect/the-2018-jcr-release-is-here/.

Editorial Office of Zoological Research. 2016. A clarification of authorship in an old publication. *Zoological Research*, **37**(6): 366–366.

Editorial Office of Zoological Research. 2019. Author Guidelines for Submitting Manuscripts to Zoological Research. http://www.zoores.ac.cn/EN/column/column117.shtml

International Committee of Medical Journal Editors. 2017. Defining the role of authors and contributors. http://www.icmje.org.

International Committee of Medical Journal Editors. 2018. Recommendations for the conduct, reporting, editing, and publication of scholarly work in medical journals. http://www.icmje.org/recommendations/.

Liu SQ. 2016. Who is innocent in authorship misconduct?. *Zoological Research*, **37**(3): 117–118.

Yao YG, Jiang XL. 2018. 2018 New Year Address of *Zoological Research*. *Zoological Research*, **39**(1): 1–2.

Prolonged milk provisioning and extended maternal care in the milking spider *Toxeus magnus*: biological implications and questions unresolved

Bing Dong[1,3], Rui-Chang Quan[2,*], Zhan-Qi Chen[1,*]

[1] *CAS Key Laboratory of Tropical Forest Ecology*, *Xishuangbanna Tropical Botanical Garden*, *Chinese Academy of Sciences*, *Xishuangbanna Yunnan* 666303, *China*

[2] *Center for Integrative Conservation*, *Xishuangbanna Tropical Botanical Garden*, *Chinese Academy of Sciences*, *Xishuangbanna Yunnan* 666303, *China*

[3] *University of Chinese Academy of Sciences*, *Beijing* 100049, *China*

Prolonged milk provisioning and extended parental care for nutritionally independent offspring, previously considered to only co-occur in long-lived mammals (Clutton-Brock, 1991; Royle et al., 2012), were recently reported in the reproduction of the milking spider, *Toxeus magnus* (Chen et al. 2018). Newly hatched *T. magnus* spiderlings require 53 days to develop to maturity, with an average adult body length of 6.6 mm. The mother provides milk droplets to her newly hatched spiderlings until they develop into subadults (~38 days old), during which their body lengths increase from 0.9 mm at birth to 5.3 mm at weaning. Although spiderlings can forage for themselves at around 20 days old, they remain in the breeding nest for weeks after maturity. These results were published in *Science* as a report in November 2018 (Chen et al., 2018).

T. magnus is not the first recorded invertebrate to provide a milk-like substance to nourish offspring. Examples of maternal nutrient liquid provisioning are reported across different arthropod clades, such as flies, cockroaches, burying beetles, bees, swaps, and ants (Benoit et al., 2015; Bilinski et al., 2018; Ostrovsky et al., 2016; Wong et al., 2013). Examples also appear in Arachnida, including scorpions and pseudoscorpions (Ostrovsky et al., 2016). However, there are two distinct differences that emphasize the uniqueness of *T. magnus* compared with the above examples. First, *T. magnus* mothers progressively feed their young with secretions from the hatchling stage until sub-adulthood, whereas those mentioned above only provide nutritional liquid pre-birth, known as insect viviparity, or for newly-hatched young. Second, *T. magnus* provides maternal care for sexually mature offspring, which has not been reported in other examples. These two characteristics suggest that *T. magnus* is comparable to long-lived social mammals in reproduction.

Milk is a unique type of maternally secreted fluid found across the animal kingdom and plays an integrative role in nourishment and immunological protection for young (Ward & German, 2004). Nutritionally, essential and non-essential amino acids and bioactive proteins in milk are indispensable for newborn survival (Demmelmair et al., 2017). In addition to nourishment and immunological functions, milk provisioning in mammals can further affect litter size, sex ratio, offspring size, and brain size at weaning (McCGraham, 1964; McClure, 1987; Page et al., 2009; Taylor et al., 2005). However, despite the unique benefits, lactation is considered the costliest part of reproduction for mothers (Gittleman & Thompson, 1988), with a mean caloric intake for females during lactation 66%−188% greater than that for non-reproductive females (Gélin et al., 2015; Glazier, 1985; McCGraham, 1964; Millar, 1978). In addition to the costs of lactation, the deposition of fat prior to breeding and during gestation may function as a supplementary energy supply to meet the needs of milk production (George et al., 2010; McClure, 1987). We speculate that the extremely high cost of milk provisioning is one of the main barriers for the evolution of lactation in non-mammals. The discovery of similar milking behavior of *T. magnus* implies that tiny-bodied arthropods can afford the costs of "lactation"; however, what costs are incurred by mothers in regard to this "lactation" remain unidentified. Therefore, prospective studies are required to examine the costs of milk provisioning to the mother, as well as future

Received: 13 May 2019; Accepted: 28 May 2019; Online: 4 June 2019

Foundation items: This study was supported by the National Natural Science Foundation of China (30800121)

*Corresponding authors, E-mail: quanrc@xtbg.ac.cn; chenzhanqi@xtbg.ac.cn

DOI: 10.24272/j.issn.2095-8137.2019.041

reproduction opportunities, longevity, predation pressure, and energy costs of milk production. These investigations should help clarify the specific factors that contribute to the occurrence of "lactation".

Mammalian milk is secreted from the mammary gland, which is considered to have evolved from sweat or skin glands, with the nipple thought to have evolved from relevant hair follicles (Clutton-Brock, 1991; Royle et al., 2012; Vorbach et al., 2006). There are three possible criteria for the origin of the mammary gland: (1) enhancement of offspring survivorship at the early birth stage by supplying additional nutrition (Hayssen, 1993), (2) provision of water to keep the early mammalian parchment-like eggs moist (Oftedal, 2002), and (3) establishment of immunological protection for young to reduce infection risks (Vorbach et al., 2006). In *T. magnus*, however, we found no evidence for the physiological process of milk secretion or immunological effects of milk. Hence, histological, transcriptomic, and metabolic analyses are required to confirm where and how the spider milk is secreted. Furthermore, behavioral and biochemical studies are necessary to examine the immunological functions of milk. These results should enhance our understanding on the origin and evolution of milk secretions across different animal clades.

Parental care often stops once offspring acquire the ability to forage for themselves (Royle et al., 2012). Caring for nutritionally independent offspring is unusual, with exceptions mainly reported in long-lived vertebrates, such as the bonobo (*Pan paniscus*) (Clutton-Brock, 1991; Royle et al., 2012). The rarest form of parental care is for sexually mature offspring, which appears to be restricted to long-lived social vertebrates (Clutton-Brock, 1991; Royle et al., 2012). This prolonged parental care may increase fitness by enabling offspring to devote more time to learning life skills, such as foraging (Hoppitt et al., 2008), anti-predation, defense against brood parasites, social skills, and mate selection (Brown & Laland, 2001; Curio, 1993; Davies & Welbergen, 2009). For example, bonobo mothers usually assistant their sexually mature sons to win intrasexual competitions for social status and mates (Surbeck et al., 2011). The milking spider, *T. magnus*, is the first recorded invertebrate species to provide parental care to adult offspring, although it remains unknown whether offspring gain long-term benefits from extended parental care as obtained in long-lived social vertebrates. Therefore, further research is required to examine the correlations between extended parental care and long-term fitness of offspring. Future studies should examine whether offspring provided with extended parental care are more competitive than those without when competing for high-quality mates and food resources. Furthermore, if extended parental care enhances offspring fitness, how are the long-term benefits achieved? Such studies will greatly expand our knowledge on the long-term benefits of extended parental care in a wider range of animal clades.

The evolutionary process and current "lactation" in the spider clade (Araneae) are also worth investigating, which will help to understand the evolutionary history and current patterns and factors that contribute to or restrict milk provisioning and extended parental care in non-mammals. Thus, additional species from the same family (Salticidae) and across other families are required for molecular and behavioral phylogenic reconstruction. Furthermore, genomic analyses of milk secretions and extended parental care in spiders remain to be undertaken.

In conclusion, *T. magnus* is the first non-mammalian species found to provide both milk and extended maternal care for their young (Chen et al., 2018), which was previously thought to only co-occur in long-lived social vertebrates. Based on the current results, a series of focused studies, ranging from ecological to genetic research, should be conducted to further our understanding of the evolution and adaptation of lactation and extended parental care in non-mammals.

COMPETING INTERESTS

The authors declare that they have no competing interests.

AUTHORS' CONTRIBUTIONS

B. D., R. C. Q., and Z. Q. C. designed the study. Z. Q. C. wrote the first manuscript. B.D. and R.C.Q. revised the manuscripts. All the authors read and approved the final version of the manuscript.

ACKNOWLEDGEMENTS

We thank Francis Commercon for English revision.

REFERENCES

Benoit JB, Attardo GM, Baumann AA, Michalkova V, Aksoy S. 2015. Adenotrophic viviparity in tsetse flies: potential for population control and as an insect model for lactation. *Annual Review of Entomology*, **60**(1): 351–371.

Bilinski SM, Jaglarz MK, Halajian A, Tworzydlo W. 2018. Unusual morphological adaptations and processes associated with viviparity in an epizoic dermapteran. *PLoS One*, **13**(4): e0195647.

Brown C, Laland K. 2001. Social learning and life skills training for hatchery reared fish. *Journal of Fish Biology*, **59**(3): 471–493.

Chen ZQ, Corlett RT, Jiao XG, Liu SJ, Charles-Dominique T, Zhang SC, Li H, Lai R, Long CB, Quan RC. 2018. Prolonged milk provisioning in a jumping spider. *Science*, **362**(6418): 1052–1055.

Clutton-Brock TH. 1991. The Evolution of Parental Care. Princeton, NJ: Princeton University Press.

Curio E. 1993. Proximate and developmental aspects of antipredator behavior. *Advances in the Study of Behavior*, **22**: 135–238.

Davies NB, Welbergen JA. 2009. Social transmission of a host defense against cuckoo parasitism. *Science*, **324**(5932): 1318–1320.

Demmelmair H, Prell C, Timby N, Lönnerdal B. 2017. Benefits of lactoferrin, osteopontin and milk fat globule membranes for infants. *Nutrients*, **9**(8): 817.

Gélin U, Wilson ME, Coulson G, Festa-Bianchet M. 2015. Experimental manipulation of female reproduction demonstrates its fitness costs in kangaroos. *Journal of Animal Ecology*, **84**(1): 239–248.

George LA, Uthlaut AB, Long NM, Zhang L, Ma Y, Smith DT, Nathanielsz

PW, Ford SP. 2010. Different levels of overnutrition and weight gain during pregnancy have differential effects on fetal growth and organ development. *Reproductive Biology and Endocrinology*, **8**(1): 75.

Gittleman JL, Thompson SD. 1988. Energy allocation in mammalian reproduction. *American Zoologist*, **28**(3): 863–875.

Glazier DS. 1985. Relationship between metabolic rate and energy expenditure for lactation in Peromyscus. *Comparative Biochemistry and Physiology Part A: Physiology*, **80**(4): 587–590.

Hayssen V. 1993. Empirical and theoretical constraints on the evolution of lactation. *Journal of Dairy Science*, **76**(10): 3213–3233.

Hoppitt WJE, Brown GR, Kendal R, Rendell L, Thornton A, Webster MM, Laland KN. 2008. Lessons from animal teaching. *Trends in Ecology & Evolution*, **23**(9): 486–493.

McCGraham N. 1964. Energy exchanges of pregnant and lactating ewes. *Australian Journal of Agricultural Research*, **15**(1): 127–141.

McClure PA. 1987. The energetics of reproduction and life histories of cricetine rodents. *Symposium of the Zoological Society of London*, **57**: 241–258.

Millar JS. 1978. Energetics of reproduction in *Peromyscus leucopus*: the cost of lactation. *Ecology*, **59**(5): 1055–1061.

Oftedal OT. 2002. The origin of lactation as a water source for parchment-shelled eggs. *Journal of Mammary Gland Biology and Neoplasia*, **7**(3): 253–266.

Ostrovsky AN, Lidgard S, Gordon DP, Schwaha T, Genikhovich G, Ereskovsky AV. 2016. Matrotrophy and placentation in invertebrates: a new paradigm. *Biological Reviews*, **91**(3): 673–711.

Page KC, Malik RE, Ripple JA, Anday EK. 2009. Maternal and postweaning diet interaction alters hypothalamic gene expression and modulates response to a high-fat diet in male offspring. *American Journal of Physiology-Regulatory, Integrative and Comparative Physiology*, **297**(4): R1049–R1057.

Royle NJ, Smiseth PT, Kölliker M. 2012. The Evolution of Parental Care. Oxford, UK: Oxford University Press.

Surbeck M, Mundry R, Hohmann G. 2011. Mothers matter! Maternal support, dominance status and mating success in male bonobos (*Pan paniscus*). *Proceedings of the Royal Society B-Biological Sciences*, **278**(1705): 590–598.

Taylor PD, McConnell J, Khan IY, Holemans K, Lawrence KM, Asare-Anane H, Persaud SJ, Jones PM, Petrie L, Hanson MA, Poston L. 2005. Impaired glucose homeostasis and mitochondrial abnormalities in offspring of rats fed a fat-rich diet in pregnancy. *American Journal of Physiology-Regulatory, Integrative and Comparative Physiology*, **288**(1): R134–R139.

Vorbach C, Capecchi MR, Penninger JM. 2006. Evolution of the mammary gland from the innate immune system?. *Bioessays*, **28**(6): 606–616.

Ward RE, German JB. 2004. Understanding milk's bioactive components: a goal for the genomics toolbox. *The Journal of Nutrition*, **134**(4): 962S–967S.

Wong JW, Meunier J, Köelliker M. 2013. The evolution of parental care in insects: the roles of ecology, life history and the social environment. *Ecological Entomology*, **38**(2): 123–137.

ZOOLOGICAL RESEARCH

On the road to Mandalay: contribution to the *Microhyla* Tschudi, 1838 (Amphibia: Anura: Microhylidae) fauna of Myanmar with description of two new species

Nikolay A. Poyarkov, Jr.[1,2,*], Vladislav A. Gorin[1], Than Zaw[3], Valentina D. Kretova[1], Svetlana S. Gogoleva[2,4,5], Parinya Pawangkhanant[6], Jing Che[7,8]

[1]*Department of Vertebrate Zoology, Biological Faculty, Lomonosov Moscow State University, Moscow* 119234*, Russia*
[2] *Joint Russian-Vietnamese Tropical Research and Technological Center, Nghia Do, Cau Giay, Hanoi, Vietnam*
[3]*Zoology Department, Mohnyin Degree College, Mohnyin, Kachin State* 1111*, Myanmar*
[4]*A.N. Severtsov Institute of Ecology and Evolution, Russian Academy of Sciences, Moscow* 119071*, Russia*
[5]*Zoological Museum of the Lomonosov Moscow State University, Moscow* 125009*, Russia*
[6]*Bansomdejchaopraya Rajabhat University, Thon Buri, Bangkok* 10600*, Thailand*
[7]*State Key Laboratory of Genetic Resources and Evolution, Kunming Institute of Zoology, Chinese Academy of Sciences, Kunming Yunnan* 650223*, China*
[8]*Southeast Asia Biodiversity Research Institute, Chinese Academy of Sciences, Yezin Nay Pyi Taw* 05282*, Myanmar*

ABSTRACT

We present a morphological and molecular assessment of the *Microhyla* fauna of Myanmar based on new collections from central (Magway Division) and northern (Kachin State) parts of the country. In total, six species of *Microhyla* are documented, including *M. berdmorei*, *M. heymonsi*, *M. butleri*, *M. mukhlesuri* and two new species described from the semi-arid savanna-like plains of the middle part of the Irrawaddy (Ayeyarwady) River Valley. We used a 2 481 bp long 12S rRNA – 16S rRNA fragment of mtDNA to hypothesize genealogical relationships within *Microhyla*. We applied an integrative taxonomic approach combining molecular, morphological, and acoustic lines of evidence to evaluate the taxonomic status of Myanmar *Microhyla*. We demonstrated that the newly discovered populations of *Microhyla* sp. from the Magway Division represent two yet undescribed species. These two new sympatric species are assigned to the *M. achatina* species group, with both adapted to the seasonally dry environments of the Irrawaddy Valley. *Microhyla fodiens* **sp. nov.** is a stout-bodied species with a remarkably enlarged shovel-like outer metatarsal tubercle used for burrowing and is highly divergent from other known congeners (*P*-distance⩾8.8%). *Microhyla irrawaddy* **sp. nov.** is a small-bodied slender frog reconstructed as a sister species to *M. kodial* from southern India (*P*-distance=5.3%); however, it clearly differs from the latter both in external morphology and advertisement call parameters. *Microhyla mukhlesuri* is reported from Myanmar for the first time. We further discuss the morphological diagnostics and biogeography of *Microhyla* species recorded in Myanmar.

Keywords: Narrow-mouth frogs; Burma; Indochina; Magway; Kachin; Biodiversity; Taxonomy; mtDNA; Morphology; Acoustics; Advertisement call

INTRODUCTION

Narrow-mouth or pygmy frogs of the genus *Microhyla* Tschudi, 1838 represent the largest genus of the Asian subfamily Microhylinae. The genus currently includes 46 species of

Received: 29 November 2018; Accepted: 07 March 2019; Online: 17 June 2019

Foundation items: This study was partially supported by the Russian Science Foundation (19-14-00050) to N. A. P., Southeast Asia Biodiversity Research Institute, CAS (Y4ZK111B01: 2017CASSEAB RIQG002), and Animal Branch of the Germplasm Bank of Wild Species, CAS (Large Research Infrastructure Funding) to J.C.

*Corresponding author, E-mail: n.poyarkov@gmail.com

DOI: 10.24272/j.issn.2095-8137.2019.044

mostly small to miniature ground-dwelling frogs (Frost, 2019). *Microhyla* frogs occur in various habitats across the East (southern China, including Taiwan and Hainan islands, and Ryukyu Archipelago of Japan), Southeast (Myanmar and Indochina, Malayan Peninsula, Sumatra, Java, Bali, Borneo, and some Philippine islands), and South Asia (Bangladesh, Nepal, Indian subcontinent to northern Pakistan in the west and Sri Lanka in the south) (Frost, 2019; Parker, 1934). Many *Microhyla* species are miniaturized, representing possibly the smallest known Asian tetrapods (Das & Haas, 2010). Taxonomic diversity of *Microhyla* is undoubtedly underestimated (Matsui et al., 2011; Poyarkov et al., 2014), with over half of currently recognized species being described within the last 15 years (Frost, 2019). Molecular phylogenetic methods have proven to be useful for uncovering cryptic diversity in *Microhyla* frogs (e.g., Hasan et al., 2014; Matsui et al., 2011, 2013; Seshadri et al., 2016; Vineeth et al., 2018; Wijayathilaka et al., 2016; Yuan et al., 2016; Zhang et al., 2018).

The Republic of the Union of Myanmar, formerly known as Burma, is the largest country of mainland Southeast Asia. However, it remains one of the least herpetologically studied areas in the region (Grismer et al., 2018a; Mulcahy et al., 2018; Zaw et al., 2019). To date, only five species of *Microhyla* have been recorded from the country and data on their distribution and variation are scarce (see Mulcahy et al., 2018; Wogan et al., 2008). Herpetological exploration of Myanmar (Burma) started with the expeditions of William Theobald in 1855 to 1873, with the first published data on Burmese *Microhyla* appearing in Mason (1860). Later, based on Theobalds' collections from Pegu in southern Burma (now Bago, Bago Division), Blyth (1856) described a new species named *Engystoma berdmorei* Blyth, 1856, now regarded as *Microhyla berdmorei* (Blyth, 1856). This species was later found to be widely distributed across the country, recorded in Karin Biapo (Kayah State; Bourret, 1942), Chin Hills (Chin State; Shreve, 1940), and later in the Rakhine and Shan States, and Magway, Sagaing, Tanintharyi, and Yangon Divisions (Mulcahy et al., 2018; Wogan et al., 2008).

Microhyla butleri Boulenger, 1900, which was originally described from the Malayan Peninsula, was reported from Burma by Parker (1934, p. 131), though without voucher information. This species was later reported from eastern and southern parts of the country, including the He-Ho Valley in southern Shan State (Bourret, 1942), Kayah State (Hallermann et al., 2002; based on historical collection from an expedition of L. Fea to Burma in 1885), Yangon (Wogan et al., 2008), and Tanintharyi divisions (Mulcahy et al., 2018).

In his monograph on Microhylidae, Parker (1934, p. 140) reported on *M. ornata* (Duméril et Bibron, 1841) from Moulmein (now Mawlamyine, Mon State) and Pegu based on the collections of Theobald and from Thayetmyo (now Thayet, Magway Division) based on the collections of Watson. The species was first mentioned for the country by Mason (1860) as *Engystoma carnaticum* Jerdon, 1854 "1853". Recent molecular studies demonstrated that *M. ornata*, previously considered to be a widely-distributed taxon, in fact represents a polyphyletic group of morphologically similar, but phylogenetically distant cryptic species (Garg et al., 2018a; Hasan et al., 2012, 2014, 2015; Howlader et al., 2015; Matsui et al., 2005; Yuan et al., 2016). These studies, however, did not include samples from Myanmar in their analyses. The recent review of Myanmar herpetodiversity by Mulcahy et al. (2018) mentioned *M. fissipes* Boulenger, 1884 (type locality "Formosa", Taiwan) for Yangon, Sagaing, Bago, Mandalay, and Magway. In contrast, based on molecular study, Yuan et al. (2016) recently demonstrated that *M. fissipes* sensu stricto only occurs north of the Red River Valley, with populations from Indochina assigned to *M. mukhlesuri* Hasan, Islam, Kuramoto, Kurabayashi et Sumida, 2014, which was recently described from eastern Bangladesh. Hence, the taxonomic status of Myanmar populations previously regarded as *M. ornata* or *M. fissipes* remains unclear and requires further clarification.

Microhyla heymonsi Vogt, 1911 (originally described from "Formosa", Taiwan, China) was first recorded from Myanmar in the He-Ho Valley (Shan State) by Bourret (1942). The species was later recorded in Kayah State (Hallermann et al., 2002), Kachin State, and Tanintharyi and Yangon divisions (Wogan et al., 2008), and more recently in the Bago and Mandalay divisions (Mulcahy et al., 2018).

Finally, *M. rubra* (Jerdon, 1854), originally described from Karnataka in southern India, was first mentioned to occur in Myanmar by Parker (1934, p. 143) based on a specimen collected by W. Theobald in Moulmein (specimen number BMNH87.2.26.24). This record was later repeated by Dutta (1997). Wogan et al. (2008) reported *M. rubra* from the Magway Division as a first record for the country, and also mentioned sympatric populations of *M. berdmorei*, *M. ornata*, and an undescribed species of *Microhyla*. Recently, Mulcahy et al. (2018) examined the 16S rRNA gene sequence of a Magway specimen identified as *M. rubra* by Peloso et al. (2016), reporting that the Magway population was not conspecific with *M. rubra* from Sri Lanka and India (Mulcahy et al., 2018, p. 117), and was therefore designated as "*Microhyla* sp. B". Mulcahy et al. (2018) also reported on a new population of *Microhyla* from Chatthin (Sagaing Division), which could not be assigned to any currently recognized species, and which they nominated as "*Microhyla* sp. A". Thus, the taxonomic status of these populations, as well as the undescribed species from the Magway Division mentioned by Wogan et al. (2008), is understudied and requires an integrative taxonomic approach for clarification.

During herpetological surveys in the Magway Division and southern Kachin State of Myanmar (see survey sites in Figure 1) in July 2018, we encountered a number of *Microhyla* specimens, which were assigned to five tentative morphospecies (Figure 2). We applied molecular, morphological, and acoustic analyses to evaluate their taxonomic status and herein describe two new species of the genus *Microhyla*.

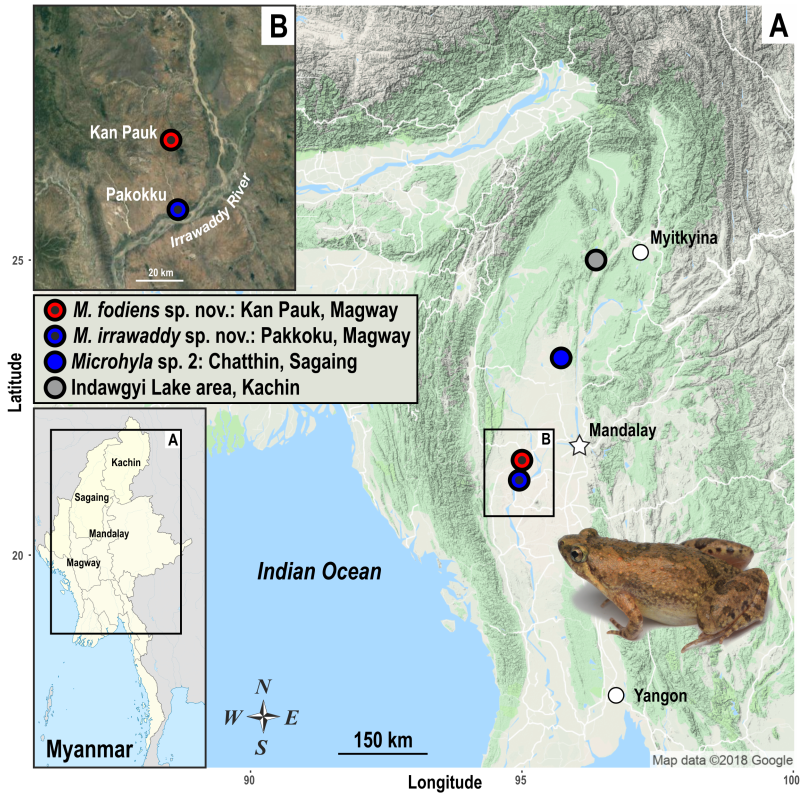

Figure 1 Map of Myanmar (A) showing geographic location of survey sites, including the close-up of Irrawaddy River Valley near Pakokku, Magway Division (B)

Colors of localities correspond to B those used in Figure 3. Photo shows female *Microhyla irrawaddy* **sp. nov.** Photo by Nikolay A. Poyarkov. Map data – courtesy of Google Maps (2018).

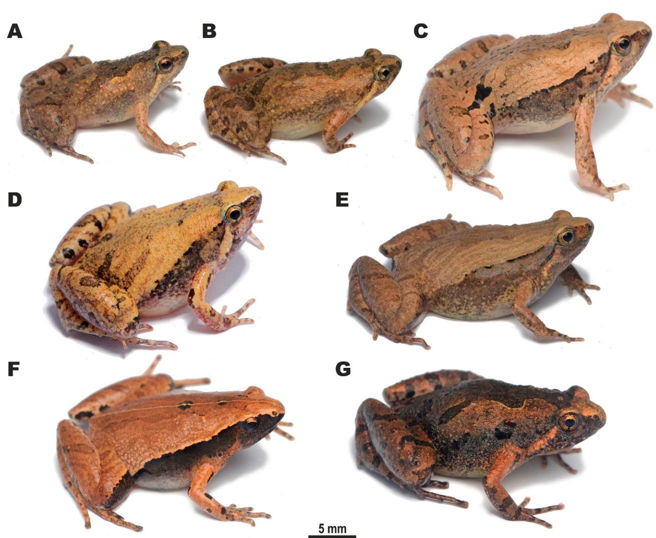

Figure 2 Species of *Microhyla* encountered during our herpetological surveys in the Magway Division and Kachin State of Myanmar

A: Male *Microhyla irrawaddy* **sp. nov.** from Pakokku, Magway (paratype); B: Female *Microhyla irrawaddy* **sp. nov.** from Kan Pauk, Magway (paratype); C: Male *Microhyla fodiens* **sp. nov.** from Kan Pauk, Magway (holotype); D: Male *M. mukhlesuri* from Pakokku, Magway; E: Male *M. mukhlesuri* from Ingyin Taung Mt., Kachin; F: Male *M. heymonsi* from Ingyin Taung Mt., Kachin; G: Male *M. butleri* from Ingyin Taung Mt., Kachin. Photos by Nikolay A. Poyarkov.

MATERIALS AND METHODS

Sample collection

Fieldwork was carried out in central and northern Myanmar, including the Magway Division and Kachin State, from 14–21 July 2018. In the Magway Division, *Microhyla* specimens were collected by hand near breeding areas (e. g., temporary rain pools, paddy fields, or swamps) in two localities, including the environs of Pakokku city on the banks of the Irrawaddy River and near Kan Pauk village, Yesagyo Township, ~30 km north of Pakokku (Figure 1). In Kachin State, the *Microhyla* spp. were collected in forest clearings surrounded by montane evergreen tropical forest and bamboo forest in the Ingyin Taung Mountain, Indawgyi Lake area, Kachin State (Figure 1). Geographic coordinates and elevation were obtained using a Garmin GPSMAP 60CSx GPS receiver and recorded in datum WGS 84. Specimens were euthanized by 20% benzocaine and tissue samples for genetic analysis were taken and stored in 96% ethanol (femoral muscles) prior to preservation. Specimens were subsequently preserved in 70% ethanol and deposited in the herpetological collections of the Zoological Museum of Moscow State University (ZMMU) in Moscow, Russia, and Zoological Institute, Russian Academy of Sciences in St. Petersburg (ZISP), Russia. Other museum abbreviations include the Natural History Museum (BMNH), London, United Kingdom. In total 13 specimens of five putative morphospecies were subjected to molecular analyses (see Table 1 for details). For the two new species described below, we measured eight males, six females, and five subadult specimens (see species description sections for details).

Table 1 Sequences and voucher specimens of *Microhyla* and outgroup taxa used in this study

No.	Specimen ID	Species	Locality	GenBank accession No.	
				12S rRNA	16S rRNA
	Ingroup				
1	MZB Amp 16402	*Microhyla achatina*	Ungaran, Java, Indonesia	AB634598	AB634656
2	MDK 24	*Microhyla achatina*	Gede Pangrango, Java, Indonesia	AB634599	AB634657
3	KUHE 53373	*Microhyla annectens*	Genting, Selangor, Malaysia	AB634600	AB634658
4	KUHE 52438	*Microhyla annectens*	Cameron, Pahang, Malaysia	AB634601	AB634659
5	ITBC2-4360	*Microhyla aurantiventris*	Kon Ka Kinh N.P., Gia Lai, Vietnam	MH286426	
6	ITBC2-4361	*Microhyla aurantiventris*	Kon Ka Kinh N.P., Gia Lai, Vietnam	MH286427	
7	CIBBL002	*Microhyla beilunensis*	Beilun, Ningbo, Zhejiang, China	MH234521	MH234535
8	CIBBL003	*Microhyla beilunensis*	Beilun, Ningbo, Zhejiang, China	MH234522	MH234536
9	KUHE 52034	*Microhyla berdmorei*	Gombak, Selangor, Malaysia	AB598314	AB598338
10	MZB Amp 16413	*Microhyla berdmorei*	Bengkulu, Sumatra, Indonesia	AB634602	AB634660
11	MZB Amp 15270	*Microhyla berdmorei*	Paramasan, Kalimantan, Indonesia	AB634603	AB634661
12	KUHE 52373	*Microhyla berdmorei*	Besut, Terengganu, Malaysia	AB634604	AB634662
13	KUHE 21992	*Microhyla berdmorei*	Mae Yom, Phrae, Thailand	AB634609	AB634667
14	KUHE 53165	*Microhyla borneensis*	Serapi, Sarawak, Malaysia	AB598305	AB598329
15	KUHE 53938	*Microhyla borneensis*	Serapi, Sarawak, Malaysia	AB634605	AB634663
16	KUHE 40591	*Microhyla butleri*	A Luoi, A Roang, Vietnam	AB634606	AB634664
17	KUHE 44203	*Microhyla butleri*	Tainan, Taiwan, China	AB634607	AB634665
18	ZMMU NAP-08282	*Microhyla butleri*	Ingyin Taung Mt., Kachin, Myanmar	MK208937*	
19	ZMMU NAP-08283	*Microhyla butleri*	Ingyin Taung Mt., Kachin, Myanmar	MK208938*	
20	USNM 586947	*Microhyla butleri*	Yangon, Myanmar	—	MG935892
21	KUHE 32943	*Microhyla fissipes*	Huangshan, Anhui, China	AB201174	AB201185
22	CAS 215851	*Microhyla fodiens* **sp. nov.**	Kan Pauk, Magway, Myanmar	—	KM509166
23	ZMMU A5960	*Microhyla fodiens* **sp. nov.**	Kan Pauk, Magway, Myanmar	MK208926*	
24	ZMMU A5961	*Microhyla fodiens* **sp. nov.**	Kan Pauk, Magway, Myanmar	MK208927*	
25	MZB Amp 15291	*Microhyla gadjahmadai*	Lampung, Sumatra, Indonesia	AB634622	AB634680
26	MZB Amp 16328	*Microhyla gadjahmadai*	Bengkulu, Sumatra, Indonesia	AB634623	AB634681
27	KUHE 23856	*Microhyla heymonsi*	Ranong, Thailand	AB598312	AB598336
28	KUHE UN (K1845)	*Microhyla heymonsi*	Kanchanaburi, Thailand	AB201179	AB201190
29	ZMMU NAP-08277	*Microhyla heymonsi*	Ingyin Taung Mt., Kachin, Myanmar	MK208932*	
30	USNM 587130	*Microhyla heymonsi*	Bago, Myanmar	—	MG935907

Continued

No.	Specimen ID	Species	Locality	GenBank accession No.	
				12S rRNA	16S rRNA
	Ingroup				
31	USNM 587138	*Microhyla heymonsi*	Mandalay, Myanmar	—	MG935906
32	ZMMU A5966	*Microhyla irrawaddy* **sp. nov.**	Pakkoku, Magway, Myanmar	MK208928*	
33	ZMMU A5967	*Microhyla irrawaddy* **sp. nov.**	Pakkoku, Magway, Myanmar	MK208929*	
34	ZMMU A5975	*Microhyla irrawaddy* **sp. nov.**	Kan Pauk, Magway, Myanmar	MK208930*	
35	ZMMU A5976	*Microhyla irrawaddy* **sp. nov.**	Kan Pauk, Magway, Myanmar	MK208931*	
36	NCBS-AY587	*Microhyla kodial*	Mangaluru, Karnataka, India	—	MF919453
37	NCBS-AY588	*Microhyla kodial*	Mangaluru, Karnataka, India	—	MF919454
38	BNHS 5965	*Microhyla laterite*	Manipal, Karnataka, Udupi, India	KT600670	KT600663
39	BNHS 5967	*Microhyla laterite*	Manipal, Karnataka, Udupi, India	KT600671	KT600664
40	KUHE 53018	*Microhyla malang*	Serapi, Sarawak, Malaysia	AB598295	AB598319
41	BORNEENSIS 9211	*Microhyla malang*	Tawau, Sabah, Malaysia	AB598301	AB598325
42	MZB Amp 16364	*Microhyla malang*	Balikpapan, Kalimantan, Indonesia	AB634619	AB634677
43	KUHE 52556	*Microhyla mantheyi*	Temerloh, Pahang, Malaysia	AB598310	AB598334
44	KUHE 15726	*Microhyla mantheyi*	Gombak, Selangor, Malaysia	AB598309	AB598333
45	KUHE 32455	*Microhyla marmorata*	Xamneua, Houapan, Laos	AB634610	AB634668
46	DZ 1468	*Microhyla mihintalei*	Anuradhapura, Sri Lanka	—	KU214861
47	DZ 1410	*Microhyla mihintalei*	Maakandura, Sri Lanka	—	KU214857
48	DZ 1445	*Microhyla mihintalei*	Mihintale, Sri Lanka	—	KU214858
49	CIB 20070248	*Microhyla mixtura*	Sichuan, China	AB634611	AB634669
50	CIBZMH2017061203	*Microhyla mixtura*	Shaanxi, Hanzhong, China	MH234528	MH234534
51	CIB20170526001	*Microhyla mixtura*	Sichuan, Hua'e Shan, China	MH234529	MH234540
52	KUHE 22064	*Microhyla mukhlesuri*	Bangkok, Thailand	AB634608	AB634666
53	ZMMU NAP-08311	*Microhyla mukhlesuri*	Ingyin Taung Mt., Kachin, Myanmar	MK208934*	
54	ZMMU NAP-08252	*Microhyla mukhlesuri*	Pakkoku, Magway, Myanmar	MK208933*	
55	USNM 587159	*Microhyla mukhlesuri*	Mandalay, Myanmar	—	MG935905
56	USNM 587110	*Microhyla mukhlesuri*	Bago, Myanmar	—	MG935902
57	USNM 587166	*Microhyla mukhlesuri*	Magway, Myanmar	—	MG935901
58	USNM 586949	*Microhyla mukhlesuri*	Yangon, Myanmar	—	MG935897
59	IABHUF5012 BdMsp77	*Microhyla mymensinghensis*	Char Nilokhia, Bangladesh	—	AB530534
60	IABHUF5012 BdMsp78	*Microhyla mymensinghensis*	Char Nilokhia, Bangladesh	—	AB530535
61	DFBGBAU Msp 306	*Microhyla mymensinghensis*	Mymensingh, Bangladesh	—	AB530536
62	DB-Hi-FROG 12005	*Microhyla nilphamariensis*	Parbatipur, Dinajpur, Bangladesh	AB201176	AB201187
63	KUHE 12840	*Microhyla okinavensis*	Amamioshima, Japan	AB201173	AB201184
64	MZB Amp 16259	*Microhyla orientalis*	Batu Karu, Bali, Indonesia	AB634621	AB634679
65	ZSIK-A9119	*Microhyla ornata*	Karnataka, India	AB201177	AB201188
66	MZB Amp 16255	*Microhyla palmipes*	Bedegul, Bali, Indonesia	AB634612	AB634670
67	MZB Amp 16323	*Microhyla palmipes*	Bengkulu, Sumatra, Indonesia	AB634613	AB634671
68	KUHE UN	*Microhyla perparva*	Balikpapan, Kalimantan, Indonesia	AB634614	AB634672
69	KUHE 53675	*Microhyla perparva*	Mulu, Sarawak, Malaysia	AB634615	AB634673
70	BORN 22412	*Microhyla petrigena*	Maliau Basin, Sabah, Malaysia	AB634616	AB634674
71	KUHE 53743	*Microhyla petrigena*	Bukit Kana, Sarawak, Malaysia	AB634617	AB634675
72	KUHE 22113	*Microhyla pulchra*	Pilok, Kanchaburi, Thailand	AB634618	AB634676
73	KUHE 35119	*Microhyla pulchra*	Phu Luan, Loei, Thailand	AB201180	AB201191

Continued

No.	Specimen ID	Species	Locality	GenBank accession No.	
				12S rRNA	16S rRNA
	Ingroup				
74	ZMMU A5006-18	*Microhyla rubra*	Bapatla, Andhra Pradesh, India	MK208935*	
75	ZMMU A5006-19	*Microhyla rubra*	Bapatla, Andhra Pradesh, India	MK208936*	
76	MRK; released (toe tip)	*Microhyla rubra*	Karnataka, India	AB201181	AB201192
77	ATREE_MISH_1	*Microhyla sholigari*	Manipal, Karnataka, Udupi, India	KT600667	KT600674
78	ATREE_MISH_2	*Microhyla sholigari*	Manipal, Karnataka, Udupi, India	KT600668	KT600675
79	KUHE 52558	*Microhyla superciliaris*	Temerloh, Pahang, Malaysia	AB634624	AB634682
80	KUHE 53371	*Microhyla superciliaris*	Kenaboi, Negeri Sembilan, Malaysia	AB634625	AB634683
81	NHM-TU-17A-0110	*Microhyla taraiensis*	Mechi, Jhapa, Jamun Khadi, Nepal	MF496241	
82	BORN 8480	*Microhyla* sp. 1	Crocker, Sabah, Malaysia	AB634620	AB634678
83	USNM 523975	*Microhyla* sp. 2	Chatthin, Sagaing, Myanmar	—	MG935884
84	USNM 537450	*Microhyla* sp. 2	Chatthin, Sagaing, Myanmar	—	MG935885
	Outgroup				
85	KUHE 44148	*Calluella yunnanensis*	Pet trade	AB634626	AB634684
86	KUHE 35163	*Calluella guttulata*	Pilok, Kanchanaburi, Thailand	AB634627	AB634685
87	KUHE 52463	*Calluella minuta*	Temerloh, Pahang, Malaysia	AB598316	AB598340
88	KUHE 35182	*Glyphoglossus molossus*	Barrnta, Tak, k Thailand	AB201182	AB201193
89	BORN 8478	*Chaperina fusca*	Crocker, Sabah, Malaysia	AB598318	AB598342
90	KUHE UN	*Kaloula picta*	Pet trade	AB634628	AB634686
91	KUHE 32313	*Kaloula baleata*	Sumba, Indonesia	AB634629	AB634687
92	KUHE 33139	*Kaloula borealis*	Cheju, Korea	AB634630	AB634688
93	KUHE 35178	*Kaloula mediolineata*	Barrntak, Tak, Thailand	AB634631	AB634689
94	KUHE 22206	*Kaloula pulchra*	Nong Khai, Thailand	AB634632	AB634690
95	KUHE 37252	*Kaloula taprobanica*	Sri Lanka	AB634633	AB634691
96	KUZ 21655	*Metaphrynella pollicaris*	Fraser's Hill, Pahang, Malaysia	AB634634	AB634692
97	BORN 8191	*Metaphrynella sundana*	Crocker, Sabah, Malaysia	AB634635	AB634693
98	UKMHC 820	*Phrynella pulchra*	Hulu Trengganu, Trengganu, Malaysia	AB634636	AB634694
99	KUHE 20497	*Micryletta inornata*	Mae Yom, Phrae, Thailand	AB598317	AB598341
100	KUHE 23858	*Micryletta inornata*	Ranong, Thailand	AB634637	AB634695
101	KUHE 35937	*Micryletta steinegeri*	Yunlin, Taiwan, China	AB634638	AB634696
102	BORN 8089	*Kalophrynus heterochirus*	Crocker, Sabah, Malaysia	AB634639	AB634697
103	USNM GZ 33787	*Kalophrynus interlineatus*	Chatthin, Myanmar	AB634640	AB634698
104	KUHE 52454	*Kalophrynus palmatissimus*	Pahang, Temerloh, Malaysia	AB634641	AB634699
105	MZB Amp 15295	*Kalophrynus pleurostigma*	Sumatra, Lampung, Indonesia	AB634642	AB634700
106	KUHE 53284	*Kalophrynus* sp.	Pulai, Johol, Malaysia	AB634643	AB634701
107	KUHE 35230	*Kalophrynus stellatus*	Pet trade	AB634644	AB634702
108	KUHE 53145	*Kalophrynus subterrestris*	Tubau, Sarawak, Malaysia	AB634645	AB634703
109	KUHE 15531	*Kalophrynus yongi*	Cameron, Pahang, Malaysia	AB634646	AB634704
110	UKM HC 279	*Gastrophrynoides immaculatus*	Negeri Sembilan, Malaysia	AB634647	AB634705

Continued

No.	Specimen ID	Species	Locality	GenBank accession No.	
				12S rRNA	16S rRNA
	Outgroup				
111	KUHE 33150	*Dyscophus guineti*	Pet trade	AB634648	AB634706
112	KUHE 35001	*Dyscophus insularis*	Pet trade	AB634649	AB634707
113	KUHE 33224	*Gastrophryne olivacea*	Dimmit, Texas, USA	AB634650	AB634708
114	MZB Amp 16265	*Oreophryne monticola*	Batu Karu, Bali, Indonesia	AB634651	AB634709
115	KUHE 33277	*Phrynomantis bifasciatus*	Pet trade	AB634652	AB634710
116	KUHE 34977	*Scaphiophryne gottlebei*	Pet trade	AB634653	AB634711
117	—	*Rhacophorus schlegelii*	Hiroshima, Japan	AB202078	

For sampling localities in Myanmar see Figure 1. Sequences generated in this study are marked with an asterisk (*); En-dash (–) denotes no data available.

Morphological description

The *Microhyla* specimens were photographed in life and after preservation. Measurements were taken using a digital caliper to the nearest 0.01 mm, subsequently rounded to 0.1 mm. We used a stereoscopic light binocular microscope when necessary. All measurements were taken on the right side of the examined specimen. Statistical analyses were performed with Statistica 6.0 (StatSoft, Inc., 2001).

Morphometric and character terminology followed Poyarkov et al. (2014, 2018), including: (1) snout-vent length (SVL; distance from tip of snout to cloaca); (2) head length (HL; distance from tip of snout to hind border of jaw angle); (3) snout length (SL; distance from anterior corner of eye to tip of snout); (4) eye length (EL; distance between anterior and posterior corners of eye); (5) nostril-eye length (N-EL; distance between anterior corner of eye and nostril center); (6) head width (HW; maximum width of head at level of mouth angles in ventral view); (7) internarial distance (IND; distance between central points of nostrils); (8) interorbital distance (IOD; shortest distance between medial edges of eyeballs in dorsal view); (9) upper eyelid width (UEW; maximum distance between medial edge of eyeball and lateral edge of upper eyelid); (10) forelimb length (FLL; length of straightened forelimb to tip of third finger); (11) lower arm and hand length (LAL; distance between elbow and tip of third finger); (12) hand length (HAL; distance between proximal end of outer palmar (metacarpal) tubercle and tip of third finger); (13) first finger length (1FL, distance between tip and distal end of inner palmar tubercle); (14) inner palmar tubercle length (IPTL; maximum distance between proximal and distal ends of inner palmar tubercle); (15) outer palmar tubercle length (OPTL; maximum diameter of outer palmar tubercle); (16) third finger disk diameter (3FDD); (17) hindlimb length (HLL; length of straightened hindlimb from groin to tip of fourth toe); (18) tibia length (TL; distance between knee and tibiotarsal articulation); (19) foot length (FL; distance between distal end of tibia and tip of fourth toe); (20) inner metatarsal tubercle length (IMTL; maximum length of inner metatarsal tubercle); (21) first toe length (1TOEL), distance between distal end of inner metatarsal tubercle and tip of first toe; (22) fourth toe disk diameter (4TDD); and (23) outer metatarsal tubercle length (OMTL; maximum length of outer metatarsal tubercle). For the holotype description, we additionally took the following measurements: (24–26) second to fourth finger lengths (2–3FL-O, 4FL-I; outer side (O) of second and third, inner side (I) of fourth, distance between tip and junction of neighboring finger); (27–30) second to fifth toe lengths (outer lengths for toes II–IV, inner length for toe V; 2–5TOEL).

Terminology for describing eye coloration in living individuals followed Glaw & Vences (1997) and toe webbing and subarticular tubercle formulas were in accordance with those of Savage (1975). The sex and maturity of the specimens were checked by minor dissections and direct observation of calling in living males prior to collection.

Diagnosis of the genus *Microhyla* and morphological characters for comparison were taken from original descriptions and taxonomic reviews of the genus, including the following works: Andersson (1942); Atmaja et al. (2019); Bain & Nguyen (2004); Blyth (1856); Boulenger (1884, 1897, 1900); Bourret (1942); Das & Haas (2010); Das et al. (2007); Duméril & Bibron (1841); Dutta & Ray (2000); Fei et al. (2010); Fernando & Siriwardhane (1996); Garg et al. (2018b); Hallowell (1861); Hasan et al. (2014); Howlader et al. (2015); Hu et al. (1966); Inger & Frogner (1979); Inger (1989); Jerdon (1854); Khatiwada et al. (2017a); Matsui (2011); Matsui et al. (2013); Nguyen et al. (2019); Parker (1928, 1934); Parker & Osman (1948); Pillai (1977); Poyarkov et al. (2014); Schenkel (1901); Seshadri et al. (2016); Smith (1923); Stejneger (1901); Taylor (1934); von Tschudi (1838); Vineeth et al. (2018); Vogt (1911); Wijayathilaka et al. (2016); and Zhang et al. (2018).

DNA isolation, polymerase chain reaction (PCR), and sequencing

For molecular phylogenetic analyses, we extracted total genomic DNA from ethanol-preserved femoral muscle tissue using standard phenol-chloroform-proteinase K extraction with consequent isopropanol precipitation, for a final concentration of ~1 mg/mL (protocols followed Hillis et al., 1996 and

Sambrook et al., 2001). We visualized the isolated total genomic DNA using agarose electrophoresis in the presence of ethidium bromide. We measured the concentration of total DNA in 1 µl using NanoDrop 2000 (Thermo Scientific), which was consequently adjusted to ~100 ng DNA/µL.

We amplified mtDNA fragments covering partial sequences of 12S rRNA and 16S rRNA mtDNA genes and a complete sequence of the $tRNA^{Val}$ gene to obtain a 2 481 bp length continuous fragment of mtDNA. The 16S rRNA gene is widely applied in biodiversity surveys in amphibians (Vences et al., 2005a, 2005b; Vieites et al., 2009) and, together with 12S rRNA partial sequences, has been used in most recent phylogenetic studies on Microhylinae (Matsui et al., 2011; Peloso et al., 2016). These fragments are particularly useful in studies of the genus *Microhyla* (e.g., Hasan et al., 2012, 2014, 2015; Howlader et al., 2015; Khatiwada et al., 2017a; Matsui 2011; Matsui et al., 2013; Peloso et al., 2016; Wijayathilaka et al., 2016). We performed DNA amplification in 20 µL reactions using 50 ng of genomic DNA, 10 nmol of each primer, 15 nmol of each dNTP, 50 nmol of additional $MgCl_2$, Taq PCR buffer (10 mmol/L Tris-HCl, pH 8.3, 50 mmol/L KCl, 1.1 mmol/L $MgCl_2$, and 0.01% gelatin), and 1 U of Taq DNA polymerase. Primers used for PCR and sequencing followed Nguyen et al. (2019) and included four forward primers: Micro-1F-12stail (ACGCTAAAATGWACCCTAAAAAGT; Nguyen et al., 2019), Micro-500F-12stail (CCACTTGAACCCACGACAG CTAGRAMACAA; Nguyen et al., 2019), 12sA-L (AACTGGGA TTAGATACCCCACTAT; Palumbi et al., 1991), L-2188 (AAAGTGGGCCTAAAAGCAGCCA; Matsui et al., 2006), and four reverse primers: Micro-600R-12stail (TAGAGGAGCCTG TTCTATAATCGATTC; Nguyen et al., 2019), Micro-1200R-12stail (AGTAAAGGCGATYAAAAAATRTTTCAAAG; Nguyen et al., 2019), R-1169 (GTGGCTGCTTTTAGGCCCACT; Wilkinson et al., 2002), and 16H-1 (CTCCGGTCTGAACTCA GATCACGTAGG; Hedges, 1994). The PCR conditions included an initial denaturation step of 5 min at 94 °C and 43 cycles of denaturation for 1 min at 94 °C, primer annealing for 1 min with the TouchDown program from 65 °C to 55 °C reducing 1 °C every cycle, extension for 1 min at 72 °C, and final extension step for 5 min at 72 °C.

We loaded PCR products onto 1% agarose gels in the presence of ethidium bromide, which were then visualized using agarose electrophoresis. If distinct bands were produced, we purified the PCR products using 2 µL of a 1:4 dilution of ExoSapIT (Amersham, Buckinghamshire, UK) per 5 µL of PCR product prior to cycle sequencing. The 10 µL sequencing reaction included 2 µL of template, 2.5 µL of sequencing buffer, 0.8 µL of 10 pmol primer, 0.4 µL of BigDye Terminator v3.1 Sequencing Standard (Applied Biosystems, USA), and 4.2 µL of water. The cycle sequencing included 35 cycles of 10 s at 96 °C, 10 s at 50 °C, and 4 min at 60 °C. We purified the cycle sequencing products by ethanol precipitation. We carried out sequence data collection and visualization on an ABI 3730xl Automated Sequencer (Applied Biosystems, USA). The obtained sequences were deposited in GenBank under the accession Nos. MK208926–MK208938 (Table 1).

Phylogenetic analyses

To hypothesize matrilineal genealogy, we used the 12S rRNA and 16S rRNA Microhylidae dataset of Matsui et al. (2011) with the addition of sequences from several recently reported Southeast Asian *Microhyla* (Hasan et al., 2014; Khatiwada et al., 2017a, 2017b; Mulcahy et al., 2018; Nguyen et al., 2019; Peloso et al., 2016; Vineeth et al., 2018; Wijayathilaka et al., 2016; Zhang et al., 2018) and our newly obtained sequences (summarized in Table 1). In total, we obtained 12S rRNA and 16S rRNA data from 117 specimens. This consisted of 84 samples from 32 species of *Microhyla* (representing almost three quarters of recognized species within the genus), 32 outgroup sequences of other microhylid representatives, and a sequence of *Rhacophorus schlegelii* (Günther) (Sano et al., 2005), which was used to root the tree.

We initially aligned nucleotide sequences using MAFFT v.6 (Katoh et al., 2002) with default parameters, and then checked and slightly adjusted them by eye using BioEdit 7.0.5.2 (Hall, 1999) and MEGA 6.0 (Tamura et al., 2013). We determined mean uncorrected genetic distances (*P*-distances) between sequences with MEGA 6.0. We used MODELTEST v. 3.6 (Posada & Crandall, 1998) to estimate the optimal evolutionary models for dataset analysis. The best-fitting model was the GTR+G model of DNA evolution, as suggested by the Akaike Information Criterion (AIC) for three partitions: 12S rRNA, $tRNA^{Val}$, and 16S rRNA.

We inferred matrilineal genealogy using maximum likelihood (ML) and Bayesian inference (BI) approaches. We conducted ML analyses using the RAxML web server (http: //embnet.vital-it.ch/raxml-bb/; Kozlov et al., 2018), which was used to search the ML trees based on the gamma model of rate heterogeneity option. We assessed nodal confidence for 12S rRNA–16S rRNA analysis by non-parametric bootstrapping (BS) with 1 000 pseudoreplicates (Felsenstein, 1985). We conducted BI in MrBayes 3.1.2 (Ronquist & Huelsenbeck, 2003); Metropolis-coupled Markov chain Monte Carlo (MCMCMC) analyses were run with one cold chain and three heated chains for twenty million generations, sampled every 2 000 generations. Five independent MCMCMC runs were performed and 1 000 trees were discarded as burn-in. We checked the convergence of the runs and that the effective sample sizes (ESS) were all above 200 by exploring the likelihood plots using TRACER v1.6 (Rambaut et al., 2014).

In both datasets, we *a priori* regarded tree nodes with BS values of 75% or greater and PP values over 0.95 to be sufficiently resolved. BS values between 75% and 50% and PP values between 0.95 and 0.90 were regarded as tendencies. Lower values indicated unresolved nodes (Huelsenbeck & Hillis, 1993).

Acoustic analysis

Advertisement calls of *Microhyla* sp. were recorded at breeding sites on the banks of a temporary pond in the Irrawaddy River Valley in Pakokku, Pakoku District, Magway Division, Myanmar (coordinates N21.316°, E95.053°; elevation 59 m a.s.l.) on 14 July 2018 at 2327 h and at

21.5 °C using a portable digital audio recorder Zoom h5 (ZOOM Corporation, Tokyo, Japan) in stereo mode with 48 kHz sampling frequency and 16-bit precision. The temperature was measured at the calling site immediately after the audio recording with a digital thermometer KTJ TA218A Digital LCD Thermometer-Hydrometer.

Calls were analysed using Avisoft SASLab Pro software v. 5.2.05 (Avisoft Bioacoustics, Germany). Before analysis, we reduced the background noise using a low-pass filter (up to 300 Hz). All temporal parameters were analysed with the standard marker cursor in the main window of Avisoft and frequencies of the maximum amplitude of calls and pulses were measured in the power spectrum. The spectrogram for analysis was created using a Hamming window, with FFT-length 1 024 points, frame 75%, and overlap 93.75%. For graphic representation of spectrograms, we lowered the sampling rate to 22.05 kHz. Figures of spectrograms were created using a Hamming window, with FFT-length 512 points, frame 75%, and overlap 87.5%. In total, we measured 50 calls from two *Microhyla* males.

We measured five temporal parameters: i. e., call duration, number of pulses per call, duration of pulses, intervals between successive pulses, and pulse period; and two power parameters: i. e., frequency of maximum amplitude (Fpeak) of calls and of pulses. Additionally, we calculated the pulse repetition rate (pulses/s) by counting the number of pulses within each call minus one and dividing that number by the call duration. Descriptive statistics were performed using STATISTICA, v. 10 (StatSoft, Tulsa, OK, USA). Most numeral parameters are given as means±*SD*, except the number of pulses per call (median±interquartile range), and the minimum and maximum values are given in parentheses (min-max).

RESULTS

Phylogenetic analyses

Sequences and statistics: Final alignment of the 12S rRNA–16S rRNA fragment contained 2 481 aligned characters, with 701 conserved sites and 761 variable sites, of which 599 were parsimony-informative. The transition-transversion bias (R) was estimated at 2.52 (all data given for ingroup only). Nucleotide frequencies were 31.64% (A), 22.82% (T), 24.37% (C), and 21.17% (G).

mtDNA genealogy: Both BI and ML analyses resulted in similar topologies, which differed only in several poorly supported nodes (Figure 3). The obtained topology is generally consistent with the results of Matsui et al. (2011), Peloso et al. (2016), and Nguyen et al. (2019). Analyses achieved high phylogenetic resolution at species complexes and species-level groups, with most nodes showing strong support (PP⩾0.95; BS>90%). However, several major nodes showing phylogenetic relationships among outgroup taxa and major lineages of *Microhyla* presented low or insignificant levels of support.

The BI genealogy (Figure 3) inferred the following set of phylogenetic relationships:

1) Monophyly of *Microhyla* is rejected (in agreement with Matsui et al., 2011), suggesting that the genus is monophyletic with respect to *Glyphoglossus*. *Microhyla* sensu lato is thus divided into two major groups, the first corresponding to the *M. annectens* species group (*Microhyla*–I, see Figure 3) and the second encompassing all remaining species (*Microhyla*–II, see Figure 3).

2) Within the *M. annectens* species group, species are clustered into two reciprocally monophyletic clades: one joining *M. annectens* Boulenger, 1900 and *M. marmorata* Bain & Nguyen, 2004 from mainland Indochina and peninsular Malaysia (1.0/93; hereafter nodal support values given for PP/BS, respectively), and another joining Bornean species *M. petrigena* Inger & Frogner, 1979 and *M. perparva* Inger & Frogner, 1979 (1.0/100).

3) Within the second species group of *Microhyla*, *M. palmipes* Boulenger, 1897 is reconstructed as a sister species to all remaining taxa, although with low node support (0.87/53). All remaining species are grouped in six well-supported clades 1–6.

4) Clade 1 (1.0/91) joins *M. superciliaris* Parker, 1928 from the Malayan Peninsula with two species from southern India: *M. sholigari* Dutta & Ray, 2000 and *M. laterite* Seshadri, Singal, Priti, Pavikanth, Vidisha, Saurabh, Pratik & Gururaja 2016, the latter two species are closely related and form a monophyly (1.0/100).

5) Clade 2 (1.0/100) joins *M. butleri* with a closely related species *M. aurantiventris* Nguyen, Poyarkov, Nguyen, Nguyen, Tran, Gorin, Murphy & Nguyen, 2019 from the Central Plateau of Vietnam. Two specimens of *Microhyla* sp. (ZMMU NAP-08282 and NAP-08283; Figure 2G) from Ingyin Taung Mt., Kachin State, unambiguously fall into the radiation of *M. butleri*.

6) Clade 3 (1.0/100) corresponds to the *M. ornata* species group and joins a number of taxa from the Indian subcontinent and is divided in two subclades. The first subclade joins two species with stout body habitus and large outer metatarsal tubercle used for burrowing, from arid areas of southern and eastern India (*M. rubra*) and Sri Lanka (*M. mihintalei* Wijayathilaka, Garg, Senevirathne, Karunarathna, Biju & Meegaskumbura, 2016). The second subclade includes smaller species from India, Nepal, and Bangladesh: *M. ornata*, *M. taraiensis* Khatiwada, Shu, Wang, Thapa, Wang & Jiang, 2017, and *M. nilphamariensis* Howlader, Nair, Gopalan & Merilä, 2015.

7) Clade 4 (1.0/100) joins two large-bodied species, *M. berdmorei* (widely distributed across Indochina and Sundaland and also occurring in Myanmar) and *M. picta* Schenkel, 1901; the latter species has a stout body habitus and enlarged shovel-like outer metatarsal tubercle.

8) Clade 5 (1.0/100) corresponds to the *M. fissipes* species group and consists of two subclades. The first subclade joins three species of *Microhyla* occurring in East Asia: *M. mixtura* Liu & Hu, 1966 in Hu et al. (1966) and *M. beilunensis* Zhang, Fei, Ye, Wang, Wang & Jiang, 2018 from China, and *M. okinavensis* Stejneger, 1901 from the Ryukyu Archipelago in Japan. The second subclade joins taxa from the southern part

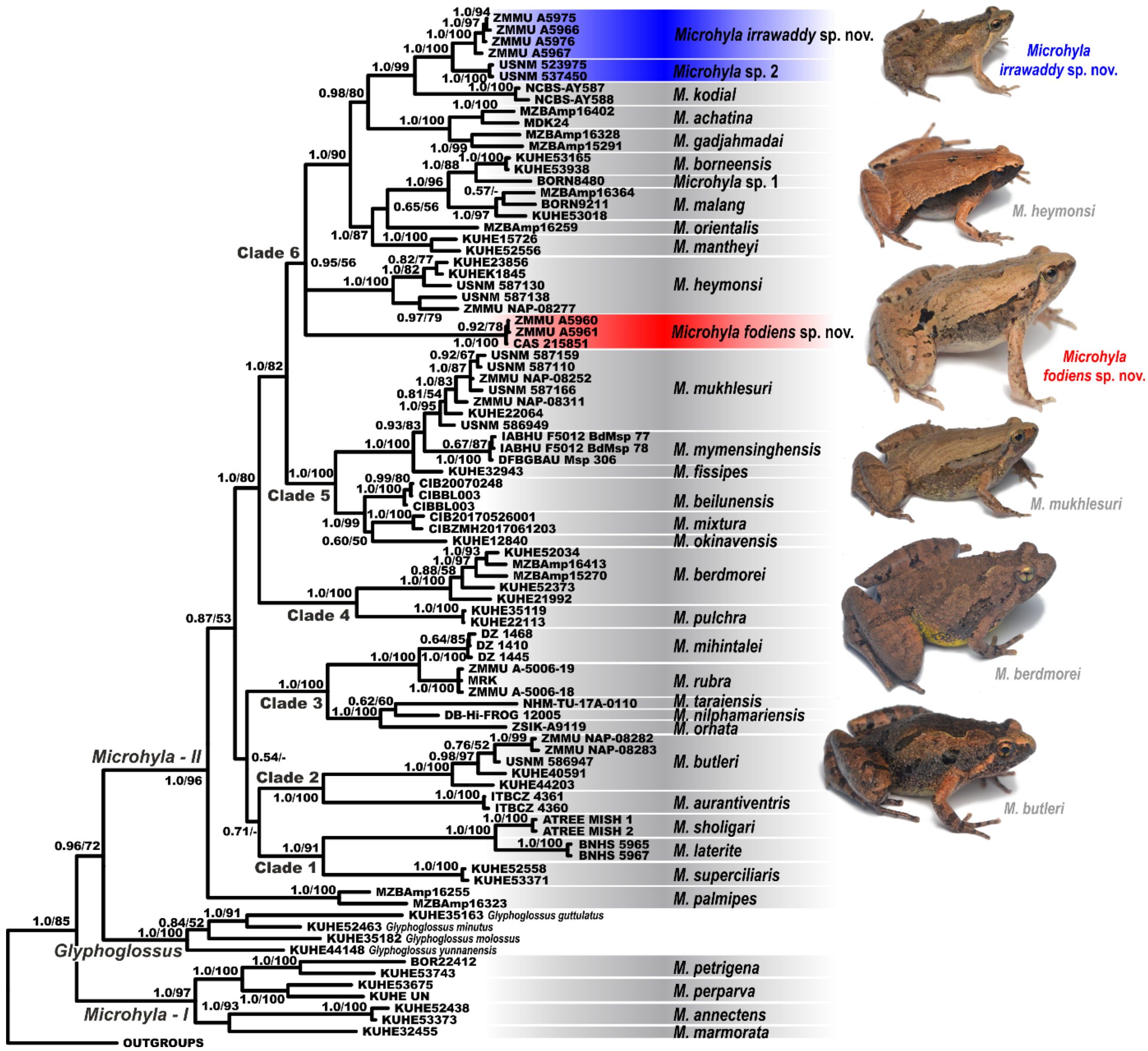

Figure 3 Bayesian inference tree of *Microhyla* derived from analysis of 2 481 bp long alignment of 12S rRNA, tRNA^{Val}, and 16S rRNA gene fragments

For voucher specimen information and GenBank accession Nos. see Table 1. Red and blue denote new species of *Microhyla* from Myanmar (see Figure 1). Numbers at tree nodes correspond to BI PP/ML BS support values, respectively. Outgroup taxa not shown. Photos showing six species of *Microhyla* recorded from Myanmar taken by Nikolay A. Poyarkov.

of China and Indochina, including *M. fissipes* from southern China, Taiwan, and northern Vietnam, *M. mymensinghensis* Hasan, Islam, Kuramoto, Kurabayashi et Sumida, 2014 from Bangladesh, and *M. mukhlesuri* from Indochina. Two specimens of *Microhyla* sp. from Pakkoku, Magway (ZMMU NAP-08252; Figure 2D) and from Ingyin Taung Mt., Kachin State (ZMMU NAP-08311; Figure 2E) were assigned to *M. mukhlesuri* and grouped with other Myanmar specimens of this species (USNM 587110, 587159, 587166). *Microhyla mukhlesuri* and *M. mymensinghensis* form a moderately supported clade (0.93/83).

9) Clade 6 shows moderate support (0.93/56) and joins members of the *M. achatina* species group and related taxa. The stout-bodied *Microhyla* sp. (ZMMU A5960–A5961; Figure 2C) from Kan Pauk, Magway Division, are grouped and appear to be conspecific with *M.* “*rubra*” of Peloso et al.

(2016) (CAS 215851) with high support (1.0/100); this species has an unresolved position within Clade 6 and is not closely related to *M. rubra* sensu stricto from India.

10) The position of *M. heymonsi* within Clade 6 is also unresolved; a specimen of *Microhyla* sp. from Ingyin Taung Mt., Kachin State (ZMMU NAP-08277; Figure 2F), is placed within the radiation of *M. heymonsi*, which is subdivided into two moderately divergent major lineages. Other specimens of *M. heymonsi* from Myanmar belong to two different lineages of *M. heymonsi* (USNM 587130 and USNM 587138).

11) A number of species from Sundaland form a subclade (1.0/87) within Clade 6: *M. mantheyi* Das, Yaakob & Sukumaran, 2007 (Malayan Peninsula) and *M. borneensis* Parker, 1928, *M. malang* Matsui, 2011, *M. orientalis* Matsui, Hamidy et Eto, 2013, and *Microhyla* sp. 1 (Borneo).

12) Sundaland species *M. achatina* Tschudi, 1838 (from Java) and *M. gadjahmadai* Atmaja, Hamidy, Arisuryanti, Matsui & Smith, 2019 (from Sumatra) form a sister lineage (0.98/80) with respect to *M. kodial* Vineeth, Radhakrishna, Godwin, Anwesha, Rajashekhar & Aravind, 2018, from southern India and two *Microhyla* sp. lineages from central Myanmar. Small-bodied slender *Microhyla* sp. specimens from the Magway Division (ZMMU A5966–A5967; A5975–A5976; Figure 2A, B) and *Microhyla* sp. 2 from the Sagaing Division (USNM 523975, 537450) form two distinct reciprocally monophyletic groups (1.0/100). *Microhyla kodial* is strongly suggested as a sister lineage to Myanmar taxa (1.0/99) (see Figure 3).

Sequence divergence: For uncorrected *P*-distances for the 16S rRNA gene fragment among and within the examined *Microhyla* species see Table 2. Intraspecific distances ranged from *P*=0% in a number of examined species to *P*=4.5% in *M. petrigena* (the latter may be explained by incomplete taxonomy of Bornean *Microhyla*). The interspecific distances within *Microhyla* varied from *P*=2.7% (between *M. rubra* and *M. mihintalei*) to *P*=13.1% (between *M. laterite* and stout-bodied *Microhyla* sp. from Kan Pauk, Magway) (Table 2). Genetic divergence within *M. mukhlesuri* was *P*=1.3%, within *M. butleri* was *P*=1.7%, and within *M. heymonsi* was *P*=2.3%. No genetic variation was observed between haplotypes within stout-bodied and slender-bodied species of *Microhyla* sp. from Magway (*P*=0.0%) (Table 2). Divergence between these taxa and their closest relatives was *P*=2.0% for small slender-bodied species of *Microhyla* sp. from the Magway Division if compared to *Microhyla* sp. 2 from Sagaing Division, and *P*=5.3% if compared with *M. kodial*; and was *P*=8.8% for stout-bodied *Microhyla* sp. from Magway Division with *M. berdmorei* (Table 2).

Taxonomy

Our field survey in Myanmar revealed two morphologically distinct species of microhylids, which belong to the genus *Microhyla* based on morphological and molecular evidence and could not be assigned to any currently recognized species (see below).

Both species were allocated to the genus *Microhyla* as they show the following diagnostic characters of the genus (Inger, 1989; Matsui et al., 2013; Parker, 1934): small to medium body size; narrow head; eyes small with circular pupil; lack of small spine-like projections of skin at heel and elbow; maxillary and vomerine teeth absent; snout less than twice diameter of eye; tongue obovate, entire and free at base; fingers without webbing; toes with basal webbing; palmar tubercles distinct; prominent inner and outer metatarsal tubercles on foot; supratympanic fold present; and, tympanum hidden under skin.

Our mtDNA genealogy analyses based on the 12S rRNA–16S rRNA 2 481 bp-long mtDNA fragment indicated that both species belong to the *M. achatina* species group (Figure 3). The stout-bodied *Microhyla* sp. from Kan Pauk represents a distinct lineage within the species group and is highly divergent in 16S rRNA gene sequences from any congener for which homologous sequences are available (*P*-distance⩾8.8%). The slender-bodied *Microhyla* sp. from the Magway Division is a sister species of an undescribed *Microhyla* sp. 2 from Sagaing Division in northern Myanmar and closely related to *M. kodial*, inhabiting southern India (*P*-distance⩾5.3%).

The phylogenetic position of *Microhyla* spp. from the Magway Division, together with the observed differences in mtDNA sequences, is congruent with evidence from diagnostic morphological characters (see "Comparisons" sections). These results strongly support our hypothesis that the newly discovered populations of *Microhyla* spp. from the Magway Division represent two previously unknown species, which we describe below.

Microhyla fodiens **sp. nov.**
Table 3; Figures 2C, 4–6.

Chresonymy:
Microhyla rubra – (?) Parker, 1934, p. 145 (B. M. 87.2.26.24, coll. from "Moulmein, Burma" by W. Theobald).
Microhyla rubra – Wogan et al., 2008, p. 84–86; Peloso et al., 2016, p. 5, 23.
Microhyla sp. B – Mulcahy et al., 2018, p. 99, 116–117.

Holotype: ZMMU A5960 (field number NAP-08268), adult male collected on the bank of an artificial pond near a Buddhist pagoda in the small village of Kan Pauk in the vicinity of Shinma Taung Mt., Yesagyo Township, Magway Division, Myanmar (coordinates N21.595°, E95.074°; elevation 232 m a.s.l.), collected on 15 July 2018 at 1900 h by Nikolay A. Poyarkov, Vladislav A. Gorin, Parinya Pawangkhanant, and Than Zaw.

Paratypes: ZMMU A5961–A5964 (field numbers NAP-08269–08272) and ZISP 13729 (field number NAP-08273), five sub-adult specimens from the same locality and with the same collection information as the holotype.

Referred specimens: CAS 215851 (field number JBS-5249), collected from the same locality as the holotype on 16 August 2000 by H. Win, T. Thin, S.W. Kyi, and H. Tun.

Table 2 Uncorrected *P*-distances (percentage) between the sequences of 12S rRNA–16S rRNA mtDNA fragments (below the diagonal) and intraspecific genetic *P*-distances (on the diagonal) of *Microhyla* species included in phylogenetic analyses

Species	1	2	3	4	5	6	7	8	9	10	11	12	13	14	15	16	17	18	19	20	21	22	23	24	25	26	27	28	29	30	31	32	33	34	35
1. *M. borneensis*	**0.0**																																		
2. *Microhyla* sp. 1	3.0	–																																	
3. *M. malang*	2.6	3.6	**3.0**																																
4. *M. orientalis*	4.3	5.7	5.4	–																															
5. *M. mantheyi*	5.3	5.3	6.3	5.2	**1.0**																														
6. *M. fodiens* **sp. nov.**	11.4	11.6	11.3	11.2	10.8	**0.0**																													
7. *M. achatina*	6.4	7.7	7.4	5.9	6.1	10.1	**2.8**																												
8. *M. gadjahmadai*	6.2	6.9	6.9	6.4	5.5	11.3	5.3	**2.6**																											
9. *M. kodial*	6.9	7.7	8.0	7.1	6.6	11.4	7.4	7.5	**0.4**																										
10. *M. irrawaddy* **sp. nov.**	7.7	7.9	8.0	7.7	7.7	11.2	7.0	7.0	5.3	**0.0**																									
11. *M. heymonsi*	6.7	6.8	6.5	7.0	7.4	9.1	7.9	8.4	7.1	7.5	**2.3**																								
12. *M. mukhlesuri*	8.2	9.3	8.1	7.6	7.6	10.7	8.1	8.1	7.0	7.9	7.1	**1.3**																							
13. *M. fissipes*	7.5	8.1	7.7	6.7	6.9	10.3	7.7	7.5	6.5	7.1	6.7	2.4	–																						
14. *M. mymensinghensis*	7.9	8.7	8.0	8.1	7.7	10.7	7.5	8.3	6.9	7.4	6.8	4.2	3.1	**0.1**																					
15. *M. okinavensis*	8.1	8.7	8.2	6.9	6.9	9.7	6.9	6.7	7.7	8.1	7.1	6.1	4.9	6.4	–																				
16. *M. beilunensis*	7.0	8.2	7.2	6.6	6.5	9.3	7.0	6.7	6.6	6.4	6.4	4.7	3.6	4.7	3.2	**0.1**																			
17. *M. mixtura*	7.7	9.3	8.0	7.9	7.4	9.2	7.9	7.6	7.5	7.3	7.4	5.7	4.6	5.0	4.5	3.2	**0.8**																		
18. *M. berdmorei*	9.9	9.9	10.2	9.4	9.4	8.8	8.0	9.3	11.6	10.7	9.8	10.0	9.4	10.4	9.3	9.5	9.8	**1.6**																	
19. *M. pulchra*	11.6	11.0	10.7	11.0	10.6	10.3	8.7	9.9	11.4	11.0	9.6	9.7	9.5	9.9	8.9	8.5	9.9	7.9	**0.0**																
20. *M. nilphamariensis*	9.1	9.8	9.1	9.8	9.3	10.2	8.8	8.9	10.0	9.6	9.9	8.5	8.3	8.3	9.6	8.3	8.7	8.9	8.9	–															
21. *M. taraiensis*	10.5	10.8	10.9	11.8	10.1	11.4	11.5	10.8	10.8	11.4	11.3	10.0	9.1	9.7	11.4	10.2	10.3	10.4	10.5	5.1	–														
22. *M. ornata*	11.0	11.8	10.6	11.6	11.3	10.3	10.1	11.0	12.0	11.8	10.2	9.2	8.9	8.9	9.7	9.9	9.9	9.3	9.5	4.9	6.7	–													
23. *M. rubra*	9.9	11.2	10.6	10.5	10.2	11.4	9.7	10.0	11.2	11.2	9.9	9.3	9.2	10.2	10.1	9.9	10.1	9.5	9.7	6.1	7.1	7.8	**0.4**												
24. *M. mihintalei*	9.6	10.4	10.3	10.0	9.5	11.0	9.8	9.5	10.8	11.2	9.6	9.8	9.2	10.2	9.6	9.7	10.0	9.8	9.4	6.2	7.6	8.0	2.7	**0.1**											
25. *M. aurantiventris*	10.8	11.2	10.5	11.2	10.3	10.1	11.3	10.9	10.6	12.0	10.1	11.4	10.8	10.5	10.5	9.4	9.9	11.3	10.1	8.1	9.9	9.5	11.0	10.2	**0.0**										
26. *M. butleri*	10.9	11.4	10.5	11.2	11.0	12.2	10.9	11.3	11.1	11.5	10.6	10.8	10.3	11.2	11.3	9.6	10.8	10.9	10.8	9.6	11.0	11.3	9.5	10.1	6.6	**1.7**									
27. *M. superciliaris*	11.1	10.6	10.6	11.1	10.1	11.3	11.3	11.5	10.7	11.3	8.7	9.3	8.6	9.7	10.6	9.3	10.2	10.4	11.3	8.8	8.6	9.2	8.7	8.5	8.8	8.1	**0.2**								
28. *M. laterite*	11.8	11.8	11.9	11.6	11.1	10.8	11.6	11.8	12.7	13.1	11.1	11.2	10.8	11.6	12.2	11.3	11.2	11.3	12.4	10.6	12.2	11.0	11.4	11.5	8.4	11.1	9.7	**0.0**							
29. *M. sholigari*	11.6	11.6	11.8	11.6	11.0	10.8	11.6	12.0	12.3	12.9	10.8	10.6	10.8	11.4	12.5	10.9	11.4	10.2	11.6	9.4	10.2	10.0	10.0	10.5	9.4	10.5	9.5	4.5	**0.0**						
30. *M. palmipes*	11.5	12.3	11.4	12.3	11.8	11.1	12.0	11.1	11.4	10.4	9.7	9.4	8.7	10.2	10.5	9.3	11.2	12.0	11.0	9.1	10.2	9.1	10.1	10.3	10.0	10.5	9.3	12.0	11.5	**2.8**					
31. *M. petrigena*	11.3	12.3	11.6	11.5	11.0	11.8	11.1	11.2	10.5	11.1	10.2	10.9	10.5	10.9	11.4	9.9	10.9	10.2	11.3	10.2	11.0	10.8	10.5	10.1	10.8	11.0	9.7	12.6	11.6	10.0	**4.5**				
32. *M. perparva*	11.0	11.7	11.1	11.7	11.6	11.5	12.0	11.3	10.8	11.2	10.1	10.3	9.6	10.0	11.2	10.1	11.0	11.5	11.6	10.8	11.2	10.5	11.4	11.2	10.0	10.9	10.0	11.7	11.8	9.3	6.0	**4.3**			
33. *M. annectens*	10.8	11.2	11.4	11.6	11.3	11.5	11.6	12.1	11.9	11.4	10.7	11.7	10.7	11.6	12.2	11.1	11.9	9.5	11.8	10.9	12.1	11.1	11.0	11.6	10.9	10.7	10.7	12.8	11.7	11.1	7.2	7.4	**0.6**		
34. *M. marmorata*	8.9	10.1	9.2	10.3	10.6	11.0	10.3	10.2	11.1	10.8	9.7	10.3	9.3	9.7	10.5	9.5	10.2	10.3	10.8	9.3	10.5	9.3	9.7	10.6	10.3	9.7	10.0	10.8	11.0	9.9	6.8	6.3	5.2	–	
35. *Microhyla* sp. 2	7.5	8.1	8.4	7.5	7.5	11.2	6.6	7.4	5.5	2.0	8.4	8.2	7.7	7.7	8.7	7.4	8.3	10.9	11.4	9.8	12.0	12.0	11.2	10.6	11.8	12.0	12.3	12.2	12.3	11.3	11.5	11.6	11.8	11.0	**0.0**

Diagnosis: *Microhyla fodiens* **sp. nov.** is characterized by a combination of the following morphological attributes: (1) males with medium body size, SVL 20.8 – 29.12 mm in two adult individuals, body habitus stout; (2) head flattened, triangular, much wider than long, snout rounded in dorsal and bluntly rounded in lateral views, notably protruding above lower jaw in ventral aspect; *canthus rostralis* rounded, indistinct; (3) skin on dorsum and flanks feebly granular with numerous small round tubercles, ventral surfaces smooth; (4) dorsolateral skinfold presents as row of large tubercles ventrally underlined with black stripe; (5) mid-vertebral skin ridge and dorsomedial stripe absent; (6) supratympanic fold almost indistinct; (7) finger I well developed, notably less than one-half length of finger II; (8) finger and toe tips lacking disks and median longitudinal grooves; (9) two large palmar tubercles (inner palmar tubercle ovoid, slightly elongated; outer palmar tubercle almost rounded); (10) two very prominent metatarsal tubercles (inner metatarsal tubercle large, bean-shaped, outer metatarsal tubercle greatly enlarged, shovel-shaped); (11) limbs short, tibiotarsal articulation of adpressed limb not reaching eye level; (12) toe webbing basal, reaching proximal tubercles; webbing formula: I 1–2 II 1¾–3 III 2¾–3¾ IV 4 – 2¾ V; (13) superciliary tubercles absent; (14) dorsum beige-brown with "teddy-bear-shaped" dark-brown marking running from interorbital to sacral region; two large dark-black inguinal spots continuing on dorsal surfaces of thighs; posterior surfaces of thighs and cloacal region with regular black stripes; chin and throat marbled with gray, chest and belly whitish, limbs ventrally pink. Interspecific genetic *P*-distances in 16S rRNA gene fragment between new species and congeners vary from 9.1% to 12.4%.

Description of holotype (Figures 2C, 4 – 6): Medium-sized male specimen in good state of preservation, SVL 20.1 mm; habitus stout (Figure 4A), head small, much shorter than wide (HL/HW 78.6%); snout rounded in dorsal view (Figure 4A), bluntly rounded in lateral profile (Figure 4C), notably protruding above lower jaw in ventral view (Figure 4B), longer than eye diameter (EL/SL 83.8%); eye small, rounded, almost not protuberant in dorsal (Figure 4A) and lateral views (Figure 4C), pupil circular (Figure 4C); dorsal surface of head flattened, *canthus rostralis* indistinct, rounded; loreal region vertical, not concave; nostril rounded with lateral orientation, located much closer to tip of snout than to eye (Figure 4C); tympanum hidden under skin of temporal region, supratympanic fold smooth, weak, almost indistinct, running ventroposteriorly from posterior corner of eye to axilla; maxillary and vomerine teeth absent, tongue obovate, entire and free at base, lacking papillae; vocal sac single, subgular.

Forelimbs short, three times shorter than hindlimbs (FLL/HLL 33.9%); hand short, notably shorter than lower arm (HAL/LAL 65.5%) and two times shorter than forelimb length (HAL/FLL 52.8%); fingers short, thick, rounded in cross-section, first finger well developed, but two times shorter than second finger (1FL/2FL 46.9%); relative finger lengths: I<IV<II<III (see Figures 4D, 5A). Finger webbing and dermal fringes absent; tips of all fingers rounded, not enlarged, lacking terminal disks and median longitudinal furrows or grooves; subarticular tubercles on volar surface of fingers very large, distinct, rounded, prominent; finger subarticular tubercle formula: 1:1:2:2 (hereafter, given for fingers I:II:III:IV, respectively); nuptial pad absent; two metacarpal (palmar) tubercles: inner palmar tubercle slightly elongated, ovoid-shaped, two times longer than wide; outer palmar tubercle flattened, large, rounded, notably longer than inner (IPTL/OPTL 81.8%); medial or supernumerary palmar tubercles absent; inner and outer palmar tubercles separated by deep groove.

Hindlimbs massive and comparatively short, tibia length slightly longer than half of snout-vent length (TL/SVL 53.4%), hindlimb length less than 1.5 times longer than snout-vent length (HLL/SVL 145.0%); tibiotarsal articulation of adpressed limb not reaching orbit level; foot slightly longer than tibia (FL/TL 137.2%); relative toe lengths: I<II<V<III<IV; tarsal fold on inner surface of tarsus absent; tips of all toes rounded, not enlarged, not forming terminal disks (Figures 4E, 5B); toes thick, short, slightly flattened in cross-section, with weak dermal fringes present on toes II–V reaching level of penultimate phalanges (Figures 4E, 5B); basal webbing developed between all toes, webbing formula: I 1–2 II 1¾–3 III 2¾–3¾ IV 4–2¾ V; subarticular tubercles on toes very distinct, protruding, rounded, toe subarticular tubercle formula: 1:2:3:3:2 (hereafter, given for toes I:II:III:IV:V, respectively); nuptial pad absent; two large metatarsal tubercles: inner metatarsal tubercle elongated, prominent, bean-shaped; outer metatarsal tubercle very large, shovel-shaped, with prominent outer edge (OMTL/IMTL 118.6%) (Figure 5B).

Dorsal skin feebly tubercular with numerous small granules and tubercles evenly scattered on dorsum; more distinct in life (Figure 6A) than in preservative (Figure 4A); upper eyelids almost smooth with few flat tubercles on medial edges of eyelids, superciliary tubercles or projections absent; mid-vertebral dermal ridge absent; indistinct dorsolateral skinfold running from posterior eye corner towards groin, consisting of row of larger glandular warts (Figure 6A); skin on dorsolateral surfaces smooth with rare small granules; dorsal surface of limbs smooth with few small tubercles, ventral sides of trunk, head, and limbs smooth.

Coloration of holotype in life: Dorsal surfaces of head and trunk with beige background (Figure 6); weak brown interorbital bar between eyelids posteriorly forming "teddy-bear"-like (see Rakotoarison et al., 2017) or hourglass-shaped dark-brown markings, running posteriorly to scapular region, widening at level of axilla, narrowing at mid-dorsum and widening again towards groin; thin brownish lines on lateral sides of dorsum forming three nested reverse V-shaped figures, parallel to edges of "teddy-bear"-like dark marking; sacral region with irregular brownish vermiculated pattern; two large dark-black inguinal spots in groin area continuing posteriorly on dorsal surfaces of thighs, forming thick dark-black cross-bands (Figure 6A). Dorsolateral lines ventrally edged with black; body flanks with numerous small blackish and dark-brown spots and mottling; ventral edge of

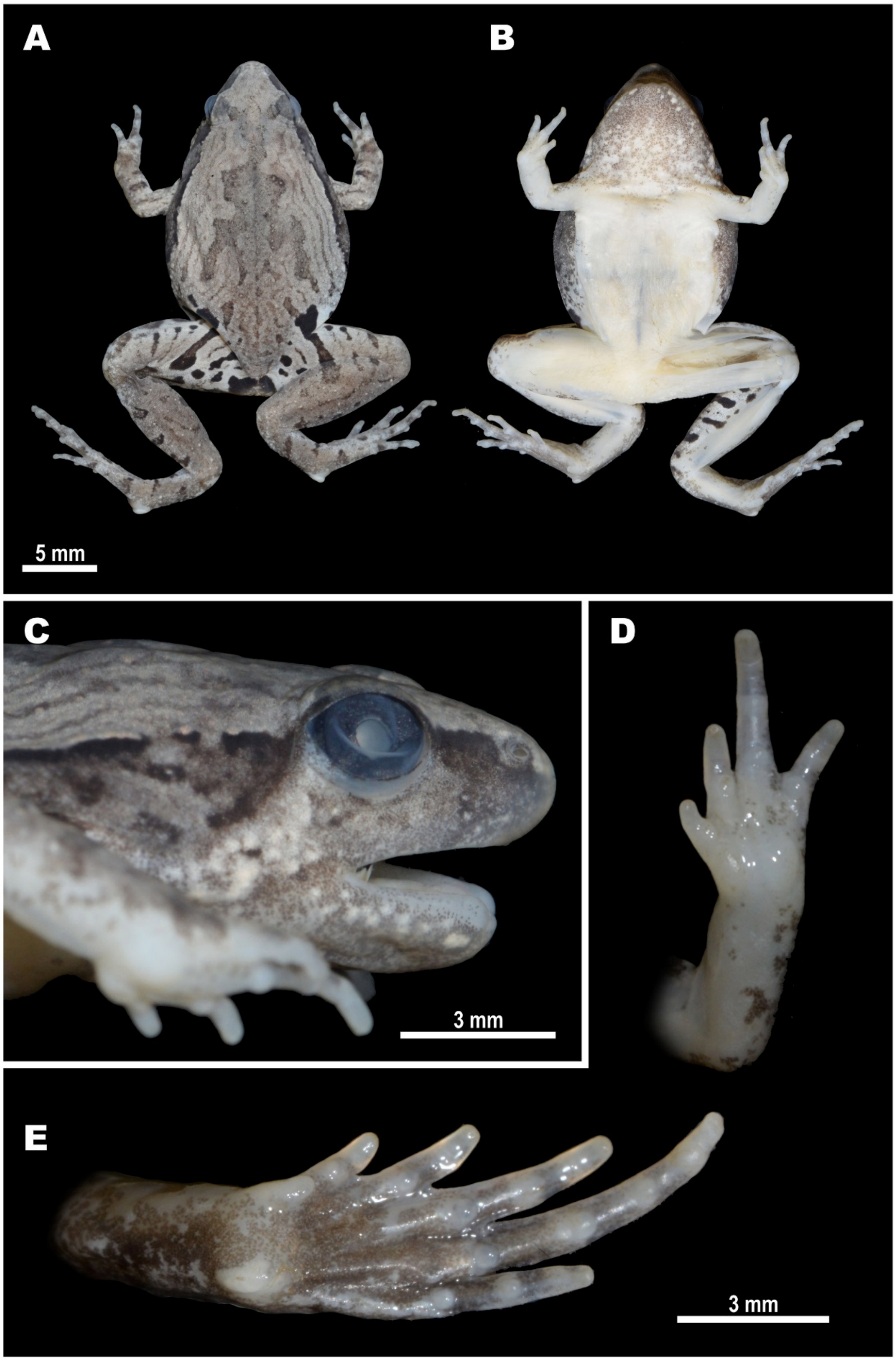

Figure 4 Holotype of *Microhyla fodiens* sp. nov. (ZMMU A5960), male, in preservative
A: Dorsal view; B: Ventral view; C: Lateral view of head; D: Volar view of left hand; E: Plantar view of right foot. Photos by Nikolay A. Poyarkov.

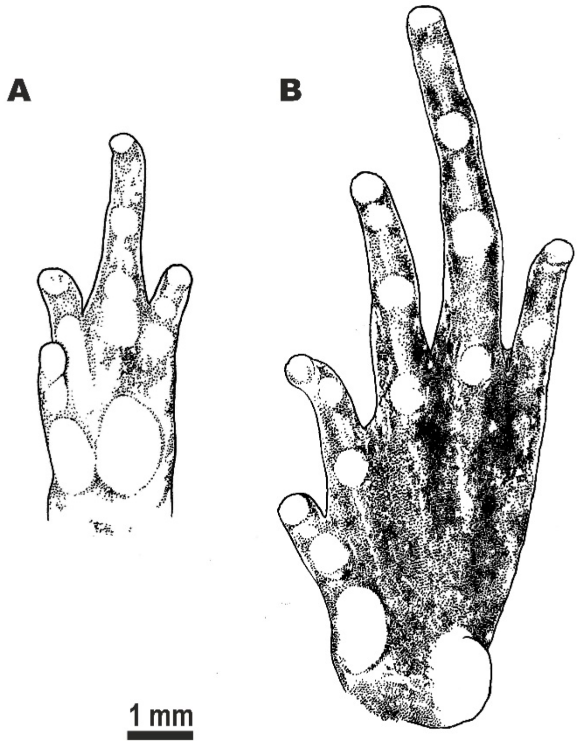

Figure 5 Morphological details of holotype of *Microhyla fodiens* sp. nov. (ZMMU A5960), male, in preservative
A: Volar view of the left hand; B: Plantar view of left foot. Scale bar: 1 mm. Drawings by Valentina D. Kretova.

eyelids dark-brown; lateral sides of head with weak brownish mottling; supratympanic dark-brown with light yellowish-beige stripe ventrally, running from posterior edge of eye towards axilla; dorsal surfaces of limbs beige-brown with few brownish blotches; two narrow dark-brown bars on dorsal surfaces of forearm on each forelimb; three wide black transverse interrupted cross-bands on dorsal and posterior surfaces of proximal part of thighs forming tiger-like pattern, cloacal region with large dark-black blotch (Figure 6C); dorsal surfaces of tibia and tarsus brownish with rare dark transverse blotches alternating on each hindlimb: four large spots on right shank, three large dark spots on left shank; two dark short stripes on each tarsus (Figure 6A, C); fingers and toes dorsally gray with brown cross-bars; throat and chest with gray mottling, chest and venter whitish; ventral surfaces of limbs pinkish to gray-violet; hand and foot ventrally pinkish-gray; pupil black, circular, edged with narrow golden line, dense golden reticulations throughout iris except for dark vertical bar at ventral part of iris; sclera bluish (Figure 6A, B).

Coloration of holotype in preservative: After initial fixation in formalin and preservation in ethanol for six months, dorsal coloration significantly faded and turned light grayish-brown (Figure 4A), ventral surface of chest, belly, and limbs changed to whitish (Figure 4B); dorsal pattern and dark stripes on dorsal surfaces of limbs and body unchanged; iris coloration faded and turned dark-gray (Figure 4C).

Measurements of holotype (in mm): SVL 20.8; HL 6.5; SL 2.9; EL 2.4; N-EL 1.7; HW 8.3; IND 1.7; IOD 2.4; UEW 1.2; FLL 10.2; LAL 8.2; HAL 5.4; IPTL 0.7; OPTL 0.9; 3FDD 0.4; HLL 30.2; TL 11.1; FL 15.2; IMTL 1.2; 4TDD 0.6; OMTL 1.4; 1FL 0.9; 2FL 1.9; 3FL 2.9; 4FL 1.6; 1TOEL 1.5; 2TOEL 2.6; 3TOEL 3.8; 4TOEL 5.5; 5TOEL 2.8.

Variation: Morphometric variation of the type series is presented in Table 3. The paratypes are subadult specimens and are notably smaller in body size than the holotype (SVL 12.6–17.9 mm; mean 15.2±1.38 mm; *n*=5). Paratype coloration does not significantly differ from that described for the holotype, with the exception of the throat, which is off-white and lacks blackish mottling. All type specimens have large black inguinal spots; location and shape of black markings on posterior surfaces of thighs and cloacal area, as well as shape of "teddy-bear"-shaped brown dorsal marking, may vary insignificantly. Adult male CAS 215851 (see Referred materials) from the type locality is larger than the holotype (SVL 29.1 mm) but agrees well with the holotype description in general morphology and coloration, although it has more dark spots in the axilla area compared to the holotype. CAS 215851 has a very large and shovel-shaped outer metatarsal tubercle, notably protruding in dorsal view. Chromatic differences include coloration of the throat, which is uniform black-gray in male CAS 215851; coloration gets darker towards lower jaw edges.

Natural history: Pakokku District is located in the heart of the dry zone of central Myanmar, which is characterized by low precipitation and high temperatures, with a hot semi-arid tropical savanna-like climate (Peel et al., 2007). On average, Pakokku receives around 560 mm of precipitation annually. April is the warmest month, with an average temperature of 31.5 °C, whereas January is the coldest month, with an average temperature of 21.5 °C. The highest rainfall is observed in August and September, with 113 and 130 mm of precipitation, respectively (data from https: //en. climate-data. org).

All specimens of *Microhyla fodiens* **sp. nov.** were collected at night from 1900 to 2100 h on the banks of a large, permanent, likely artificial pond near a small Buddhist pagoda in the center of Kan Pauk village, located in a dry and open habitat with rare vegetation in the vicinity of Shinma Taung Mountain – the only hill in the area with an elevation of 514 m a. s. l. (Figure 7A). The pond is used by local people as a watering area for livestock. Subadult specimens were recorded on the banks of the pond hiding in cracks, whereas the adult male holotype was collected from the stone fence of the pagoda, hiding in a crevice. Thus, the new species appears to be a good burrower. During the survey, the weather remained hot and dry and the *Microhyla fodiens* **sp. nov.** specimens were inactive and hid in shelters; no calling was recorded. We also examined several paddy-fields and

Figure 6 Holotype of *Microhyla fodiens* sp. nov. (ZMMU A5960), male, in life

A: Dorsolateral view *in situ*; B: Lateral view of head; C: Posterior view of thighs and inguinal region showing regular black markings. Photos by Nikolay A. Poyarkov (A) and Parinya Pawangkhanant (B, C).

Table 3 Measurements of type series of *Microhyla fodiens* sp. nov. (in mm)

No.	Specimen ID	Type status	SVL	HL	SL	EL	N-EL	HW	IND	IOD	UEW	FLL	LAL	HAL	1FL	IPTL	OPTL	3FDD	HLL	TL	FL	IMTL	1TOEL	4TDD	OMTL
	Male																								
1	ZMMU A5960	Holotype	20.8	6.5	2.9	2.4	1.7	8.3	1.7	2.4	1.2	10.2	8.2	5.4	0.9	0.7	1.1	0.4	30.2	11.1	15.2	1.2	1.5	0.6	1.4
	Sub adults																								
2	ZMMU A5961	Paratype	17.9	5.4	2.6	2.2	1.4	7.5	1.4	2.0	1.3	9.4	7.2	4.8	0.8	0.8	1.0	0.4	25.5	9.2	13.0	1.0	1.5	0.5	1.1
3	ZMMU A5962	Paratype	15.9	5.6	2.3	2.3	1.4	6.7	1.4	1.9	1.1	7.4	6.6	4.2	0.8	0.6	0.9	0.3	22.4	8.5	11.3	0.8	1.5	0.4	0.8
4	ZMMU A5963	Paratype	15.1	5.0	2.4	2.2	1.3	6.3	1.4	1.8	1.2	8.9	6.7	4.3	0.8	0.7	0.9	0.4	24.1	8.0	11.0	0.9	1.4	0.6	0.8
5	ZMMU A5964	Paratype	14.5	4.7	2.3	1.9	1.4	5.5	1.5	2.0	1.1	8.0	6.3	4.0	0.9	0.7	0.8	0.4	22.5	8.1	11.0	0.8	1.5	0.4	1.0
6	ZISP 13729	Paratype	12.6	4.2	2.2	2.0	1.2	5.1	1.3	2.0	1.0	6.6	5.6	3.6	0.7	0.6	0.8	0.3	19.0	6.8	9.4	0.6	1.3	0.4	0.7
		Mean	16.1	5.2	2.4	2.2	1.4	6.2	1.5	2.0	1.2	8.4	6.8	4.4	0.8	0.7	0.9	0.4	23.9	8.6	11.8	0.9	1.5	0.5	0.9
		SD	*2.9*	*0.8*	*0.3*	*0.2*	*0.2*	*1.0*	*0.2*	*0.2*	*0.1*	*1.4*	*0.9*	*0.6*	*0.1*	*0.1*	*0.1*	*0.0*	*3.7*	*1.5*	*2.0*	*0.2*	*0.1*	*0.1*	*0.1*
		Min	12.6	4.2	2.2	1.9	1.2	5.1	1.3	1.8	1.0	6.6	5.6	3.6	0.7	0.6	0.8	0.3	19.0	6.8	9.4	0.6	1.3	0.4	0.7
		Max	20.8	6.5	2.9	2.4	1.7	7.5	1.7	2.4	1.3	10.2	8.2	5.4	1.1	0.8	1.1	0.4	30.2	11.1	15.2	1.2	1.7	0.6	1.1

Min: Minium; Max: Maximum. For other abbreviations see Materials and Methods.

other large waterbodies within a 2 km radius around Kan Pauk village; however, *Microhyla fodiens* **sp. nov.** was not recorded in any other locality. Diet, larval stages, and eggs of the new species are unknown.

Other microhylids recorded in sympatry with *Microhyla fodiens* **sp. nov.** included new congeneric species *Microhyla irrawaddy* **sp. nov.** (see below) and *Kaloula pulchra* Gray, 1831, which appear to share the same breeding site during the reproductive season. Other anurans such as *Fejervarya* sp., *Hoplobatrachus* cf. *tigerinus* (Daudin, 1802), *Sphaerotheca*

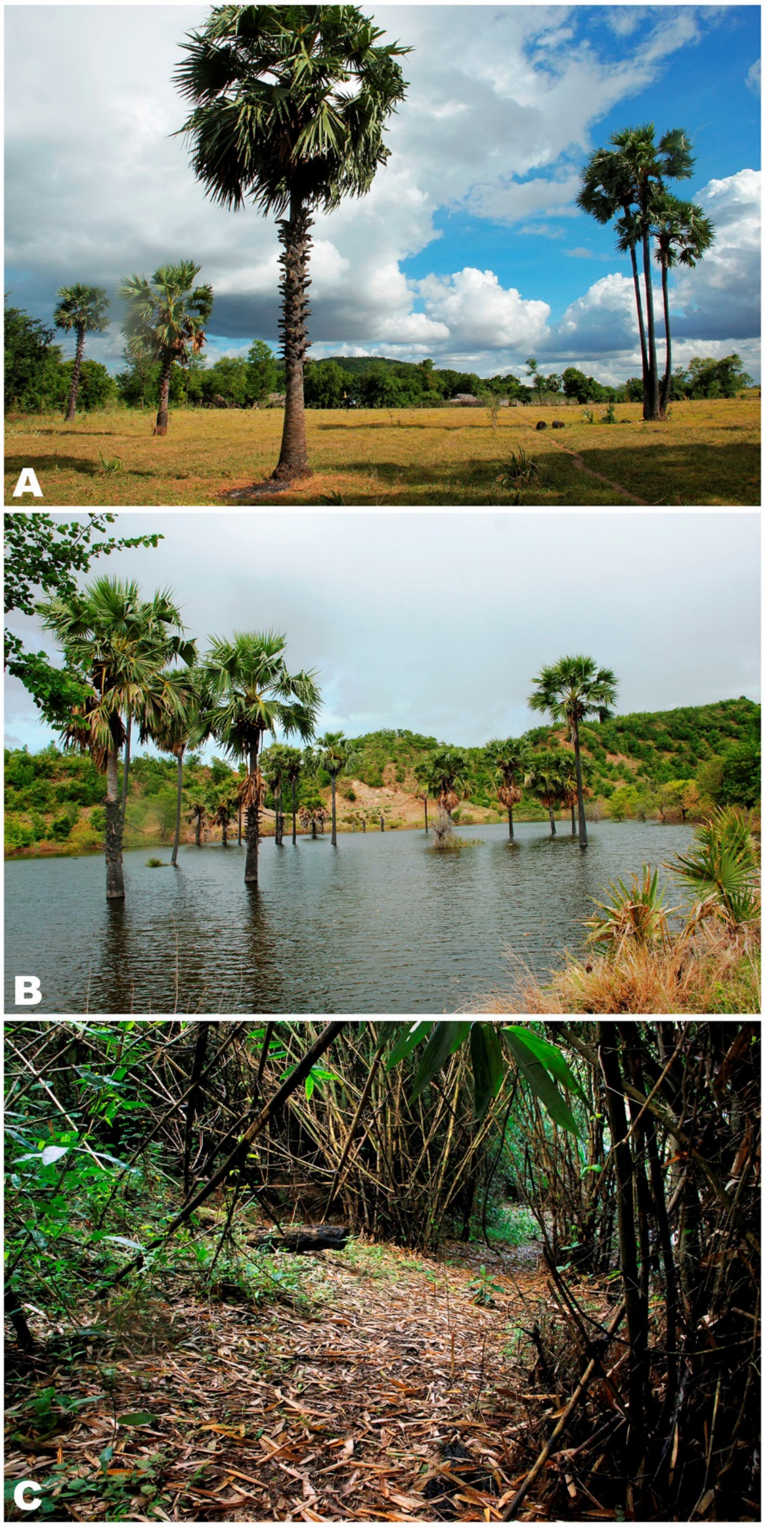

Figure 7 Natural habitats of *Microhyla* in Myanmar

A: Natural habitat of *Microhyla fodiens* **sp. nov.** at Kan Pauk village, Magway (type locality), green hill in background is Shinma Taung Mountain; B: Breeding habitat of *Microhyla irrawaddy* **sp. nov.** from Pakokku, Magway (type locality); C: Natural habitat of *M. heymonsi*, *M. butleri*, and *M. mukhlesuri* in bamboo forest on slopes of Ingyin Taung Mt., Indawgyi Lake region, Kachin. Photos by Parinya Pawangkhanant.

sp., and *Duttaphrynus melanostictus* (Schneider, 1799) also occurred in sympatry.

Distribution: *Microhyla fodiens* **sp. nov.** is currently known only from the type locality in Kan Pauk, Yesagyo Township, Magway Division, Myanmar (Figure 1). The species was recorded at an elevation of 230 m a.s.l. The actual distribution of the new species is unknown, but it is likely to be found in other arid areas of the Irrawaddy River Valley in the region of the Irrawaddy and Chindwin interfluve; discovery of new localities in Magway, Sagaing, and Mandalay divisions is anticipated. The record of "*Microhyla rubra*" from "Moulmein, Burma" (now Mawlamyine) by Parker (1934) based on W. Theobald's collection comes from Mon State in southern Myanmar—a region with a much milder tropical monsoon climate—might refer to a different species. The taxonomic status of this record requires clarification by further studies.

Conservation status: At present, the new species is known from several specimens from a single locality in Yesagyo Township, Magway Division; however, a wider distribution in other arid areas of central Myanmar is anticipated. As the actual range and population trend of the new species are currently unknown, we suggest *Microhyla fodiens* **sp. nov.** be considered as a Data Deficient species following IUCN's Red List categories (IUCN Standards and Petitions Subcommittee, 2017).

Etymology: The specific name "*fodiens*" is a Latin adjective in the nominative singular derived from "*fodio*" — Latin verb meaning "to dig" or "to burrow" referring to the distinctive enlarged shovel-shaped outer metatarsal tubercle of the new species, suggesting that it is a good burrower, which may serve as an adaptation to the dry climate of the Irrawaddy River Valley in central Myanmar. The recommended common name in English is "*Burrowing narrow-mouth frog*". The recommended common name in Burmese is "*Twin Aoung Thaephar*".

Comparisons: Only a few species of *Microhyla* have a stout body habitus with an enlarged spade- or shovel-shaped outer metatarsal tubercle as an adaptation for digging, including, *M. rubra* from southern India, *M. mihintalei* from Sri Lanka, *M. taraiensis* from eastern Nepal, and *M. picta* from southern Vietnam. Comparisons of *Microhyla fodiens* **sp. nov.** with the abovementioned species appear to be the most pertinent; from all remaining species of the genus, the new species can be easily distinguished by its stout body habitus and enlarged shovel-shaped outer metatarsal tubercle (vs. slender to stout body habitus and small or no outer metatarsal tubercle in other species of *Microhyla*).

Microhyla rubra was originally described by Jerdon (1854) from "Carnatic near rivers" and "also Ceylon"; the holotype is considered to be lost. Recently, Wijayathilaka et al. (2016) restricted the distribution of *M. rubra* to southern India and Garg et al. (2018b) designated a neotype for this species. *Microhyla fodiens* **sp. nov.** can be distinguished from *M. rubra* from southern and eastern India by the following characteristics: first finger notably shorter than half of second finger (vs. equal), thigh shorter than foot length, TL=8.6±1.5 mm, FOL=11.8±2.0 mm, *n*=6 (vs. thigh longer than foot length, male, TL 13.8±0.5 mm, FOL 12.4±0.4 mm, *n*=8; data from Wijayathilaka et al., 2016), comparatively shorter hindlimbs with tibiotarsal articulation not reaching eye level (vs. reaching over eye level but shorter than snout tip), comparatively better developed webbing between toes, toe webbing formula: I 1–2 II 1¾–3 III 2¾–3¾ IV 4–2¾ V (vs. I 1½–2 II 1½–3 III 2½–3 IV 4–2½ V), and dorsal pattern with brown "teddy-bear"-shaped marking, thin brownish lines on lateral sides of dorsum forming three nested reverse V-shaped figures (vs. almost uniform reddish-brown dorsum).

Microhyla fodiens **sp. nov.** can be distinguished from *M. mihintalei* from Sri Lanka by the following characteristics: granular skin on dorsum (vs. shagreened or sparsely granular skin on dorsum), thigh shorter than foot length, TL=8.6±1.5 mm, FOL=11.8±2.0 mm, *n*=6 (vs. thigh equal to foot length, male, TL 11.6±0.6 mm, FOL 11.6±0.6 mm, *n*=14; data from Wijayathilaka et al., 2016), comparatively better developed foot webbing (vs. toe webbing reduced), dorsal pattern with brown "teddy-bear"-shaped marking, thin brownish lines on lateral sides of dorsum forming three nested reverse V-shaped figures (vs. almost uniform orange-brown or reddish-brown dorsum), and three wide black transverse cross-bands on dorsal and posterior surfaces of thighs forming tiger-like pattern, cloacal region with large black blotch (vs. tiger-like pattern and dark cloacal blotch absent).

The new species can be readily diagnosed from *M. taraiensis* from eastern Nepal by the following characteristics: red spots and tubercles on dorsum absent (vs. light red dots dispersed over dorsal surfaces), large shovel-shaped outer metatarsal tubercle (vs. rounded outer metatarsal tubercle), second finger longer than fourth finger (vs. shorter), comparatively shorter hindlimbs with tibiotarsal articulation not reaching eye level (vs. reaching nostril level), inner palmar tubercle ca. 1.5 times smaller than outer palmar tubercle (vs. inner palmar tubercle two times greater than outer palmar tubercle), single subarticular tubercle on second finger and two subarticular tubercles on third finger (vs. two tubercles on second finger and three tubercles on third finger), and single subarticular tubercle on second toe and two subarticular tubercles on third toe (vs. two tubercles on second toe and three tubercles on third toe).

Finally, *Microhyla fodiens* **sp. nov.** can be distinguished from *M. picta* from southern Vietnam by the following characteristics: generally smaller body size, adult SVL 20.8–29.1 mm (vs. adult SVL 25.2–33.4 mm), better developed webbing on feet, toe webbing formula: I 1–2 II 1¾–3 III 2¾–3¾ IV 4–2¾ V (vs. I 2–2¾ II 1¾–2¾ III 2¾–3¾ IV 4–2½ V), dorsal pattern with brown "teddy-bear"-shaped marking, thin brownish lines on lateral sides of dorsum forming three nested reverse V-shaped figures (vs. brown dorsal markings in shape of irregular blotches or reverse V-shaped figures but always edged with white or light beige), pronounced dorsolateral fold as row of enlarged tubercles (vs. no dorsolateral fold), bright-yellow coloration in groin area absent (vs. present), and black

iris with dense golden reticulations (vs. dark iris with bronze to reddish-bronze color of reticulations).

Microhyla irrawaddy **sp. nov.**
Table 4; Figures 2A–B, 8–10.

Chresonymy
Microhyla sp. A – (?) Mulcahy et al., 2018, p. 99, 116–117.

Holotype: ZMMU A5965 (field number NAP-08241), adult male collected while calling from holes/hollows in the bank of a temporary pond in the Irrawaddy (Ayeyarwady) River Valley, in the suburbs of Pakokku, Pakoku District, Magway Division, Myanmar (coordinates N21.316°, E95.053°; elevation 59 m a. s. l.), collected on 14 July 2018 at 1900 h by Nikolay A. Poyarkov, Vladislav A. Gorin, Parinya Pawangkhanant, and Than Zaw.

Paratypes: ZMMU A5966–A5970 (field numbers NAP-08238–08240; NAP-08242 – 08243), and ZISP 13730 (field number NAP-08244), six adult males from the same locality and with the same collection information as the holotype; ZMMU A5971 – A5974 (field numbers NAP-08245 – 08248), four adult females from the same locality and with the same collection information as the holotype; ZMMU A5975–A5976 (field numbers NAP-08274 – 08275), two adult females collected on the bank of a paddy field in the vicinity of Kan Pauk village, near Shinma Taung Mt., Yesagyo Township, Magway Division, Myanmar (coordinates N21.594°, E95.082°; elevation 217 m a. s. l.), collected on 15 July 2018 at 1900 h by Nikolay A. Poyarkov, Vladislav A. Gorin, Parinya Pawangkhanant, and Than Zaw.

Diagnosis: *Microhyla irrawaddy* **sp. nov.** is distinguished by the following combination of morphological characters: (1) small adult body size: males SVL 12.3 – 17.1 mm, females SVL 16.7 – 20.9 mm, body habitus very slender; (2) head small, triangular, wider than long, snout acuminate with rounded tip in dorsal view and rounded in lateral view, slightly protruding above lower jaw in ventral aspect; *canthus rostralis* indistinct; (3) skin on dorsum and flanks granular with irregularly scattered numerous large and small round tubercles, ventral surfaces completely smooth; (4) dorsolateral skinfold and dark lateral band absent; (5) mid-vertebral skin ridge and dorsomedial stripe absent; (6) supratympanic fold distinct; (7) finger I well developed, slightly longer than one-half length of finger II; (8) tips of fingers II – IV and toes II – V weakly dilated, not forming conspicuous disks; peripheral grooves ventrally present on tips of fingers II–IV and toes II–IV; fingers and toes lacking dorsal median grooves or distal notches; (9) two small palmar tubercles (inner palmar tubercle rounded, prominent; outer palmar tubercle smaller and less distinct than inner, rounded, flattened); (10) two small metatarsal tubercles (inner metatarsal tubercle elongated, ovoid, flattened; outer metatarsal tubercle small, rounded, prominent); (11) limbs comparatively short, tibiotarsal articulation of adpressed limb reaching eye level; (12) toe webbing completely reduced; webbing formula: I 2–3 II 2–3 III 3 – 4½ IV 4½ – 2¾ V; (13) superciliary tubercles absent; (14) dorsum yellowish-brown with dark-brown contrasting "teddy-bear"-shaped marking running from interorbital to sacral region; larger tubercles on dorsum orange to red; body flanks grayish with darker mottling not clearly separated from dorsum coloration; dorsal surfaces of thighs and shanks with two to three dark crossbars; chin and throat with grayish mottling (blackish in males), body and limbs ventrally cream to whitish at belly. Interspecific genetic *P*-distances in the 16S rRNA gene fragment between the new species and other currently recognized species of *Microhyla* vary from 5.7% to 12.9%.

Description of holotype (Figures 8 – 9, 10A): Small-sized male specimen in good state of preservation, SVL 15.6 mm; habitus very slender (Figure 8A), head small, notably shorter than wide (HL/HW 73.3%); snout acuminate with rounded tip in dorsal view (Figure 8A), gently rounded in lateral profile (Figure 8C), slightly projecting above lower jaw in ventral aspect (Figure 8B); snout longer than eye diameter (EL/SL 87.9%); eyes rounded, notably protuberant in dorsal (Figure 8A) and lateral views (Figures 8C, 10A), pupil circular (Figure 8C); head dorsally flattened, *canthus rostralis* rounded, indistinct; loreal region slightly concave; nostril lateral, rounded, located much closer to tip of snout than to eye (Figure 8C); tympanum hidden, supratympanic fold distinct, prominent, gently curving ventroposteriorly from posterior corner of eye towards forelimb insertion; maxillary and vomerine teeth absent, tongue obovate with pointed tip, smooth margins, lingual papillae absent; vocal sac single, subgular.

Forelimbs comparatively short, three times length of hindlimbs (FLL/HLL 33.9%); hand short, shorter than lower arm (HAL/LAL 62.0%), two times forelimb length (HAL/FLL 51.2%); fingers comparatively long and thin, rounded in cross-section, first finger well developed, notably longer than half of second finger length (1FL/2FL 56.0%); relative finger lengths: I <II=IV<III (see Figures 8D, 9A). Finger webbing and dermal fringes absent; tip of finger I rounded, not enlarged, lacking terminal disk and median longitudinal furrow; tips of fingers II–IV slightly dilated, not forming conspicuous disks and lacking dorsal median grooves; peripheral grooves ventrally present on tips of fingers II–IV (Figures 8D, 9A). Subarticular tubercles on volar surface of fingers rounded, with indistinct borders, rather flattened, finger subarticular tubercle formula: 1 : 1 : 2 : 2; nuptial pad absent; two palmar tubercles: inner palmar tubercle rounded, slightly prominent, with distinct borders; outer palmar tubercle flattened, large, rounded, with indistinct borders, larger than inner (IPTL/OPTL 83.8%); supernumerary palmar tubercles absent.

Hindlimbs comparatively short and thin, tibia length equal to half of snout-vent length (TL/SVL 50.7%), hindlimb length around 1.5 times longer than snout-vent length (HLL/SVL 145.0%); tibiotarsal articulation of adpressed limb reaching eye level; foot notably longer than tibia (FL/TL 144.9%); relative toe lengths: I<V<II<III<IV; tarsal fold absent; tip of toe I rounded, not forming terminal disk; tips of toes II – V weakly dilated, not forming conspicuous disks; peripheral grooves

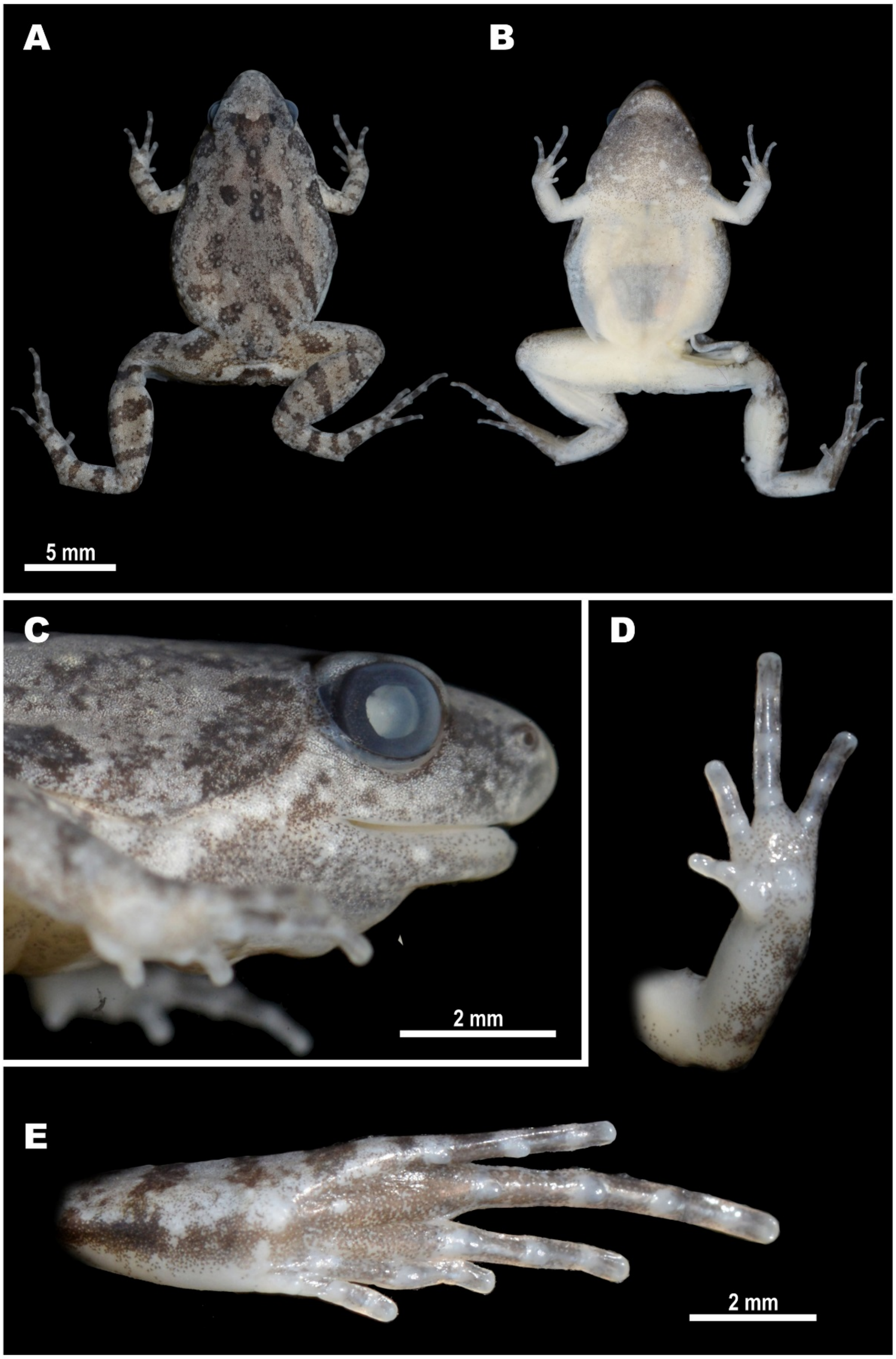

Figure 8 Holotype of *Microhyla irrawaddy* sp. nov. (ZMMU A5965), male, in preservative
A: Dorsal view; B: Ventral view; C: Lateral view of head; D: Volar view of left hand; E: Plantar view of right foot. Photos by Nikolay A. Poyarkov.

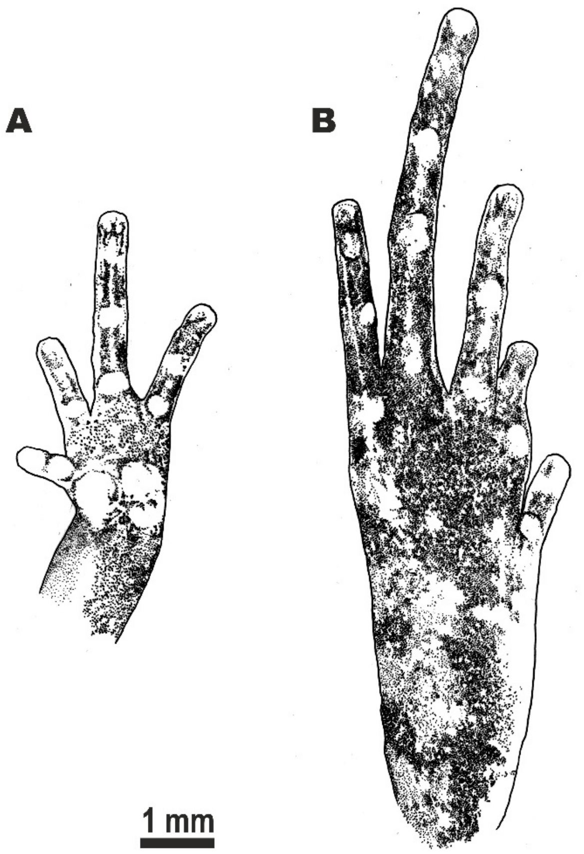

Figure 9 Morphological details of holotype of *Microhyla irrawaddy* sp. nov. (ZMMU A5965), male, in preservative

A: Volar view of left hand; B: Plantar view of right foot. Scale bar: 1 mm. Drawings by Valentina D. Kretova.

ventrally present on toe tips II–IV (Figures 8E, 9B); toes thin, long, rounded in cross-section, lacking dermal fringes (Figures 8E, 9B); webbing completely reduced between all toes, webbing formula: I 2–3 II 2–3 III 3–4½ IV 4½–2¾ V; subarticular tubercles on toes distinct, rounded, protruding, toe subarticular tubercle formula: 1:1:2:3:2; nuptial pad absent; two small metatarsal tubercles, inner metatarsal tubercle elongated, ovoid, flattened; outer metatarsal tubercle small, rounded, prominent, around one third length of inner metatarsal tubercle (OMTL/IMTL 35.6%).

Dorsal skin granular with numerous small granules and larger tubercles irregularly scattered on dorsum; distinct in life (Figure 10A) as in preservative (Figure 8A); upper eyelids with numerous small tubercles scattered medially; superciliary tubercles or projections absent; mid-vertebral dermal ridge and dorsolateral folds absent; skin on dorsolateral surfaces with smaller flattened granules and pustules; dorsal surface of forearms, thighs, shanks, and tarsus with evenly scattered small tubercles; skin on ventral sides of trunk, head, and limbs smooth.

Coloration of holotype in life: Head and trunk dorsally with yellowish-brown background coloration (Figure 10A); dark-brown interorbital bar between eyelids forming V-shaped marking oriented posteriorly towards scapular region; dark-brown markings on dorsum "teddy-bear"-like shape: narrowing at head basis, widening to diamond-shape on scapular region (four blackish round spots forming cross), narrowing posteriorly, forming two pairs of dark stripes towards groin and sacral area. Indistinct brownish lines and blotches on sacral area and axillary region. Gray-brownish line with unclear edges running from posterior corner of eye along upper flanks toward groin. Thin dark-brown stripe from anterior corner of eye along *canthus rostralis* toward nostril. Lateral sides of head and trunk grayish to yellowish-gray (Figure 10A). Limbs dorsally yellowish-brown with darker brownish markings alternating on each limb: two brown cross-bars on forearms, brownish spots on dorsal surfaces of hands and fingers; two dark-brown blotches on dorsal surfaces of thighs, distal one continuing to shanks; shanks dorsally with three dark-brown cross-bars; dorsal surface of tarsus with two brown cross-bars; feet and toes with brownish spots. Ventral surfaces of chest and belly pale cream; throat with dense dark-gray mottling, getting darker toward margins of lower jaw and lower margin of upper jaw; light yellow pigmentation at junction of forelimbs; limbs ventrally pinkish. Tubercles and granules on dorsal surfaces of body, head, and thighs orange to bright-red (Figure 10A); superciliary area of upper eyelids lighter than medial area; supratympanic fold brown; light yellowish-cream stripe from posterior corner of eye toward forelimb insertion; cloacal region brownish. Pupil black, circular, edged with golden line, dense bronze-green to golden reticulations throughout iris; sclera greenish-yellow (Figure 10A).

Coloration of holotype in preservative: After preservation in formalin and storage in ethanol for six months, coloration of dorsal surfaces faded to grayish-brown (Figure 8A), ventral surface of chest, belly, and limbs changed to whitish-gray (Figure 8B). Dorsal pattern, brownish markings on dorsal surfaces of limbs and body unchanged; iris coloration completely faded to black (Figure 8C).

Measurements of holotype (in mm): SVL 15.6; HL 5.1; SL 2.4; EL 2.1; N-EL 1.4; HW 6.9; IND 1.3; IOD 1.8; UEW 1.1; FLL 7.7; LAL 6.3; HAL 3.9; IPTL 0.6; OPTL 0.7; 3FDD 0.4; HLL 22.6; TL 7.9; FL 11.5; IMTL 0.7; 4TDD 0.4; OMTL 0.3; 1FL 0.9; 2FL 1.6; 3FL 2.8; 4FL 1.6; 1TOEL 1.5; 2TOEL 2.6; 3TOEL 3.3; 4TOEL 5.4; 5TOEL 2.5.

Variation: Variation in morphometric characters within the type series is shown in Table 4. In general, all paratypes agree well with the description of the holotype. Specimens vary significantly in body size, coloration of dorsal surface, form of dark "teddy-bear"-shaped brown markings on dorsum, extent of spotting on dorsum and flanks, and coloration of ventral surfaces. Males have generally much smaller body size than females: SVL in males 12.3–17.1 mm (mean 14.9±1.8 mm; *n*= 7) and SVL in females 16.7–20.9 mm (mean 18.1±1.5 mm; *n*=

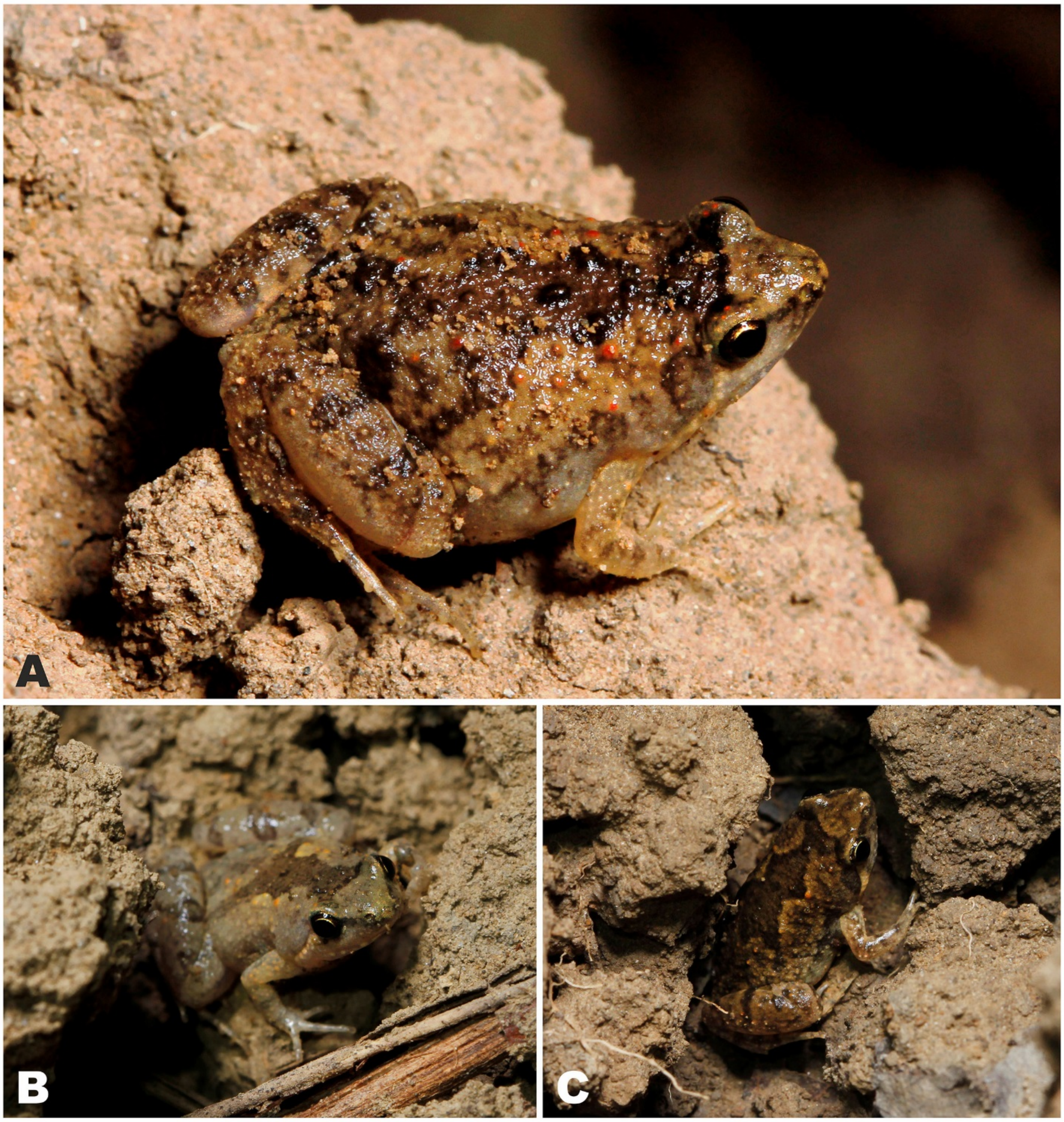

Figure 10 ***Microhyla irrawaddy*** **sp. nov. type series** ***in situ***

A: Dorsolateral view of holotype (ZMMU A5965); B, C: Paratype males (ZMMU A5966 and A5967) in calling position in hollows and buffalo footprints in dirt at type locality. Photos by Parinya Pawangkhanant.

6). Females have generally lighter coloration, with less contrast in light-brown dorsal marking and fewer bright reddish tubercles on dorsum (Figure 2B) than males (Figures 2A, 10A). In female ZMMU NAP-08274, the dorsal "teddy-bear"-like marking on the dorsum is interrupted and represented by a number of large grayish-brown irregular blotches (Figure 2B). Females have a more gray-olive tint in dorsal coloration than males (Figure 2A, B). Males have a grayish-black subgular vocal sac, whereas females have lighter grayish-white throats. Gravid females contained unpigmented eggs, visible through the semi-translucent belly skin near the groin area. Background dorsal coloration of

breeding males may vary from light-gray (paratype ZMMU A5966, see Figure 10B) to beige (holotype ZMMU A5965, see Figure 10A) and light yellowish-brown (paratype ZMMU A5967, see Figure 10C).

Table 4 Measurements of type series of *Microhyla irrawaddy* sp. nov. (in mm)

No.	Specimen ID	Type status	SVL	HL	SL	EL	N-EL	HW	IND	IOD	UEW	FLL	LAL	HAL	1FL	IPTL	OPTL	3FDD	HLL	TL	FL	IMTL	1TOEL	4TDD	OMTL
	Males																								
1	ZMMU A5965	Holotype	15.6	5.1	2.4	2.1	1.4	6.9	1.3	1.8	1.1	7.7	6.3	3.9	0.9	0.6	0.7	0.4	22.6	7.9	11.5	0.7	1.5	0.4	0.3
2	ZMMU A5966	Paratype	17.1	5.3	2.4	2.3	1.3	6.9	1.3	1.9	1.2	7.8	6.6	3.9	0.9	0.6	0.6	0.3	23.6	8.0	11.2	0.6	1.4	0.4	0.3
3	ZMMU A5967	Paratype	15.4	4.9	2.5	2.2	1.2	7.0	1.3	1.9	1.2	7.6	6.0	3.7	0.7	0.5	0.6	0.3	22.9	7.7	10.9	0.7	1.2	0.3	0.4
4	ZMMU A5968	Paratype	12.4	4.1	1.7	1.7	1.2	5.1	1.3	1.5	1.1	6.8	5.5	3.4	0.8	0.3	0.6	0.3	18.9	6.7	10.1	0.6	1.3	0.3	0.2
5	ZMMU A5969	Paratype	16.0	5.1	2.3	2.2	1.3	6.2	1.3	1.8	1.1	8.2	7.1	4.5	0.9	0.6	0.7	0.4	24.3	8.3	12.2	0.6	1.6	0.4	0.4
6	ZMMU A5970	Paratype	15.3	5.2	2.3	1.8	1.1	6.7	1.3	1.7	1.3	8.5	6.9	4.2	0.8	0.5	0.7	0.3	22.6	7.9	11.3	0.5	1.4	0.3	0.4
7	ZISP 13730	Paratype	12.3	4.1	1.8	1.7	1.1	4.7	1.3	1.4	0.9	6.6	5.2	3.5	0.8	0.4	0.6	0.3	18.6	6.5	9.7	0.5	1.3	0.4	0.2
		Mean	14.9	4.8	2.2	2.0	1.2	6.2	1.3	1.7	1.1	7.6	6.2	3.9	0.8	0.5	0.7	0.3	21.9	7.6	11.0	0.6	1.4	0.4	0.3
		SD	*1.8*	*0.5*	*0.3*	*0.3*	*0.1*	*1.0*	*0.0*	*0.2*	*0.1*	*0.7*	*0.7*	*0.4*	*0.1*	*0.1*	*0.1*	*0.0*	*2.2*	*0.7*	*0.8*	*0.1*	*0.1*	*0.1*	*0.1*
		Min	12.3	4.1	1.7	1.7	1.1	4.7	1.3	1.4	0.9	6.6	5.2	3.4	0.7	0.3	0.6	0.3	18.6	6.5	9.7	0.5	1.2	0.3	0.2
		Max	17.1	5.3	2.5	2.3	1.4	7.0	1.3	1.9	1.3	8.5	7.1	4.5	0.9	0.6	0.7	0.4	24.3	8.3	12.2	0.7	1.6	0.4	0.4
	Females																								
8	ZMMU A5971	Paratype	16.7	5.1	2.0	2.2	1.2	7.2	1.4	1.9	1.0	7.5	6.2	3.6	1.0	0.6	0.9	0.3	23.3	8.0	11.9	0.6	1.6	0.4	0.4
9	ZMMU A5972	Paratype	17.6	5.3	2.5	2.2	1.4	7.7	1.6	2.1	1.2	9.5	7.4	4.7	1.1	0.7	0.7	0.4	26.7	9.4	13.3	0.6	1.8	0.4	0.4
10	ZMMU A5973	Paratype	17.7	5.4	2.2	2.2	1.3	6.7	1.5	2.0	1.1	9.2	6.6	4.8	1.0	0.6	0.7	0.4	26.5	9.2	12.6	0.4	1.7	0.4	0.4
11	ZMMU A5974	Paratype	17.5	5.3	2.2	2.2	1.4	7.7	1.6	2.1	1.4	9.2	7.4	4.8	0.9	0.6	0.8	0.4	25.4	8.9	13.0	0.6	1.6	0.5	0.5
12	ZMMU A5975	Paratype	20.9	6.3	2.5	2.4	1.5	7.8	1.5	2.1	1.3	9.5	7.4	4.8	1.0	0.7	1.0	0.4	28.1	10.0	14.1	0.7	1.6	0.5	0.5
13	ZMMU A5976	Paratype	18.2	5.4	2.3	2.2	1.3	7.4	1.5	2.0	1.3	9.2	7.6	4.5	0.9	0.7	0.8	0.5	24.7	8.8	12.2	0.6	1.6	0.5	0.4
		Mean	18.1	5.5	2.3	2.2	1.3	7.4	1.5	2.0	1.2	9.0	7.1	4.5	1.0	0.6	0.8	0.4	25.8	9.0	12.8	0.6	1.7	0.4	0.4
		SD	*1.5*	*0.4*	*0.2*	*0.1*	*0.1*	*0.4*	*0.1*	*0.1*	*0.1*	*0.8*	*0.6*	*0.4*	*0.1*	*0.1*	*0.1*	*0.0*	*1.7*	*0.7*	*0.8*	*0.1*	*0.1*	*0.1*	*0.1*
		Min	16.7	5.1	2.0	2.2	1.2	6.7	1.4	1.9	1.0	7.5	6.2	3.6	0.9	0.6	0.7	0.3	23.3	8.0	11.9	0.4	1.6	0.4	0.4
		Max	20.9	6.3	2.5	2.4	1.5	7.8	1.6	2.1	1.4	9.5	7.6	4.8	1.1	0.7	1.0	0.5	28.1	10.0	14.1	0.7	1.8	0.5	0.5

Min: Minium; Max: Maximum. For other abbreviations see Materials and Methods.

Advertisement call: The *Microhyla irrawaddy* **sp. nov.** male advertisement call represents a characteristic rattling sound, resembling the sound of a ratchet to the human ear, similar to "*krrrrr… kkrrrrr… kkrrrrr…*". Advertisement signal calls were of 0.184±0.07 s duration (0.004–0.277 s, *n*=50), consisting of 1–5 pulses (4±2, *n*=50) (Figure 11). The pulse duration was 4±0.1 ms (2–5 ms, *n*=194) and the interval between successive pulses within a call varied from 5 to 99 ms (59±2.11 ms, *n*=144). Thus, the pulse period was 63±2.12 ms (9–103 ms, *n*=144) and pulse rate varied from 11.89 to 57.14 pulses/s (17.3±1.05 pulses/s, *n*=49). The maximum amplitude frequency of pulses varied within a call from pulse to pulse and the mean value of this parameter was 3 700±570 Hz, *n*=194 (1 870–4 120 Hz). The maximum amplitude frequency of the call varied from 2 810 to 4 120 Hz (3 780±350 Hz, *n*=50).

Natural history: Same as *Microhyla fodiens* **sp. nov.**, the new species inhabits the dry zone of central Myanmar with a hot semi-arid savanna-like climate (see above). The new species was recorded in two habitats within the Pakokku District of Magway Division, but was always observed in close proximity to comparatively large waterbodies, including temporary and permanent pools in the Irrawaddy River Valley (Figure 7B) in suburbs of Pakokku city, or paddy fields and water reservoirs in the vicinity of Kan Pauk village.

Specimens of *Microhyla irrawaddy* **sp. nov.** were collected at night from 1830 h to 2100 h. Males did not normally sit in the open and were recorded calling from small cracks and holes in the banks of the waterbody, often hiding in footprints of buffalo hooves (Figure 10B, C). Males called from 1900 h to approximately 0200 h. Females were recorded while hiding in grass in close proximity to water-filled pools. Clutch size is unknown; one female (ZMMU A5972) laid ca. 30 eggs in a plastic bag after capture. Eggs of the new species are 0.8–0.9 mm in diameter and yellowish-white in color with a brownish animation pole. Larval stages of *Microhyla irrawaddy* **sp. nov.** are unknown. Diet of the new species is unknown.

At the type locality, *Microhyla irrawaddy* **sp. nov.** was found in sympatry with congeneric species *M. mukhlesuri* (Figure 2D), and also with *Fejervarya* sp.; these species shared the

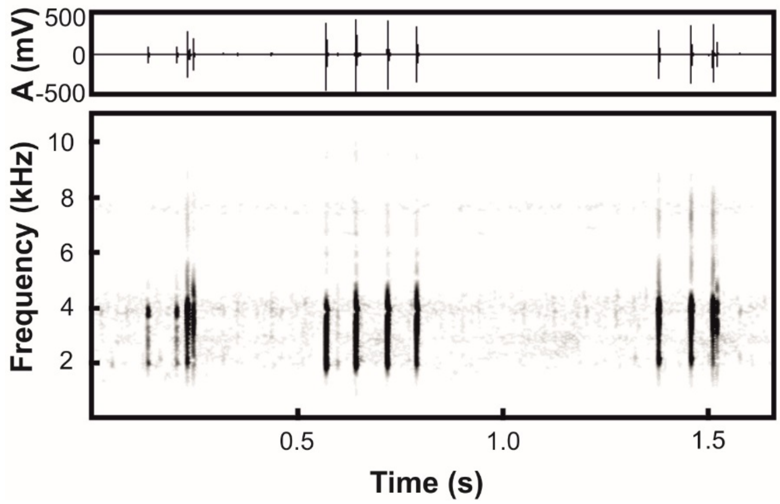

Figure 11 Oscillogram (top) and sonogram (bottom) of male advertisement call of *Microhyla irrawaddy* sp. nov. recorded at 21.5 °C (suburbs of Pakokku, Pakoku District, Magway Division, Myanmar)

same breeding site with the new species. In the vicinity of Kan Pauk village, the new species was recorded in sympatry with *Microhyla fodiens* **sp. nov.**, *Kaloula pulchra*, *Fejervarya* sp., *Hoplobatrachus* cf. *tigerinus*, *Sphaerotheca* sp., and *Duttaphrynus melanostictus.*

Distribution: *Microhyla irrawaddy* **sp. nov.** is at present known from two closely located areas in Pakokku District of Magway Division, central Myanmar: i. e., suburbs of Pakokku city on the bank of the Irrawaddy River (the type locality) and in the vicinity of Kan Pauk village, Yesagyo Township (ca. 30 km north of type locality) (Figure 1). The species was recorded from elevations of 60 to 220 m a.s.l.. A genealogically closely related population of *Microhyla* (herein indicated as *Microhyla* sp. 2, see Table 1) was recorded from the vicinity of Chatthin in Sagaing Division of northern Myanmar by Mulcahy et al. (2018). Considering the notable genetic divergence between Sagaing and Magway populations (*P*=2.0%), further research is needed to clarify whether *Microhyla* sp. 2 is conspecific with *Microhyla irrawaddy* **sp. nov.** The actual distribution of the new species is unknown and discoveries of new localities within the middle part of the Irrawaddy River Valley are anticipated.

Conservation status: Currently, the actual distribution range and population trends of *Microhyla irrawaddy* **sp. nov.** remain unknown and require further study. Given the information available, we suggest *Microhyla irrawaddy* **sp. nov.** be considered as a Data Deficient species following IUCN's Red List categories (IUCN Standards and Petitions Subcommittee, 2017).

Etymology: The new species name "*irrawaddy*" is given as a noun in apposition in reference to the Irrawaddy (or, officially, Ayeyarwady) River – the greatest water basin in Myanmar and western Indochina, and the cradle of Burmese civilization. The new species is known to occur in dry areas of the central part of the Irrawaddy Valley in the Magway Division, but likely has a wider distribution in the dry zone of central Myanmar. The recommended common name in English is "*Irrawaddy narrow-mouth frog*". The recommended common name in Burmese is "*Myanmar Thaephar*".

Morphological comparisons: In having toes with almost completely reduced webbing (webbing I 2–3 II 2–3 III 3–4½ IV 4½–2¾ V), *Microhyla irrawaddy* **sp. nov.** can be easily distinguished from those members of the genus that have fully developed webbing reaching to disks at most toes (usually with the exception of toe IV), including: *M. annamensis* Smith, 1923, *M. annectens*, *M. berdmorei* (including *M. fowleri* Taylor, 1934, which is considered a synonym of *M. berdmorei* by Matsui et al., 2011), *M. darevskii* Poyarkov, Vassilieva, Orlov, Galoyan, Tran, Le, Kretova & Geissler, 2014, *M. malang*, *M. mantheyi*, *M. marmorata*, *M. nanapollexa* Bain & Nguyen, 2004, *M. perparva*, *M. petrigena*, *M. pulchella* Poyarkov, Vassilieva, Orlov, Galoyan, Tran, Le, Kretova & Geissler, 2014, *M. pulverata* Bain & Nguyen, 2004, and *M. superciliaris* (detailed by Poyarkov et al., 2014).

A number of *Microhyla* species have toe webbing that reaches the level of the penultimate (distal) subarticular tubercles on at least some toes and, thus, can be easily diagnosed from *Microhyla irrawaddy* **sp. nov.**, where toe webbing is completely reduced. These species include *M. arboricola* Poyarkov, Vassilieva, Orlov, Galoyan, Tran, Le, Kretova & Geissler, 2014, *M. darreli* Garg, Suyesh, Das, Jiang, Wijayathilaka, Amarasinghe, Alhadi, Vineeth, Aravind, Senevirathne, Meegaskumbura & Biju, 2018 "2019", *M. karunaratnei* Fernando & Siriwardhane, 1996, *M. palmipes*, *M. pulchra* (Hallowell, 1861), *M. sholigari*, and *M. zeylanica* Parker & Osman-Hill, 1948. In *M. butleri* and *M. aurantiventris* toe webbing is better developed than in *Microhyla irrawaddy* **sp. nov.** reaching the level between the two distal tubercles on the third toe.

The new species has a very slender body habitus and can be easily distinguished from those species of *Microhyla* that have a stout body habitus and enlarged spade- or shovel-shaped outer metatarsal tubercle as an adaptation for digging, including: *M. rubra*, *M. mihintalei*, *M. taraiensis*, *M. picta*, and *Microhyla fodiens* **sp. nov.** (see above). The presence of scattered red spots or dots over the dorsum was previously reported only for *M. taraiensis*; thus, with the exception of the presence of red or reddish dorsal tubercles, the new species can be distinguished from all remaining species of *Microhyla*.

The following species of *Microhyla* have notable longitudinal grooves on the dorsal surface of fingers and toes (also known as dorso-terminal grooves) and, thus, can be readily distinguished from the new species, which lacks such grooves: *M. achatina*, *M. annamensis*, *M. annectens*, *M. arboricola*, *M. aurantiventris*, *M. beilunensis* (on toes only), *M. borneensis*, *M. darreli*, *M. gadjahmadai*, *M. heymonsi* (usually present), *M. karunaratnei*, *M. kodial*, *M. malang*, *M. mantheyi*, *M. marmorata*, *M. minuta* Poyarkov, Vassilieva, Orlov, Galoyan, Tran, Le, Kretova & Geissler, 2014, *M. nanapollexa*, *M. orientalis*, *M. perparva* (on toes only), *M. petrigena*, *M. pineticola* Poyarkov, Vassilieva, Orlov, Galoyan, Tran, Le, Kretova & Geissler, 2014, *M. pulchella*, *M. pulverata*, *M. sholigari*, and *M. superciliaris* (two latter species have grooves on toes only).

Microhyla irrawaddy **sp. nov.** has a notably granular skin on dorsum, which readily distinguishes it from those species of *Microhyla* that have smooth or shagreened dorsal skin without prominent granular projections, including: *M. achatina*, *M. annectens*, *M. chakrapanii* Pillai, 1977, *M. darreli*, *M. fusca* Andersson, 1942, *M. gadjahmadai*, *M. heymonsi*, *M. karunaratnei*, *M. laterite*, *M. malang*, *M. marmorata*, *M. mukhlesuri*, *M. mymensinghensis*, *M. nanapollexa*, *M. perparva*, *M. pineticola*, *M. pulchella*, *M. pulverata*, *M. sholigari*, and *M. superciliaris*.

The new species has a well-developed first finger, longer than one half of the second finger length, whereas in a number of its congeners the first finger is reduced or is shorter than one half of the second finger length, including: *M. achatina*, *M. annamensis*, *M. annectens*, *M. arboricola*, *M. beilunensis*, *M. berdmorei*, *M. borneensis* (reduced to a nub), *M. darreli*, *M. fissipes*, *M. fusca*, *M. gadjahmadai*, *M. heymonsi* (smaller or equal to one half of second finger length), *M. malang*, *M. mantheyi*, *M. marmorata*, *M. mihintalei*, *M. minuta* (smaller or equal to one half of second finger length), *M. mixtura*, *M. nanapollexa* (reduced to a nub), *M. orientalis*, *M. palmipes* (reduced to a nub), *M. perparva* (reduced to a nub), *M. petrigena* (reduced to a nub), *M. picta*, *M. pineticola*, *M. pulchella*, *M. pulchra*, *M. pulverata*, and *M. superciliaris*.

Microhyla irrawaddy **sp. nov.** can be distinguished from *M. maculifera* Inger, 1989 from Borneo by the following characteristics: generally larger body size, adult males SVL 12.3–17.1 mm, adult females SVL 16.7–20.9 mm (vs. adult males SVL 12.0–13.3 mm, adult females 11.8 mm), two metatarsal tubercles on feet (vs. single metatarsal tubercle), dorsum irregularly covered with tubercles of various sizes (vs. two lateral rows of tubercles), and weak disks on fingers II–IV (vs. no disks on fingers). The new species can be distinguished from *M. nilphamariensis* from the lowlands of Nepal and northern India by the following characteristics: notably granular skin (vs. smooth or shagreened), first finger longer than one half of second finger length (vs. equal), and reduced webbing on toes, toe webbing formula: I 2–3 II 2–3 III 3–4½ IV 4½–2¾ V (vs. comparatively better developed foot webbing, toe webbing formula: I 2–2¾ II 2–3½ III 3–4 IV 4¼–2¾ V). The new species can also be distinguished from *M. okinavensis* by the following characteristics: smaller body size, adult males SVL 12.3–17.1 mm, adult females SVL 16.7–20.9 mm (vs. adult males SVL 22.5–28.2 mm, adult females SVL 26.5–30.8 mm), notably granular skin (vs. smooth or shagreened), presence of weak disks on fingers and toes (vs. absent), comparatively shorter hindlimbs with tibiotarsal articulation of adpressed hindlimb reaching eye level (vs. reaching snout tip), and reduced webbing on feet, toe webbing formula: I 2–3 II 2–3 III 3–4½ IV 4½–2¾ V (vs. comparatively better developed foot webbing, toe webbing formula: I 1½–2 II 1½–3¼ III 2¾–4 IV 4–2½ V).

Microhyla irrawaddy **sp. nov.**, can be further distinguished from its sister species *M. kodial* from southern India by the following characteristics: larger and more prominent tubercles (vs. comparatively less granular skin with small flat tubercles), no olive dorsal markings, red or orange dorsal tubercles and brown "teddy-bear"-shaped marking present dorsally (vs. olive-green markings on dorsum and lacking red-colored tubercles and brown "teddy-bear"-shaped marking on dorsum), dorsolateral line of tubercles and dark stripe present (vs. dorsolateral row of tubercles and dorsolateral dark stripe absent), and dorsal notches absent on digits (vs. short dorsal notches on finger- and toe-tips).

Acoustic comparisons: Comparison of advertisement call parameters is based on data from the current study and from Dehling (2010), Garcia-Rutledge & Narins (2001), Heyer (1971), Kanamadi et al. (1994), Khatiwada et al. (2017a), Kuramoto & Joshy (2006), Kurniati (2013), Le et al. (2016a, b), Matsui (2011), Nguyen et al. (2019), Vineeth et al. (2018), and Wijayathilaka & Meegaskumbura (2016). Comparison of current bio-acoustic analyses with available data is presented in Table 5.

Microhyla irrawaddy **sp. nov.** has a unique combination of acoustic parameters, such as a relatively low number of pulses per call, low pulse rate, and relatively high call frequency of maximum amplitude (see Table 5). According to most acoustic parameters, *Microhyla irrawaddy* **sp. nov.** is similar to *M. kodial* from southern India: i. e., frequency of maximum amplitude (3 780±350 Hz vs. 3 752.16±233.06 Hz), number of pulses per call (4±2 vs. 6±2), and pulse rate (17.3±1.05 pulses/s vs. 14.97±1.38 pulses/s). However, the advertisement signal of *Microhyla irrawaddy* **sp. nov.** significantly differs from *M. kodial* by call duration (0.18±0.07 s vs. 0.33±0.07 s).

Call duration in *Microhyla irrawaddy* **sp. nov.** (0.18±0.07 s) is similar to that of *M. malang* (0.17±0.04 s), *M. rubra* (0.17±

Table 5 Bio-acoustic comparison of *Microhylairrawaddy* sp. nov. with other members of the genus *Microhyla*

Species	Call duration (s) (Mean±*SD*)	Call duration (s) (Min–Max)	Pulses/call (Median±inter-quartile range)	Pulses/call (Min–Max)	Pulse rate, pulses/s (Mean±*SD*)	Fpeak, Hz (Mean±*SD*)	Fpeak, Hz (Min–Max)	Reference
M. irrawaddy **sp. nov.**	0.18±0.07	0.004–0.28	4±2	1–5	17.3±1.05	3780±350	2810–4120	Present study
M. kodial	0.33±0.07 0.26±0.03	0.11–0.42 0.23–0.29	6±2 6±0.5	2–7 5–7	14.97±1.38 18±0.5	3752.16±233.06 3800	3359.2–4220.5 3800	Garg et al., 2019; Vineeth et al., 2018
M. darreli	0.65±0.06	0.59–0.74	68±5.5	63–78	105.6±1.2	3600	3600	Garg et al., 2019
M. mymensinghensis	0.47±0.01	0.45–0.48	21±1.1	19–22	43.1±2.9	3600±400	3500–3600	Garg et al., 2019
M. nilphamariensis	0.34±0.02	0.31–0.37	11±0.8	10–12	29.6±0.4	2300	2300	Garg et al., 2019
M. achatina	0.38±0.04 0.23±0.07	0.26–0.51 0.12–0.29	N/A 8±2	6–11 4–9	21.6±2.6 26.4±1.1	2976±143.1 3300±800	2718–3375 3200–3400	Garg et al., 2019; Kumiati, 2013
M. malang	0.17±0.04	0.10–0.24	N/A	4–8	30.3±1.4	2404±94	2250–2530	Dehling, 2010 Matsui, 2011
M. petrigena	0.13±0.03	0.07–0.18	12.1±3*	6–17	89±5	4430±322	3850–5050	Dehling, 2010
M. heymonsi	0.48 0.34±0.09	N/A 0.28–0.38	N/A N/A	11 11	23*** 25.7±1.6	N/A 2367±132	1700–3000 N/A	Garcia–Rutledge & Narins, 2001; Heyer, 1971; Kurniati, 2013
M. borneensis	0.17±0.04 N/A	0.10–0.24 0.70–0.73	5.7±1.1* N/A	4–8 2–9	30.3±1.4 N/A	2404±94 N/A	2250–2530 3000–5500	Dehling, 2010 Kurniati, 2013
M. taraiensis	0.75±0.12	0.70–0.91	N/A	13–14	17.3	3305.50±95.46	3433–3101	Khatiwada et al., 2017
M. orientalis	0.07±0.01 0.06±0.01	0.01–0.08 0.04–0.07	N/A 5±0.9	3–5 3–5	N/A 57.7±8.5	3400±100 3700	3200–3600 3700	Garg et al., 2019; Matsui et al., 2013
M. ornata	0.27±0.02 0.30±0.06 0.28±0.03 0.33±0.02	N/A 0.21–0.80 0.21–0.35 0.32–0.38	10.9±0.86** 13±1 11±1.75 13±0.4	N/A 9–14 9–14 13–14	35.5±1.1 41.6±1.5 38.63±1.74 37.3±1.4	2600 3100±400 2656.34±103.46 2600	N/A 2200–3400 2497.9–2842.4 2600	Garg et al., 2019; Kuramoto & Joshy, 2006; Vineeth et al., 2018; Wijayathilaka & Meegaskumbura, 2016
M. mukhlesuri (as *M. ornata*)	N/A	0.23–0.31	N/A	10–18	53–60***	N/A	1200–3500	Heyer, 1971

Continued

Species	Call duration (s) (Mean±*SD*)	Call duration (s) (Min–Max)	Pulses/call (Median±inter-quartile range)	Pulses/call (Min–Max)	Pulse rate, pulses/s (Mean±*SD*)	Fpeak, Hz (Mean±*SD*)	Fpeak, Hz (Min–Max)	Reference
M. sholigari	0.73±0.04 0.93±0.05	0.66–0.82 0.90–1.01	63±4 72±3.7	56–69 70–79	86±3.84 77.3±0.4	3673.55±159.54 3400	3316.1–3962.1 3400	Garg et al., 2019; Vineeth et al., 2018
M. laterite	0.70±0.05 0.81±0.06	0.6–0.85 0.73–0.89	90±6.75 104±7	79–103 94–113	128.24±3.98 128.0±1.2	3670.96±97.10 3600±400	3531.4–3789.8 3500–3600	Garg et al., 2019; Vineeth et al., 2018
M. rubra	0.17±0.03* 0.13±0.01	0.14–0.23 0.12–0.14	18±0.2* 11±1	15–21 10–12	N/A 80.4±3.8	2268±43* 2200±700	N/A 2000–2200	Garg et al., 2019; Kanamadi et al., 1994
M. karunaratnei	0.87±0.1 0.87±0.13	0.7–1.17 0.77–1.00	66.5±14, 2 60±13	50–95 56–86	76.9±5.8 76.1±4.4	3300±100 3200±140	3100–3400 3100–3400	Garg et al., 2019; Wijayathilaka & Meegaskumbura, 2016
M. zeylanica	1.85±0.12 1.76±0.04	1.5–2 1.71–1.80	84±5 86±3.6	61–92 81–90	44.5±3.2 48.4±1.0	2600±200 2700±290	2200–2900 2300–3000	Garg et al., 2019; Wijayathilaka & Meegaskumbura, 2016
M. mihintalei	0.19±0.02 0.16±0.004	0.14–0.25 0.16–0.17	13±2.5 12±0.4	9–15 11–12	58.6±2.8 68.4±2.1	2100±400 2300±100	1300–2600 2300–2400	Garg et al., 2019; Wijayathilaka & Meegaskumbura, 2016
M. butleri	0.32±0.01	0.3–0.35	36.4±1.3**	34–40	109±4.5	3000±30	2900–3000	Nguyen et al., 2019
M. aurantiventris	0.14±0.02	0.11–0.23	17.9±1.45**	15–26	122.7±6.45	2100±100	1800–2200	Nguyen et al., 2019
M. marmorata	N/A	N/A	N/A	9–13	N/A	2857±81	2756–3015	Le et al., 2016a
M. pulchra	0.42±0.19	0.22–0.84	N/A	38–80	N/A	2334±44	2240–2412	Le et al., 2016b
M. berdmorei	N/A	0.09–0.26	N/A	3–9	33－35***	N/A	1500–1800	Heyer, 1971
M. fissipes	0.24±0.01	0.21–0.25	15±0.5	15–16	61.8±0.4	3000±100	3000–3100	Garg et al., 2019
M. palmipes	0.11±0.04	0.06–0.16	11±3.2	6–13	79.8±7.6	3500±300	3400–3500	Garg et al., 2019

N/A: Data not available; *: Mean±*SE*; **: Mean±*SD*; ***: Range; Min: Minium; Max: Maximum.

0.03 s), and *M. mihintalei* (0.19±0.02 s); however, other call parameters among these species are different: for example, number of pulses per call (4±2 vs. NA, 18±0.2, and 13±2.5, respectively), pulse rate (17.3±1.05 pulses/s vs. 30.3±1.4, NA, and 58.6±2.8 pulses/s, respectively), and frequency of maximum amplitude (3 780±350 Hz vs. 2 404±94, 2 268±43, and 2 100±400 Hz, respectively).

Microhyla irrawaddy **sp. nov.** has a similar frequency of maximum amplitude (3 780±350 Hz) to *M. sholigari* (3 673.55±159.54 Hz) and *M. laterite* (3 670.96±97.10 Hz), but differs from these two species by values of temporal parameters, such as call duration (0.18±0.07 s vs. 0.73±0.04 and 0.70±0.05 s, respectively), number of pulses per call (4±2 vs. 63±4 and 90±6.75, respectively), and pulse rate (17.3±1.05 pulses/s vs. 86±3.84 and 128.24±3.98 pulses/s, respectively).

DISCUSSION

Myanmar remains one of the least herpetologically studied countries in Southeast Asia. However, its vast area and diversity of lowland and montane habitats with varying climatic conditions make Myanmar a promising area for discovery of yet unknown herpetofaunal diversity (Grismer et al., 2017a, 2017b; Mulcahy et al., 2018). In recent years, significant progress has been made in describing the diversity of Myanmar amphibians (e.g., Dever, 2017; Dever et al., 2012; Grismer et al., 2018b; Pawangkhanant et al., 2018; Sheridan & Stuart, 2018; Suwannapoom et al., 2016; Wilkinson et al., 2003, 2012, 2014; Wogan, 2012; Wogan et al., 2003; Zaw et al., 2019; Zug, 2015), although almost all new species discovered have been encountered in hilly or montane wet areas covered with tropical forests. In the present paper, we describe two new species of *Microhyla* from the driest and hottest part of Myanmar–the Irrawaddy (Ayeyarwady) River Valley in the central part of the country. This area has the lowest level of precipitation in Myanmar and is characterized by a semi-arid savanna-like climate (Peel et al., 2007). Previous studies have shown that the hilly regions within the Irrawaddy Basin are notable for harboring endemic species of lizards (Grismer et al., 2018a, 2018c). Our study shows that the dry plains of the central Irrawaddy River Basin also harbor an unknown endemic diversity of frogs.

Both newly described *Microhyla* species appear to be well adapted to the seasonally dry environment, especially *Microhyla fodiens* **sp. nov.**, which is notable for its stout body habitus and large shovel-like outer metatarsal tubercle used for burrowing. Several species of *Microhyla* have developed similar adaptations and inhabit arid and often sandy areas in southern India (*M. rubra*), Sri Lanka (*M. mihintalei*), northern India and Nepal (*M. taraiensis*), and south-eastern Vietnam (*M. picta*). The phylogenetic position of *M. picta* is unknown; however, our mtDNA genealogy analysis indicated that stout-bodied burrowing species belong to at least two distinct species groups of *Microhyla* and adaptations to arid environments in the genus likely evolved independently.

Our data provide an important contribution to knowledge on the *Microhyla* fauna of Myanmar. In agreement with previous studies, we confirmed the presence of *M. heymonsi* and *M. butleri* in the country; the latter species recorded for the first time in Kachin State. A recent study by Nguyen et al. (2019) demonstrated significant divergence within *M. butleri*, which consists of two main lineages–one inhabiting southern mainland China and Taiwan, China and the other found in Indochina and the Malayan Peninsula (divergence level *P*=1.7%). The Myanmar population of *M. butleri* from Kachin State belongs to the Indochinese lineage. We also confirmed significant phylogenetic structuring within *M. heymonsi*, with Myanmar populations falling into at least two distinct lineages within the species (divergence level *P*=2.3%); however, further studies are required to clarify the phylogeographic structure of the *M. heymonsi* species complex. Our study did not confirm the results of Mulcahy et al. (2018), who assigned Myanmar populations of the former "*M. ornata*" species complex to *M. fissipes*. Results of our phylogenetic analyses clearly indicate that they belong to *M. mukhlesuri*, a species originally described from eastern Bangladesh (Hasan et al., 2014), but recently shown to inhabit almost all Indochina south of the Red River basin (Yuan et al., 2016). Thus, our work raises the number of *Microhyla* species known for Myanmar to six, and the total number of species recognized within the genus to 48.

Our knowledge on *Microhyla* diversity in Myanmar is still far from complete. Mulcahy et al. (2018) reported a population of *Microhyla* sp. from the vicinity of Chatthin in Sagaing Division, indicated in the present study as *Microhyla* sp. 2. Our phylogenetic analyses recovered this population as a sister taxon of *Microhyla irrawaddy* **sp. nov.** from the Magway Division. Though these two lineages showed a moderate level of genetic divergence (*P*=2.0%), this differentiation is comparable with genetic distances between some recognized species of *Microhyla* (e.g., *M. fissipes* and *M. mukhlesuri* *P*=2.4%; *M. borneensis* and *M. malang* *P*=2.6%; see Table 2). Hence, we consider that morphological and acoustic data are needed to test whether *Microhyla* sp. 2 is conspecific with *Microhyla irrawaddy* **sp. nov.** Further sampling and research on genetic and morphological differentiation of *Microhyla* frogs in Myanmar might lead to discovery of yet unknown lineages and species.

The phylogenetic position of *Microhyla irrawaddy* **sp. nov.** is of special interest, as it is reconstructed as a sister species with respect to *M. kodial* from southern India. The latter species was recently described and found to be the only member of the mostly Southeast Asian *M. achatina* species group reported for the Indian subcontinent (Vineeth et al., 2018). Vineeth et al. (2018) argued that the possible explanation for this biogeographic pattern could be the introduction of *M. kodial* from somewhere in Southeast Asia, and noted that the type locality of this species is adjacent to the New Mangalore Port "where timber logs imported from Myanmar, Malaysia and Indonesia used to be dumped until recently" (Vineeth et al., 2018, p. 175). According to Vineeth et al. (2018), a population of *M. kodial* could have been introduced from South East Asia and established in the lowlands of southern India several decades ago. Our

discovery of a closely related but still significantly divergent lineage in arid areas of central Myanmar represents a possible "stepping stone" between Southeast Asia and India and suggests that a past dispersal event from Myanmar to the Indian subcontinent should not be excluded in explaining the biogeographic origin of *M. kodial*. Amphibians, especially small frogs such as *Microhyla*, are usually sensitive to minor changes in temperature and humidity; an unintended transfer of such miniaturized frogs on ships with timber seems an unrealistic scenario. On the other hand, the establishment of a monsoon climate and the consequent aridification starting ca. 10 mya has been shown to have influenced diversification in at least four groups of Indian lizards: i. e., *Cyrtopodion*, *Cyrtodactylus*, *Ophisops*, and *Sitana* (Agarwal et al., 2014; Agarwal & Karanth, 2015; Agarwal & Ramakrishnan, 2017; Deepak & Karanth, 2018). Progressing aridification of India could favor dispersal of species adapted to drier environments from the Eurasian mainland to the Indian subcontinent (Deepak & Karanth, 2018; Solovyeva et al., 2018). Further sampling and molecular phylogenetic and biogeographic studies are required to elucidate the biogeographic history of *Microhyla* and the processes of faunal exchange between the Indian subcontinent and Eurasian landmass.

Key to species of *Microhyla* Tschudi, 1838 from Myanmar

The following key can be used as a guide for the identification of *Microhyla* species occurring in Myanmar.

1a) Body habitus stout; outer metatarsal tubercle large, shovel-like; large black blotch in inguinal region ··*Microhyla fodiens* **sp. nov.**

1b) Body habitus slender or stocky; outer metatarsal tubercle small or absent ···**2**

2a) Webbing on toes complete except toe IV; limbs long, tibiotarsal articulation of adpressed hindlimb reaching well beyond snout; in life inguinal region and ventral surface of thighs with yellowish tint··················*Microhyla berdmorei*

2b) Webbing on toes reaching distal tubercles or rudimentary; limbs short, tibiotarsal articulation of adpressed hindlimb reaching snout or shorter; in life no yellowish tint in inguinal region and ventral surface of thighs ···············**3**

3a) Webbing on toe III reaching level between two distal tubercles; dorsum with dark hourglass-shaped or "teddy-bear"-shaped figure edged with light border ···*Microhyla butleri*

3b) Webbing on toe rudimentary; no dark figure with light edging on dorsum ··**4**

4a) Finger I length subequal to one half of finger II length; body and head sides dark-brown to black, clearly separated from light-brown coloration of dorsum; light dorsomedial stripe with black spot in scapular region ··*Microhyla heymonsi*

4b) Finger I length greater than one half of finger II length; body and head sides not black, dorsomedial stripe and black scapular spot absent ·····································**5**

5a) Medium-sized species (adult males SVL 16.5–21.0 mm); disks on digits absent; tibiotarsal articulation of adpressed hindlimb reaching snout; skin on dorsum smooth; dorsum with light-brown longitudinal lines resembling wood pattern ····································*Microhyla mukhlesuri*

5b) Small-sized species (adult males SVL 12.3–17.1 mm); disks on digits present; tibiotarsal articulation of adpressed hindlimb reaching eye level; skin on dorsum granular with numerous reddish tubercles ···*Microhyla irrawaddy* **sp. nov.**

COMPETING INTERESTS

The authors declare that they have no competing interests.

AUTHORS' CONTRIBUTIONS

N.A.P., V.A.G., T.Z., and J.C. designed the study; N.A.P., V.A.G., T.Z., and P. P. collected materials for the study; N.A.P., V.A.G., T.Z., V.D.K., S.S.G., P.P., and J.C. discussed the results of the study, N.A.P., V.A.G., and S.S.G. prepared the manuscript; N.A.P., V.D.K., S.S.G., and P.P. provided photographs and figures for the study; N.A.P., V.A.G., and V.D.K. performed morphological analyses; V.A.G. and N.A.P. performed molecular and phylogenetic analyses; N.A.P. and J.C. provided funding for the study and revised the manuscript. All authors read and approved the final version of the manuscript.

NOMENCLATURAL ACTS REGISTRATION

The electronic version of this article in portable document format will represent a published work according to the International Commission on Zoological Nomenclature (ICZN), and hence the new names contained in the electronic version are effectively published under that Code from the electronic edition alone (see Articles 8.5–8.6 of the Code). This published work and the nomenclatural acts it contains have been registered in ZooBank, the online registration system for the ICZN. The ZooBank LSIDs (Life Science Identifiers) can be resolved and the associated information can be viewed through any standard web browser by appending the LSID to the prefixhttp: //zoobank.org/.

Publication LSID:
urn: lsid: zoobank.org: pub: 2F9BC231-22D5-44DE-A919-79E66229EA34.
Microhyla fodiens LSID:
urn: lsid: zoobank.org: act: 6251923B-3A4C-4E38-840B-3EBB2A654EB4.
Microhyla irrawaddy LSID:
urn: lsid: zoobank.org: act: 1FBF2CEE-57FF-4389-AB66-4E1B22ED629D.

ACKNOWLEDGEMENTS

We thank the Ministry of Natural Resources and Environmental Conservation Forest Department for the collection and export permits. We thank Hein Thu Aung and U Soe Kyi (Pakokku) for logistical support and hospitality. We are also extremely grateful to the people of Kan Pauk village and especially to the local football team for their hospitality and selfless help during the field surveys. NAP thanks Duong Van Tang and Anna S. Dubrovskaya for help during lab work; and Evgeniy S. Popov for support. For permission to study specimens under their care and permanent support, we thank Valentina F. Orlova (ZMMU), Roman A. Nazarov (ZMMU), and Konstantin D. Milto (ZISP). We are grateful to Justin Lee

(USNM) for help with examining additional *Microhyla* specimens from CAS. We thank Natalia Ershova for proofreading. We are grateful to two anonymous reviewers for their kind help and useful comments, which helped us to improve the previous version of this manuscript.

REFERENCES

Agarwal I, Bauer AM, Jackman TR, Karanth KP. 2014. Cryptic species and miocene diversification of palaearctic naked-toed geckos (Squamata: Gekkonidae) in the Indian dry zone. *Zoologica Scripta*, **43**(5): 455–471.

Agarwal I, Karanth KP. 2015. A phylogeny of the only ground-dwelling radiation of *Cyrtodactylus* (Squamata, Gekkonidae): diversification of *Geckoella* across peninsular India and Sri Lanka. *Molecular Phylogenetics and Evolution*, **82**: 193–199.

Agarwal I, Ramakrishnan U. 2017. On the antiquity of Indian grassy biomes: a phylogeny of open-habitat lizards (Squamata: Lacertidae: *Ophisops*) supports the antiquity of Indian grassy biomes. *Journal of Biogeography*, **44**(9): 2021–2032.

Andersson LG. 1942. A small collection of frogs from Annam collected in the years 1938−39 by Bertil Bjorkegren. *Arkiv for Zoologi*, **34**A(6): 1–11.

Atmaja VY, Hamidy A, Arisuryanti T, Matsui M, Smith EN. 2019. A new species of *Microhyla* (Anura: Microhylidae) from Sumatra, Indonesia. *Treubia*, **45**: 25–46.

Bain RH, Nguyen QT. 2004. Three new species of narrow-mouth frogs (Genus: *Microhyla*) from Indochina, with comments on *Microhyla annamensis* and *Microhyla palmipes*. *Copeia*, **2004**(3): 507–524.

Blyth E. 1856. Report for October meeting, 1855. *Journal of the Asiatic Society of Bengal*, **24**: 711–723.

Boulenger GA. 1884. Descriptions of new species of reptiles and batrachians in the British Museum. Part. II. *Journal of Natural History*, **13**(77): 396–398.

Boulenger GA. 1897. Descriptions of new Malay frogs. *Journal of Natural History*, **19**(109): 106–108.

Boulenger GA. 1900. Descriptions of new batrachians and reptiles from the Larut Hills, Perak. *Annals and Magazine of Natural History, Series* 7, **6**(32): 186–193.

Bourret R. 1942. Les Batraciens de l'Indochine. Ha Noi: Institut Océanographique de l'Indochine. (in French)

Das I, Haas A. 2010. New species of *Microhyla* from Sarawak: Old World's smallest frogs crawl out of miniature pitcher plants on Borneo (Amphibia: Anura: Microhylidae). *Zootaxa*, **2571**(1): 37–52.

Das I, Yaakob NS, Sukumaran J. 2007. A new species of *Microhyla* (Anura: Microhylidae) from the Malay Peninsula. *Hamadryad*, **31**(2): 304–314.

Deepak V, Karanth P. 2018. Aridification driven diversification of fan-throated lizards from the Indian subcontinent. *Molecular Phylogenetics and Evolution*, **120**: 53–62.

Dehling JM. 2010. Advertisement calls of two species of *Microhyla* (Anura: Microhylidae) from Borneo. *Salamandra*, **46**(2): 114–116.

Dever JA, Fuiten AM, Konu Ö , Wilkinson JA. 2012. Cryptic torrent frogs of Myanmar: An examination of the *Amolops marmoratus* species complex with the resurrection of *Amolops afghanus* and the identification of a new species. *Copeia*, 2012(1): 57–76.

Dever JA. 2017. A new cryptic species of the *Theloderma asperum* complex (Anura: Rhacophoridae) from Myanmar. *Journal of Herpetology*, **51**(3): 425–436.

Duméril AHC, Bibron G. 1841. Erpétologie Genérale ou Histoire Naturelle Complète des Reptiles. Vol. 8. Paris: Librarie Enclyclopedique de Roret, III–792. (in French)

Dutta SK. 1997. Amphibians of India and Sri Lanka. Bhubaneswar: Odyssey Publishing House, 342.

Dutta SK, Ray P. 2000. *Microhyla sholigari*, a new species of microhylid frog (Anura: Microhylidae) from Karnataka, India. *Hamadryad*, **25**: 38–44.

Fei L, Ye C, Jiang J. 2010. Colored Atlas of Chinese Amphibians. Sichuan: Sichuan Publishing Group, Sichuan Publishing House of Science & Technology, 519.

Felsenstein J. 1985. Confidence limits on phylogenies: an approach using the bootstrap. *Evolution*, **39**(4): 783–791.

Fernando P, Siriwardhane M. 1996. *Microhyla karunaratnei* (Anura: Microhylidae), a new species of frog endemic to Sri Lanka. *Journal of South Asian Natural History*, **2**(1): 135–142.

Frost DR. 2019 Amphibian Species of the World: an Online Reference. *Version* 6.0 (22/01/2019). New York, USA: American Museum of Natural History, Electronic database accessible at http: //research. amnh. org/ herpetology/amphibia/index.html.

Garcia-Rutledge EJ, Narins PM. 2001. Shared acoustic resources in an old-world frog community. *Herpetologica*, **57**(1): 104–116.

Garg S, Das A, Kamei RG, Biju SD. 2018a. Delineating *Microhyla ornata* (Anura, Microhylidae): mitochondrial DNA barcodes resolve century-old taxonomic misidentification. *Mitochondrial DNA Part B*, **3**(2): 856–561.

Garg S, Suyesh R, Das A, Jiang JP, Wijayathilaka N, Amarasinghe AAT, Alhadi F, Vineeth KK, Aravind NA, Senevirathne G, Meegaskumbura M, Biju SD. 2018b. Systematic revision of *Microhyla* (Microhylidae) frogs of South Asia: a molecular, morphological, and acoustic assessment. *Vertebrate Zoology*, **69**(1): 1–71.

Glaw F, Vences M. 1997. Anuran eye colouration: definitions, variation, taxonomic implications and possible functions. *Herpetologia Bonnensis. SEH Proceedings, Bonn*, 125–138.

Grismer LL, Wood PL Jr , Quah ESH, Murdoch ML, Grismer MS, Herr MW, Espinoza RE, Brown RM, Lin A. 2018a. A phylogenetic taxonomy of the *Cyrtodactylus peguensis* group (Reptilia: Squamata: Gekkonidae) with descriptions of two new species from Myanmar. *PeerJ*, **6**: e5575; doi: 10.7717/peerj.5575

Grismer LL, Wood, PL Jr , Quah ESH, Thura MK, Espinoza RE, Grismer MS, Murdoch ML, Lin A. 2018b. A new species of crocodile newt *Tylototriton* (Caudata: Salamandridae) from Shan State, Myanmar (Burma). *Zootaxa*, **4500**(4): 442–573.

Grismer LL, Wood PL Jr , Thura MK, Grismer MS, Brown RM, Stuart BL. 2018c. Geographically structured genetic variation in *Ptychozoon lionotum* (Squamata: Gekkonidae) and a new species from an isolated volcano in Myanmar. *Zootaxa*, **4514**(2): 202–214.

Grismer LL, Wood PL Jr., Thura MK, Zin T, Quah ESH, Murdoch ML, Grismer MS, Lin A, Kyaw H, Ngwe L. 2017a. Twelve new species of *Cyrtodactylus* Gray (Squamata: Gekkonidae) from isolated limestone habitats in east-central and southern Myanmar demonstrate high localized diversity and unprecedented microendemism. *Zoological Journal of the Linnean Society*, **182**(4): 862–959.

Grismer LL, Wood PL Jr., Thura MK, Zin T, Quah ESH, Murdoch ML, Grismer MS, Lin A, Kyaw H, Ngwe L. 2017b. Phylogenetic taxonomy of *Hemiphyllodactylus* Bleeker, 1860 (Squamata: Gekkonidae) with

descriptions of three new species from Myanmar. *Journal of Natural History*, **52**(13–16): 881–915.

Hall TA. 1999. BioEdit: a user-friendly biological sequence alignment editor and analysis program for Windows 95/98/NT. *In*: Nucleic Acids Symposium Series. London: Information Retrieval Ltd., c1979-c2000, 95–98.

Hallermann J, Ananjeva N, Orlov N, Tillack F. 2002. Leonardo Fea's historical collections of Amphibia and Reptilia from Burma deposited at the Zoologisches Museum Hamburg. *Mitteilungen aus dem Hamburgischen Zoologischen Museum und Institut*, **99**: 139–153.

Hallowell E. 1861. Report upon the Reptilia of the North Pacific Exploring Expedition, under command of Capt. John Rogers, U.S.N. *Proceedings of the Academy of Natural Sciences of Philadelphia*, **1860**: 480–510.

Hasan M, Islam MM, Khan MMR, Alam MS, Kurabayashi A, Igawa T, Kuramoto M, Sumida M. 2012. Cryptic anuran biodiversity in Bangladesh revealed by mitochondrial 16S rRNA gene sequences. *Zoological Science*, **29**(3): 162–172.

Hasan M, Islam MM, Kuramoto M, Kurabayashi A Sumida M. 2014. Description of two new species of *Microhyla* (Anura: Microhylidae) from Bangladesh. *Zootaxa*, **3755**(5): 401–408.

Hasan M, Razzaque MA, Sarker AK, Kuramoto M Sumida M. 2015. Genetic variation, advertisement call, and morphometry of *Microhyla nilphamariensis* from Bangladesh. *Philippine Journal of Systematic Biology*, **9**: 63–80.

Hedges SB. 1994. Molecular evidence for the origin of birds. *Proceedings of the National Academy of Sciences*, **91**(7): 2621–2624.

Heyer WR. 1971. Mating calls of some frogs from Thailand. *Fieldiana Zoology*, **58**(6): 61–82.

Hillis DM, Moritz C, Mable BK, Graur D. 1996. Molecular Systematics (Vol. 23). Sunderland, MA: Sinauer Associates.

Howlader MSA, Nair A, Gopalan SV, Merilä J. 2015. A new species of *Microhyla* (Anura: Microhylidae) from Nilphamari, Bangladesh. *PLoS One*, **10**(3): e0119825.

Hu SC. 1966. A herpetological survey of the Tsinling and Ta-Pa Shan region. *Acta Zoologica Sinica*, **18**: 57–89. (in Chinese).

Huelsenbeck JP, Hillis DM. 1993. Success of phylogenetic methods in the four-taxon case. *Systematic Biology*, **42**(3): 247–264.

Inger RF, Frogner KJ. 1979. New species of narrow-mouth frogs (genus *Microhyla*) from Borneo. *The Sarawak Museum Journal*, **27**: 311–322.

Inger RF. 1989. Four new species of frogs from Borneo. *Malayan Nature Journal. Kuala Lumpur*, **42**: 229–243.

IUCN Standards and Petitions Subcommittee. 2017[12 November 2018]. Guidelines for Using the IUCN Red List Categories and Criteria. Version 13. Prepared by the Standards and Petitions Subcommittee. Downloadable from: http: //www.iucnredlist.org/documents/RedListGuidelines.pdf.

Jerdon TC. 1854. Catalogue of reptiles inhabiting the Peninsula of India. *Journal of the Asiatic Society of Bengal*, **22**: 522–534.

Kanamadi RD, Hiremath CR, Schneider H. 1994. Courtship, amplexus and advertisement call of the frog, *Microhyla rubra*. *Current Science*, **66**: 683–684.

Katoh K, Misawa K, Kuma K, Miyata T. 2002. MAFFT: a novel method for rapid multiple sequence alignment based on fast Fourier transform. *Nucleic Acids Research*, **30**(14): 3059–3066.

Khatiwada JR, Shu GC, Wang SH, Thapa A, Wang B, Jiang J. 2017a. A new species of the genus *Microhyla* (Anura: Microhylidae) from Eastern Nepal. *Zootaxa*, **4254**(2): 221–239.

Khatiwada JR, Wang S, Shu G, Xie F, Jiang J. 2017b. The mitochondrial genome of the *Microhyla taraiensis* (Anura: Microhylidae) and related phylogenetic analyses. *Conservation Genetics Resources*, **10**(3): 441–444.

Kozlov A, Darriba D, Flouri T, Morel B, Stamatakis A. 2018. RAxML-NG: A fast, scalable, and user-friendly tool for maximum likelihood phylogenetic inference. *BioRxiv*, 447110.

Kuramoto M, Joshy SH. 2006. Morphological and acoustic comparisons of *Microhyla ornata*, *M. fissipes*, and *M. okinavensis* (Anura: Microhylidae). *Current Herpetology*, **25**(1): 15–27.

Kurniati H. 2013. Vocalizations of *Microhyla achatina* Tschudi, 1838 (Anura: Microhylidae) from the foot hills of Mount Salak, West Java. *Jurnal Biologi Indonesia*, **9**(2): 301–310.

Le DT, Ninh TH, Luong MA, Nguyen TQ. 2016a. Advertisement call and description of the tadpole of *Microhyla marmorata* Bain & Nguyen, 2004 from Xuan Son National Park, Phu Tho Province. *Vietnam Journal of Biology*, **38**(2): 154–164.

Le DT, Ninh TH, Luong MA, Nguyen LHS, Tran DL. 2016b. Advertisement call and description of the tadpole of *Microhyla pulchra* Hallowell, 1861 from Dong Nai Culture and Nature Reserve. *In*: Proceedings of the 3nd National Scientific Workshop "Amphibians and Reptiles in Vietnam", Hanoi: Publishing House for Science and Technology, 160–168.

Mason F. 1860. Burmah, its People and Natural Productions. London: Publ. Trubner, 480.

Matsui M. 2011. Taxonomic revision of one of the Old World's smallest frogs, with description of a new bornean *Microhyla* (Amphibia, Microhylidae). *Zootaxa*, **2814**(1): 33–49.

Matsui M, Hamidy A, Belabut DM, Ahmad N, Panha S, Sudin A, Khonsue W, Oh HS, Yong HS, Jiang JP, Nishikawa K. 2011. Systematic relationships of oriental tiny frogs of the family Microhylidae (Amphibia, Anura) as revealed by mtDNA genealogy. *Molecular Phylogenetics and Evolution*, **61**(1): 167–176.

Matsui M, Hamidy A, Eto K. 2013. Description of a new species of *Microhyla* from Bali, Indonesia (Amphibia, Anura). *Zootaxa*, **3670**(4): 579–590.

Matsui M, Ito H, Shimada T, Ota H, Saidapur SK, Khonsue W, Tanaka-Ueno T, Wu GF. 2005. Taxonomic relationships within the pan-oriental narrow-mouth toad *Microhyla ornata* as revealed by mtDNA analysis (Amphibia, Anura, Microhylidae). *Zoological Science*, **22**(4): 489–495.

Matsui M, Shimada T, Liu WZ, Maryati M, Khonsue W, Orlov N. 2006. Phylogenetic relationships of oriental torrent frogs in the genus *Amolops* and its allies (Amphibia, Anura, Ranidae). *Molecular Phylogenetics and Evolution*, **38**(3): 659–666.

Mulcahy DG, Lee JL, Miller AH, Chand M, Thura MK, Zug GR. 2018. Filling the BINs of life: Report of an amphibian and reptile survey of the Tanintharyi (Tenasserim) Region of Myanmar, with DNA barcode data. *ZooKeys*, **757**: 85–152.

Nguyen LT, Poyarkov NA Jr, Nguyen TT, Nguyen TA, Nguyen VH, Gorin VA, Murphy RW, Nguyen SN. 2019. A new species of the genus *Microhyla* Tschudi, 1838 (Amphibia: Anura: Microhylidae) from Tay Nguyen Plateau, Central Vietnam. *Zootaxa*, **4543**(4): 549–580.

Palumbi S R, Martin A, Romano S, McMillan W O, Stice L, Grabowski G. 1991. The Simple Fool's Guide to PCR, Version 2.0. Privately published document compiled by S. Palumbi, Department of Zoology, University of Hawaii, Honolulu, 96822. http://palumbi.stanford.edu/SimpleFoolsMaster.pdf.

Parker HW. 1928. LXIII. — The brevicipitid frogs of the genus *Microhyla*. *Journal of Natural History*, **2**(11): 473–499.
Parker HW. 1934. Monograph of the Frogs of the Family Microhylidae. London: Trustees of the British Museum, 208.
Parker HW, Osman HWC. 1948. LI. — Frogs of the genus *Microhyla* from Ceylon. *Journal of Natural History*, **1**(10): 759–764.
Pawangkhanant P, Poyarkov NA Jr, Duong TV, Naiduangchan M, Suwannapoom C. 2018. A new species of *Leptobrachium* (Anura, Megophryidae) from western Thailand. *PeerJ*, **6**: e5584.
Peel MC, Finlayson BL, McMahon TA. 2007. Updated world map of the Köppen – Geiger climate classification. *Hydrology and Earth System Sciences Discussions*, **11**: 1633–1644.
Peloso PL, Frost DR, Richards SJ, Rodrigues MT, Donnellan S, Matsui M, Raxworthy CJ, Biju S, Lemmon EM, Lemmon AR, Wheeler WC. 2016. The impact of anchored phylogenomics and taxon sampling on phylogenetic inference in narrow-mouthed frogs (Anura, Microhylidae). *Cladistics*, **32**(2): 113–140.
Pillai R. 1977. On two frogs of the family Microhylidae from Andamans including a new species. *Proceedings of the Indian Academy of Sciences, Section-B*, **86**(2): 135–138.
Posada D, Crandall KA. 1998. Modeltest: testing the model of DNA substitution. *Bioinformatics*, **14**(9): 817–818.
Poyarkov NA, Nguyen TV, Duong TV, Gorin VA, Yang JH. 2018. A new limestone-dwelling species of *Micryletta* (Amphibia: Anura: Microhylidae) from northern Vietnam. *PeerJ*, **6**: e5771.
Poyarkov NA Jr, Vassilieva AB, Orlov NL, Galoyan EA, Tran D, Le DTT, Kretova VD, Geissler P. 2014. Taxonomy and distribution of narrow-mouth frogs of the genus *Microhyla* Tschudi, 1838 (Anura: Microhylidae) from Vietnam with descriptions of five new species. *Russian Journal of Herpetology*, **21**(2): 89–148.
Rakotoarison A, Scherz MD, Glaw F, Köhler J, Andreone F, Franzen M, Glos J, Hawlitschek O, Jono T, Mori A, Ndriantsoa SH, Raminosoa NR, Riemann JC, Rödel MO, Rosa GM, Vieites DR, Crottini A, Vences M. 2017. Describing the smaller majority: integrative taxonomy reveals twenty-six new species of tiny microhylid frogs (genus *Stumpffia*) from Madagascar. *Vertebrate Zoology*, **67**(3): 271–398.
Rambaut A, Suchard M, Xie W, Drummond A. 2014. Tracer v. 1.6. Institute of Evolutionary Biology, University of Edinburgh. Available at: http: //tree.bio.ed.ac.uk/software/tracer/.
Ronquist F, Huelsenbeck JP. 2003. MrBayes 3: Bayesian phylogenetic inference under mixed models. *Bioinformatics*, **19**(12): 1572–1574.
Sambrook J, Russell DW. 2001. Molecular Cloning: A Laboratory Manual (3rd edition). New York: Cold Spring Harbor Laboratory Press.
Sano N, Kurabayashi A, Fujii T, Yonekawa H, Sumida M. 2005. Complete nucleotide sequence of the mitochondrial genome of Schlegel's tree frog *Rhacophorus schlegelii* (family Rhacophoridae): duplicated control regions and gene rearrangements. *Genes & Genetic Systems*, **80**(3): 213–224.
Savage JM. 1975. Systematics and distribution of the Mexican and Central American stream frogs related to *Eleutherodactylus rugulosus*. *Copeia*, **1975**(2): 254–306.
Schenkel E. 1901. Achter Nachtrag zum Katalog der herpetologischen Sammlung des Basler Museums. *Verhandlungen der Naturforschenden Gesellschaft in Basel*, **13**(1): 142–199. (in German).
Seshadri KS, Singal R, Priti H, Ravikanth G, Vidisha MK, Saurabh S, Pratik M, Gururaja KV. 2016. *Microhyla laterite* sp. nov., a new species of *Microhyla* Tschudi, 1838 (Amphibia: Anura: Microhylidae) from a laterite rock formation in South West India. *PLoS One*, **11**(3): e0149727.
Sheridan JA, Stuart BL. 2018. Hidden species diversity in *Sylvirana nigrovittata* (Amphibia: Ranidae) highlights the importance of taxonomic revisions in biodiversity conservation. *PLoS One*, **13**(3): e0192766.
Shreve B. 1940. Reptiles and amphibians from Burma with descriptions of three new skincs. *Proceedings of the New England Zoölogical Club*, **18**: 17–26.
Smith M. 1923. Notes on reptiles and batrachians from Siam and Indo-China (No. *2). Journal of the Natural History Society of Siam*, **6**(1): 47–53.
Solovyeva EN, Lebedev VS, Dunayev EA, Nazarov RA, Bannikova AA, Che J, Murphy RW, Poyarkov NA. 2018. Cenozoic aridization in Central Eurasia shaped diversification of toad-headed agamas (*Phrynocephalus*; Agamidae, Reptilia). *PeerJ*, **6**: e4543.
Stejneger L. 1901. Diagnoses of eight new batrachians and reptiles from the Riu Kiu Archipelago, Japan. *Proceedings of the Biological Society of Washington*, **14**: 189–191.
Suwannapoom C, Yuan ZY, Chen JM, Hou M, Zhao HP, Wang LJ, Nguyen TQ, Murphy RW, Sullivan J, McLeod DS, Che J. 2016. Taxonomic revision of the Chinese *Limnonectes* (Anura, Dicroglossidae) with the description of a new species from China and Myanmar. *Zootaxa*, **4093**(2): 181–200.
Tamura K, Stecher G, Peterson D, Filipski A, Kumar S. 2013. MEGA6: molecular evolutionary genetics analysis version 6.0. *Molecular Biology and Evolution*, **30**(12): 2725–2729.
Taylor EH. 1934. Zoological results of the third De Schauensee Siamese Expedition, Part III. Amphibians and reptiles. *Proceedings of the Academy of Natural Sciences of Philadelphia*, **86**: 281–310.
Tschudi JJV. 1838. Classification der Batrachier mit Berücksichtigung der fossilen Thiere dieser Abtheilung der Reptilien. Neuchâtel: Petitpierre, 124. (in German).
Vences M, Thomas M, Bonett RM, Vieites DR. 2005a. Deciphering amphibian diversity through DNA barcoding: chances and challenges. *Philosophical Transactions of the Royal Society of London B: Biological Sciences*, **360**(1462): 1859–1868.
Vences M, Thomas M, Van der Meijden A, Chiari Y, Vieites DR. 2005b. Comparative performance of the 16S rRNA gene in DNA barcoding of amphibians. *Frontiers in Zoology*, **2**(1): 5.
Vieites DR, Wollenberg KC, Andreone F, Köhler J, Glaw F, Vences M. 2009. Vast underestimation of Madagascar's biodiversity evidenced by an integrative amphibian inventory. *Proceedings of the National Academy of Sciences*, **106**(20): 8267–8272.
Vineeth KK, Radhakrishna U, Godwin R., Anwesha S, Rajashekhar KP, Aravind N. 2018. A new species of *Microhyla* Tschudi, 1838 (Anura: Microhylidae) from West Coast of India: an integrative taxonomic approach. *Zootaxa*, **4420**(2): 151–179.
Vogt T. 1911. Beitrag zur Amphibien-fauna der Insel Formosa. *Sitzungsberichte der Gesellschaft Naturforschender Freunde zu Berlin*, **1911**: 179–184. (in German)
Wijayathilaka N, Garg S, Senevirathne G, Karunarathna N, Biju S, Meegaskumbura M. 2016. A new species of *Microhyla* (Anura: Microhylidae) from Sri Lanka: an integrative taxonomic approach. *Zootaxa*, **4066**(3): 331–342.
Wijayathilaka N, Meegaskumbura M. 2016. An acoustic analysis of the

genus *Microhyla* (Anura: Microhylidae) of Sri Lanka. *PLoS One*, **11**(7): e0159003.

Wilkinson JA, Drewes RC, Tatum OL. 2002. A molecular phylogenetic analysis of the family Rhacophoridae with an emphasis on the Asian and African genera. *Molecular Phylogenetics and Evolution*, **24**(2): 265–273.

Wilkinson JA, Sellas AB, Vindum JV. 2012. A new species of *Ansonia* (Anura: Bufonidae) from northern Tanintharyi Division, Myanmar. *Zootaxa*, **3163**: 54–68.

Wilkinson JA, Win H, Thin T, Lwin KS, Shein AK, Tun H. 2003. A new species of *Chirixalus* (Anura: Rhacophoridae) from western Myanmar (Burma). *Proceedings of the California Academy of Sciences*, **54**: 17–26.

Wilkinson M, Presswell B, Sherratt E, Papadopoulou A, Gower DJ. 2014. A new species of striped *Ichthyophis* Fitzinger, 1826 (Amphibia: Gymnophiona: Ichthyophiidae) from Myanmar. *Zootaxa*, **3785**(1): 45–58.

Wogan GOU. 2012. A new species of *Leptobrachium* from Myanmar (Anura: Megophryidae). *Zootaxa*, **3415**: 23–36.

Wogan GOU, Vindum JV, Wilkinson JA, Koo MS, Slowinski JB, Win H, Thin T, Kyi SW, Oo SL, Lwin KS, Shein AK. 2008. New country records and range extensions for Myanmar amphibians and reptiles. *Hamadryad*, **33**: 83–96.

Wogan GOU, Win H, Thin T, Lwin KS, Shein AK, Kyi SW, Tun H. 2003. A new species of *Bufo* (Anura: Bufonidae) from Myanmar (Burma), and redescription of the little-known species *Bufo stuarti* Smith, 1929. *Proceedings of the California Academy of Sciences*, **54**: 141–153.

Yuan ZY, Suwannapoom C, Yan F, Poyarkov NA, Nguyen SN, Chen HM, Chomdej S, Murphy RW, Che J. 2016. Red River barrier and Pleistocene climatic fluctuations shaped the genetic structure of *Microhyla fissipes* complex (Anura: Microhylidae) in southern China and Indochina. *Current Zoology*, **62**(6): 531–543.

Zaw T, Lay P, Pawangkhanant P, Gorin VA, Poyarkov NA. 2019. A new species of Crocodile Newt, genus *Tylototriton* (Amphibia, Caudata, Salamandridae) from mountains of Kachin State, northern Myanmar. *Zoological Research*, **40**(3): 151–174.

Zhang M, Fei L, Ye C, Wang Y, Wang B, Jiang J. 2018. A new species of genus *Microhyla* (Amphibia: Anura: Microhylidae) from Zhejiang Province, China. *Asian Herpetological Research*, **9**(3): 135–148.

Zug GR. 2015. Morphology and systematics of *Kalophrynus interlineatus* - *pleurostigma* populations (Anura: Microhylidae: Kalphryninae) and a taxonomy of the genus *Kalophrynus* Tschudi, Asian Sticky Frogs. *Proceedings of the California Academy of Sciences*, **62**: 135–190.

Natural history of Valentin's rock lizard (*Darevskia valentini*) in Armenia

Eduard Galoyan[1,4,*], Alisa Bolshakova[2], Manush Abrahamyan[3], Ruzanna Petrosyan[3], Valeria Komarova[4], Victor Spangenberg[5], Marine Arakelyan[3]

[1] *Zoological Museum of the Lomonosov Moscow State University, Moscow* 125009, *Russia*
[2] *Department of Zoology, Biological Faculty of Moscow State University, Moscow* 119992, *Russia*
[3] *Department of Zoology, Biological Faculty of Yerevan State University, Yerevan* 0025, *Armenia*
[4] *Severtsov Institute of Ecology and Evolution of the Russian Academy of Sciences, Moscow* 119071, *Russia*
[5] *Vavilov Institute of General Genetics, Russian Academy of Sciences, Moscow* 119991, *Russia*

ABSTRACT

Valentin's rock lizard (*Darevskia valentini*) is suggested to be the parent for several parthenogenetic species (e.g., *D. armeniaca*, *D. bendimahiensis, D. sapphirina*, and *D. unisexualis*) that evolved through hybridization. Complex evolutionary processes (including reticulate evolution) are occurring within the areas where Valentin's rock lizard coexists with these and other rock lizards. Hence, a detailed biological specification of this species is important for understanding how vertebrates evolve. Valentin's rock lizard is a long-lived (up to 9 years), small diurnal lizard with larger females than males, which is unlike other species of the genus. Their relatively large eggs and early reproduction period, which occurs just after emergence from winter shelters, are adaptations for living in a high elevation climate (higher than 2 000 m a.s.l.). Their body temperatures (31–32 °C) are comparable to body temperatures of rock lizards living in milder climates, though female body temperature is more dependent on substrate temperature and basking due to their lower activity than that found in males. Population density fluctuates from several individuals to several hundred per hectare and is not affected by parthenogen coexistence, although hybrids do occur in sexually biased populations where males are more common than females. The male home range is larger than that of females, though these home ranges broadly overlap. Prey is not limited in the mountain meadows and Valentin's rock lizards feed on a great variety of arthropods. Infanticide occurs in high-density populations.

Keywords: *Darevskia valentini*; Reproduction; Population density; Skeletochronology; Home range; Seasonal activity

INTRODUCTION

Rock lizards belong to the genus *Darevskia* (Arribas, 1999; Arribas et al., 2017) or the recently suggested genus *Caucasilacerta* (Busack et al., 2016), which comprises about 30 relatively small species, seven of which reproduce parthenogenetically. The lizards of this genus are distributed in the Caucasus Mountains, Armenian highlands, northern Iran, western Turkmenistan, eastern Turkey, and Crimean Peninsula. Due to hybrid speciation in this genus, Caucasian rock lizards are important model organisms for the study of evolutionary mechanisms (Danielyan et al., 2008; Darevsky, 1967; Freitas et al., 2016; Ryskov et al., 2017; Spangenberg et al., 2017; Tarkhnishvili et al., 2013). However, information on the ecological traits and requirements of most *Darevskia* species is limited. Their biological features were first partially described by Darevsky (1967), with other researchers since undertaking studies on niche differentiation (Tarkhnishvili et al., 2010), age estimation (Arakelyan, 2002; Kurnaz et al., 2017; Sergeev, 1937; Tsellarius & Tsellarius, 2009), foraging and prey composition (Darevsky & Danielyan, 1967; Lukina, 1963), and spacing and social behavior (Galoyan, 2010, 2013a; Tsellarius & Tsellarius, 2001; Tsellarius et al., 2016,

Received: 09 August 2018; Accepted: 03 February 2019; Online: 28 March 2019

Foundation items: This work was supported by the Russian Foundation for Basic Research (RFBR) KOMFI 17-00-00430 (K) and 17-00-00425 and Arm_a 18-54-05020 and Russian National Foundation N14-50-00029

*Corresponding author, E-mail: saxicola@mail.ru

DOI: 10.24272/j.issn.2095-8137.2019.036

2017). However, there is still a general lack of information on the natural history of rock lizards. Moreover, our basic understanding of the underlying mechanisms of modern geographical distribution and evolutionary scenarios needs to be improved, in particular the specific ecological traits within the genus *Darevskia*.

Valentin's rock lizard (*Darevskia valentini* (Boettger, 1892)) is a rock-dwelling lizard that mainly inhabits meadows at elevations between 1 900 and 3 110 m a. s. l. in the Small Caucasus, particularly in northern Armenia, southern Georgia, northern Iran, and eastern Turkey (Arakelyan et al., 2011; http: //reptile-database. reptarium. cz, 2017). This taxon was previously described as *Lacerta saxicola terentjevi* (Darevsky, 1957) and then synonymized with the earlier suggested name *Lacerta saxicola valentini* (Darevsky, 1965). The high elevation and extreme climate have contributed to the distinct natural history of this species. Furthermore, this species is of interest due to its evolutionary role in the origin of several parthenogens, namely *D. armeniaca*, *D. bendimahiensis*, *D. sapphirina*, and *D. unisexualis* (Fu et al., 2000; Tarkhnishvili et al., 2016). Among mtDNA clades, according to their phylogeny (Ahmadzadeh et al., 2013; Murphy et al., 2000), this species belongs to the "rudis" clade. The hybrid origin of parthenogenetic rock lizards is not controversial (Darevsky et al., 1985; Murphy et al., 2000; Tarkhnishvili et al., 2017). It is suggested that *D. valentini* is the paternal species for those listed above. Triploid and even tetraploid hybrids between parental and parthenogenetic species have also been described previously for sympatric populations (Danielyan et al., 2008; Darevsky & Kupriyanova, 1985); however, their evolutionary role is still unrecognized. Hence, understanding the hybridization conditions, ecological preferences, and biological specification of the parental species is crucial for our understanding of the appearance of parthenogens.

The aims of this study were to consolidate data on the autecology of Valentin's rock lizard from allopatric and sympatric populations and to describe the main biological traits of the species, which are important for predicting evolutionary output within rock lizards. Here we present considerable data compiled from different areas and years by our research team and provide a general overview of the ecological characteristics of Valentin's rock lizard.

MATERIALS AND METHODS

Study object

Among rock lizards, Valentin's rock lizard is a relatively large species with a snout-vent length (SVL) body size of up to 77 mm. According to Darevsky (1967, p. 104), the dorsum coloration is greenish-brown or bright-green and the venter is yellow or white (Figure 1A, B). A black temporal stripe bears one to three longitudinal rows of rounded, bright (bluish in pectoral zone) spots forming the centers of fused, dark ocelli. The upper side of the head has black, irregular blotches and spots. Males differ in body proportion, with a relatively wide head, and bright coloration. Daughter parthenogenetic species *D. unisexualis* differs from *D. valentini* by grey dorsum coloration with a reticulate pattern (Figure 1C). Unlike in *D. armeniaca* (Figure 1D), there are several, not one, rows of scales between the tympanic shield and mid temporal scale (Figure 1E, F; Darevsky, 1967, fig. 39, p. 52). *Darevskia armeniaca* differs from *D. valentini* by dull-green dorsal coloration with light spots along the flanks and pale-yellow venter with white throat (Figure 1D). The adult triploid hybrids between parthenogenetic *D. unisexualis* and *D. valentini* are often larger and more robust than the adult diploid individuals (Danielyan et al., 2008) and can be distinguished by green dorsum coloration with distinct reticulate pattern similar to that in *D. unisexualis* (Figure 1G). Hybrids between parthenogenetic *D. armeniaca* and *D. valentini* are larger than the diploids but exhibit no any obvious differences from *D. armeniaca*.

Study area

Valentin's lizard is widely distributed along the Armenian highlands, mostly in the central and northern parts of the country. We used the data on distribution of *D. valentini* (Arakelyan et al., 2011; Petrosyan et al., 2019) and open access in ArcGIS 10.2 applying World Topographic Map, published by ESRI (services. arcgisonline. com) application to make the distribution map (Figure 2). We collected data for the present work between 2006 and 2017 from four locations in Armenia (Figure 2): Mets Sepasar (area of Ashotsk City, Shirak Province, 2 030 m a.s.l.), Kuchak (area of Aparan City, Aragatsotn Province, 1 900 m a.s.l.), Lchashen (Gegharkunik Province, 1 900 m a.s.l.), and Sotk (Gegharkunik Province, 2 030 m a. s. l.). Kuchak and Mets Sepasar were the main survey areas as they represent two population models with high and low population densities. In all studied localities, Valentin's rock lizards occupy highlands with cold snowy winters, chilly and rainy springs and short, relatively hot and dry summers (Figure 3). Although the climatic conditions are similar in these areas, Mets Sepasar experiences heavier snowfalls in winter and, in general, colder temperatures. High-elevation meadows with dense grass vegetation of up to 40–50 cm in height dominate the landscape. In the survey areas, rock lizards inhabit stony mounds (Figure 4A), rocky outcrops of glacial origin, and steep rocks along roads (Figure 4B), riverbanks, and cliffs on lakeshores and river valleys. All listed population areas are subject to cattle grazing.

There are two population types: allopatric, where *D. valentini* is the only one species of rock lizards; and sympatric (Figure 2), where *D. valentini* coexists with the parthenogenetic Armenian rock lizard (*D. armeniaca* Meheli, 1909) and *D. unisexualis* (Darevsky, 1966).

Population density and structure

We used distance sampling (Buckland et al., 1993) to estimate lizard population densities. Age and sex structure, microhabitat use, as well as seasonal and daily activities were estimated on the same line transects (Table 1). One line transect was placed in the high-elevation meadow area near Mets Sepasar (allopatric population) and another included the path along the bank of the Akhuryan River valley and where

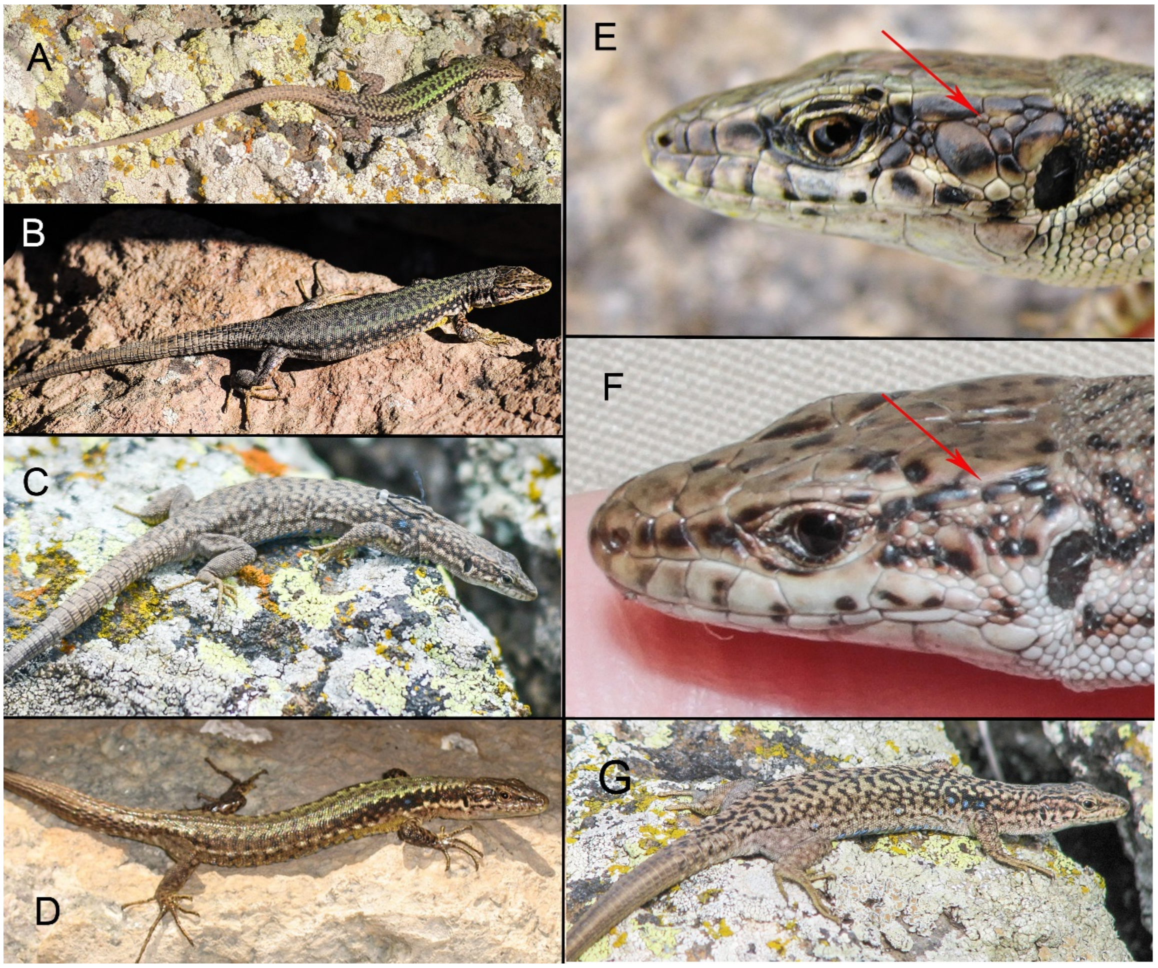

Figure 1 Morphology and external view of studied lizards

A: Male *Darevskia valentini*; B: Female *D. valentini*; C: *D. unisexualis*; D: *D. armeniaca*; E: Head of *D. armeniaca* with one row of scales between tympanic shield and mid temporal scale; F: Head of *D. valentini* female; G: Female triploid hybrid between *D. valentini* and *D. unisexualis*.

an old nineteenth century stone bridge crosses the river (sympatric population). The transect near Kuchak village crossed a meadow (sympatric population). Counting was performed by three scientists with the help of binoculars. All participants were experienced in joint work to calibrate their results. The perpendicular distance from the transect line to each detected lizard was noted in a field book. We visually identified the lizards to species and hybrids according to experience and described characteristics (Danielyan et al., 2008). We also noted age and sex categories: i. e., adult females, adult males, and young. The latter included subadults and juveniles due to difficulties in their discrimination. Prior to each survey, we recorded the temperatures above the surface in the shade and substrate temperatures in the sun. Encounter surveys were performed on selected transects from 0600 h to 1900 h during warm sunny days: one in Kuchak (23 June 2013) and two in Mets Sepasar (14 June 2016). This allowed us to estimate daily activity patterns of lizards and to define the maximum number of lizards per day for population density calculation.

Population density (D) is commonly calculated as the number of detected animals (n) within the boundaries of the occupied area (A). We calculated population density via the formula $D=N/2lwPa$, where l is the length of the transect, w is half the width of the transect, N is the number of estimated lizards, and Pa is the proportion of animals detected in the covered area ($2lw$) (Kendeigh, 1944). The number of animals over substantial distances can be underestimated. To estimate the proportion of animals detected within the covered area, at different distances from the line of the transect, we divided the width of the transects into segments, which included perpendicular distances to each registered lizard: 0–1 m to 9–10 m. The detection function (df) for different distances from the counting transect was estimated, and the probability of underestimated individuals was calculated using the formula $Pa=S_{df}/S_{ed}$, where S_{df} is the area under the detection function and S_{ed} is the area under uniform distribution within the detection range (Buckland et al., 1993; Gonzalez et al., 2017).

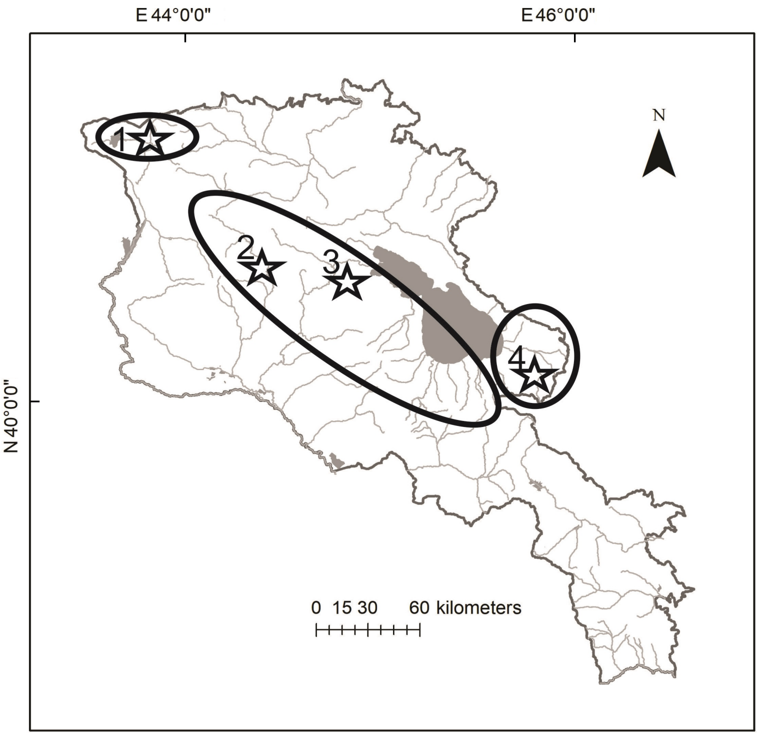

Figure 2 Distribution map of Valentin's lizard *(D. valentini*) in Armenia and adjacent areas (Arakelyan et al., 2011 with changes)

Survey areas are marked by stars, 1: Mets Sepasar (*D. valentini*; *D. raddei nairensis*; *D. armeniaca*), 2: Kuchak (*D. valentini*; *D. armeniaca*; *D. unisexualis*), 3: Lchashen (*D. valentini*; *D. armeniaca; D. unisexualis*), 4: Sotk populations (*D. valentini*; *D. armeniaca*).

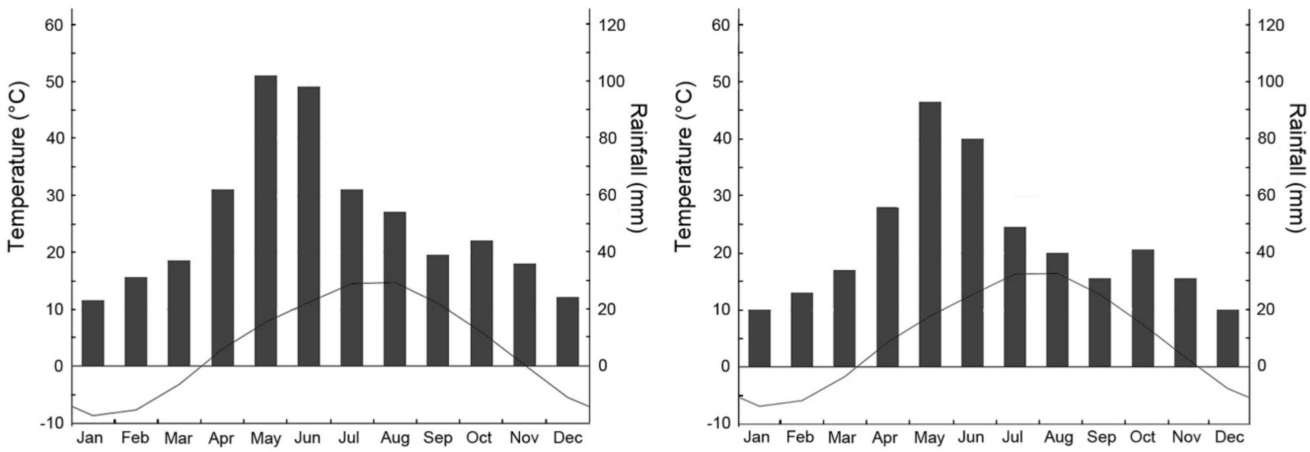

Figure 3 Climatographs (data from https://ru.climate-data.org) for cities closest to the main survey areas

A: Ashotsk (Shirak Province, area of Mets Sepasar); B: Aparan (Aragatsotn Province, area of Kuchak).

Detection functions were determined during daylong monitoring and fitted to half-normal distribution (Table 1; Supplementary Figure 1). The differences in *Pa* between the study areas were explained by low temperatures and strong winds in the meadow near Mets Sepasar village; hence, lizard activity was higher on the stones, where the probability of being detected by an observer was also higher. Further recalculations to the area A were established, which is, in our case, equal to one hectare. Calculations were performed using the "Distance" package in R software. Average lizard density was calculated for the samplings at activity peaks and is given with the standard errors (*SE*) for each line transect. Average population density (±*SE*) was calculated from the activity peaks (the highest number of lizards registered on the transect during the whole-day registrations). Although the distance sampling method might underestimate actual population density (Smolensky &

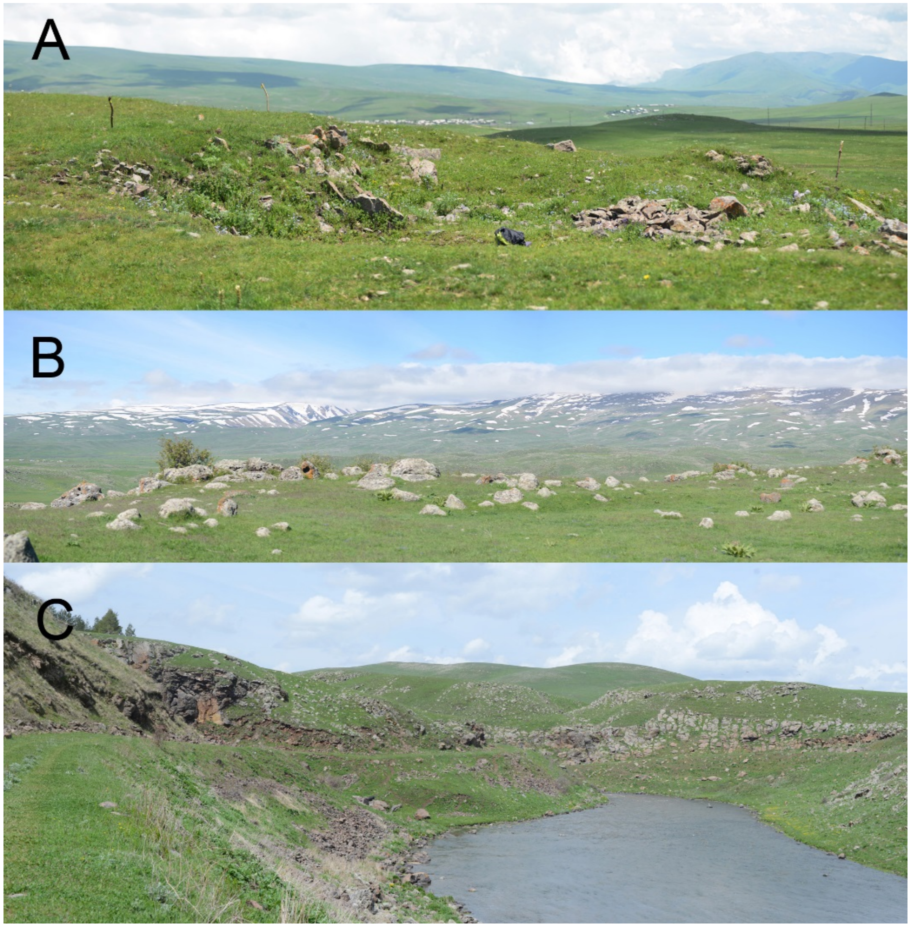

Figure 4 Typical landscapes inhabited by *D. valentini*

High-elevation meadows with stony outcrops in Mets Sepasar (A) and Kuchak (B). Steep cliffs in the Akhuryan River valley in the Mets Sepasar area (C).

Table 1 Data for population density and structure estimation

Area	Mets Sepasar (Allopatric)	Mets Sepasar (Sympatric)	Kuchak (Sympatric)
Survey dates	20., 21., 29. 05. 2016, 01., 14. 06. 2016	14. 06. 2016	17., 18., 23. 06. 2013
N_{ad} (*D. valentini*/*D.* spp)	317	320/98	15/783
N_y	804	174	567
l (m)	800	1 000	1 000
L (m)	13 600	11 000	19 000
w	10	10	10
*P*a	0.779	0.318	0.253

N_{ad}: Number of detected adult individuals; N_y: Number of detected young animals; *l*: Transect length, *L*: Total length of all transects, *w*: Transect width, *P*a: Probability of underestimated individuals.

Fitzgerald, 2010), it is important for describing seasonal and daily activity both in terms of age and sex structure of the population. A similar method has been used in previous studies on *Darevskia* (Galoyan, 2010; Tsellarius & Tsellarius, 2001), facilitating comparison with our data.

Local population density was also estimated by the capture-mark-recapture method (CMR) in the sampling areas in Kuchak (3 600 m^2) and Mets Sepasar (1 300 m^2). Lizards were captured and individually marked by amputation of the distal phalanx and by two color beads sewn by a nylon line

through the skin fold on their back (Fisher & Muth, 1989). The latter method allows observing and distinguishing individuals from a distance. These two humane methods have no negative impact on lizard behavior (Galoyan, 2017; Husak & Fox, 2003; Nicholson & Richards, 2011; Tsellarius & Tsellarius, 2001).

In total, 118 lizards were marked in 2013 in the study area near Kuchak village (92 *D. armeniaca*, six possible *D. armeniaca×D. valentini* hybrids, 11 *D. unisexualis*, six *D. unisexualis×D. valentini* hybrids, and three *D. valentini* males) and in 2016, 176 lizards were marked within the study area near Mets Sepasar (*D. valentini*, allopatric population). Most lizards were marked in the first days after emergence from winter shelters, with newcomers marked if they occurred in the study area afterwards. For each individual, we measured body length with a caliper to an accuracy of 0.5 mm; photographs were taken for further identification of the specific coloration pattern; for skeletochronological studies, the removed finger was measured and dried. To estimate the population density in the sampling areas, we used the Petersen-Lincoln index (Southwood & Henderson, 2000) using the formula $N=Kn/k$, where N is the number of animals in the population, K is the number of animals captured the second time, n is the number of animals marked the first time, and k is the number of recaptured animals marked. Population density was estimated for seven pairs of full observation days (26 May–5 June 2016) in Mets Sepasar and for five pairs of full observation days (23 May–5 June 2016) in Kuchak.

Age determination

The lizards oviposit in late June – August (Darevsky, 1967). The first wintering of juvenile rock lizards occurs when SVL is about 30 – 40 mm (Arakelyan & Danielyan, 2000; Tsellarius & Tsellarius, 2009). This was supported in the present work for *D. valentini* by skeletochronological age estimation for four individuals (32–36 mm). The age of young animals (1–3 years old) was partly based on SVL measurements; lizards with SVL=32.4±0.96 (n=9, May – June) were considered juveniles (juv). Subadults (sad) were defined as those lizards which survived two and three winters and showed an SVL of up to 60 mm. Individuals with an SVL higher than 60 mm and which survived more than four winters were defined as adults. Age estimations of 65 older individuals from Mets Sepasar, 22 from Lchashen, 10 from Kuchak, and 15 from Sotk were based on the skeletochronological method (Castanet, 1994; Smirina, 1974). The amputated digits were prepared and analysed following standard methods (Galoyan, 2013a; Kurnaz et al., 2017; Tsellarius & Tsellarius, 2009). The phalanxes were decalcified in 5% nitric acid and microscopic sections (10–15 μm) were prepared on a sledge microtome MC-2. The sections were colored by Ehrlich's hematoxylin.

Space use

Visual observations of individually marked lizards took place from 15 May – 14 June 2014, 13 May – 15 June 2016, and 25 September 2016 in Mets Sepasar and 21 May – 22 July 2013 in Kuchak. Each sampling area was mapped in detail. Visual observations of active lizards were performed between 0800 h and 1800 h on days with favorable weather. Focal observations were made from 5 – 10 m or closer, especially if the lizards were habituated to the presence of an observer. The observer chose a focal lizard and observed it for 10 – 15 min before switching to another individual. Location, contacts, including mating and mating attempts, and foraging behavior were recorded using a Nikon D600. Total observation time was 30 d (143 h) in 2013 in Kuchak and 17 d (49.5 h) in 2014 and 19 d (65.5+78.5 h) in 2016 in Mets Sepasar. The position of the focal animal was noted each minute and converted into location points for range estimation.

Here, we defined home range as the minimum convex polygon (MCP), with the exclusion of occasional sallies beyond the home range and characterized by specific behavior (Tsellarius & Tsellarius, 2005). Range structure was defined for residents by approximately 300 location points, which included at least 75% of the range area (Galoyan, 2013a; 2017).

Seasonal activity and reproduction cycle

During the visual observations, we noted and described successful copulation and mating attempts. We considered the mating season as the period between the first mating attempts and the appearance of females with obvious marks on their bellies (i.e., jaw bite traces) and last observed mating attempts. The oviposition period was defined as the time between the appearance of the first and last females who laid eggs within the study area. The skin fold along the body flank, just after clutching, was used to distinguish oviposited females. Fourteen females were caught within one week before egg laying and kept in a terrarium. The number of eggs per clutch was counted and egg size parameters were measured with a caliper. The eggs and females were returned to the population after the study.

Feeding

We used two methods to estimate prey item composition and proportion: visual observations and contents of feces collected in the field. The observations were recorded with a camera in video mode and prey items were determined from the images. The prey items from the feces were determined under a binocular after fecal maceration in warm water. In total, 54 fecal samples, which included 205 prey items, and 32 records were analysed.

We also estimated prey density in the study area. Total counts of invertebrates in grass, on substrate surfaces, and in shallow surface areas were performed within a random 25 cm× 25 cm plot (n=19) (Tsellarius & Tsellarius, 2001). The numbers of feeding objects were counted on a cold day (19 June) in Mets Sepasar, when flying insects were immobile on the surface and could easily be detected in the grass.

Thermal biology

Body temperature (T_b) was measured from 3–15 June 2016 in Mets Sepasar and from 15 – 20 June 2015 in Kuchak. We measured active lizards captured in the field (41 records in Mets Sepasar and 23 in Kuchak) by inserting a cloacal

thermometer (Miller-Weber cloacal thermometer). Subsequently, 10 females and 10 males from Mets Sepasar were brought to the laboratory to estimate the thermal preferences of lizards. Lizards were acclimated for 3 d prior to the experiment. In the laboratory, we created a thermal gradient ranging from 15–53 °C in an indoor 100 cm×50 cm×50 cm glass terrarium by suspending light bulbs and ice blocks. Every hour from 0800 h to 2000 h, we measured the body temperature of the lizards and ambient temperature using a Miller-Weber cloacal thermometer.

Statistical analyses

All means are given with standard errors (*SE*). We used the independent sample *t*-test to compare range areas between males and females after applying the Shapiro-Wilk normality test for choosing criteria (parametric or nonparametric). We used the Wilcoxon test for comparison of the SVL of males and females of the same age and body temperature of males and females from the same and different populations. Spearman rank correlation (*R*s) was calculated to estimate the correlation between age and SVL of lizards, body temperatures and ambient temperatures, and body temperatures and substrate temperatures.

RESULTS

Population density

The average population density of the Valentin's lizard varied in different locations from 3 to 66 ind./ha (DSM census). Local density within a sample site (CMR census) reached up to 400 ind./ha (Table 2). This number was comparable with the population density of parthenogenetic species in Kuchak (*D. armeniaca* and *D. unisexualis* and their hybrids with *D. valentini*), where Valentin's lizard coexists.

Table 2 Average (±*SE*) population density of adult lizards, calculated by the distance-sampling method (DSM), on the line transects at activity peaks in three populations

	Elevation (m)	Biotope	*D. valentini* (ind./ha)		*D.* spp. (ind./ha)	
Method			DSM	CMR	DSM	CMR
Mets Sepasar (Allopatric)	2 030	Meadow	25.7±1.60	433.9±28.40	–	–
Mets Sepasar (Sympatric, Akhuryan gorge)	2 030	Gorge, river valley	66.0±6.55	No data	18.9±1.57	No data
Kuchak (Sympatric)	1 900	Meadow	3.0±0.99	5.6±0.79	159.6±6.06	194.4±7.04

Mets Sepasar allopatric; Mets Sepasar sympatric; Kuchak sympatric: (*L*=4 800, 3 000, 4 000 m; *N*=192, 162, 329 ind.; *Pa*=0.779, 0.318, 0.253, respectively, where *L*: total route distance on the transects; *N*: number of detected animals; *Pa*: "average" detectability of animals on route). Local average (±*SE*) population density at studied settlements determined by capture-mark-recapture method (CMR) in two locations: Mets Sepasar (A= 1 300 m^2) allopatric and Kuchak (A=3 600 m^2) sympatric. A: Correspondingly, where A is the sampling area. –: Not available.

The ratio of *D. valentini* to other species of rock lizards differed among sites (Tables 2, 3). For instance, *D. valentini* was twice as common as *D. armeniaca* in the Akhuryan River gorge, although in the Kuchak population, individuals in the biparental species were extremely scarce (Tables 2, 3).

Population structure

The male/female proportion in *D. valentini* was close to 1:2 in the allopatric population and about 1:1 in the sympatric population in Mets Sepasar. If we included the parthenogenetic *D. armeniaca*, the male to female proportion was the same (Table 3). The sex ratio was dramatically biased in Kuchak, where the number of *D. valentini* females was five times lower than that of males, with males compensating for their absence by interactions with females of parthenogenetic *D. unisexualis* and *D. armeniaca*.

The proportion of adults to juveniles was considerably biased to the young in the Mets Sepasar meadow (Table 3) and, albeit to a lesser extent, in the Akhuryan River valley and the sympatric population in Kuchak.

Table 3 Proportions of males and females of biparental species *D. valentini*, parthenogenetic *D. armeniaca*, and young animals (Sad) on the transects on 14 June 2016 in Mets Sepasar and 23 June 2013 in Kuchak

Transect	*D. valentini* F (%)	*D. valentini* M (%)	*D.* spp. Ad (%)	*D.* spp. + *D. valentini* Sad (%)	Length of route per transect (m)	*n*	*N*
Mets Sepasar allopatric	18.1±2.21	10.4±1.45	–	71.5±5.19	1 900	16	1 096
Mets Sepasar sympatric	21.6±1.92	24.5±1.56	23.2±3.27	30.8±4.70	1 000	11	494
Kuchak sympatric	0.2±0.16	1.0±0.32	58.8±2.15	40.0±2.23	1 900	19	1 369

n: Number of routes per transect, *N*: Number of registered lizards. M: Male; F: Female. Ad: Adult; Sad: Subadult.

Age and body length

The oldest lizards were one male and one female, which survived at least nine winter hibernations. Only a few males that survived more than six winters were found, which suggests that, on average, females reach higher ages than males (Table 4).

Table 4 Mean (±*SE*) body length (mm) values of male and female *D. valentini* from Kuchak, Lchashen, Mets Sepasar, and Sotk; ages defined by skeletochronological analysis

	Juv 1	Sad 2	Sad 3	Ad 4	Ad 5	Ad 6	Ad 7	Ad 8	Ad 9
	Winter	Winters	Winters	Winters	Winters	Winters	Winters	Winters	Winters
M	32.4±1.44	53.5±0.40	58.2±1.05	64.4±0.96	66.2±0.56	67.4±0.87	No data	69	68
F		48.6±1.58	58.0±1.76	62.1±1.50	70.2±0.74	71.7±1.06	73.6±1.35	No data	76
N	4	3M+8F	7M+5F	11M+10F	17M+16F	5M+11F	0M+9F	1M+0F	1M+ 1F

N: Number of individuals. M: Males; F: Females. Juv: Juvenile; Sad: Subadult; Ad: Adult.

The maximum SVL was 79 mm (a female from the Mets Sepasar population). The growth rates of males and females in Mets Sepasar were almost the same before the fourth winter (Wilcoxon test, P>0.05); however, male growth slowed after the fifth wintering, whereas females continued to grow (Figure 5, Table 4) and became significantly larger than males of the same age (Figure 5, W=16, P=0.04 and W=3.5, P=0.03, respectively, for five and six winter hibernations).

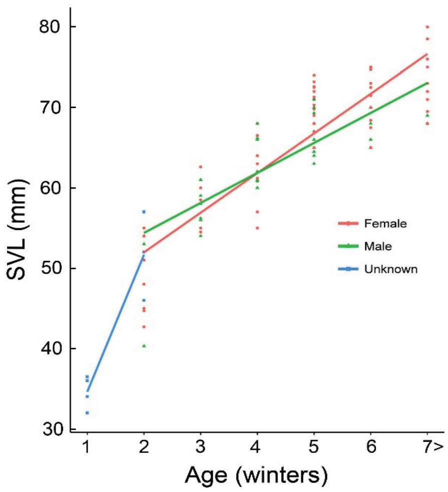

Figure 5 Body lengths and ages of lizards from four populations (Mets Sepasar, Sotk, Lchashen, and Kuchak)

n=112 ind. There was a positive correlation between age and SVL for males and females (Rs=0.740, P<0.0001 in males and Rs=0.825, P< 0.0001 in females).

Space use

Lizards were concentrated in areas with stony mounds and rocky outcrops on the highland meadows in both Kuchak and Mets Sepasar. The highest concentration of lizards was observed around winter shelters, where the local density of lizards (CMR) was significantly higher in the observation areas compared to the average density on the transect at the same area (Table 2).

Not all lizards observed within the survey areas lived continuously within the same range. The number of residential individuals (observed during the entire observation period) in the Mets Sepasar allopatric population was 32 (19% of all captured animals in 2016). Among the 148 lizards captured in Kuchak in 2013, only three residential *D. valentini* males (2%) were observed.

The home ranges of Valentin's lizards consisted of stony mounds and solitary stones, which were used as shelters and basking sites. Two types of individual home ranges were detected: monolite (basking sites close to each other and connected by permanent routes, one core area) and fragmented (basking sites far from each other and not connected by permanent routes, more than one core area). Residential individuals could use both of types of home ranges. Fragmented home ranges (121.1±12.38 m^2) were larger for males than monolite home ranges (46.6±5.56 m^2) (t= 5.49; P=0.0003, n_1=8, n_2=17), and male monolite home ranges were larger than that of females (22.1±4.56 m^2) (t= 3.41; P=3.4074; P=0.002; n_1=17, n_2=14). Several females jointly used an area and often basked on the same stones simultaneously, sometimes with one male. Males were aggressive towards each other; however, their ranges could also overlap. Some males seemed to have harems comprising residential and switching females. Males in the Kuchak population also had social and sexual interactions with *D. armeniaca* and *D. unisexualis* females.

Seasonal and daily activity

Emergence of *D. valentini* in the area of Mets Sepasar after winter hibernation was observed from 15 May in 2014 and from 12 May in 2016. Spring activity in the morning started at about 1000 h, when the ambient temperature reached 10 °C and the shelter temperature was 7 °C. The sex ratio just after leaving the winter shelters was 1: 1. Due to permanent rains and cloudy weather in May in Kuchak, mass emergence from the winter shelter in 2013 appeared on 21 and 22 May, when ambient air temperature was 11 °C, whereas in 2016, the first appearance of lizards was detected on 20 April, with massive emergence in the first days of May.

Lizard activity in late May and June showed two peaks (morning and evening) (Figure 6). Due to the low ambient temperatures, lizards basked and spent more time on the surface and were thus more visible in May than in the summertime; hence, the maximum number of lizards per one route on the transect on the transect was higher.

In late May to early July, air temperatures increased, and daily activity started at 0800 h, though some individuals could be observed as early as 0700 h (Figures 5; 6A, B). In spring, lizards entered shelters at about 1700 h, whereas in mid-summer, they entered shelters between 1900 h to 2000 h. On

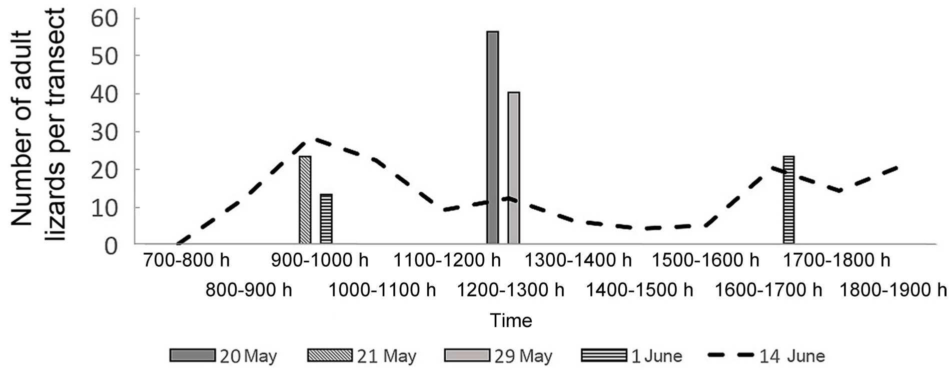

Figure 6 Number of observed adult lizards on the transect in Mets Sepasar on the high-elevation meadow in 2016

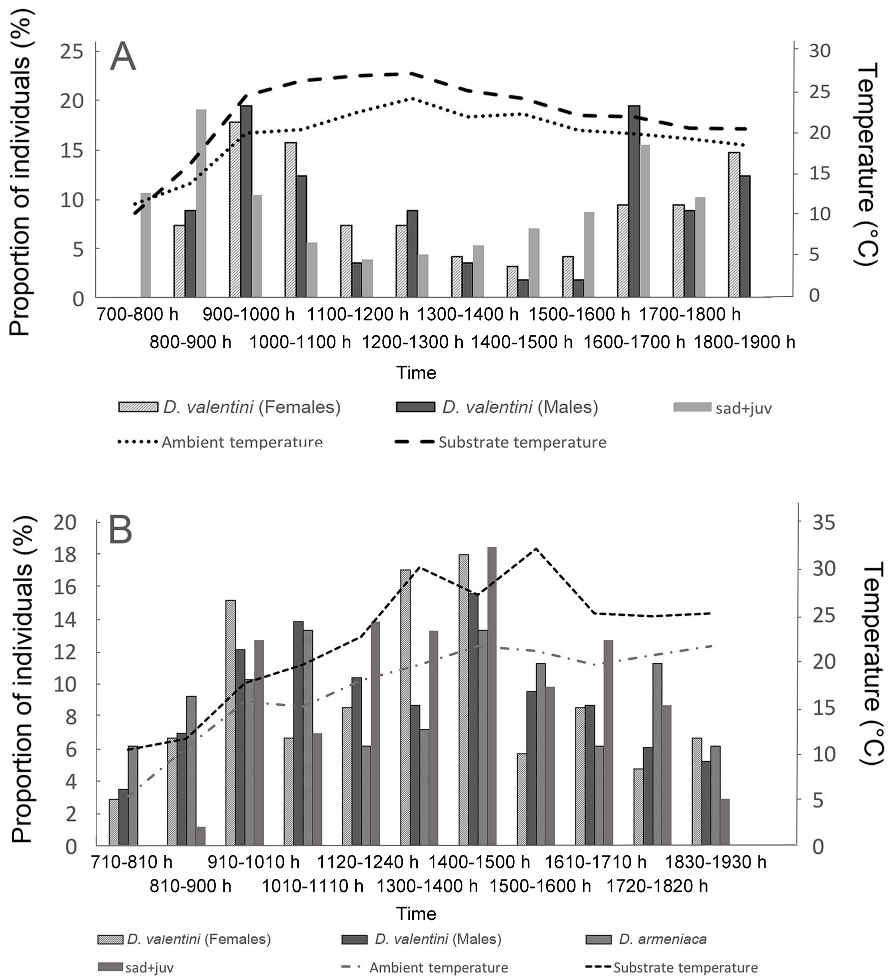

Figure 7 Daily activity of *D. valentini* in Mets Sepasar on the high-elevation meadow (A) and Akhuryan River valley (B) on 14 June 2016
Juveniles and subadults of these two species look similar from a distance and were therefore combined.

25 September 2016, lizards were still recorded on the surface and were mainly found basking near their winter shelters.

Reproductive cycles and intersexual behavior

The mating period of *D. valentini* started just after leaving the hibernation shelters at the beginning of April and lasted until early June. We recorded three mating attempts in 2014 between 19 and 31 May and 10 mating attempts between 19 and 27 May in 2016 in the Mets Sepasar population. In the Kuchak population, with the low density of female *D. valentini*,

we observed 11 mating attempts of *D. valentini* males with parthenogenetic females of *D. armeniaca* and *D. unisexualis* from 21 May to 9 June 2013.

During the mating period, the male and female often basked together, with physical contact: i. e., a male could lay on a female or vice versa, and they often crawled over each other (Figure 8A). This kind of behavior was considered as social (affiliative). Males could switch from this activity to sexual behavior. We also observed other types of sexual behavior, including a male chasing a female and attempting to mate without preliminary social contact (sexual aggression). During coitus, the male took the female's lateral fold in his jaws and coiled over her, restraining the female by hugging her in the crest area via his hind limbs (Figure 8B). The intraspecies coitus lasted on average 19.9±3.33 min (n=7), with a maximum duration of 37 min. Mating attempts, even unsuccessful ones, resulted in jaw-prints on the flanks of the female. These marks were used as an indicator of such an attempt but did not necessarily indicate successful mating. Larger females with a SVL > 65 mm mated earlier than smaller individuals.

Figure 8 Joint basking (A) of male N149 and female N140 in 2016; mating (B) of male N8 and female N13 in 2014

Females oviposited from 14 to 29 June 2016 (n=10) in the Mets Sepasar population. Pregnancy in Valentin's lizard lasted 45–50 d. Not all adult females laid eggs: three (SVL=65, 67, and 70 mm) were observed to mate within the study area in the Mets Sepasar population, but did not oviposit. The average number of eggs per clutch in adult females older than three years and larger than 60 mm of SVL was 6.0±0.50 (n=26). The maximum number of eggs per clutch was greater in larger and older females, but this number was not strongly correlated with the SVL of females (Rs=0.43, P=0.027, n=26), (Table 5). Mean egg size was 14.8±0.23 mm×8.1±0.13 mm (n=33).

Table 5 Snout-vent length (SVL) and number of eggs per clutch of Valentin's lizards from the Mets Sepasar population

Age	3	4	5	6	> 7
SVL (mm)	57.5	63.0±2.73	70.6±1.01	72.4±1.73	73, 71
Number of eggs per clutch	2	5.5±1.04	6.1±0.64	7.8±2.17	6, 2
Number of females	1	4	8	4	2

Age was estimated via the skeletochronological method.

Feeding

While Valentin's rock lizards are primarily insectivores, we did observe consumption of a small amount of vegetation (e. g., plants, flowers) in the current study (Figures 9, 10). The abundance of possible prey was relatively high in the Mets Sepasar population (mean number of feeding objects 4.5±0.69, n=18 samples of 25 cm×25 cm frames). According to the feeding objects found in feces, *D. valentini* mainly fed on beetles (Coleoptera). Direct observations indicated that flies (Diptera) were also a favorable food, which they hunted from the stems of plants or in flight (Figure 10), with Hymenoptera, Lepidoptera, and Aranea consumed rarely. During our observations, two cases of infanticide were observed (one male and one female ate a juvenile). We also recorded remains of juveniles in feces (Figures 8, 9).

The lizards rarely actively searched for prey outside their main activity areas. Most often, they preyed within and near basking sites or on the move (during cruising foraging, *sensu* Regal, 1983). We recorded hunting behaviour (e. g., chasing and ambushing) exhibited in adults preying on juveniles.

Thermal biology

No significant differences between the body temperatures of adult lizards (within and between sexes) were revealed in the Kuchak and Mets Sepasar populations during the study periods (Wilcoxon test, P>0.05), although substrate temperatures were higher in the Mets Sepasar allopatric population (Table 6).

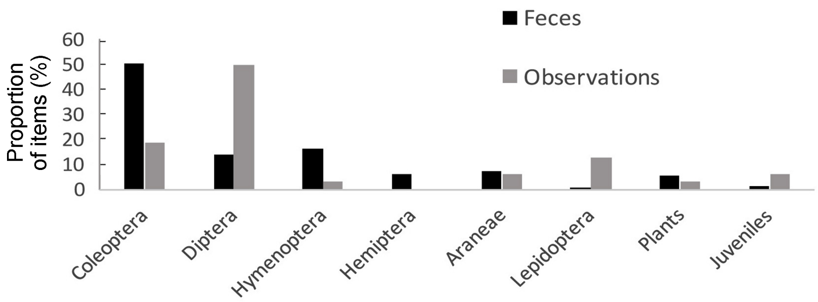

Figure 9 Distribution of feeding objects found in feces of Valentin's lizards (*n*=205) and by observation (*n*=32)

Figure 10 Feeding observations of the Valentin's rock lizards

A: Adult female eating a juvenile; B: Subadult eating "forget-me-not"; C: Female catching a locust.

Table 6 Average (±*SE*) body temperature (T_b) of active adult male and female *D. valentini* from Kuchak and Mets Sepasar, determined via a thermo-gradient apparatus

	Male T_b (°C)	Female T_b (°C)	Substrate *T* (°C)	Ambient *T* (°C)
Kuchak	31.8±0.44 (*n*=19)	32.7±0.76 (*n*=4)	27.6±1.00	26.7±1.09
Mets Sepasar	31.7±0.90 (*n*=8)	32.3±0.53 (*n*=21)	32.0±1.23	23.0±0.56
Thermal gradient apparatus	31.5±0.39 (*n*=10)	31.8±0.59 (*n*=9)	32.4±0.60	32.4±0.60

n: Number of individuals.

Body temperatures of adult lizards that had just left their shelters were almost the same as the ambient temperatures at the capture site (T_b=28.5±3.07 °C and *T*air=25.3±2.18 °C, *n*=4, respectively). Hence, basking is an obligate activity for Valentin's lizards, enabling them to reach higher temperatures to perform activities (T_b=31–32 °C, Table 6). Lizards came out of their shelters and flattened themselves on a stone, exposing the maximum amount of their body surface to the sun. They could also obtain heat from the stones when the sun disappeared behind clouds. Thus, lizards managed to maintain a high body temperature even when air temperatures were 14–16 °C or less. Lizards switched to shuttling behavior (Spellerberg, 1972) during hot days and moved from the shade to sunny spots to maintain stable temperatures. Activity decreased with increasing temperatures in July; lizards were almost absent on the surface after 1400 h when the substrate temperature approached 30 °C (Figure 11).

Unlike females, males demonstrated no correlation between substrate temperature and body temperature (Figure 11). This was also the case for ambient temperature and body temperature.

We found no difference between the body temperatures of active male and female Valentin's lizards measured in nature and in the thermogradient apparatus (Wilcoxon test, *P*>0.05). Several females of parthenogenetic *D. armeniaca* and gonochoristic *D. valentini* preferred slightly higher ambient and substrate temperatures in the thermogradient apparatus than males of *D. valentini* (Figure 12), although no significant differences were revealed between females of these two species or between females and males of Valentin's lizard (Wilcoxon test, *P*>0.05, Figure 12).

DISCUSSION

The population density of *D. valentini* varied greatly from relatively low (1–2 ind./ha) to several hundred ind./ha, which exceeded the density of other biparental species such as *D. brauneri* (25 ind./ha, DSM, Tsellarius & Tsellarius, 2001) and *D. portschinskii* (5–6 ind./ha, DSM, Galoyan, 2010; Trofimov,

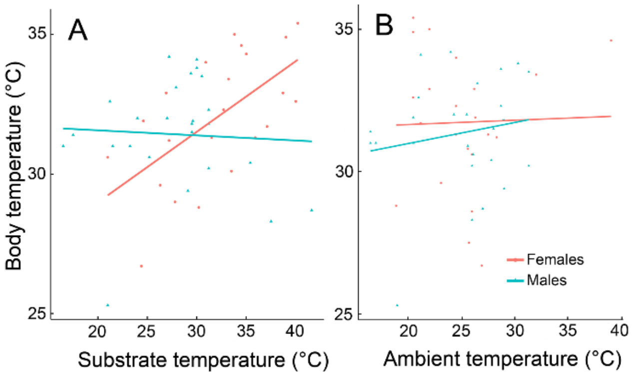

Figure 11 Lizard body, substrate and ambient temperatures

A: Measurements of body temperature of male and female *D. valentini* from Sepasar and Kuchak (*n*=25F+27M). There was a positive correlation between female body temperature and substrate temperature (*R*s=0.644, *P*=0.002), but not between male body temperature and substrate temperature (*R*s=−0.0256, *P*=0.90. B: No relationship was found between body temperature and ambient temperature (Males: *R*s=0.0778, *P*=0.70; Females: *R*s=0.1208, *P*=0.38).

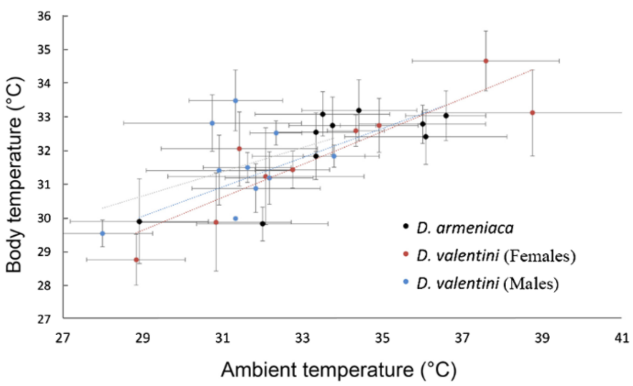

Figure 12 Mean (±*SE*) body and preferred ambient temperature of female parthenogenetic *D. armeniaca* (*n*=10), female *D. valentini* (*n*=9), and male *D. valentini* (*n*=10) from Mets Sepasar

Each individual was measured 12 times throughout the day.

1981) (Table 2). Populations of parthenogenetic species *D. armeniaca* and *D. unisexualis* have also been reported to reach high densities (100−300 ind./ha, DSM, Galoyan, 2010; Tarkhnishvili et al., 2010; Trofimov, 1981; CMR, Danielyan, 1971). The possible explanation for the relatively high population density of *D. valentini* could be joint space use, as observed in parthenogenetic rock lizards (Galoyan, 2013b; Trofimov, 1981). The high population density with a high proportion of juveniles indicated good breeding and feeding conditions in Mets Sepasar. However, such a high population density may also have disadvantages. We suggest that the considerable number of lizards in a relatively small area may be why some females did not lay eggs, even after mating. Pregnancy termination, known as the Bruce effects, has been described in rodents (Blumstein, 2000) and may also occur in rock lizards. Another consequence of the large number of animals and high proportion of juveniles was infant cannibalism (Figures 9, 10). Infanticide has been observed for a variety of reptilian taxa (Ataev, 1985; Bogdanov, 1965; Jenssen et al., 1989), including rock lizards (Tsellarius et al., 2008). In some reptiles, eating unrelated juveniles of the same species may increase parental protection and may even be a possible reason for social evolution towards nuclear family formation (O'Connor & Shine, 2004). There are no studies devoted to this phenomenon in reptiles; however, a long-term study on barn swallows (*Hirundo rustica*) demonstrated decreased infanticide in a decreasing population (Møller, 2004).

Interspecies competition for resources can decrease the population size of competitors (MacArthur, 1958; Pianka, 1973; Schoener, 1971). Due to a faster reproduction rate, parthenogenetic species of rock lizards are likely better competitors, which should outrange related biparental species in overlapping areas in number (Tarkhnishvili et al., 2010). In some sympatric populations, the number of parthenogenetic rock lizards far exceeds the number of biparental relatives, as observed in Kuchak (Danielyan et al., 2008; unpublished data). However, this was not the rule in our study: the ratio of parthenogenetic and biparental species in the Akhuryan River valley was about 1: 2, whereas the ratio of parthenogenetic Armenian lizards to female Valentin's lizards was 1: 1 (Table 3). In Sotk and Lchashen, *D. valentini* was also a common species (Figure 2). In our surveys on 23 June 2010 and 1 July 2010 in Sotk, we detected 19 adult *D. valentini* among 27 captured lizards of other rock lizards, whereas in Lchashen, we observed 24 Valentin's lizards among 32 other individuals of the genus *Darevskia*. The deprivation of females belonging to biparental species in Kuchak may lead to regular hybridization between male Valentin's lizards and parthenogens, whose proportions have exceeded 50% in some years (Arakelyan et al., 2011; Danielyan et al., 2008). No *D. armeniaca*×*D. valentini* hybrids were observed in the Akhuryan River gorge, and they were also extremely rare in Lchashen. Contrary to the Mets Sepasar population, for which a high density of females and males of *D. valentini* was described, in the Kuchak population, we revealed other interactions and social behaviors between *D. valentini* males and other parthenogenetic lizards (*D. armeniaca* and *D. unisexualis*) as a result of a deficit in females of their own species. Therefore, the three different species in Kuchak function as single population, where males are represented by *D. valentini* and females are represented by parthenogenetic species *D. armeniaca* and *D. unisexualis*. Moreover, in the Akhurian population where *D. valentini* coexisted with only one parthenogenetic species, we did not detect any interspecific hybrids, which is evidence that Valentin's males in an area with a high density of females of their own species do not mate with other females of another species.

The estimated home range size of the Valentin's rock lizard was comparable with the home range size in other species of rock lizards (Galoyan, 2013a; Tsellarius & Tsellarius, 2005). As in other saurian species, the home range of males was larger than that of females (Perry & Garland, 2002). The average

home range of residential individuals was only about 20–40 m^2, though some males had very large ranges (more than 100 m^2). We suggest that females aggregating around small areas filled with stones, where they can find shelters and suitable basking sites, may explain the relatively small individual areas in males. Hence, males concentrated around these areas to maintain close proximity to females. This hypothesis should be further evaluated, although it might be supported by the knowledge that space use in females is more dependent on resource availability and distribution, whereas the behavior of males is more 'female-orientated' (Baird et al., 2003; Davies, 1992; Stamps, 1977; Tsellarius et al., 2017). Hence, small and overlapping home ranges favor high population densities and facilitate joint basking.

The Valentin's rock lizard is characterized by unique morphological and ecological adaptations to extreme habitats on high elevations. It was active at low ambient temperatures (Figure 11) and had a relatively large body size in comparison with that of other species of rock lizards. The female-biased sexual size dimorphism has been reported previously (Arakelyan, 2002; Darevsky, 1967) and is supported by our data. Unlike in other small lacertids with a similar lifespan where females grow faster (Kolarov et al., 2010), the growth trajectory in male and female Valentin's lizard before the fourth winter was similar; however, after this, only females continued to grow (Figure 8; Kurnaz et al., 2017). The maximum body length for females was 79 mm, which is larger than that recorded for *D. valentini* from the highland population in Balahor (Turkey, 2 400 m a.s.l.) (Kurnaz et al., 2017). The body size of female Valentin's lizard is close to the upper limits reported for rock lizards. Only triploid hybrids between parthenogenetic and biparental species exceeds 80 mm in body length (Arakelyan, 2002).

Valentin's lizards occupy areas with stable cold climates, where minus temperatures are common from December to March and cold nights are customary from October to April (Figure 2). Larger body size of species living in cold climates has been described for lizards, although it is not a steadfast rule (Pincheira-Donoso et al., 2008) and the weight/SVL proportion does not appear to be affected by mean environmental temperatures (Meiri, 2010). Smaller species of rock lizards (e. g., *D. caucasica*) are also known to exist at such elevations. Such lizards generally shelter within narrow crevices between rocks, deep enough to maintain stable positive temperatures (Darevsky, 1967); however, such shelters are too small for larger individuals, who are thus more likely to die during cold winters. This might be a possible explanation for the arrested growth in the studied species. Arrested growth also affects the results of skeletochronological study and reduces maximal age of the animals due to absence of new marks of growth. That is why previous studies suggest a lifespan of seven years for this species, as estimated by skeletochronology (Arakelyan, 2002). The average lifespan of biparental and parthenogenetic rock lizards has been estimated at five to six years (Arakelyan & Danielyan, 2000). Our observations support this suggestion, although a prolonged lifespan of nine years is possible for *D. valentini* from Turkey (Kurnaz et al., 2017) and parthenogenetic *D. armeniaca* (Galoyan, 2013a). Still, the only way of evaluating the actual lifespan of long-lived reptiles is via prolonged visual observations. According to Tsellarius & Tsellarius (2009), the lifespan of Brauner's rock lizard is 14 years and might differ between residential and non-residential as well as territorial and wandering animals. Our observations suggest that male Valentin's lizards have a shorter life span than that of females (Figure 6), although this should be clarified in future studies.

The reproductive period differs among species of rock lizards (Darevsky, 1967). We observed first matings in Valentin's rock lizard just after emergence from winter hibernation shelters in mid-May. Some other species (*D. brauneri*) start mating after two or three weeks of activity (Tsellarius & Tsellarius, 2001). The gonadal ripening and mating period in *D. raddei nairensis* in Lchashen occur one month later than that in *D. valentini* in the same locality (Danielyan, 1965). Our observations indicate that *D. portschinskii*, which occurs on the steppes at lower elevations of 1 500 m a.s.l. (Arakelyan et al., 2011), started to reproduce in early spring (May) within a short time after emergence, unlike *D. raddei* with which it coexists (own observations). Early reproduction might be an adaptation to harsh conditions at high elevations, but this suggestion should be tested among different species.

According to our findings and those of Darevsky (1967), female Valentin's lizards have, on average, five to six eggs per clutch (Table 6; Darevsky, 1967), reaching, according to our data, up to 12 eggs. Egg size in Valentin's lizard was larger than that in most related species at 14 – 15 mm×8 – 9 mm (Darevsky, 1967; unpublished data), although smaller than that in *D. zchzerbaki* and *D. rudis macromaculata* (Table 36 in Darevsky, 1967), which are not high-elevation species. Hence, egg size can't be the obvious adaptation for the living at the high elevation conditions as well.

The high abundance of diverse prey in the meadows (unpublished data) is comparable with that in deciduous forests (Tsellarius & Tsellarius, 2001). The high taxonomic variety of prey items indicated diverse foraging tactics (Figure 9). Valentin's lizards are active foragers, mostly searching for prey in a cruising foraging mode: animals catch prey in the basking area or on the move. Flies of the Bombyliidae and Sarcophagidae families were common prey items, which were caught in mid-jump from stems or even directly in flight. Hunting juveniles also requires good reactions. The high proportion of immobile objects in their diets, such as larvae, further demonstrated that Valentin's rock lizards are good searchers and would often find such prey under stones and in the grass. Hence, this species is a universal forager with a great variety of prey items and searching strategies.

Different species or unisexual and biparental rock lizards demonstrate a similar preferred body temperature of about 31–32°C, although they inhabit biotopes with different temperature and light conditions: e. g., dense deciduous forests or highland meadows (Galoyan, 2010; Tsellarius & Tsellarius, 2001; Table 6). Primarily, Valentin's lizards

achieved their relatively high body temperature by basking, a common behavior for poikilothermic reptiles (Pianka & Vitt, 2003) and especially relevant in the cold climate highlands. Such conditions explain their late emergence (1000–1100 h) and mid-day activity peak in spring. The breeding season coincidences with this period, with males then able to find females above the surface for mating and communication. This became almost impossible when temperatures increased in mid-summer (Figures 5, 6). Besides direct basking, Valentin's rock lizards also use the heat from stones and aggregate together on the stony mounds in joint basking, often with physical contact. Several females of *D. valentini* cooperated in such a joint basking. A single male could join them, however, two and more males were never observed to bask close to each other. Such joint basking might help increase body temperatures in cold climates. Because the relatively small and compact home ranges often overlapped, the basking areas of individuals also often coincided.

Although we found no differences in body temperatures between males and females, the latter were more dependent on substrate temperature (Figure 11). This may be explained by lower activity (also indicated by smaller range sizes) in females. As prey items were abundant around basking sites, the main reason for male activity was mate searching and guarding, and they could achieve high body temperatures by metabolic heat from muscles during movement.

COMPETING INTERESTS

The authors declare that they have no competing interests.

AUTHORS' CONTRIBUTIONS

E.G. and M. A. designed the study and wrote the manuscript. M. A. and R. P. made the experimental part in thermal gradient apparatus, V. K., A. B. and V. S. took part in the field work. All authors read and approved the final version of the manuscript.

ACKNOWLEDGEMENTS

Many thanks to Aleksey Gusakov for his patient and precise help in feces content and insect determination. We are also grateful to the head of Mets Sepasar village, Sergo, and his family for their kind help and to the director Arain Petrosyan and the staff of Lake Arpi National Park. Many thanks to the reviewers for their work in manuscript editing and improvement. We also grateful to Dr. Christine Watts for her editing of the present MS.

REFERENCES

Ahmadzadeh F, Flecks M, Carretero MA, Mozaffari O, Böhme W, Harris DJ, Freitas S, Rödder D. 2013. Cryptic speciation patterns in Iranian rock lizards uncovered by integrative taxonomy. *PLoS One*, **8**(12): e80563.

Anonymus. https://ru.climate-data.org. Accessed: 05.*01*.2018.

Arakelyan MS. 2002. The study of age, growth, and longevity in the triploid hybrids of rock lizards of the genus *Darevskia* in Armenia. *Russian Journal of Herpetology*, **9**(1): 63–68.

Arakelyan MS. 2012. Processes of species origin in sympatric populations of biparental species of rock lizards of *Darevskia* genus. *Biological Journal of Armenia*, **64**: 10–15.(in Russian)

Arakelyan MS, Danielyan FD. 2000. Growth and age composition of some parthenogenetic and biparental species of Armenian Rock Lizards. *Entomological Review*, **80**: 161–166.

Arakelyan MS, Danielyan FD, Corti C, Sindaco R, Leviton AE. 2011. Herpetofauna of Armenia and Nagorno–Karabakh. Salt Lake City: Society for Study of Amphibians and Reptiles.

Arribas OJ. 1999. Phylogeny and relationships of the mountain lizards of Europe and Near East (archaeolacerta mertens 1921, sensu lato) and their relationships among the Eurasian lacertid radiation. *Russian Journal of Herpetology*, **6**(1): 1–22.

Arribas OJ, Ananjeva NB, Carranza S, Doronin IV, Harris DJ, Orlov NL, Orlova VF. 2017. The pernicious effect of retroactive changes in the code: *Darevskia* and nomenclatorial stability, a reply to Busacket al. *Basic and Applied Herpetology*, **31**: 125–129.

Ataev CA. 1985. Reptiles of the Mountains of Turkmenistan. TSSR Academy of Sciences, Ashkabad. (in Russian)

Baird TA, Timanus DK, Sloan CL. 2003. Intra– and intersexual variation in sexual behaviour: effects of ontogeny, phenotype, resources, and season. *In*: Fox SF, McCoy JK, Baird TA. Lizard Social Behaviour. Baltimor and London: The Johns Hopkins University Press, 7–46.

Blumstein D. 2000. The evolution of infanticide in rodents: a comparative analysis. *In*: van Schaik CP, Janson CH (eds). Infanticide by Males and Its Implications Cambridge: Cambridge University Press, 178–198.

Bogdanov OP. 1965. Ecology of Reptiles of Middle Asia. Nauka, Tashkent.

Buckland ST, Burnham KP, Anderson DR, Thomas L. 1993. Distance Sampling Estimation of Abundance of Biological Populations. London: Chapman and Hall.

Busack SD, Salvador A, Bauer AM, Kaiser H. 2016. *Darevskia* and *Iberolacerta* (reptilia, lacertidae): arribas, 1997 or 1999? The correct dating of two nomenclatural acts affecting palearctic lizards, and validation of the name *Caucasilacerta* harris, Arnold & Thomas, 1998. *Bionomina*, **10**: 61–73.

Castanet J. 1994. Age estimation and longevity in reptiles. *Gerontology*, **40**(2–4): 174–192.

Danielyan F, Arakelyan M, Stepanyan I. 2008. Hybrids of *Darevskia valentini*, *D. armeniaca* and *D. unisexualis from a sympatric population in Armenia. Amphibia-Reptilia*, **29**(4): 487–504.

Danielyan FD. 1965. Mechanisms of reproductive isolation in some forms of rock lizards(*Lacerta saxicola* eversmann), distributed in Armenia. *Izvestia Nauk Armyanskoy SSR*, **18**: 75–80.(in Russian)

Danielyan FD. 1971. A comparative study of the population density and migrations of parthenogenetic and bisexual rock lizards in Armenia. *Russian Journal of Zoology*, **10**: 145–147.(in Russian)

Darevsky IS. 1957. Systematics and ecology of rock lizards(*Lacerta saxicola* eversmann). *Sbornik Akademii Nauk Armenskoy SSR*, **10**: 27–57. (in Russian)

Darevsky IS. 1965. About one forgotten description of rock lizard (*Lacerta saxicola valentini* Boettger) from Armenia. *Izvestia Nauk Armyansoy SSR*, **18**: 71–74.(in Russian)

Darevsky IS. 1967. Rock Lizards of the Caucasus (Systematics, Ecology, and Phylogeny of the Polymorphic Lizards of the Caucasus of the

Subgenus *Archaeolacerta*). Nauka, Saint Petersburg Leningrad: Published for Smithsonian Institution and the National Science Foundation, Washington D. C. by the Indian National Scientific Documentation Centre, New Dehli.

Darevsky IS, Danielyan FD. 1967. Comparative study of foraging in rock lizard (*Lacerta saxicola* eversmann) in the conditions of Armenia. *Biologiya*, **105**: 81–86.(in Russian)

Darevsky IS, Grechko VV, Kupriyanova LA. 2000. Lizards, reproducing without males. *Priroda*, **9**: 131–133.(in Russian)

Darevsky IS, Kupriyanova LA. 1985. Parthenogenesis in reptiles. *In*: Uzzell T. Biology of the Reptilia, Vol. 15, Development B. New York: John Wiley and Sons, 412–526.

Darevsky IS, Kupriyanova LA, Bakradze MA. 1977. Residual biparentality in parthenogenetic species of rock lizards of *Lacerta* genus. *Journal Obshey Biologii*, **38**: 772–779.(in Russian)

Darevsky IS, Uzzel T, Kupriyanova LA, Danielyan FD. 1973. Hybrid triploid males in sympartric populations of parthenogenetic and biparental species of *Lacerla* genus. *Buliten Moskovskogo Obshestva Estesvoispitateley Prirodi*, **78**: 48–57.(in Russian)

Darevsky IS, Kupriyanova LA, Uzzel T. 1985. Parthenogenesis in reptiles. *In:* Gans C, Billet F (eds). Biology of the Reptilian, Vol. 15. New York, NY: John Wiley and Sons Inc., 412–526.

Davies NB. 1992. Mating system. *In*: Krebs JR, Davies NB. Behavioural Ecology: An Evolutionary Approach. Oxford: Blackwell, 263–294.

Fisher JW, Muth A. 1989. A technique for permanently marking lizards. *Herpetological Review*, **20**:45–46.

Freitas S, Rocha S, Campos J, Ahmadzadeh F, Corti C, Sillero N, Ilgaz C, Kumlutas Y, rakelyan M, Harris J, Carretero MA. 2016. Parthenogenesis through the ice ages: a biogeographic analysis of Caucasian rock lizards (genus *Darevskia*). *Molecular Phylogenetics and Evolution*, **102**:117–127.

Fu J, Murphy RW, Darevsky IS. 2000. Divergence of the cytochrome b gene in the *Lacerta raddei* complex and its parthenogenetic daughter species: evidence for recent multiple origins. *Copeia*, **2000** (2): 432–440.

Galoyan EA. 2010. Distribution of parthenogenetic rock lizards (*Darevskia armeniaca, Darevskia unisexualis*) in northern Armenia and their comparison with biparental species. *Russian Journal of Zoology*, **89**: 470–474.(in Russian)

Galoyan EA. 2013a. Joint space use in a parthenogenetic Armenian rock lizard (*Darevskia armeniaca*) suggests weak competition among monoclonal females. *Journal of Herpetology*, **47**(1): 97–104.

Galoyan EA. 2013b. Inter – and intraspecies relations in rock lizards of *Darevskia* genus. *In*: Ananyeva NB, Syromyatnikova EV, Doronin IV. Modern Herpetology: Problems and Ways to Solve. Articles by materials of the first international youth conference of herpetologists of Russia and adjustment countries. Saint Petersburg, 61–66. (in Russian)

Galoyan EA. 2017. Unstable social structre indicates low diversity of relationships in the spotted forest skink *Sphenomorphus maculatus*. *Amphibia-Reptilia*. **38**(3): 383–393.

Gonzalez RP, Thomas L, Marques TA. 2017. Estimation bias under model selection for distance sampling detection functions. *Environmental and Ecological Statistics*. **24**(3): 399–414.

Husak JF, Fox SF. 2003. Adult male collared lizards, *Crotaphytus collaris*, increase aggression towards displaced neighbours. *Animal Behaviour*, **65**(2):391–396.

Jenssen, TA, Marcellini DL, Buhlmann KA, Goforth PH. 1989. Differential infanticide by adult curly – tailed lizards, *Leiocephalus schreibersi*. *Animal Behaviour*, **38**(6): 1054–1061.

Kendeigh SC. 1944. Measurement of bird populations. *Ecological Monographs*, **14**(1): 67–107.

Kolarov TN, Ljubisavljevic LK, Polovic L, Dzukic G, Kalezic ML. 2010. The body size, age structure and growth pattern of the endemic balkan mosor rock lizard (*Dinarolacerta mosorensis* kolombatovic, 1886). *Acta Zoologica Academiae Scientiarum Hungaricae*, **56**(1): 55–71.

Kurnaz M, Eroğlu Aİ, Bülbül U, Koç H, Kutrup B. 2017. The life–history traits in a breeding population of *Darevskia valentini* from Turkey. *Acta Herpetologica*, **12**(2): 167–173.

Lukina GP. 1963. Systematic position and biology of rock lizard *Lacerta saxicola* eversmann on the northwest border of distribution area of the species within Caucasus. *Izvestiya Akademii Nauk Azerbaydjanskoy SSR*, **6**: 53–61.(in Russian)

Macarthur RH. 1958. Population ecology of some warblers of northeastern coniferous forests. *Ecology*, **39**(4): 599–619.

Meiri S. 2010. Length – weight allometries in lizards. *Journal of Zoology*, **281**(3): 218–226.

Møller AP. 2004. Rapid temporal change in frequency of infanticide in a passerine bird associated with change in population density and body condition. *Behavioural Ecology*, **15**(3): 462–468.

Murphy RW, Fu J, Macculloch RD, Darevsky IS, Kupriyanova LA. 2000. A fi ne line between sex and unisexuality: the phylogenetic constraints on parthenogenesis in lacertid lizards. *Zoological Journal of the Linnean Society*, **130**(4): 527–549.

Nicholson KE, Richards PM. 2011. Home–range size and overlap within an introduced population of the cuban knight anole, *Anolis equestris* (squamata: iguanidae). *Phyllomedusa*, **10**(1): 65–73.

O’Connor DE, Shine R. 2004. Parental care protects against infanticide in the lizard *Egernia saxatilis* (scincidae). *Animal Behaviour*, **68**(6): 1361–1369.

Perry G, Garland T. 2002. Lizard home ranges revisited: effects of sex, body size, diet, habitat, and phylogeny. *Ecology*, **83**(7): 1870–1885.

Petrosyan VG, Osipov FA, Bobrov VV, Dergunova N, Danielyan FD, Arakelyan MS. 2019. Ew records of *Darevskia rmeniaca* (Meheli, 1909) and *Darevskia valentini* (Boettger, 892) (Squamata Sauria, Lacertidae) from Armenia and updated geographic distribution maps. *Check List*, **15**(1): 21–31.

Pianka ER. 1973. The structure of lizard communities. *Annual Review of Ecology and Systematics*. **4**: 53–74.

Pianka ER, Vitt LJ. 2003. Lizards: Windows to the Evolution of Diversity. Berkeley, Los Angeles & London: University of California Press.

Pincheira–Donoso D, Hodgson DJ, Tregenza T. 2008. The evolution of body size under environmental gradients in ectotherms: why should bergmann's rule apply to lizards?. *BMC Evolutionary Biology*, **8**: 68.

Smirina EM. 1974. Prospects of age determination by bone layers in reptiles. *Russian Journal of Zoology*, **53**:111–117.(in Russian)

Smolensky NL, Fitzgerald LA. 2010. Distance sampling underestimates population densities of dune – dwelling lizards. *Journal of Herpetology*, **44**(3): 372–381.

Spellerberg IF. 1972. Thermal ecology of allopatric lizards(*sphenomorphus*) in southeast Australia. *Oecologia*, **9**(4): 385–398.

Regal PJ. 1983. The adaptive zone and behaviour of lizards. *In*: Huey RB,

Pianka ER, Schoener TW. Lizard Ecology. Cambridge: Harvard University Press, 105–118.

Ryskov AP, Osipov FA, Omelchenko AV, Semyenova SK, Girnyk AE, Korchagin VI, Vergun AA, Murphy RW. 2017. The origin of multiple clones in the parthenogenetic lizard species *Darevskia rostombekowi*. *PLoS One*, **12**(9): e0185161.

Schoener TW. 1971. Theory of feeding strategies. *Annual Review of Ecology and Systematics*, **2**: 369–404.

Southwood TRE, Henderson PA. 2000. Ecological Methods, 3rd edn. Oxford: Blackwell Science.

Sergeev AM. 1937. Materials to the question of the postembryonic growth of reptiles. *Russian Journal of Zoology*, **16**: 723–734.

Spangenberg V, Arakelyan M, Galoyan E, Matveevsky S, Petrosyan R, Bogdanov Y, Danielyan F, Kolomiets O. 2017. Reticulate evolution of the rock lizards: meiotic chromosome dynamics and spermatogenesis in diploid and triploid males of the genus *Darevskia*. *Genes*, **8**(6): E149.

Stamps JA. 1977. Social behavior and spacing patterns in lizards. *In*: Gans C, Tinkle DW. Biology of the Reptilia, Vol. 7. New York: John Wiley and Sons, 265-334.

Tarkhnishvili D, Gabelaia M, Mumladze L, Murtskhvaladze M. 2016. Mitochondrial phylogeny of the *Darevskia saxicola* complex: two highly deviant evolutionary lineages from the easternmost part of the range. *The Herpetological Journal*, **26**: 175–182.

Tarkhnishvili D, Gavashelishvili A, Avaliani A, Murtskhvaladze M, Mumladze L. 2010. Unisexual rock lizard might be outcompeting its biparental progenitors in the caucasus. *Biological Journal of the Linnean Society*, **101**(2): 447–460.

Tarkhnishvili D, Murtskhvaladze M, Anderson CL. 2017. Coincidence of genotypes at two loci in two parthenogenetic rock lizards: How backcrosses might trigger adaptive speciation. *Biological Journal of the Linnean Society*, **121**(2): 365–378.

Tarkhnishvili D, Murtskhvaladze M, Gavashelishvili A. 2013. Speciation in Caucasian lizards: climatic dissimilarity of the habitats is more important than isolation time. *Biological Journal of the Linnean Society*, **109**(4): 876–892.

Trofimov AG. 1981. Population Spatial Structure of Some Parthenogenetic and Gonochoristic Rock Lizards from the Caucasus. Ph. D. Dissertation, Taras Shevchenko Kyiv University, Kyev. (in Russian)

Tsellarius AY, Tsellarius EY. 2001. Dynamics of population spatial structure in *Lacerta saxicola* in deciduous forests of the Navagir mountain ridge. *Russian Journal of Zoology*, **80**: 1–8.(in Russian)

Tsellarius AY, Tsellarius EY. 2005. Space use pattern and mating system of the rock lizard *Lacerta saxicola* (reptilia, sauria). *Journal of Modern Herpetology*, **3**: 99–110.(in Russian)

Tsellarius AY, Tsellarius EY. 2009. Length of life and mortality factors in the rock lizard *darevskia brauneri* (sauria) according to long–term observations on the Navagir mountain ridge. *Russian Journal of Zoology*, **88**: 1276–1280. (in Russian)

Tsellarius AY, Tsellarius EY, Galoyan EA. 2008. Interrelation of adults and juveniles of rock lizards — *Darevskia brauneri* (reptilia, sauria) in the Navagir mountain ridge. *Journal of Modern Herpetology*, **8**: 170 – 186. (in Russian)

Tsellarius AY, Tsellarius EY, Galoyan EA. 2016. Social relations between males and females of the rock lizard *Darevskia brauneri* (lacertidae) 1. *Friendly monogyny n Males and Polyandry in Females. Biology Bulletin*. **43**(9): 1077–1086.

Tsellarius AY, Tsellarius EY, Galoyan EA. 2017. Social relations between males and females of the rock lizard *Darevskia brauneri* (lacertidae) 3. *competition between females and it's role in the formation of intersexual friendly relations. Russian Journal of Zoology*, **96**: 439–448.(in Russian)

Uetz Peter. Darevskia valentini. http://reptile-database. reptarium. cz. Accessed: 23.12.2017.

ZOOLOGICAL RESEARCH

Allele-specific expression and alternative splicing in horse×donkey and cattle×yak hybrids

Yu Wang[1], Shan Gao[1], Yue Zhao[1], Wei-Huang Chen[1], Jun-Jie Shao[1], Ni-Ni Wang[1], Ming Li[1], Guang-Xian Zhou[1], Lei Wang[2], Wen-Jing Shen[3], Jing-Tao Xu[2], Wei-Dong Deng[4], Wen Wang[3], Yu-Lin Chen[1], Yu Jiang[1,*]

[1] *Key Laboratory of Animal Genetics*, *Breeding and Reproduction of Shaanxi Province*, *College of Animal Science and Technology*, *Northwest A&F University*, *Yangling Shaanxi* 712100, *China*

[2] *Stake Key Laboratory of Plateau Ecology and Agriculture*, *Qinghai Academy of Animal Science and Veterinary Medicine*, *Qinghai University*, *Xining Qinghai* 810016, *China*

[3] *State Key Laboratory of Genetic Resources and Evolution*, *Kunming Institute of Zoology*, *Chinese Academy of Sciences*, *Kunming Yunnan* 650223, *China*

[4] *Faculty of Animal Science and Technology*, *Yunnan Agricultural University*, *Kunming Yunnan* 650223, *China*

ABSTRACT

Divergence of gene expression and alternative splicing is a crucial driving force in the evolution of species; to date, however the molecular mechanism remains unclear. Hybrids of closely related species provide a suitable model to analyze allele-specific expression (ASE) and allele-specific alternative splicing (ASS). Analysis of ASE and ASS can uncover the differences in *cis*-regulatory elements between closely related species, while eliminating interference of *trans*-regulatory elements. Here, we provide a detailed characterization of ASE and ASS from 19 and 10 transcriptome datasets across five tissues from reciprocal-cross hybrids of horse× donkey (mule/hinny) and cattle×yak (dzo), respectively. Results showed that 4.8%–8.7% and 10.8%–16.7% of genes exhibited ASE and ASS, respectively. Notably, lncRNAs and pseudogenes were more likely to show ASE than protein-coding genes. In addition, genes showing ASE and ASS in mule/hinny were found to be involved in the regulation of muscle strength, whereas those of dzo were involved in high-altitude adaptation. In conclusion, our study demonstrated that exploration of genes showing ASE and ASS in hybrids of closely related species is feasible for species evolution research.

Keywords: Allele-specific alternative splicing; Allele-specific expression; *Cis*-regulatory elements; Hybrid species

INTRODUCTION

The accumulation of genetic variations in a genome sequence results in phenotypic diversity and adaptive evolution, with the majority of genetic variations functioning in gene expression regulation (Keane et al., 2011; Kwan et al., 2008). Therefore, identification of changes in the gene expression profiles, including expression levels and alternative splicing, between closely related species (e. g., horse and donkey, cattle and yak) could help clarify the genetic basis of species adaptive evolution. However, it is widely accepted that environmental factors can also affect gene expression (Forrest et al., 2014; Prabhakar et al., 2008; Villar et al., 2015), which can hinder comparisons of gene expression profiles between species (Brown et al., 2014).

Hybrids of closely related species provide a good model for interspecific comparisons of gene expression profiles at the allelic level (Tirosh et al., 2009). The relative expression profiles of two alleles of a heterozygous variant can be assessed by allele-specific expression (ASE) and allele-specific splicing (ASS). To date, most studies on ASE and

Received: 01 April 2019; Accepted: 02 July 2019; Online: 3 July 2019

Foundation items: This work was supported by grants from the National Natural Science Foundation of China (31572381), National Thousand Youth Talents Plan of the International Science and Technology Cooperation Project of China (2013DFA31420), and Science and Technology Innovation Capability Promotion Program of the Science and Technology Department of Qinghai Province (2015-ZJ-712)

*Corresponding author, E-mail: yu.jiang@nwafu.edu.cn

DOI: 10.24272/j.issn.2095-8137.2019.042

ASS genes have been primarily identified in model organisms, such as the mouse (Eckersley-Maslin & Spector, 2014; Pinter et al., 2015; Wood et al., 2015). Crowley et al. (2015) used highly divergent mouse crosses to analyze ASE and found that more than 80% of genes exhibited *cis*-regulatory variation, thus suggesting that pervasive gene expression regulatory variation can influence complex genetic traits and thereby contributed to the adaptive evolution of mice. In addition, ASS has also been identified using hybrids of divergent C57BL/6J and SPRET/EiJ mouse strains, which showed that *cis*-regulatory changes resulted in alternative splicing in the evolution of mice (Gao et al., 2015). In the current study, we expanded ASE and ASS research to large mammals (horse×donkey and cattle×yak hybrids) and explored changes in gene expression in regard to adaptive evolution.

Horse (*Equus caballus*) and donkeys (*Equus asinus*) are domesticated members of *Equus* that diverged approximately 4.0–4.5 million years ago (Orlando et al., 2013). The main difference between these species is in muscle strength, with horses exhibiting greater initial power over short distances and donkeys showing greater stamina over longer distances. Cattle (*Bos taurus*) and yaks (*Bos grunniens*) are members of the bovine family and diverged approximately 4.9 million years ago (Qiu et al., 2012). The most remarkable difference between these species is the ability of yaks to adapt to high-altitude environments. However, the molecular bases of the adaptive evolution between the above closely related species remain unclear.

In this study, we used reciprocal-cross hybrids of horse× donkey and cattle×yak to calculate ASE and imprinting genes and to explore the evolution of *cis*-regulatory gene expression and alternative splicing (Figure 1). In addition, to elucidate fixed expression changes between closely related species, those genes showing ASE in all biological replicates were retained and individually specific ASE genes were filtered. Our results demonstrated that both gene expression and alternative splicing contributed to the divergence between closely related species. Furthermore, genes showing ASE and ASS participated in the regulation of phenotype differences, including muscle strength in mule/hinny and high-altitude adaptation in dzo.

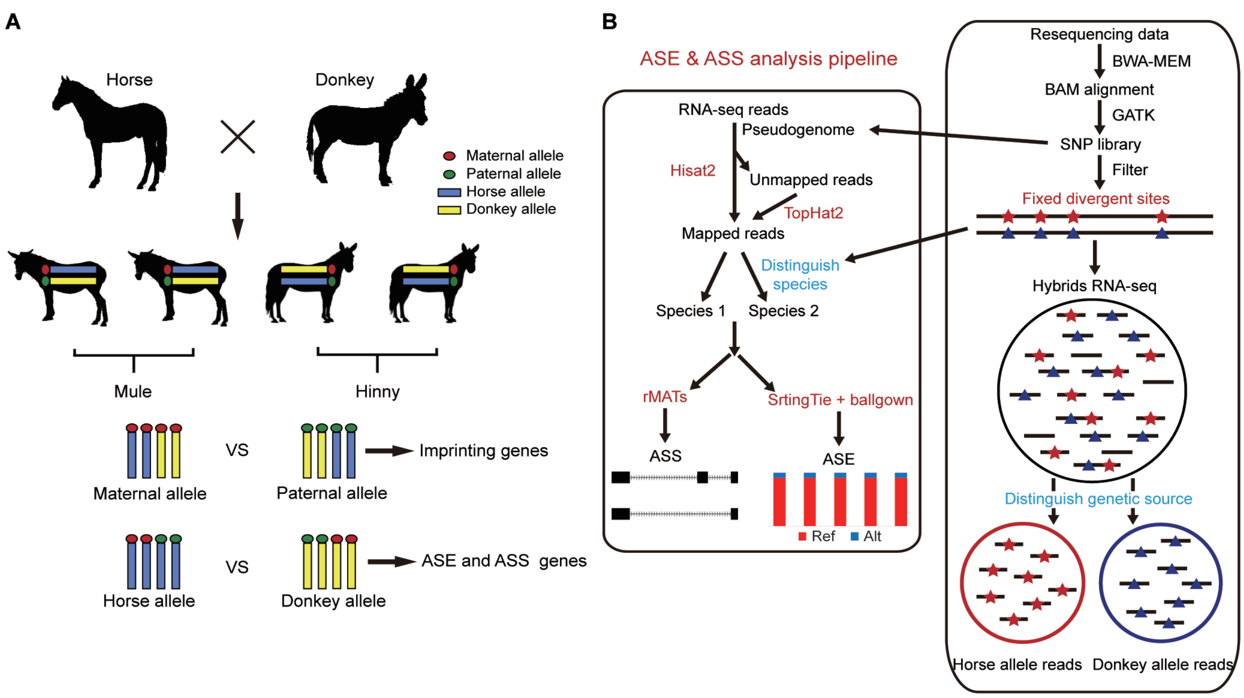

Figure 1 Pipeline for ASE and ASS analysis

Resequencing data were mapped to the genome using BWA. Divergent site calling was then performed by GATK. The pseudogenome was constructed. Divergent sites were filtered by RNA-seq data and used to calculate ASE. Hybrid transcriptomes were divided into two genetic allelic samples using fixed divergent sites. Separated genetic allelic samples were used to calculate ASS. rMATS: Replicate multivariate analysis of transcript splicing. Ref: Reference allele; Alt: Alternative allele.

MATERIALS AND METHODS

Samples

Samples from hybrids of horse and donkey (10-year-old mules/hinnies) were obtained from Yulin City, Shaanxi Province (see Supplementary Table S1 for detailed sample information). Samples from hybrids of cattle and yak (two- to five-year-old dzos) were obtained from Xining City, Qinghai

Province (ear tissue) and Diqing City, Yunnan Province (liver tissue) (see Supplementary Table S2 for detailed sample information). The skin (back of neck, *n*=7, three mule and four hinny samples), brain (prefrontal lobe, *n*=5, three mule and two hinny samples), muscle (semitendinosus muscle, *n*=7, three mule and four hinny samples), liver (*n*=4, three true and one false dzo samples), and ear (*n*=6, two true and four false dzo samples) were dissected and rinsed with PBS. In addition, two skin, two brain, and two muscle tissue samples from donkeys, two liver and four ear tissue samples from cattle, and three liver and two ear tissue samples from yaks were also dissected for RNA sequencing (RNA-seq) (Figure 2D, E). The samples were frozen in liquid nitrogen and stored at −80 °C freezer until required. The study was approved by the Institutional Animal Care and Use Committee of Northwest A&F University (Permit Number: NWAFAC1019).

RNA-seq library construction and sequencing

Total RNA from the frozen samples was extracted using TRIzol reagent (Invitrogen, USA) following the protocols stated by the manufacturer. Genomic DNA contamination was first removed using RNA-free DNase I, and RNA integrity and quality were then analyzed using a bioanalyzer (Agilent, USA). The RNA integrity threshold was RIN⩾6.8. The PolyA(+) RNA-seq libraries were constructed using a NEBNext® Ultra™ RNA Library Prep Kit for Illumina® (NEB, USA) according to the manufacturer's recommendations. The resulting cDNA was first cleaved into 300–500 bp fragments to construct libraries according to the manufacturer's instructions, with the libraries then sequenced using the Illumina HiSeq 2000/2500 platform (USA). As a result, we obtained an average of 20 million 100–125 bp paired reads per sample (Supplementary Table S1, S2).

Trimming and alignment of RNA reads

The RNA-seq raw reads were cleaned, and the adapter sequences were trimmed using Trimmomatic (v0.33) (Bolger et al., 2014). Reads longer than 70 bp were retained as high-quality clean data. The purified reads acquired from the mule/hinny samples were aligned to the horse reference genome (*Equus caballus* EquCab2.0) and the donkey pseudogenome using HISAT2 (v2.0.3) (Kim et al., 2015). We constructed pseudogenomes by replacing the divergent sites without changing the genome coordinates using the method described by Wang et al. (2013). Because the genome and pseudogenome had the same genome coordinates, their mapping results were merged to eliminate mapping bias. Similarly, the purified reads acquired from the dzo samples were aligned to the cattle reference genome (*Bos taurus* Bos_taurus_UMD_3.1.1) and yak pseudogenome. To improve the mapping ratio, unmapped reads were extracted and further aligned to the corresponding genome using TopHat2 (v2.1.1) (Trapnell et al., 2009) with at most five tolerated mismatches. Reads uniquely mapped to both the genome and pseudogenome were merged for further analysis.

Identification of fixed divergent sites and pseudogenome construction

Orlando et al. (2013) identified 22.6 million divergent sites between horses and donkeys (homozygous in both horse and donkey but different between horse and donkey). Divergent sites between cattle and yak were obtained through *de novo* calling. In brief, resequencing data previously obtained from six yaks (97.4G) (Qiu et al., 2012) were downloaded from the National Center for Biotechnology Information database (NCBI accession Nos.: SRR1047220, SRR1047221, SRR962824, SRR962825, SRR962826, and SRR962827) and mapped to the cattle genome using Burrows-Wheeler Alignment (BWA) (v0.7.10-r789) (Li & Durbin, 2009). Divergent site calling was then performed using the Genome Analysis ToolKit (GATK) (v3.2-2), and low-quality sites were filtered using QUAL<30.0 as a cutoff. We filtered heterozygote sites in the cattle or yak that diverged approximately 4.9 million years ago. Multiple allelic sites, including GA and GT, were also filtered to avoid inaccuracy. Finally, 20.8 million divergent sites between cattle and yak were used for analysis (Figure 1). We mapped the RNA-seq reads to the pseudogenome because mapping RNA-seq reads from hybrids to only the reference genome using the same cut-off for both reads (read arising from the reference and that from alternative alleles) can create genome mapping bias toward the reference allele. To avoid mapping bias in the hybrid transcriptome, the donkey pseudogenome was constructed by replacing the horse genome divergent sites with donkey sites using the method described by Wang et al. (2013). In brief, the donkey pseudogenome was constructed by incorporating the single nucleotide variants (SNVs) into the horse genome using the vcf2diploid tool (v0.2.6) in the AlleleSeq pipeline. We selected three horse, three donkey, and three hybrid transcriptomes, which were then mapped to the horse and donkey as well as the donkey pseudogenome to evaluate the mapping rate. Results showed that our method avoided mapping bias (Supplementary Table S3). The yak pseudogenome was constructed using the same approach. In addition, the divergent sites in the exonic region were further filtered through the cattle and yak RNA-seq data (two liver and four ear samples from cattle, two liver and two ear samples from yaks), and the divergent sites between horses and donkeys were similarly filtered using two brain, two muscle, and two skin tissue samples from donkeys and three pooled tissue samples from horses (accession numbers: ERR593552, ERR593553, and ERR593554). In addition, 647 247 and 512 588 fixed divergent sites (FDSs) located in the exonic region were used to identify the genes showing ASE and ASS of mule/hinny and dzo, respectively.

Assignment of genetic origin of reads uniquely mapped to hybrid transcriptomes

Reads uniquely mapped to each hybrid transcriptome were assigned a genetic allele origin based on the FDSs (Figure 1). Using the dzo samples as an example, the number of cattle and yak allelic sites in all uniquely mapped paired-end reads was calculated. If the paired-end reads contained only cattle

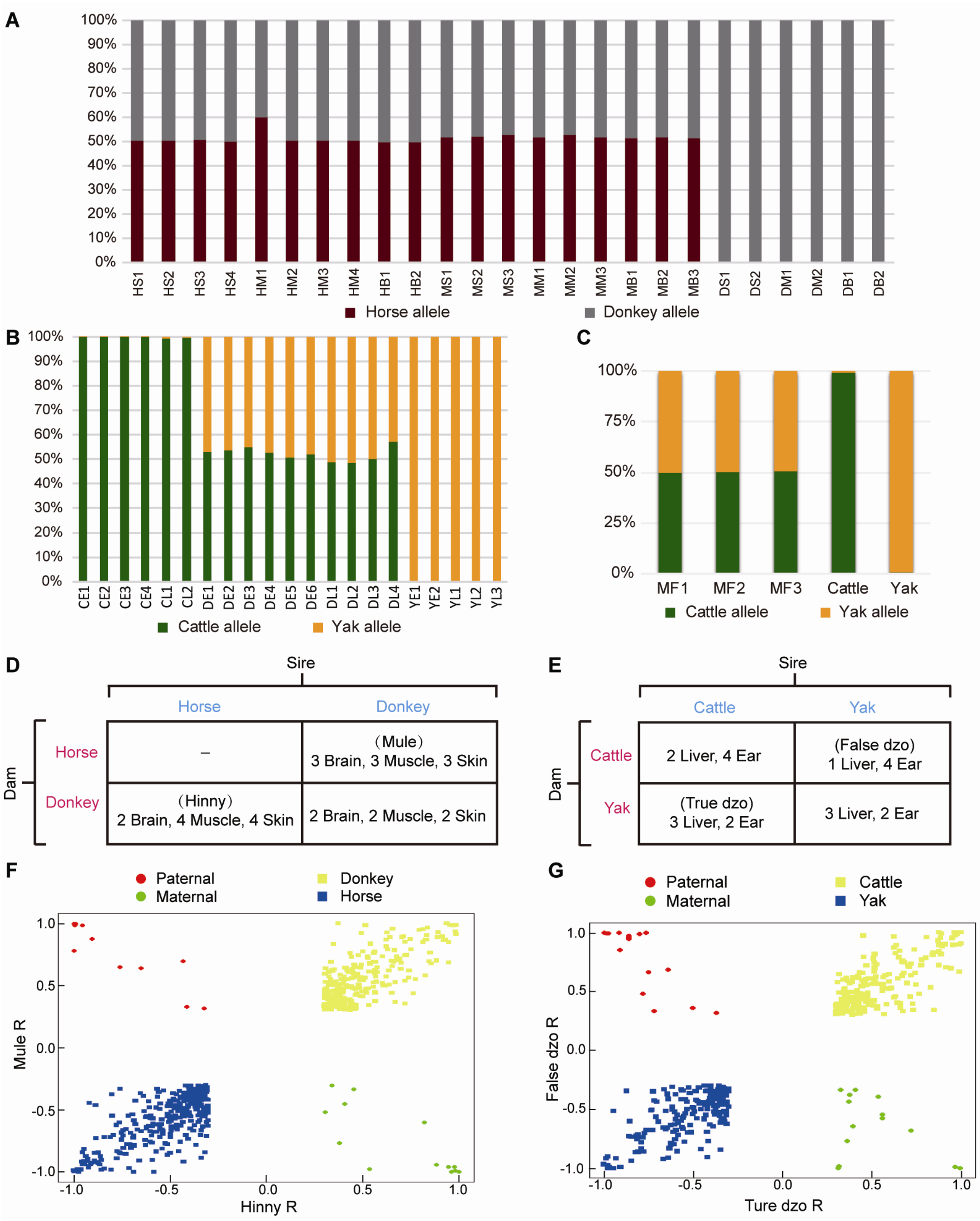

Figure 2 Reciprocal-cross hybrid samples to identify ASE

A: RNA-seq paired-end reads of mule/hinny and donkey were assigned a genetic allele origin. Proportions of the horse and donkey allele origins are shown. HS: Hinny skin tissue; HM: Hinny muscle tissue; HB: Hinny brain tissue; MS: Mule skin tissue; MM: Mule muscle tissue; MB: Mule brain tissue; DS: Donkey skin tissue; DM: Donkey muscle tissue; DB: Donkey brain tissue. B: RNA-seq reads of cattle, yak, and dzo were assigned a genetic allele origin. Proportions of cattle and yak allele origin are shown. CE: Cattle ear tissue; CL: Cattle liver tissue; DE: Dzo ear tissue; DL: Dzo liver tissue; YE: Yak ear tissue; YL: Yak liver tissue. C: Mock hybrid transcriptomes were assigned a genetic allele origin. MF: Mock hybrids. D: Sample and diallel crossing scheme of horse and donkey, mule (female horse×male donkey), and hinny (male horse×female donkey). E: Sample and diallel crossing scheme of cattle and yak, true dzo (male cattle×female yak), and false dzo (female cattle×male yak). F: Distribution of skew (*R*) values (where read ratio *R*=(horse−donkey)/(horse+donkey)) from −1 to 1 for genes showing ASE (yellow, blue) and imprinting genes (red, green) in mule and hinny brain tissues. G: Distribution of skew (*R*) values in true and false dzo ear tissues (*R*= (cattle−yak)/(cattle+yak)).

or yak allelic sites, they were regarded as being expressed from one cattle or yak allele, respectively. The paired-end reads containing both cattle and yak allele sites or those without FDSs were not included in subsequent analyses (Figure 1). Finally, 23%–42% of uniquely mapped reads from all hybrid samples were accurately assigned a genetic allele origin (Figure 2A, B; Supplementary Table S1, 2). To assess the accuracy of this result, mock hybrid transcriptomes were constructed by mixing the same amount of reads from cattle and yak (50 million). The reads of the mock hybrid transcriptomes were precisely assigned using the above-described methods (Figure 2C), and the samples of each hybrid were divided into two genetic allelic samples for ASS analysis.

Analysis of genetic allele-specific alternative splicing

The separated genetic allelic samples were used for the detection of ASS events (Figure 1). A replicate multivariate analysis of transcript splicing (rMATS, v3.2.5) (Shen et al., 2014) was performed for the identification and comparison of gene alternative splicing events, including exon skipping (SE), mutually exclusive exons (MXEs), alternative 5' splice sites (A5SSs), alternative 3' splice sites (A3SSs), and retained introns (RIs). The likelihood-ratio method was used to test the significance of rMATS by calculating the *P* value based on the differential ψ values, also known as "percent spliced-in" (PSI). To ensure high-accuracy detection of ASS events, the splicing events were supported by at least 100 reads, with rigorous statistical criteria (i. e., $|\Delta\psi|$ >10% and false discovery rate (FDR) $\leqslant$1%) used to quantify the ASS events.

Analysis of genes showing genetic allele-specific expression

Gene expression levels (fragments per kilobase of transcript (FPKMs)) were quantified using StringTie (v1.2.2) coupled with the R (v3.5.1) package Ballgown (v2.12.0) based on the known set of transcripts: horse, GCF_000002305.2_EquCab2.0_genomic. gff; cattle, GCF_000003055.6_Bos_taurus_UMD_3.1.1_genomic. gff (Pertea et al., 2016). Genes showing ASE were detected by comparing the read counts of two genetic alleles. Analysis of ASE revealed that the paternal allele was more highly expressed than the maternal allele, indicating male dominance in ASE in certain tissues. Male dominance in ASE results from an imprinting effect. In this study, we identified genetic ASE in reciprocal cross hybrids to exclude the effect of imprinting. To overcome the mapping bias of the reads, allelic expression ratios were calculated using the average read counts from the pseudogenome and reference genome. To improve the accuracy of analysis, the allelic expression ratios of each gene were calculated by combining all FDSs in the gene. In addition, those genes showing ASE were filtered under certain criteria (i. e., at least three FDSs in the exonic regions and at least 20 reads, on average, in each biological replicate). The resulting genes were used for the calculation of allelic expression ratios. In this study, the statistical significance of genes showing ASE was calculated using the Storer-Kim test (Storer & Kim, 1990). For the mule/hinny genes showing ASE, p1 and p2 were defined as the expression ratios from the horse allele and donkey allele, respectively. The expressed genes with balanced alleles showed the following expression ratio: p1=p2=0.5. We expected the genes showing ASE to have expression ratios of p1=0 and p2=1 or p1=1 and p2=0. The null hypothesis p2−p1=0 was tested, and the *P* values were corrected using the R package "qvalue" with the Benjamini-Hochberg algorithm. An adjusted *P* value of <0.05 was used. Here, to identify genes showing the most allelic imbalance, we used cutoff ratios based on previous study (Wang, 2013), that is, p1>0.65 and p2<0.35 for horse allele-specific expression and p1<0.35 and p2>0.65 for donkey allele-specific expression.

Calculation of diversity of gene expression levels

Gene expression diversity can be reflected by the coefficient of variation (CV) of gene expression levels in biological replicates (Bellucci et al., 2014). The CV value was calculated as the ratio between the standard deviation (*SD*) and mean of gene expression levels (FPKMs) obtained for hybrid individuals. The gene expression diversity of each tissue (five brain, seven muscle, seven skin, four liver, and six ear tissue samples) was calculated separately.

Calculation of Ka/Ks value

The coding sequence (CDS) of the horse was downloaded from ensembl (ftp://ftp. ensembl. org/pub/release-88/fasta/equus_caballus/cds/) and aligned to the donkey pseudogenome using BLAT (v36x1) with the output file type set to axt. Each alignment block in an axt file contains a summary line and two sequence lines. The summary line contains chromosomal position and size information about the alignment (details inhttps://genome.ucsc.edu/goldenPath/help/axt. html). We used the axt file to calculate the Ka/Ks value using the KaKs calculator (v2.0) (Zhang et al., 2006) with "-m GMYcN" as a parameter. Similarly, the CDS of cattle was downloaded (ftp://ftp. ensembl. org/pub/release-94/fasta/bos_taurus/cds/) and then aligned to the yak pseudogenome and then treated in the same way as above.

Data archiving

The RNA-seq data obtained in this study were submitted to the National Center for Biotechnology Information (https://www.ncbi.nlm.nih.gov/) under accession Nos. PRJNA387435 and PRJNA387436.The RNA-seq data were also deposited at GSA (http://gsa.big.ac.cn/) under accession No. CRA001591.

RESULTS

Identification of genes showing allele-specific expression in hybrids

To depict the *cis*-regulatory gene expression profiles, we performed RNA-seq analysis of reciprocal-cross hybrids of donkey × horse and cattle×yak (Figure 2D, E). We developed a pipeline to detect genes showing ASE (Figure 1). Based on the exonic FDSs, approximately 76.8% and 67.4% of

expressed genes (13 643 of 17 770 in mule/hinny and 10 378 of 15 399 in dzo) harbored at least three FDSs in the exonic region, which enabled robust calculation of ASE (Supplementary Figure S1). To ensure precision, those genes showing ASE were filtered under the conditions that multiple FDSs (⩾3) and high allelic bias (0.65/0.35) were supported by at least an average of 20 uniquely mapped reads from each sample, with concordance between biological replicates. The expression divergence between the two genetic alleles was greater than the divergence between paternal and maternal alleles (Figure 2F, G). Read number differences between paternal and maternal alleles were also compared. Here, we identified 49 imprinting genes in the mules/hinnies and 40 imprinting genes in the dzos (Supplementary Figure S2) with the same cutoff as ASE genes. Among the expressed genes (FPKM⩾1), 846 (6.5%), 790 (7.3%), and 905 (6.8%) genes showing ASE were identified in the brain, muscle, and skin tissues of mule/hinny, respectively (Figure 3A, B), whereas 883 (8.7%) and 592 (4.8%) genes showing ASE were identified in the liver and ear of dzo, respectively (Figure 3A, B). When we adopted a more permissive threshold of imbalance (0.4–0.6), about 15% of genes showed ASE. Only 109 and 101 genes showing ASE were shared among the three tissues of mule/hinny and two tissues of dzo, respectively (Figure 3A). The results suggest that the genes showing ASE were tissue specific. Principal component analysis was conducted based on the allelic expression ratios (ratios of reads of two alleles), which showed that samples were clustered according to tissue type, further indicating tissue specificity in genes showing ASE (Supplementary Figure S3A, B). For example, in mule/hinny, *HPSG2* was identified as a brain-specific ASE gene (Supplementary Figure S3C) and *ST3GAL1* was identified as a muscle-specific ASE gene (Supplementary Figure S3D).

lncRNAs and pseudogenes are more likely to show ASE

Comparison of the proportions of ASE among the expressed protein-coding genes, lncRNAs, and pseudogenes showed 3.2%–6.7%, 17.3%–22.7%, and 16%–40%, respectively (Figure 3E). In addition, the distribution of allelic expression

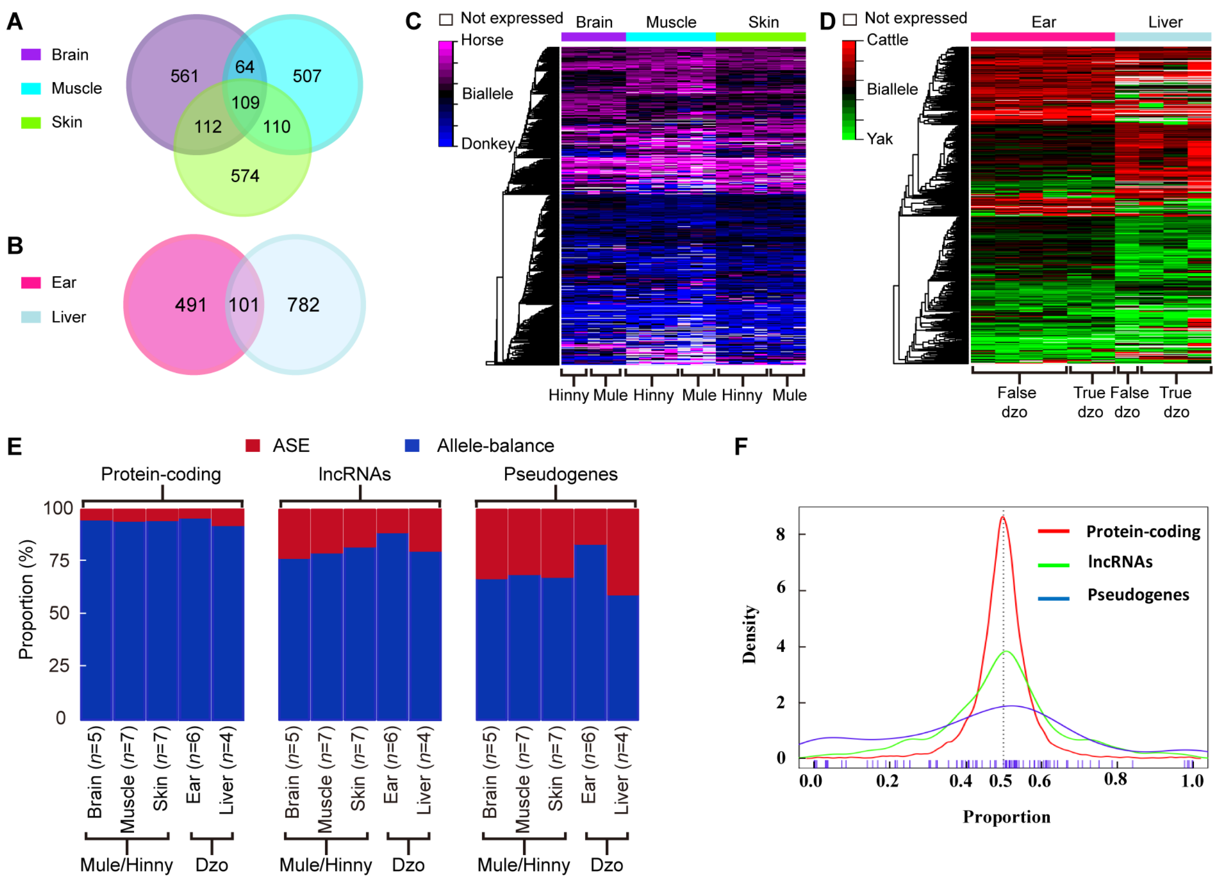

Figure 3 Genes showing ASE in mule/hinny and dzo

Number of shared and unique genes showing ASE in brain, muscle, and skin tissues of mule/hinny (A), and ear and liver tissues of dzo (B). Heatmap of genes showing ASE (*n*=2 037) in brain, muscle, and skin samples of mule/hinny (C), and ear and liver samples of dzo (D). Genes are colored based on ASE score (red-green scale from 100% – 0% horse and cattle allele expression). Side color bar shows tissues. E: Proportion of protein-coding genes, lncRNAs, and pseudogenes showing ASE and allele-balanced expression in all tested tissues of mule/hinny and dzo. Numbers of samples from each tissue are provided. F: Distribution of allelic expression ratios of protein-coding genes, lncRNAs, and pseudogenes.

ratios further indicated that more lncRNAs and pseudogenes tended to show genetic allele biases (Figure 3F). In contrast, analysis of genes showing allele-balanced expression revealed that those genes showing ASE exhibited a higher density of divergent sites in the promoter region (Figure 4A). Consistently, a significantly higher density of divergent sites in the promoter region was observed among the lncRNAs and pseudogenes compared with the protein-coding genes (Figure 4A), which was in accordance with the proportion of ASE in these three gene types (Figure 3E). Thus, the higher proportion of divergent sites in the promoter region of lncRNAs and pseudogenes may be correlated with the evolution of gene expression. In addition, among the closely related species, the expression levels of lncRNAs and pseudogenes showed more rapid changes than that of protein coding genes.

Changes in gene expression due to a lack of selection pressure

We subsequently searched for evidence showing the evolution of gene expression in closely related species under natural selection. First, the gene expression levels of genes showing ASE and allele-balanced expression were compared. As shown in Figure 4B, the expression levels of genes showing ASE were significantly lower than those showing allele-balanced expression in all tested tissues from both mule/hinny and dzo. This suggested that genes with low expression levels in hybrid tissues were more likely to show ASE. In contrast to the gene expression levels, the diversity in expression levels (CV, coefficient of variation of gene expression levels in biological replicates) of genes showing ASE was significantly higher than that of genes showing allele-balanced expression (Figure 4C). This high diversity indicated that the expression of genes showing ASE was not fully restricted, thus suggesting that the change in expression in most genes may have been achieved in the absence of selection pressure. To further explore the evolution of gene expression, the selection pressure (Ka/Ks ratio) of genes was investigated. A slightly higher Ka/Ks ratio was found for genes showing ASE than for genes showing allele-balanced expression; however, the values of these ratios were usually lower than 1 (Figure 4E), indicating that some genes showing

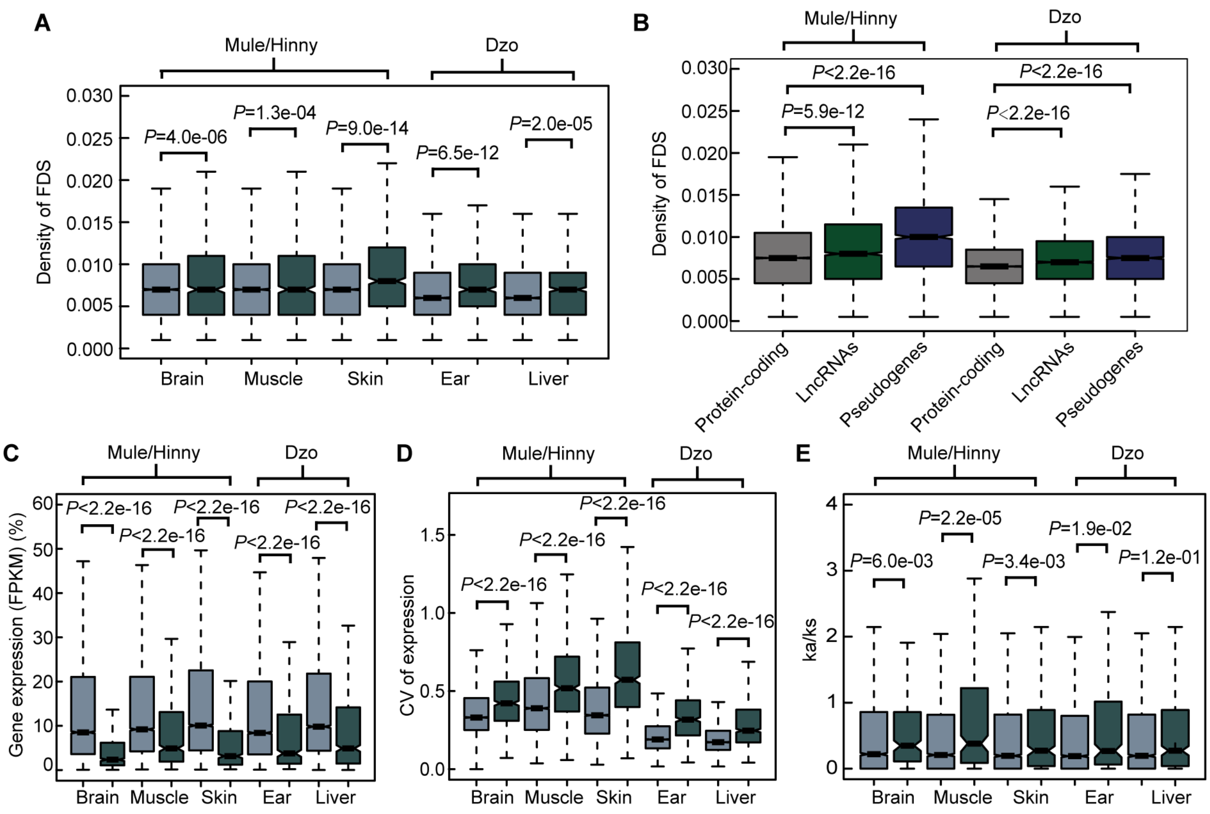

Figure 4 Features of genes showing ASE

A: Densities of FDSs in promoter (2 kb upstream of TSS) of genes showing ASE and genes showing allele-balanced expression. B: Densities of FDSs in promoter of protein-coding genes, lncRNAs, and pseudogenes. C: Distribution of expression levels of genes showing ASE and genes showing allele-balanced expression in all tested tissues. D: Distribution of expression diversities (CV) of genes showing ASE and genes showing allele-balanced expression in all tested tissues. CV: Coefficient of variation of gene expression level in biological replicates. E: Distribution of Ka/Ks values of genes showing ASE and genes showing allele-balanced expression. Genes showing ASE are in dark-gray and genes showing allele-balanced expression are in light-gray. *P*-value was from Wilcoxon test.

ASE were under relaxed selection.

Genes showing ASS are potential contributors to species evolution

Here, ASS events were identified using the hybrid transcriptomes with an assigned genetic allele origin through rMATS (Figure 1). To achieve relatively high-accuracy detection of ASS events, rigorous statistical criteria (|Δψ| > 10%, FDR⩽1%, support reads numbers ⩾100) were used to quantify ASS events. In total, 980 (13.5%), 778 (12.5%), and 839 (11.2%) ASS events were identified in the brain, muscle, and skin tissues of mule/hinny (Table 1), respectively, and 559 (16.7%) and 623 (10.8%) ASS events were identified in the liver and ear of dzo, respectively (Table 1).

We detected the density of FDSs in the splicing exons and adjacent introns of ASS and non-ASS events. As shown in Figure 5A, compared with non-ASS exons, the densities of FDSs in the ASS exons were higher, whereas the densities in upstream and downstream introns showed no differences. These results suggest that the FDSs within the exons may have led to gene splicing evolution. In addition, genes showing ASS had higher expression levels than genes showing ASE in all tested tissues (Figure 5B). In contrast, the diversity in the expression levels of genes showing ASS was lower that of genes showing ASE in all tissues, with exception of the dzo liver (Figure 5C). Thus, the evolution of *cis*-regulatory alternative splicing may be a major contributor to the adaptive evolution of a species and may be equally important to the evolution of gene expression levels.

Genes showing ASE and ASS are involved in species adaptive evolution

Genes showing ASE and ASS in mule/hinny muscle tissue have received considerable attention since the discovery of muscle strength divergence between horses and donkeys (Renaud et al., 2018). Here, four genes showing ASE (i. e., *MYOZ1*, *MYOZ2*, *MYH4*, and *MYBPH*) were detected in all mule/hinny muscle samples (Figure 6A). Notably, *MYOZ1* and *MYOZ2* are members of the same *MYO* gene family, which plays a role in myofibrillogenesis (Takada et al., 2001), with both found to be donkey specific in the current study. In contrast, however, both MYH4 and MYBPH were found to be horse specific (Figure 6A). Thus, these mule/hinny muscle-related genes showing ASE may be responsible for the divergence observed in muscle strength between horses and donkeys. Furthermore, *MYOZ3* and *MYOM2* showed ASS in the mule/hinny muscle samples (Figure 6B). Notably, *MYOZ3* also belongs to the *MYO* gene family, suggesting that the *MYO* gene family may have played an important role in the evolution of muscle strength. Thus, the above results further suggest that changes in both gene expression levels and alternative splicing have played a role in the divergence of muscle strength found between horses and donkeys.

Compared with cattle, yaks exhibit a remarkable adaptive trait to high-altitude hypoxic environments. In the current study, the *ARG2* gene showing ASE was identified in both the liver and ear of dzo (Figure 6C). *ARG2* has been identified previously as a hypoxia-related and rapidly evolving gene in yak (Qiu, 2012). In addition, the *ATP12A* gene showing ASE was identified with high expression in the yak allele of dzo (Figure 6C). This gene has been identified previously as a hypoxia-related gene in Tibetan antelope (Ge et al., 2013). In addition, we also identified *ENTPD5* and *SULT1A1* as dzo genes showing ASS (Figure 6D). These two genes are involved in metabolic processes (Gamage et al., 2006; Huitema et al., 2012), and thus may also contribute to the high-altitude adaptation of yak. Thus, the above results provide preliminary evidence demonstrating that genes showing ASE and ASS may participate in the regulation of muscle strength in mule/hinny and high-altitude adaptation in dzo.

Table 1 ASS events in mule/hinny and dzo

Species	Tissue	Event type	SE	RI	MXE	A3SS	A5SS	Total
Mule/Hinny	Brain	Total splicing events	4849	151	1246	692	337	7275
		ASS events	612	23	198	75	72	980
		ASS ratio	0.126	0.152	0.159	0.108	0.214	0.135
	Muscle	Total splicing events	3992	129	1406	460	262	6249
		ASS events	458	19	193	52	56	778
		ASS ratio	0.115	0.147	0.137	0.113	0.214	0.125
	Skin	Total splicing events	4857	196	1401	660	351	7465
		ASS events	489	31	190	72	57	839
		ASS ratio	0.101	0.158	0.136	0.109	0.162	0.112
Dzo	Liver	Total splicing events	2078	108	555	423	191	3355
		ASS events	308	23	106	76	46	559
		ASS ratio	0.148	0.213	0.191	0.180	0.241	0.167
	Ear	Total splicing events	3726	203	922	616	293	5760
		ASS events	352	47	112	59	53	623
		ASS ratio	0.094	0.232	0.121	0.096	0.181	0.108

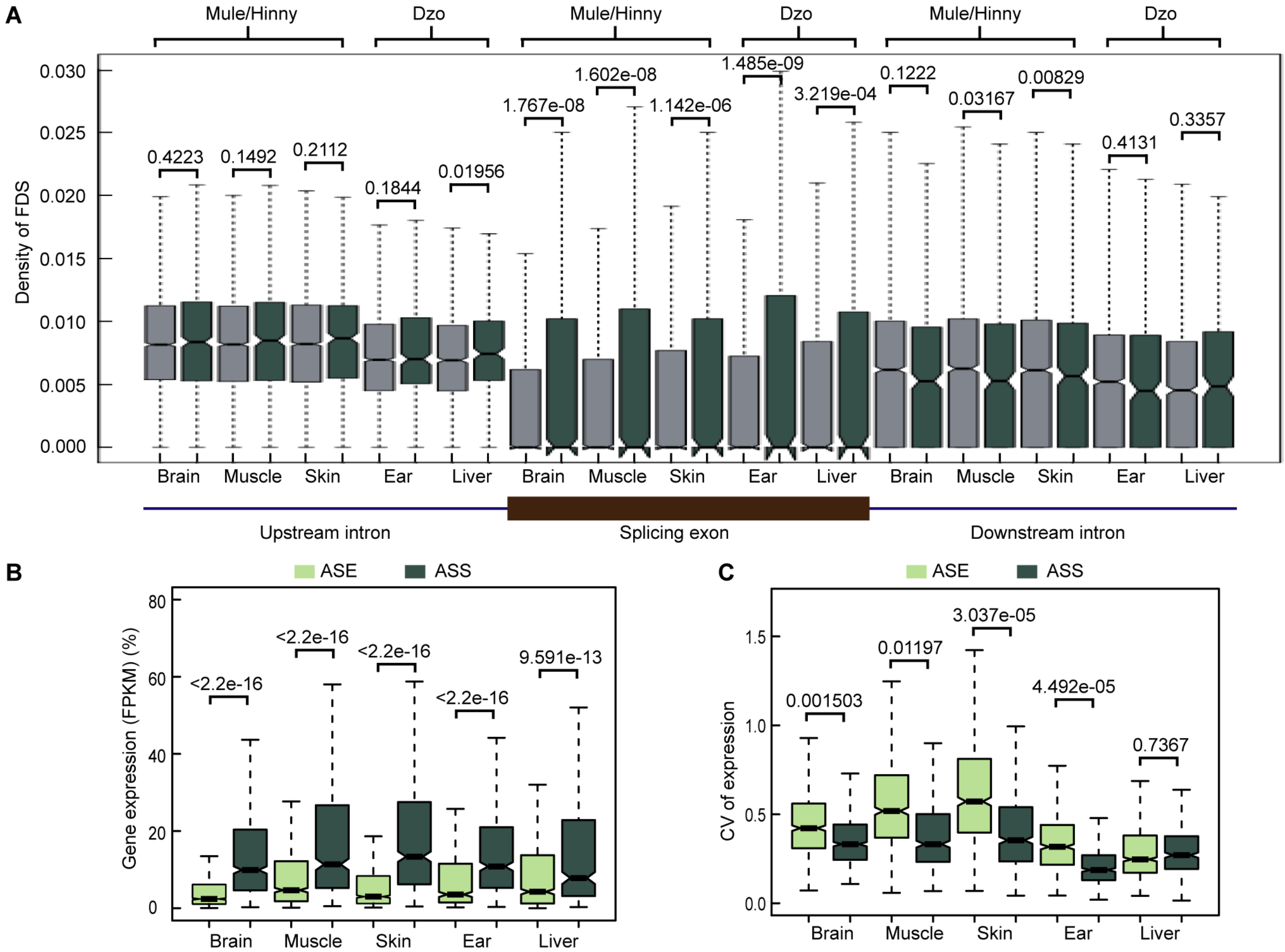

Figure 5 Features of genes showing ASS

A: Densities of FDSs in exons, upstream introns, and downstream introns of ASS and non-ASS events (Wilcoxon test). B: Comparison of expression levels of genes showing ASE and genes showing ASS. C: Comparison of expression diversities (comparison of genes) of genes showing ASE and genes showing ASS.

DISCUSSION

To date, most previous studies on genes showing ASE have been conducted on model organisms, e.g., mouse (Crowley, 2015; Gao, 2015). As their hybrids can be difficult to obtain, few studies have been reported on genes showing ASE in large mammals, particularly in regard to changes in gene expression in animal speciation and evolution. In this study, we obtained the ASE and ASS genetic profiles of horse×donkey and cattle×yak hybrids to reveal differences in gene expression and alternative splicing between closely related species. The use of closely related species with more FDSs allows for the robust and precise identification of genes showing ASE and ASS.

Protein-coding genes and lncRNAs are known to contribute to species evolution (Babbitt et al., 2010). However, previous study has indicated that the sequences of lncRNAs change more rapidly than those of protein-coding genes (Johnsson et al., 2014). For example, in humans, one of the most rapidly evolved regions ("human accelerated regions") from chimpanzees, i.e., HAR1, is a noncoding RNA gene (Pollard et al., 2006). Compared with protein-coding genes, we found that lncRNAs were more likely to show ASE. Hence, our results indicated that the expression levels of lncRNAs were also rapidly evolving between closely related species. Similar to lncRNAs, pseudogenes, which are regarded as dysfunctional DNA sequences without selective constraints and are thus silenced last (Mira, 2005), also tended to show ASE. Some detected pseudogenes showing ASE may be in the process of elimination, i.e., are expressed in one species but not in another, thus resulting in ASE. As such, most gene expression changes (e.g., ASE) may be neutral and not under evolutionary selection. However, some gene expression changes may contribute to adaptive evolution; for example, the ASE genes (*MYOZ1*, *MYOZ2*, *MYH4*, and *MYBPH*) involved in the regulation of muscle strength in mule/hinny.

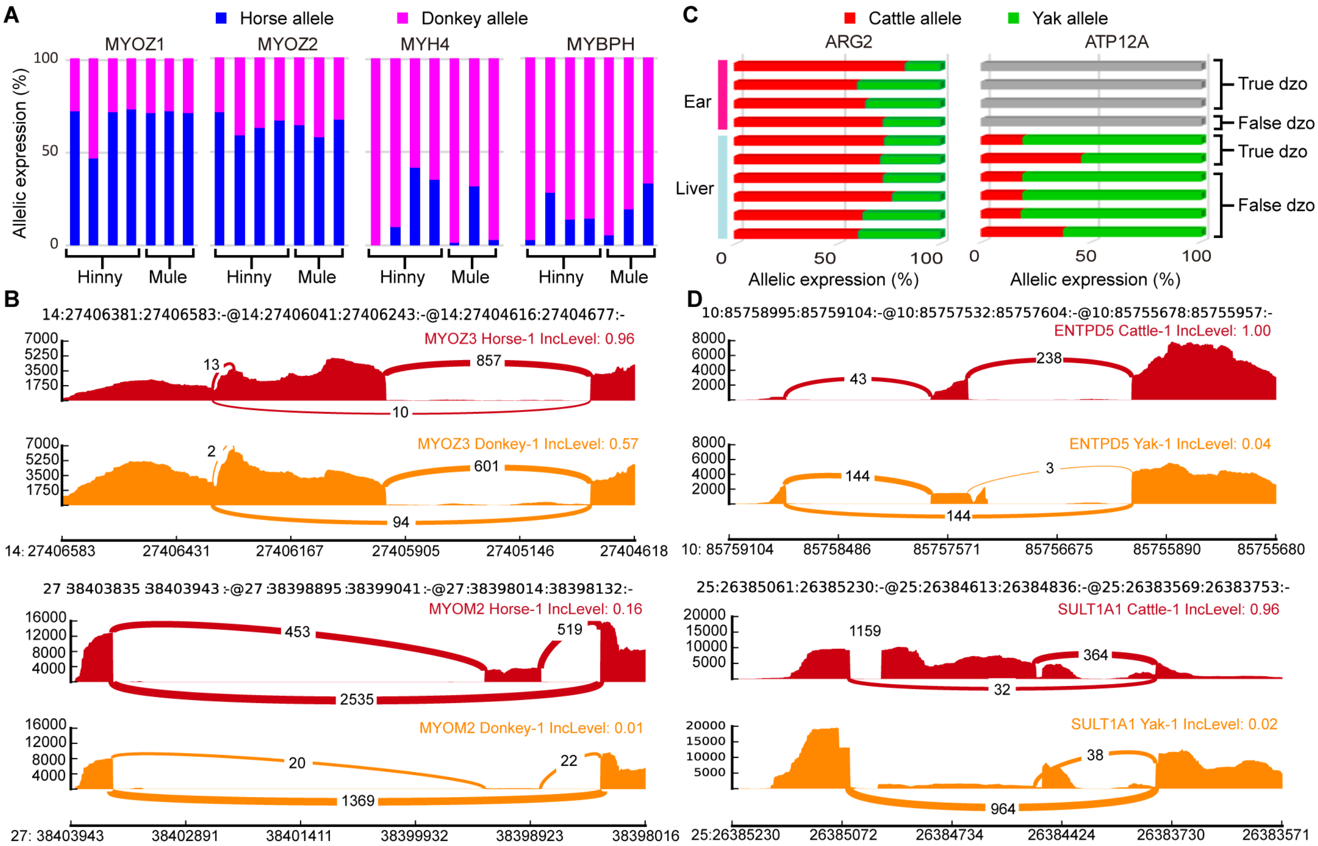

Figure 6 Functional analysis of genes showing ASE and ASS

A: Allelic expression ratios of four muscle function-related ASE genes, *MYOZ1*, *MYOZ2*, *MYH4*, and *MYBPH*, in mule/hinny muscle samples. Horse allele (blue); donkey allele (purple). B: Sashimi plot of muscle-related genes showing ASS, *MYOZ3*, and *MYOM2*, in mule/hinny muscle samples. Read densities supporting inclusion and exclusion of exons are shown. C: Proportion of *ARG2* and *ATP12A* expression levels from cattle allele (red) or yak allele (green) in four liver and six ears samples of dzo. Gray bar indicates no expression. D: Sashimi plot of two genes showing ASS (*ENTPD5* and *SULT1A1*) in dzo. Read densities supporting inclusion and exclusion of exons are shown.

These results are coincident with most genetic changes being neutral, with only a few being under positive selection. Thus, while many ASE genes may be evolutionary neutral, some may be related to the adaptive evolution of a species. Here, in each tested mule/hinny and dzo tissue using cutoff ratios of below 0.35 and above 0.65 (Wang, 2013), approximately 5% of expressed genes were identified as showing ASE. However, previous research on mice (Pinter, 2015) and *Drosophila* (León-Novelo et al., 2017) observed 20% ASE genes. We thus applied a more permissive threshold of imbalance (0.4−0.6), with results indicating that about 15% of genes showed ASE. However, to be consistent with the pipeline in Wang et al. (2013), we still used the gene list with the cutoff of 0.35−0.65. Based on this, our results suggested that most *cis*-regulatory effects on gene expression did not differ between closely related species. This is consistent with the view that gene expression evolution is conserved and strongly shaped by purifying selection (Jordan, 2004; Liao & Zhang, 2006; Zheng-Bradley et al., 2010). In addition, genes showing ASE had lower expression levels, higher expression diversity, and slightly higher Ka/Ks ratios than genes showing allele-balanced expression. These results indicate that the changes in the expression levels of most genes may have occurred in the absence of selection pressure. Gene alternative splicing is actually more prevalent than previously anticipated, with more than 90% of human genes possessing different transcription isoforms (Wang et al., 2008). We discovered that more than 10% of alternative splicing events showed significant differences between related species, which was higher than that found for ASE. In addition, the expression levels of genes showing ASS were higher than those showing ASE, whereas the diversity in the expression of genes showing ASS was lower than that for genes showing ASE. In conclusion, our study demonstrated that both gene expression and alternative splicing contribute to the divergence between closely related species.

COMPETING INTERESTS

The authors declare that they have no competing interests.

AUTHORS' CONTRIBUTIONS

Y.J. designed the study. Y.W., S.G., Y.Z., W.H.C., J.J.S, N.N.W. and M.L. performed bioinformatics analysis. G.X.Z., L.W., W.J.S., J.T.X. and W.D.D collected the samples and extracted RNA. Y.W. wrote the manuscript with the other authors' input. Y.J., W.W. and Y.L.C. revised the manuscript. All authors read and approved the final version of the manuscript.

ACKNOWLEDGEMENTS

We thank the High-Performance Computing Center (HPC) of Northwest A&F University (NWAFU) for providing computing resources. We are grateful for the magazine cover provider: Petr Meissner (picture link: https://www.flickr.com/photos/myneur/albums).

REFERENCES

Babbitt CC, Fedrigo O, Pfefferle AD, Boyle AP, Horvath JE, Furey TS, Wray GA. 2010. Both noncoding and protein-coding RNAs contribute to gene expression evolution in the Primate Brain. *Genome Biology and Evolution*, **2**: 67–79.

Bellucci E, Bitocchi E, Ferrarini A, Benazzo A, Biagetti E, Klie S, Minio A, Rau D, Rodriguez M, Panziera A, Venturini L, Attene G, Albertini E, Jackson SA, Nanni L, Fernie AR, Nikoloski Z, Bertorelle G, Delledonne M, Papa R. 2014. Decreased nucleotide and expression diversity and modified coexpression patterns characterize domestication in the Common Bean. *The Plant Cell*, **26**(5): 1901–1912.

Bolger AM, Lohse M, Usadel B. 2014. Trimmomatic: a flexible trimmer for Illumina sequence data. *Bioinformatics*, **30**(15): 2114–2120.

Brown JB, Boley N, Eisman R, May GE, Stoiber MH, Duff MO, Booth BW, Wen J, Park S, Suzuki AM, Wan KH, Yu C, Zhang D, Carlson JW, Cherbas L, Eads BD, Miller D, Mockaitis K, Roberts J, Davis CA, Frise E, Hammonds AS, Olson S, Shenker S, Sturgill D, Samsonova AA, Weiszmann R, Robinson G, Hernandez J, Andrews J, Bickel PJ, Carninci P, Cherbas P, Gingeras TR, Hoskins RA, Kaufman TC, Lai EC, Oliver B, Perrimon N, Graveley BR, Celniker SE. 2014. Diversity and dynamics of the Drosophila transcriptome. *Nature*, **512**(7515): 393–399.

Crowley JJ, Zhabotynsky V, Sun W, Huang S, Pakatci IK, Kim Y, Wang JR, Morgan AP, Calaway JD, Aylor DL, Yun Z, Bell TA, Buus RJ, Calaway ME, Didion JP, Gooch TJ, Hansen SD, Robinson NN, Shaw GD, Spence JS, Quackenbush CR, Barrick CJ, Nonneman RJ, Kim K, Xenakis J, Xie Y, Valdar W, Lenarcic AB, Wang W, Welsh CE, Fu C, Zhang Z, Holt J, Guo Z, Threadgill DW, Tarantino LM, Miller DR, Zou F, Mcmillan L, Sullivan PF, De Villena FP. 2015. Analyses of allele-specific gene expression in highly divergent mouse crosses identifies pervasive allelic imbalance. *Nature Genetics*, **47**: 353–360.

Eckersley-Maslin MA, Spector DL. 2014. Random monoallelic expression: regulating gene expression one allele at a time. *Trends in Genetics*, **30**(6): 237–244.

Forrest ARR, Kawaji H, Rehli M, Baillie JK, de Hoon MJL, Haberle V, Lassmann T, Kulakovskiy IV, Lizio M, Itoh M, Andersson R, Mungall CJ, Meehan TF, Schmeier S, Bertin N, Jorgensen M, Dimont E, Arner E, Schmidl C, Schaefer U, Medvedeva YA, Plessy C, Vitezic M, Severin J, Semple C, Ishizu Y, Young RS, Francescatto M, Alam I, Albanese D, Altschuler GM, Arakawa T, Archer JA, Arner P, Babina M, Rennie S, Balwierz PJ, Beckhouse AG, Pradhan-Bhatt S, Blake JA, Blumenthal A, Bodega B, Bonetti A, Briggs J, Brombacher F, Burroughs AM, Califano A, Cannistraci CV, Carbajo D, Chen Y, Chierici M, Ciani Y, Clevers HC, Dalla E, Davis CA, Detmar M, Diehl AD, Dohi T, Drablos F, Edge AS, Edinger M, Ekwall K, Endoh M, Enomoto H, Fagiolini M, Fairbairn L, Fang H, Farach-Carson MC, Faulkner GJ, Favorov AV, Fisher ME, Frith MC, Fujita R, Fukuda S, Furlanello C, Furino M, Furusawa J, Geijtenbeek TB, Gibson AP, Gingeras T, Goldowitz D, Gough J, Guhl S, Guler R, Gustincich S, Ha TJ, Hamaguchi M, Hara M, Harbers M, Harshbarger J, Hasegawa A, Hasegawa Y, Hashimoto T, Herlyn M, Hitchens KJ, Ho SS, Hofmann OM, Hoof I, Hori F, Huminiecki L, Iida K, Ikawa T, Jankovic BR, Jia H, Joshi A, Jurman G, Kaczkowski B, Kai C, Kaida K, Kaiho A, Kajiyama K, Kanamori-Katayama M, Kasianov AS, Kasukawa T, Katayama S, Kato S, Kawaguchi S, Kawamoto H, Kawamura YI, Kawashima T, Kempfle JS, Kenna TJ, Kere J, Khachigian LM, Kitamura T, Klinken SP, Knox AJ, Kojima M, Kojima S, Kondo N, Koseki H, Koyasu S, Krampitz S, Kubosaki A, Kwon AT, Laros JF, Lee W, Lennartsson A, Li K, Lilje B, Lipovich L, Mackay-Sim A, Manabe R, Mar JC, Marchand B, Mathelier A, Mejhert N, Meynert A, Mizuno Y, de Lima MD, Morikawa H, Morimoto M, Moro K, Motakis E, Motohashi H, Mummery CL, Murata M, Nagao-Sato S, Nakachi Y, Nakahara F, Nakamura T, Nakamura Y, Nakazato K, van Nimwegen E, Ninomiya N, Nishiyori H, Noma S, Noma S, Noazaki T, Ogishima S, Ohkura N, Ohimiya H, Ohno H, Ohshima M, Okada-Hatakeyama M, Okazaki Y, Orlando V, Ovchinnikov DA, Pain A, Passier R, Patrikakis M, Persson H, Piazza S, Prendergast JG, Rackham OJ, Ramilowski JA, Rashid M, Ravasi T, Rizzu P, Roncador M, Roy S, Rye MB, Saijyo E, Sajantila A, Saka A, Sakaguchi S, Sakai M, Sato H, Savvi S, Saxena A, Schneider C, Schultes EA, Schulze-Tanzil GG, Schwegmann A, Sengstag T, Sheng G, Shimoji H, Shimoni Y, Shin JW, Simon C, Sugiyama D, Sugiyama T, Suzuki M, Suzuki N, Swoboda RK, Hoen PAC, Tagami M, Takahashi N, Takai J, Tanaka H, Tatsukawa H, Tatum Z, Thompson M, Toyodo H, Toyoda T, Valen E, van de Wetering M, van den Berg LM, Verado R, Vijayan D, Vorontsov IE, Wasserman WW, Watanabe S, Wells CA, Winteringham LN, Wolvetang E, Wood EJ, Yamaguchi Y, Yamamoto M, Yoneda M, Yonekura Y, Yoshida S, Zabierowski SE, Zhang PG, Zhao X, Zucchelli S, Summers KM, Suzuki H, Daub CO, Kawai J, Heutink P, Hide W, Freeman TC, Lenhard B, Bajic VB, Taylor MS, Makeev VJ, Sandelin A, Hume DA, Carninci P, Hayashizaki Y. 2014. A promoter-level mammalian expression atlas. *Nature*, **507**(7493): 462–470.

Gamage N, Barnett A, Hempel N, Duggleby RG, Windmill KF, Martin JL, Mcmanus ME. 2006. Human sulfotransferases and their role in chemical metabolism. *Toxicological Sciences*, **90**(1): 5–22.

Gao Q, Sun W, Ballegeer M, Libert C, Chen W. 2015. Predominant contribution of cis-regulatory divergence in the evolution of mouse alternative splicing. *Molecular Systems Biology*, **11**(7): 816.

Ge RL, Cai Q, Shen YY, San A, Ma L, Zhang Y, Yi X, Chen Y, Yang L, Huang Y, He R, Hui Y, Hao M, Li Y, Wang B, Ou X, Xu J, Zhang Y, Wu K, Geng C, Zhou W, Zhou T, Irwin DM, Yang Y, Ying L, Bao H, Kim J, Larkin DM, Ma J, Lewin HA, Xing J, Platt RN, Ray DA, Auvil L, Capitanu B, Zhang X, Zhang G, Murphy RW, Wang J, Zhang YP, Wang J. 2013. Draft genome sequence of the Tibetan antelope. *Nature Communications*, **4**: 1858.

Huitema LFA, Apschner A, Logister I, Spoorendonk KM, Bussmann J, Hammond CL, Schulte-Merker S. 2012. Entpd5 is essential for skeletal mineralization and regulates phosphate homeostasis in zebrafish. *Proceedings of the National Academy of Sciences*, **109**(52): 21372–21377.

Johnsson P, Lipovich L, Grandér D, Morris KV. 2014. Evolutionary conservation of long non-coding RNAs; sequence, structure, function. *Biochimica Biophysica Acta*, **1840**(3): 1063–1071.

Jordan IK, Mariño-Ramírez L, Wolf YI, Koonin EV. 2004. Conservation and coevolution in the scale-free human gene coexpression network. *Molecular Biology and Evolution*, **21**(11): 2058–2070.

Keane TM, Goodstadt L, Danecek P, White MA, Wong K, Yalcin B, Heger A, Agam A, Slater G, Goodson M, Furlotte NA, Eskin E, Nellåker C, Whitley H, Cleak J, Janowitz D, Hernandez-Pliego P, Edwards A, Belgard TG, Oliver PL, Mcintyre RE, Bhomra A, Nicod J, Gan X, Yuan W, van der Weyden L, Steward CA, Bala S, Stalker J, Mott R, Durbin R, Jackson IJ, Czechanski A, Guerra-Assunção JA, Donahue LR, Reinholdt LG, Payseur BA, Ponting CP, Birney E, Flint J, Adams DJ. 2011. Mouse genomic variation and its effect on phenotypes and gene regulation. *Nature*, **477**(7364): 289–294.

Kim D, Langmead B, Salzberg SL. 2015. HISAT: a fast spliced aligner with low memory requirements. *Nature Methods*, **12**(4): 357–360.

Kwan T, Benovoy D, Dias C, Gurd S, Provencher C, Beaulieu P, Hudson TJ, Sladek R, Majewski J. 2008. Genome-wide analysis of transcript isoform variation in humans. *Nature Genetics*, **40**(2): 225–231.

León-Novelo L, Gerken AR, Graze RM, Mcintyre LM, Marroni F. 2018. Direct testing for allele-specific expression differences between conditions. *G*3, **8**(2): g3–g300139.

Li H, Durbin R. 2009. Fast and accurate short read alignment with Burrows-Wheeler transform. *Bioinformatics*, **25**(14): 1754–1760.

Liao BY, Zhang J. 2006. Evolutionary conservation of expression profiles between human and mouse orthologous genes. *Molecular Biology and Evolution*, **23**(3): 530–540.

Mira A, Pushker R. 2005. The silencing of pseudogenes. *Molecular Biology and Evolution*, **22**(11): 2135–2138.

Orlando L, Ginolhac A, Zhang G, Froese D, Albrechtsen A, Stiller M, Schubert M, Cappellini E, Petersen B, Moltke I, Johnson PLF, Fumagalli M, Vilstrup JT, Raghavan M, Korneliussen T, Malaspinas A, Vogt J, Szklarczyk D, Kelstrup CD, Vinther J, Dolocan A, Stenderup J, Velazquez AMV, Cahill J, Rasmussen M, Wang X, Min J, Zazula GD, Seguin-Orlando A, Mortensen C, Magnussen K, Thompson JF, Weinstock J, Gregersen K, Røed KH, Eisenmann V, Rubin CJ, Miller DC, Antczak DF, Bertelsen MF, Brunak S, Al-Rasheid KAS, Ryder O, Andersson L, Mundy J, Krogh A, Gilbert MTP, Kjær K, Sicheritz-Ponten T, Jensen LJ, Olsen JV, Hofreiter M, Nielsen R, Shapiro B, Wang J, Willerslev E. 2013. Recalibrating Equus evolution using the genome sequence of an early Middle Pleistocene horse. *Nature*, **499**(7456): 74–78.

Pertea M, Kim D, Pertea GM, Leek JT, Salzberg SL. 2016. Transcript-level expression analysis of RNA-seq experiments with HISAT, StringTie and Ballgown. *Nature Protocols*, **11**(9): 1650–1667.

Pinter SF, Colognori D, Beliveau BJ, Sadreyev RI, Payer B, Yildirim E, Wu CT, Lee JT. 2015. Allelic imbalance is a prevalent and Tissue-Specific Feature of the Mouse Transcriptome. *Genetics*, **200**(2): 537–549.

Pollard KS, Salama SR, Lambert N, Lambot MA, Coppens S, Pedersen JS, Katzman S, King B, Onodera C, Siepel A, Kern AD, Dehay C, Igel H, Ares MJ, Vanderhaeghen P, Haussler D. 2006. An RNA gene expressed during cortical development evolved rapidly in humans. *Nature*, **443**(7108): 167–172.

Prabhakar S, Visel A, Akiyama JA, Shoukry M, Lewis KD, Holt A, Plajzer-Frick I, Morrison H, Fitzpatrick DR, Afzal V, Pennacchio LA, Rubin EM, Noonan JP. 2008. Human-specific gain of function in a developmental enhancer. *Science*, **321**(5894): 1346–1350.

Qiu Q, Zhang G, Ma T, Qian W, Wang J, Ye Z, Cao C, Hu Q, Kim J, Larkin DM, Auvil L, Capitanu B, Ma J, Lewin HA, Qian X, Lang Y, Zhou R, Wang L, Wang K, Xia J, Liao S, Pan S, Lu X, Hou H, Wang Y, Zang X, Yin Y, Ma H, Zhang J, Wang Z, Zhang Y, Zhang D, Yonezawa T, Hasegawa M, Zhong Y, Liu W, Zhang Y, Huang Z, Zhang S, Long R, Yang H, Wang J, Lenstra JA, Cooper DN, Wu Y, Wang J, Shi P, Wang J, Liu J. 2012. The yak genome and adaptation to life at high altitude. *Nature Genetics*, **44**(8): 946–949.

Renaud G, Petersen B, Seguin-Orlando A, Bertelsen MF, Waller A, Newton R, Paillot R, Bryant N, Vaudin M, Librado P, Orlando L. 2018. Improved de novo genomic assembly for the domestic donkey. *Science advances*, **4**(4): q392.

Shen S, Park JW, Lu Z, Lin L, Henry MD, Wu YN, Zhou Q, Xing Y. 2014. rMATS: Robust and flexible detection of differential alternative splicing from replicate RNA-Seq data. *Proceedings of the National Academy of Sciences*, **111**(51): E5593–E5601.

Storer BE, Kim C. 1990. Exact properties of some exact test statistics for comparing two binomial proportions. *Journal of the American Statistical Association*, **85**(409): 146–155.

Takada F, Woude DLV, Tong HQ, Thompson TG, Watkins SC, Kunkel LM, Beggs AH. 2001. Myozenin: an alpha-actinin- and gamma-filamin-binding protein of skeletal muscle Z lines. *Proceedings of the National Academy of Sciences of the United States of America*, **98**(4): 1595–1600.

Tirosh I, Reikhav S, Levy AA, Barkai N. 2009. A yeast hybrid provides insight into the evolution of gene expression regulation. *Science*, **324**(5927): 659–662.

Trapnell C, Pachter L, Salzberg SL. 2009. TopHat: discovering splice junctions with RNA-Seq. *Bioinformatics*, **25**(9): 1105–1111.

Villar D, Berthelot C, Aldridge S, Rayner TF, Lukk M, Pignatelli M, Park TJ, Deaville R, Erichsen JT, Jasinska AJ, Turner JMA, Bertelsen MF, Murchison EP, Flicek P, Odom DT. 2015. Enhancer evolution across 20 mammalian species. *Cell*, **160**(3): 554–566.

Wang ET, Sandberg R, Luo S, Khrebtukova I, Zhang L, Mayr C, Kingsmore SF, Schroth GP, Burge CB. 2008. Alternative isoform regulation in human tissue transcriptomes. *Nature*, **456**(7221): 470–476.

Wang X, Miller DC, Harman R, Antczak DF, Clark AG. 2013. Paternally expressed genes predominate in the placenta. *Proceedings of the National Academy of Sciences of the United States of America*, **110**(26): 10705–10710.

Wood DLA, Nones K, Steptoe A, Christ A, Harliwong I, Newell F, Bruxner TJC, Miller D, Cloonan N, Grimmond SM. 2015. Recommendations for accurate resolution of gene and isoform Allele-Specific Expression in RNA-Seq Data. *PLoS One*, **10**(5): e126911.

Zhang Z, Li J, Zhao XQ, Wang J, Wong GK, Yu J. 2006. KaKs_Calculator: calculating Ka and Ks through model selection and model averaging. *Genomics, Proteomics & Bioinformatics*, **4**(4): 259–263.

Zheng-Bradley X, Rung J, Parkinson H, Brazma A. 2010. Large scale comparison of global gene expression patterns in human and mouse. *Genome Biology*, **11**(12): R124.

Effect of temperature on antioxidant defense and innate immunity in Brandt's voles

De-Li Xu[1,2], Meng-Meng Xu[2], De-Hua Wang[2,*]

[1] *College of Life Sciences*, *Qufu Normal University*, *Qufu Shandong* 273165, *China*

[2] *State Key Laboratory of Integrated Management of Pest Insects and Rodents*, *Institute of Zoology*, *Chinese Academy of Sciences*, *Beijing* 100101, *China*

ABSTRACT

Ambient temperature is an important factor influencing many physiological processes, including antioxidant defense and immunity. In the present study, we tested the hypothesis that antioxidant defense and immunity are suppressed by high and low temperature treatment in Brandt's voles (*Lasiopodomys brandtii*). Thirty male voles were randomly assigned into different temperature groups (4, 23, and 32 °C, *n*=10 for each group), with the treatment course lasting for 27 d. Results showed that low temperature increased gross energy intake (GEI) and liver, heart, and kidney mass, but decreased body fat mass and dry carcass mass. With the decline in temperature, hydrogen peroxide (H_2O_2) concentration, which is indicative of reactive oxygen species (ROS) levels, increased in the liver, decreased in the heart, and was unchanged in the kidney, testis, and small intestine. Lipid peroxidation indicated by malonaldehyde (MDA) content in the liver, heart, kidney, testis, and small intestine did not differ among groups, implying that high and low temperature did not cause oxidative damage. Similarly, superoxide dismutase (SOD) and catalase (CAT) activities and total antioxidant capacity (T-AOC) in the five tissues did not respond to low or high temperature, except for elevation of CAT activity in the testis upon cold exposure. Bacteria killing capacity, which is indicative of innate immunity, was nearly suppressed in the 4 °C group in contrast to the 23 °C group, whereas spleen mass and white blood cells were unaffected by temperature treatment. The levels of testosterone, but not corticosterone, were influenced by temperature treatment, though neither were correlated with innate immunity, H_2O_2 and MDA levels, or SOD, CAT, and T-AOC activity in any detected tissues. Overall, these results showed that temperature had different influences on oxidative stress, antioxidant enzymes, and immunity, which depended on the tissues and parameters tested. Up-regulation or maintenance of antioxidant defense might be an important mechanism for voles to survive highly variable environmental temperatures.

Keywords: Antioxidant defense; Brandt's voles (*Lasiopodomys brandtii*); Immunity; Temperature

INTRODUCTION

Ambient temperature is an important factor influencing many physiological processes in animals, including antioxidant defense and immune function (King, 2004; Marnila & Lilius, 2015). While antioxidant defense can eliminate reactive oxygen species (ROS), oxidative stress can occur when ROS production overwhelms antioxidant capacity (Dickinson & Chang, 2011; Selman et al., 2013). Oxidative stress can cause oxidative damage to biomolecules (i.e., lipids, proteins, and DNA) and is deleterious to the structure and function of cells and tissues (Marri & Richner, 2015; Raut et al., 2012). The immune system, which protects animals from infection and pathogens, plays a key role in survival and fitness (Owens & Wilson, 1999; Sheldon &Verhulst, 1996). Therefore, both antioxidant capacity and immune function are crucial for animals to maintain health and survival; however, both are markedly influenced by environmental temperature (Carroll et al., 2012; Metcalfe & Alonso-Alvarez, 2010; Zhou et al., 2015).

Received: 30 December 2018; Accepted: 22 March 2019; Online: 10 April 2019

Foundation items: This study was supported by the National Natural Science Foundation of China (31770444) and the State Key Laboratory of Integrated Management of Pest Insects and Rodents (IPM1906)

*Corresponding author, E-mail: wangdh@ioz.ac.cn

DOI: 10.24272/j.issn.2095-8137.2019.045

Several researchers have investigated the impact of temperature on antioxidant defense. For instance, cold exposure in rats has been shown to increase lipid peroxidation in the brain but decrease it in the liver (Lomakina, 1980) and enhance superoxide dismutase (SOD) activity in the heart and kidney but suppress it in the lungs and pancreas (Vasilijević et al., 2007; Yuksel et al., 2008). Moreover, cold stress is reported to increase protein oxidation in the liver and muscle but not affect brown adipose tissue in short-tailed field voles (*Microtus agrestis*) (Selman et al., 2000, 2002, 2008). Lipid peroxidation, total antioxidant capacity (T-AOC), and glutathione peroxidase activity in brown adipose tissue has been shown to increase under low temperature but decrease under high temperature in striped hamsters (*Cricetulus barabensis*) (Zhou et al., 2015). Furthermore, high temperature exposure has been shown to cause oxidative damage in broiler chickens (Tan et al., 2010) and decrease SOD activity in rat testes (Kanter et al., 2013).

Bacteria killing capacity, which entails phagocytes, opsonizing proteins, and natural antibodies acting against specific pathogens, has been used to evaluate innate immunity in mammals (Demas et al., 2011; Tieleman et al., 2005). Immune organs and total white blood cells (WBC) are indirect parameters indicative of immune function (Calder & Kew, 2002). A larger spleen is representative of a stronger immune system (Smith & Hunt, 2004), and adipose tissue is no longer regarded as a simple passive energy reserve but also as an important endocrine and immune organ (Ahima & Flier, 2000; Fantuzzi, 2005; Trayhurn, 2005). Although investigators have examined the impact of temperature on immunity in laboratory animals, including mice (Xu et al., 1992) and rats (Kozyreva & Eliseeva, 2000, 2004), research on wild rodents remains scarce or contradictory. For instance, both cellular immunity and bacteria killing capacity are reported to be unaffected by low and high temperature in female Mongolian gerbils (*Meriones unguiculatus*) (Yang et al., 2013).

Stressful conditions, such as cold or hot temperatures, can stimulate the hypothalamic-pituitary-adrenal axis, and hence secretion of glucocorticoids such as corticosterone, which is related to oxidative damage and immunity (Kim et al., 2013; Sapolsky et al., 2000). Moreover, testosterone incurs oxidative costs such as increased production of ROS according to the oxidation handicap hypothesis (Alonso-Alvarez et al., 2007, 2008). Testosterone also has suppressive effects on immune function in many species, including mammals and birds (Trigunaite et al., 2015).

Brandt's voles (*Lasiopodomys brandtii*) are primarily distributed in the grasslands of Inner Mongolia in China as well as the Republic of Mongolia and the Baikal region of Russia (Li et al., 2010; Walker, 1968). They are strictly herbivorous and feed mainly on grass (Wang et al., 2003). The climate is arid and characterized by warm, dry summers (maximum 42.6 °C) and cold winters (minimum −47.5 °C) (Chen, 1988; Zhao & Wang, 2006). Thus, this species experiences considerable seasonal fluctuations in temperature, photoperiod, and food availability (Wang et al., 2000; Zhang & Wang, 1998). Previous research has shown that resting metabolic rate (RMR) and uncoupling protein 1 (UCP1) content increase but body fat mass decreases in voles upon cold exposure (Liu et al., 2009; Wang, 2007). Both immune responses (Demas, 2004; Martin et al., 2003) and oxidative stress come at a cost (Dowling & Simmons, 2009) and life-history trade-off (Hall et al., 2010; Martin et al., 2007; Monaghan et al., 2009). Therefore, we expect that low and high temperature exposure should cause oxidative stress and immunosuppression in voles.

MATERIAL AND METHODS

Animals and experimental design

Animals used in this study were the offspring of a captive colony trapped on the Inner Mongolian grasslands in May 1999 and brought to the animal facility at the Institute of Zoology, Chinese Academy of Sciences, Beijing, China. All animal procedures were licensed under the Institutional Animal Care and Use Committee of the Institute of Zoology, Chinese Academy of Sciences (approval number: QFNUDW2012016; approval date: 20120628). The animals were housed individually after weaning in plastic cages (30 cm×15 cm×20 cm) with sawdust as bedding under a constant photoperiod (16 h:8 h light-dark cycle) and temperature (23±1 °C). Rabbit pellet chow and water were provided *ad libitum*. Thirty male voles (aged 4–6 months) were randomly assigned into the cold (4±1 °C) (n=10), warm (23±1 °C) (n=10), and hot groups (32±1 °C) (n=10) (hereafter referred to as the 4 °C, 23 °C, and 32 °C groups). The treatment course lasted for 27 d. One vole escaped after 13 d of cold treatment and another vole died after 16 d of cold treatment. Therefore, these two voles were not included in subsequent statistical analyses.

Energy intake

Body mass was recorded every 3 d and energy budgets were determined at 3-d intervals over the course of the study. Food intake was measured in metabolic cages, as described previously (Xu & Wang, 2011; Xu et al., 2011). Food was provided quantitatively. Food residue and feces were collected from each subject over 3 d before acclimation began and during the course of treatment and were separated after they were dried at 60 °C to a constant mass (Liu et al., 2003). Energy content of the food and feces was determined using a Parr 1281 oxygen bomb calorimeter (Parr Instrument, USA). Gross energy intake (GEI) was calculated according to Grodzinski & Wunder (1975) and Liu et al. (2003) using the following equation:

$$\text{GEI (kJ/d)}=\text{dry matter intake (DMI)}\times \text{energy content of food (kJ/g)} \tag{1}$$

Organ and body composition

At the end of the experiment, animals were sacrificed by CO_2 asphyxiation, after which trunk blood was collected for later measurement of WBC. Blood samples were allowed to clot for 1 h and centrifuged at 4 °C for 30 min at 4 000 r/min. Sera were collected and stored in polypropylene microcentrifuge

tubes at −80 °C for later hormone (i.e., corticosterone and testosterone) and bacterial killing capacity assays. Organ mass was measured as described previously (Xu & Wang, 2011; Xu et al., 2011). In brief, visceral organs, including the heart, liver, kidneys, testes, small intestine, and spleen, were dissected on an ice box and weighed (±1 mg). The length of the small intestine was measured by extending the organ to its unstressed length along a ruler (±1 mm) (Pei et al., 2001). The small intestine was then opened and rinsed with saline to eliminate all gut contents, blotted dry on tissue paper, and weighed. The heart, liver, kidneys, testes, and small intestine were stored at −80 °C for later antioxidant enzyme assays. The carcass was dried in an oven at 60 °C to a constant mass, and then weighed again to obtain dry mass. The difference between the wet and dry carcass mass was the water mass of the carcass. Total body fat was extracted from the dried carcass by petroleum ether extraction in a Soxhlet apparatus, and body fat content was calculated as the proportion of total body fat mass divided by wet carcass mass (Xu & Wang, 2010).

Oxidative stress marker assays

Lipid peroxidation, which is indicative of oxidative damage, was examined as described previously (Yang et al., 2013). Specifically, lipid peroxidation was evaluated by quantifying malonaldehyde (MDA) (Del Rio et al., 2005) using a thiobarbituric acid reactive substances (TBARS) assay kit (Nanjing Jiancheng, Nanjing, China) following the manufacturer's instructions. The absorbance of the eluent was monitored spectrophotometrically at 532 nm (BioTek Synergy 4 Hybrid Microplate Reader, BioTek, Winooski, Vermont, USA). The intra- and inter-assay coefficients of variation for this assay were <1.5% and <3.32%, respectively. Lipid peroxidation was expressed as nmol MDA per mg protein.

ROS levels were measured in the tissues by examining hydrogen peroxide (H_2O_2) levels (Zhou et al., 2015). The H_2O_2 levels were analyzed using a commercial kit (Nanjing Jiancheng, Nanjing, China) in accordance with the manufacturer's instructions. Levels of H_2O_2 were expressed as μmol/g protein.

Antioxidant enzymes

The activities of antioxidant enzymes, including SOD and CAT, and total antioxidant capacity (T-AOC) were also determined using commercial kits (Nanjing Jiancheng, Nanjing, China) according to the manufacturer's instructions. One unit of SOD was defined as the amount of enzyme that caused 50% inhibition of superoxide radical produced by the reaction between xanthine and xanthine oxidase at 37 °C; one unit of CAT activity was defined as the decomposition of 1 μmol H_2O_2 per min; one unit of T-AOC was defined as the extent to which optical density increased by 0.01 per milligram protein per min (Chen et al., 2014).

Immunological parameters

WBC count was determined as described previously (Xu & Wang, 2010). In brief, 20 μL of whole blood was diluted immediately in a 0.38 mL solution containing 1.5% glacial acetic acid and 1% crystal violet (Sigma). The leukocytes were then counted in an improved Neubauer chamber using a microscope. Total number of WBC was determined by counting all leucocytes in the four large corner squares of the Neubauer chamber and multiplying the raw data by 5×10^7 to obtain final values (10^9 cells/L) (Yang, 2004).

Serum bacterial killing capacity, which is indicative of innate immunity, was performed in a sterile laminar flow cabinet to assess the functional response by the animal's innate immune system against a relevant pathogen, *Escherichia coli* (Demas et al., 2011; Tieleman et al., 2005; Yang et al., 2013). Briefly, serum samples were diluted 1:20 in a CO_2-independent medium (Gibco no. 18045, Carlsbad, GA, USA). A standard number of colony-forming units (CFUs) of *E. coli* (ATCC no. 8739, Microbial Culture Collection Center of Guangdong Institute of Microbiology, China) was added to each sample at a ratio of 1:10, after which the mixture was allowed to incubate at 37 °C for 30 min to induce bacterial killing. After incubation, 50 μL of each sample was added to tryptic soy agar plates in duplicate. All plates were covered and left to incubate upside down at 37 °C for 24 h. After this, total CFUs were counted and bactericidal capacity was calculated as 100% minus the mean number of CFUs for each sample divided by the mean number of CFUs for the positive controls (containing only medium and standard bacterial solution), i.e., the percentage of bacteria killed relative to the positive control.

Serum corticosterone assays

Serum corticosterone concentrations were determined using a rat corticosterone ELISA kit (Cat. No. HR083, RapidBio Lab. Calabasas, California, USA). The lowest level of corticosterone that could be detected by this assay was 1.0 nmol/L. All procedures were in accordance with the manufacturer's instructions. Inter- and intra-assay variabilities for corticosterone were <1.1% and 7.5%, respectively.

Serum testosterone

Serum testosterone concentrations were assessed using a rat testosterone ELISA kit (Cat. No. HR083, RapidBio Lab. Calabasas, California, USA) following the manufacturer's instructions. The tested range of testosterone was 0.13–25.6 ng/mL. Intra- and inter-assay variabilities for testosterone were <9.0% and 11.0%, respectively.

Statistical analysis

Data were analyzed using SPSS 13.0 software (SPSS Inc., Chicago, IL, USA). Prior to all statistical analyses, data were examined for normality and homogeneity of variance using Kolmogorov-Smirnov and Levene tests, respectively. Changes in body mass and GEI during the experiment were analyzed with the Repeated Measure of General Linear Model (GLM). Differences in body mass at any time point, MDA and H_2O_2 levels, SOD and CAT activity, T-AOC, WBC, innate immunity, and corticosterone and testosterone concentrations in different groups were analyzed by one-way analysis of

variance (ANOVA) followed by Tukey's *post hoc* tests. Group differences in wet organ mass and GEI, with body mass as the covariate, at any time point were analyzed by a one-way analysis of covariance (ANCOVA) followed by Bonferroni *post-hoc* tests. Significant group differences were further evaluated by GLM multivariate analysis followed by Bonferroni *post hoc* tests. Pearson correlation analysis was performed to determine the correlations of corticosterone, testosterone, and antioxidant parameters. Results are expressed as means±*SE*, with P<0.05 considered to be statistically significant.

RESULTS

Body mass and energy intake

Body mass among the 4 °C, 23 °C, and 32 °C groups did not differ significantly before the experiment began (day 0, $F_{2, 25}$=0.650, P=0.531) (Figure 1A). Based on repeated measure ANOVA, body mass changed significantly over the 27 d acclimation to low and high temperature ($F_{9, 225}$=40.915, P<0.001). Body mass among the three groups show no significant differences from day 3 ($F_{2, 25}$=1.477, P=0.248) to day 12 ($F_{2, 25}$=2.822, P=0.078), whereas body mass differed significantly from day 15 ($F_{2, 25}$=4.600, P=0.020) to day 27 ($F_{2, 25}$=4.203, P=0.027) (Figure 1A). At the end of the experiment, body mass in the 4 °C, 23 °C, and 32 °C groups increased by 16.2%, 17.4%, and 32.4%, respectively, compared with body mass on day 0 (Table 1). There was no difference in GEI among the three groups on day 0 ($F_{2, 24}$=0.251, P=0.780) (Figure 1B); however, GEI changed significantly over the course of the experiment ($F_{8, 200}$=54.430, P<0.001). GEI was significantly influenced by temperature from day 3 to day 27 and was significantly higher in the 4 °C group and lower in the 32 °C group relative to the 23 °C group (day 3, $F_{2, 24}$=10657.8, P<0.001; day 27, $F_{2, 24}$=22.7, P<0.001) (Figure 1B).

Body composition and organs

Body composition (i.e., wet carcass, dry carcass, fat free dry carcass, body fat mass, and fat content) decreased, whereas organ mass (i.e., heart, liver, and kidney) and small intestine length increased, and spleen, testis, and small intestine mass remained unchanged with the decline in temperature (Table 1). Body fat mass was 37.9% lower in the 4 °C group and 62.1% higher in the 32 °C group in contrast with the 23 °C group.

Oxidative stress

H_2O_2 levels showed significant differences among the various tissues in all three treatment groups ($F_{4, 135}$=58.61, P<0.001, Figure 2A). In the 4 °C group, H_2O_2 levels were significantly higher in the small intestine than in the liver, heart, kidney, or testis (*post hoc*, P<0.05). Temperature had a significant effect on H_2O_2 levels in the liver, which were 46.7% higher in the 4 °C group and 27.9% lower in the 32 °C group compared to the 23 °C group ($F_{2, 25}$=4.584, P=0.020). H_2O_2 levels in the heart were also affected significantly by temperature and were 44.3% and 102.9% higher in the 4 °C and 32 °C groups, respectively, compared to the 23 °C group ($F_{2, 25}$=7.949, P=

Table 1 Effect of temperature on body composition and wet organ mass in Brandt's voles

Parameter	4 °C	23 °C	32 °C	Statistical summary	
				$F_{2, 25}$	P
Body composition (g)					
Initial body mass	40.2±2.7	43.0±1.8	43.8±2.3	0.650	0.531
Final body mass	46.7±2.1[b]	50.5±6.6[ab]	58.0±3.6[a]	4.203	0.027
Wet carcass	30.3±2.1[b]	35.0±1.6[b]	42.4±2.6[a]	7.819	0.002
Dry carcass	13.2±2.8[b]	16.5±1.3[ab]	22.3±2.3[a]	6.995	0.004
Body water	17.1±1.2	18.5±0.7	20.1±0.8	2.690	0.087
Fat free dry carcass	9.1±0.5[b]	9.9±0.4[ab]	11.5±0.6[a]	6.090	0.007
Body fat mass	4.1±0.5[b]	6.6±1.1[ab]	10.7±1.8[a]	6.255	0.006
Fat content (%)	30.3±1.6[b]	38.1±3.1[ab]	45.3±3.2[a]	6.584	0.005
Organ mass (mg)				$F_{2, 24}$	P
Heart	249±8[a]	213±6[b]	178±7[c]	18.116	<0.001
Liver	2331±136	1905±109	1869±125	3.617	0.042
Kidney	618±24[a]	510±19[b]	399±22[c]	18.282	<0.001
Small intestine	312±79	344±63	259±73	0.369	0.695
Small intestine length (cm)	35.1±1.0[a]	32.9±0.8[a]	29.4±0.9 [b]	7.983	0.002
Testis	813±74	929±59	796±68	1.437	0.257
Spleen	35±3	32±3	36±3	0.748	0.484

Values are means±*SE*. Values for a specific parameter that share different superscripts are significantly different at P<0.05. Body composition was analyzed by one-way ANOVA, and organ mass was determined by General Linear Model multivariate analysis followed by Bonferroni *post hoc* tests with body mass as the covariate.

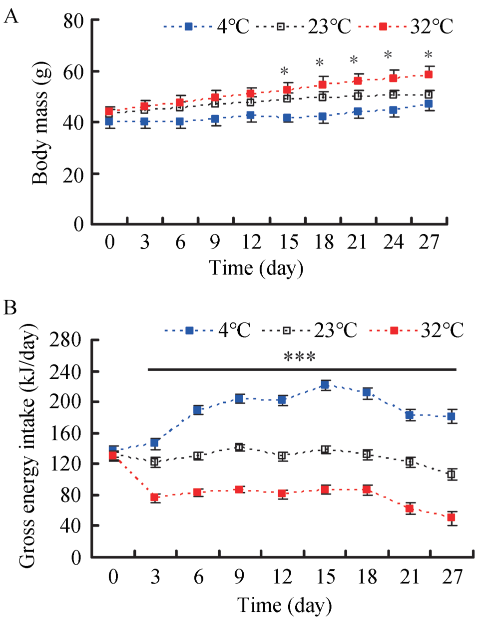

Figure 1 Effect of temperature on body mass (A) and gross energy intake (B) in Brandt's voles acclimated to 4 °C, 23 °C, and 32 °C

Data are means±*SE*. *: P<0.05, ***: P<0.001.

0.002). However, temperature had no effect on H_2O_2 levels in the kidney ($F_{2, 25}$=1.506, P=0.241), testis ($F_{2, 25}$=0.166, P=0.848), or small intestine ($F_{2, 25}$=1.649, P=0.212) (Figure 2A).

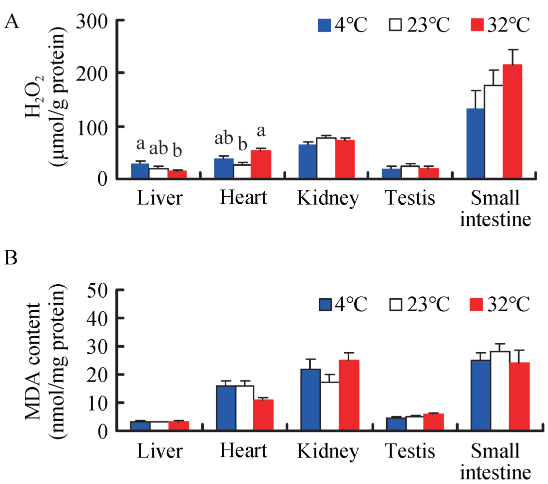

Figure 2 Effect of temperature on H_2O_2 (A) and MDA levels (B) in Brandt's voles acclimated to 4 °C, 23 °C, and 32 °C

Different letters above columns indicate significant differences at P<0.05.

MDA levels differed significantly among the various tissues ($F_{4, 135}$=59.29, P<0.001, Figure 2B), and were significantly higher in the kidney and small intestine than that in the liver, heart, or testis in the 4 °C group (*post hoc*, P<0.05). Temperature had no influence on MDA content in the liver ($F_{2, 25}$=0.247, P=0.783), kidney ($F_{2, 25}$=1.816, P=0.184), testis ($F_{2, 25}$=2.039, P=0.151), or small intestine ($F_{2, 25}$=0.356, P=0.704). However, MDA levels in the heart were 31.5% lower in the 32 °C group than that in the 23 °C group ($F_{2, 25}$=3.391, P=0.050) (Figure 2B).

Antioxidant enzymes

A significant difference in total SOD activity was found among the five tissues ($F_{4, 135}$=42.64, P<0.001, Figure 3A), with higher activity detected in the small intestine compared with the other four tissues (*post hoc*, P<0.05). There were no significant differences in total SOD activity in the liver ($F_{2, 25}$=0.531, P=0.594), heart ($F_{2, 25}$=0.076, P=0.927), kidney ($F_{2, 25}$=0.523, P=0.599), and small intestine ($F_{2, 25}$=0.184, P=0.833) among the 4 °C, 23 °C, and 32°C groups. Total SOD activity in the testis was 18.8% and 19.9% higher in the 4 °C and 32 °C groups, respectively, compared to the 23 °C group ($F_{2, 25}$=3.239, P=0.056) (Figure 3A).

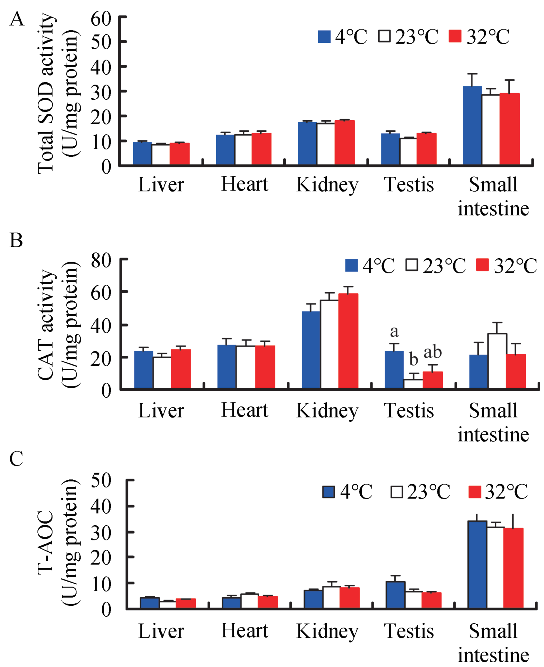

Figure 3 Effect of temperature on total SOD activity (A), CAT activity (B), and total antioxidant capacity (T-AOC) (C) in Brandt's voles

Different letters above columns indicate significant differences at P<0.05.

CAT activity exhibited significant differences among the five tissues ($F_{4, 135}$=31.17, P<0.001, Figure 3B), and was higher in the kidney than the other four tissues in the 4 °C group (*post hoc*, P<0.05). CAT activity in the testis was significantly increased in the 4 °C (304.6%) and 32 °C groups (87.3%), respectively, compared to the 23 °C group (Figure 3B). However, temperature had no significant impact on CAT activity in the liver, heart, kidney, or small intestine (liver, $F_{2, 25}$=1.165, P=0.328; heart, $F_{2,25}$=0.016, P=0.984; kidney, $F_{2,25}$=1.299,

P=0.291; small intestine, $F_{2, 25}$=1.110, P=0.345) (Figure 3B).

T-AOC differed significantly among the five tissues ($F_{4, 135}$=59.44, P<0.001, Figure 3C), and was higher in the small intestine than that in the other four tissues in the 4 °C group (*post hoc*, P<0.05). No significant differences in T-AOC were observed in the liver ($F_{2, 25}$=2.313, P=0.120), heart ($F_{2, 25}$=0.683, P=0.514), kidney ($F_{2, 25}$=0.437, P=0.651), testis ($F_{2, 25}$=2.368, P=0.114), and small intestine ($F_{2, 25}$=0.068, P=0.934) among the groups (Figure 3C). However, significant positive correlations were found between MDA levels and SOD, CAT, and T-AOC activities in the heart and small intestine and between H_2O_2 levels and MDA, SOD, and T-AOC activities in the small intestine, with some significant correlations found in the liver, kidney, and testis (Table 2).

Immunological parameters

No statistically significant differences were observed in wet spleen mass ($F_{2, 25}$=0.748 P=0.484) (Figure 4A), WBC ($F_{2, 25}$=0.504, P=0.610) (Figure 4B), or bacteria killing capacity ($F_{2, 25}$=2.822, P=0.079) (Figure 4C). Innate immunity was 118.0% and 35.5% lower in the 4 °C and 32 °C groups, respectively, compared to the 23 °C group. Innate immunity was negatively correlated with liver H_2O_2 levels and kidney MDA content, but not with body fat mass, H_2O_2 levels, or MDA content in other tissues (Table 3).

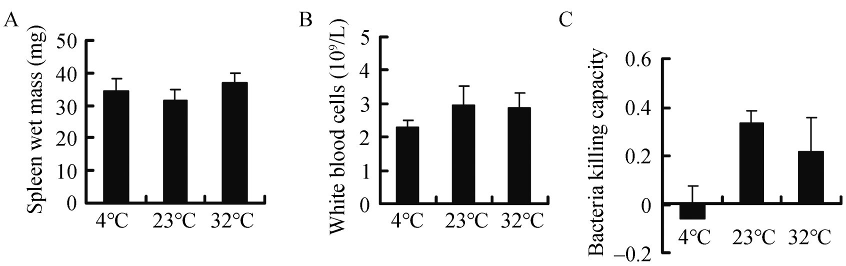

Figure 4 Effect of temperature on spleen wet mass (A), white blood cell count (B), and bacteria killing capacity (C) in Brandt's voles

Serum corticosterone

Corticosterone concentration did not differ among the groups ($F_{2, 25}$=1.818, P=0.183) (Figure 5A). Furthermore, corticosterone concentration was not correlated with H_2O_2 levels, MDA content, or SOD, CAT, and T-AOC activities in the liver, heart, kidney, testis, or small intestine, except for a negative correlation between corticosterone and SOD activity in the testis (Table 2). Moreover, no significant correlation was found between innate immunity and corticosterone concentration (r=0.206, P=0.293) (Table 3).

Serum testosterone

Testosterone concentration was significantly influenced by temperature and was 25.8% and 53.1% higher in the 4 °C and 32 °C groups, respectively, compared to the 23 °C group ($F_{2, 25}$=4.403, P=0.023) (Figure 5B). Testosterone concentration was not correlated with H_2O_2 levels, MDA content, or SOD, CAT, and T-AOC activities in the liver, heart, kidney, testis, or small intestine, except for a positive correlation with testis SOD (Table 2). Testosterone concentration was negatively correlated with corticosterone concentration (Table 2) but was not correlated with innate immunity (r=−0.119, P=0.546) (Table 3).

DISCUSSION

Ambient temperature is one of the most important factors affecting physiological processes. Contrary to our expectation, we found that temperature exerted different influences on oxidative stress, antioxidant enzymes, and immunity depending on the tissues and parameters tested. With the decline in temperature, ROS levels increased in the liver but did not change in the kidney, testis, or small intestine. ROS levels in the heart were higher in the 32 °C group than in the 23 °C group. Compared to the 23 °C group, cold exposure elevated CAT activity in the testis but not in the liver, heart, kidney, or small intestine. MDA content and SOD and T-AOC activities in the five tissues showed no response to low or high temperature. Bacteria killing capacity was nearly suppressed in the 4 °C group compared with that in the 23° C group, whereas spleen mass and WBC were unaffected by temperature treatment.

Body mass, body composition, and organs

To satisfy the augmentation in energy requirements during cold temperature, animals usually increase energy intake (Hammond & Wunder, 1995). In the present study, we also found that gross energy intake increased in the voles with the decline in temperature. However, the body masses in the 4 °C and 32 °C groups at the end of the experiment were 7.5% lighter and 14.8% heavier, respectively, than that in the 23 °C group. This may be due to an increase in energy expenditure with the decrease in temperature (Chi & Wang, 2011; Hammond & Wunder, 1995). Moreover, voles also mobilized energy reserves, including fat free carcass and body fat mass, to meet the elevated energy requirements with the decrease in temperature. In general, an increase in expensive metabolic organ mass (i.e., liver, heart, small intestine, and kidneys) and small intestine length during cold acclimation are adaptive responses to elevated energy needs and food processing capability (Daan et al., 1990; Hammond & Wunder, 1995; Konarzewski & Diamond, 1995). In our study, the liver, heart, and kidney mass and small intestine length also increased

Table 2 Pearson's correlation coefficients between H_2O_2 and MDA levels, SOD, CAT, T-AOC activity, and corticosterone and testosterone in Brandt's voles

		H_2O_2	MDA	SOD	CAT	T-AOC	CORT	T
Liver	H_2O_2	1						
	MDA	–0.096	1					
	SOD	–0.042	0.435*	1				
	CAT	0.025	0.343	0.592**	1			
	T-AOC	0.108	0.179	0.442*	0.402*	1		
	CORT	–0.352	–0.106	–0.088	–0.044	0.140	1	
	T	0.258	–0.005	0.136	0.102	–0.123	–0.840**	1
		H_2O_2	MDA	SOD	CAT	T-AOC	CORT	T
Heart	H_2O_2	1						
	MDA	–0.045	1					
	SOD	0.346	0.390*	1				
	CAT	0.107	0.520**	0.551**	1			
	T-AOC	0.087	0.566**	0.695**	0.451*	1		
	CORT	–0.085	0.208	0.056	0.089	0.219	1	
	T	0.273	–0.206	0.048	–0.057	–0.037	–0.840**	1
		H_2O_2	MDA	SOD	CAT	T-AOC	CORT	T
Kidney	H_2O_2	1						
	MDA	0.041	1					
	SOD	–0.187	–0.116	1				
	CAT	0.173	0.335	0.169	1			
	T-AOC	0.148	0.266	0.355	0.330	1		
	CORT	0.117	–0.183	–0.158	0.121	–0.023	1	
	T	–0.068	0.114	0.209	–0.114	–0.101	–0.840**	1
		H_2O_2	MDA	SOD	CAT	T-AOC	CORT	T
Testis	H_2O_2	1						
	MDA	0.248	1					
	SOD	0.212	0.324	1				
	CAT	–0.200	–0.231	0.233	1			
	T-AOC	0.228	–0.197	0.536**	0.071	1		
	CORT	–0.163	–0.322	–0.447*	–0.171	–0.207	1	
	T	0.129	0.339	0.392*	0.249	–0.036	–0.840**	1
		H_2O_2	MDA	SOD	CAT	T-AOC	CORT	T
SI	H_2O_2	1						
	MDA	0.507**	1					
	SOD	0.651**	0.636**	1				
	CAT	0.340	0.411*	0.397*	1			
	T-AOC	0.503**	0.633**	0.794**	0.329	1		
	CORT	–0.008	0.162	–0.005	0.208	–0.194	1	
	T	–0.022	–0.204	–0.111	–0.173	–0.002	–0.840**	1

SI: Small intestine; CORT: Corticosterone; T: Testosterone. *: $P<0.05$, **: $P<0.01$.

Table 3 Pearson's correlation coefficients between innate immunity, H_2O_2 and MDA levels, corticosterone, testosterone, and body fat mass in Brandt's voles

		Immunity	H_2O_2					MDA							
			Liver	Heart	Kidney	Testis	SI	Liver	Heart	Kidney	Testis	SI	CORT	T	Fat
Immunity		1													
H_2O_2	Liver	–0.441*	1												
	Heart	–0.143	–0.030	1											
	Kidney	–0.105	–0.181	–0.349	1										
	Testis	0.050	–0.066	0.229	–0.104	1									
	SI	0.032	–0.259	–0.006	–0.078	–0.061	1								
MDA	Liver	–0.171	–0.096	–0.021	0.023	–0.069	0.261	1							
	Heart	0.011	0.200	–0.045	–0.071	0.172	–0.342	–0.527**	1						
	Kidney	–0.423*	0.333	0.383*	0.041	0.000	0.078	0.099	–0.200	1					
	Testis	–0.032	0.008	0.161	–0.014	0.248	0.269	–0.121	–0.203	–0.039	1				
	SI	0.185	–0.098	–0.408	0.129	–0.114	0.507**	0.186	–0.089	–0.160	–0.075	1			
	CORT	0.206	–0.352	–0.085	0.117	–0.163	–0.008	–0.106	0.208	–0.183	–0.322	0.162	1		
	T	–0.119	0.258	0.273	–0.068	0.129	–0.022	–0.005	–0.206	0.114	0.339	–0.204	–0.840**	1	
	Fat	–0.065	–0.219	0.289	0.163	0.005	0.085	–0.435*	0.089	0.393*	0.253	–0.291	–0.111	0.132	1

SI: Small intestine; CORT: Corticosterone; T: Testosterone; Fat: Body fat mass. *: P<0.05, **: P<0.01.

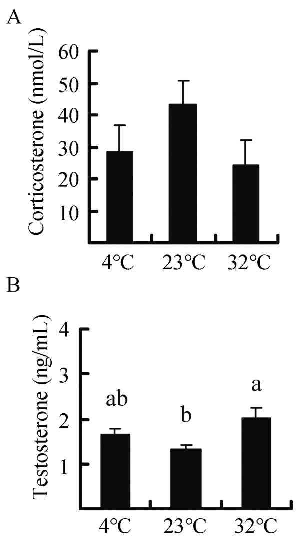

Figure 5 Effect of temperature on the concentration of corticosterone (A) and testosterone (B) in Brandt's voles acclimated to 4 °C, 23 °C, and 32 °C

significantly with the decline in temperature, consistent with previous studies (Chi & Wang, 2011; Zhang & Wang, 2006). These changes in metabolic organs would satisfy the increased energy requirements and food processing capability under cold exposure.

Oxidative stress and gross energy intake

Energy requirements usually increase across many species in cold environments (Chi & Wang, 2011; Liu et al., 2009; Zhou et al., 2015). Thus, animals adopt different adaptive strategies, such as increased food and gross energy intake, as observed in the voles in our study. The increase in GEI with the decline in temperature also indicated an elevation in the metabolic rate of voles, although resting metabolic rate was not examined in our study. Previous research has shown that cold exposure significantly increases metabolic rate in voles (Li et al., 2001; Liu et al., 2009; Zhang & Wang, 2006). According to the rate of living-free radical hypothesis, higher metabolic rates, which are achieved by enhancing mitochondrial oxidative phosphorylation, should increase the production of free radicals (i. e., ROS) (Harman, 1956; Pearl, 1928; Selman et al., 2013; Speakman et al., 2004). In the current study, the increase in ROS production with the decrease in temperature, as indicated by H_2O_2 levels in the liver, was consistent with this hypothesis, whereas the reduction of ROS in the heart and unchanged ROS in the kidney, testis, and small intestine were not compatible with this hypothesis. The reason of these disparate results might lie in the fact that an elevated metabolic rate during cold acclimation does not necessarily result in greater ROS production (Costantini, 2008; Hulbert et al., 2007). In light of the "uncoupling to survive" hypothesis, increased uncoupling proteins in response to cold temperature can decrease ROS production by lowering the potential of the inner mitochondrial membrane (Brand, 2000; Speakman et al., 2004). Several studies have also demonstrated that an increased metabolic rate is not associated with elevated ROS levels in skeletal muscle or certain organs, including the liver, heart, lungs, spleen, kidneys, and digestive tract (Chen et al., 2014; Selman et al., 2002; Stier et al., 2014). The increased UCP1 content in voles upon cold exposure in previous studies might account for the ROS results in our experiment (Liu et al., 2009; Zhang & Wang, 2006).

In the present study, high temperature led to an increase in

oxidation, as indicated by the H_2O_2 levels in the vole heart, which is consistent with previous research showing increased levels of oxidation at high temperature in broiler chickens (Tan et al., 2010). In light of the oxidation handicap hypothesis, testosterone may elevate the levels of ROS (Alonso-Alvarez et al., 2007, 2008). The increased ROS levels in voles under high temperature may also be caused by higher testosterone concentration, although no significant correlation was detected between H_2O_2 and testosterone levels.

In general, excessive ROS production can lead to oxidative damage (Burton & Jauniaux, 2011; Costantini, 2008; Finkel & Holbrook, 2000; Hulbert et al., 2007). In the present study, however, MDA content in the liver, heart, kidney, testis, and small intestine, which did not respond to high or low temperature treatment, was not related to ROS (H_2O_2) levels. This result agrees with several studies in which MDA content in the liver and serum of female Mongolian gerbils (Yang et al., 2013) or in the liver, heart, muscle, and brain of striped hamsters (Zhou et al., 2015) was not affected by high or low temperature treatment. This may be because the voles were able to maintain or increase SOD, T-AOC, and CAT activity in the five tissues, even under high or low temperature environments, which removed excessive free radicals.

Antioxidant defense and hormone profiles

In the present study, CAT activity in the testis increased upon cold exposure but did not change under high temperature. Conversely, testosterone levels increased under high temperature but did not change with cold exposure. Thus, the effects of high temperature on the voles were different from those of low temperature.

Secretion of stress hormones such as corticosterone usually increase in animals facing stressful conditions, including high or low ambient temperature (Bligh-Tynan et al., 1993; Kim et al., 2013; Sapolsky et al., 2000). In the current study, however, corticosterone concentration in voles was not affected by high or low temperature, which is inconsistent with other studies showing increased corticosterone levels under cold stress (Adels et al., 1986; Shu et al., 1993). This discrepancy may be due to the difference in cold exposure duration. Secretion of corticosterone usually increases upon acute cold exposure, whereas its levels can recover to baseline under chronic cold exposure (Bligh-Tynan et al., 1993).

Several studies have shown that exogenous corticosterone administration can increase oxidative stress and decrease SOD activity in rats (Dhanabalan et al., 2010) and birds (Alonso-Alvarez et al., 2007; Lin et al., 2004). Here, we found that corticosterone concentration did not respond to high or low temperature treatment, and it was not correlated with ROS and MDA levels or SOD, CAT, and T-AOC activities in the liver, heart, kidney, testis, and small intestine (except for a negative correlation with SOD activity in the testis). Thus, it appears that corticosterone could not fully explain the impact of hot and cold temperature on oxidative stress and antioxidant capacity in voles.

The oxidation handicap hypothesis holds that testosterone incurs oxidative costs (Alonso-Alvarez et al., 2007, 2008). Although the testosterone concentration was significantly affected by temperature in the tested voles, it was not correlated with H_2O_2 levels, MDA content, or SOD, CAT, and T-AOC activities in the five tested tissues (i. e., liver, heart, kidney, testis, and small intestine), with the exception of a positive correlation with SOD activity in the testis. This result is consistent with earlier research demonstrating that increased testosterone does not cause oxidative damage to DNA but enhances total antioxidant capacity in yellowthroat warblers (*Geothlypis trichas*) (Taff & Freeman-Gallant, 2014). Several authors have argued that detection of oxidative costs is both tissue and assay-dependent (Yang et al., 2013), suggesting that additional parameters and tissues may have identified certain direct oxidative costs of testosterone in the present study.

Immunity, body fat, and hormone profiles

Innate immunity, as indicated by bacteria killing capacity, was lower in the 4 °C group than in the 23 °C group. This may be due to the reduction of body fat in voles upon cold exposure. Adipose tissues are not only considered as endocrine and immune organs (Ahima & Flier, 2000; Trayhurn, 2005), but also as energy depots for expensive physiological processes, including immune function (Demas et al., 1997; Demas, 2004; Moret & Schmid-Hempel, 2000). Previous research has demonstrated that animals with low energy reserves choose to allocate less energy to immune defense than animals with higher reserves (Houston et al., 2007). Therefore, reductions in body fat can impair immunity (Chandra, 1996; Demas et al., 2003). In the face of energy demanding conditions, including cold environments, trade-offs may occur among different physiological processes. Voles might divert energy from less critical physiological functions such as immunity to more important processes such as thermogenesis for immediate survival during cold exposure (Liu et al., 2009; Zhang & Wang, 2006). However, further research is required to clarify whether trade-offs occur between thermogenic capacity and immune function under cold environments.

Both corticosterone and testosterone have suppressive effects on immunity (Marketon & Glaser, 2008; Sapolsky et al., 2000; Trigunaite et al., 2015). In the present study, however, we found no correlation between corticosterone and testosterone and innate immunity. Thus, these two hormones could not account for the variation in immunity observed in voles. Recently, several authors have shown that oxidative stress may also impair immune function (Costantini & Møller, 2009; Sordillo & Aitken, 2009). We found that innate immunity was negatively correlated with H_2O_2 levels in the liver and MDA content in the kidney. Suppression of innate immunity in the 4 °C group compared to the control may be caused by oxidative stress in voles.

In the current study, voles exhibited several adaptive strategies to cope with high and low temperature. Voles increased gross energy intake and active metabolic organs (i. e., heart, liver, kidneys) and mobilized energy reserves with the decline in temperature. However, voles may maintain or

increase antioxidant defense at the cost of innate immunity under cold temperature. Therefore, up-regulation or maintenance of antioxidant defenses may be crucial for voles to survive under dramatically fluctuating ambient temperatures from the perspective of oxidative ecology (Boonstra, 2013).

COMPETING INTERESTS

The authors declare that they have no competing interests.

AUTHORS' CONTRIBUTIONS

D.L.X. and D.H.W. designed the study. D.L.X. and D.H.W. supervised the analyses. D.L.X. and M.M.X examined the body mass and gross energy intake of the study. D.L.X. performed the parameters of antoxidant enzymes and oxidative stress. D.L.X. wrote the manuscript with the direction of D.H. W.. D.L.X. revised the manuscript. All authors read and approved the final version of the manuscript.

ACKNOWLEDGEMENTS

We are grateful to Xue-Ying Zhang from Institute of Zoology, Chinese Academy of Sciences for her help in the experiment. We are also grateful for the valuable suggestions provided by the anonymous reviewers and the carefully editing of the editors of Zoological Research.

REFERENCES

Adels LE, Leon M, Wiener SG, Smith MS. 1986. Endocrine response to acute cold exposure by lactating and non-lactating Norway rats. *Physiology & Behavior*, **36**(1): 179–181.

Ahima RS, Flier JS. 2000. Adipose tissue as an endocrine organ. *Trends in Endocrinology & Metabolism*, **11**(8): 327–332.

Alonso-Alvarez C, Bertrand S, Faivre B, Chastel O, Sorci G. 2007. Testosterone and oxidative stress: the oxidation handicap hypothesis. *Proceedings of the Royal Society B*, **274**(1161): 819–825.

Alonso-Alvarez C, Perez-Rodriguez L, Mateo R, Chastel O, Vinuela J. 2008. The oxidation handicap hypothesis and the carotenoid allocation trade-off. *Journal of Evolutionary Biology*, **21**(6): 1789–1797.

Bligh-Tynan ME, Bhagwat SA, Castonguay TW. 1993. The effects of chronic cold exposure on diurnal corticosterone and aldosterone rhythms in Sprague-Dawley rats. *Physiology & Behavior*, **54**(2): 363–367.

Boonstra R. 2013. The ecology of stress: a marriage of disciplines. *Functional Ecology*, **27**(1): 7–10.

Brand MD. 2000. Uncoupling to survive? The role of mitochondrial inefficiency in ageing. *Experimental Gerontology*, **35**(6–7): 811–820.

Burton GJ, Jauniaux E. 2011. Oxidative stress. *Best Practice & Research Clinical Obstetrics & Gynaecology*, **25**(3): 287–299.

Calder PC, Kew S. 2002. The immune system: *a target for functional foods? British Journal of Nutrition*, **88**: S165–176.

Carroll JA, Burdick NC, Chase CC, Coleman SW, Spiers DE. 2012. Influence of environmental temperature on the physiological, endocrine, and immune responses in livestock exposed to a provocative immune challenge. *Domestic Animal Endocrinology*, **43**(2): 146–153.

Chandra RK. 1996. Nutrition, immunity and infection: from basic knowledge of dietary manipulation of immune responses to practical application of ameliorating suffering and improving survival. *Proceeding of the National Academy of Sciences of the United States of America*, **93**(25): 14304–14307.

Chen ZZ. 1998. Land form and climate in Xilin river valley. In: The Study of Grassland Ecosystem. Beijing, China: Science Press, 13–22.

Chen KX, Wang CM, Wang GY, Zhao ZJ. 2014. Energy budget, oxidative stress and antioxidant in striped hamster acclimated to moderate cold and warm temperatures. *Journal of Thermal Biology*, **44**: 35–40.

Chi QS, Wang DH. 2011. Thermal physiology and energetics in male desert hamsters (*Phodopus roborovskii*) during cold acclimation. *Journal of Comparative Physiology B*, **181**(1): 91–103.

Costantini D. 2008. Oxidative stress in ecology and evolution: lessons from avian studies. *Ecology Letters*, **11**(11): 1238–1251.

Costantini D, Møller AP. 2009. Does immune response cause oxidative stress in birds? A meta-analysis. *Comparative Biochemistry and Physiology Part A*, **153**(3): 339–344.

Daan S, Masman D, Groenewold A. 1990. Avian basal metabolic rates: their association with body composition and energy expenditure in nature. *American Journal of Physiology-Regulatory, Integrative and Comparative Physiology*, **259**(2): R333–340.

Del Rio D, Stewart AJ, Pellegrini N. 2005. A review of recent studies on malondialdehyde as toxic molecule and biological marker of oxidative stress. *Nutrition, Metabolism and Cardiovascular Diseases*, **15**(4): 316–328.

Demas GE. 2004. The energetics of immunity: a neuroendocrine link between energy balance and immune function. *Hormones and Behavior*, **45**(3): 173–180.

Demas GE, Drazen DL, Nelson RJ. 2003. Reductions in total body fat decrease humoral immunity. *Proceedings of the Royal Society B*, **270**(1518): 905–911.

Demas GE, Chefer V, Talan MI, Nelson RJ. 1997. Metabolic costs of mounting an antigen-stimulated immune response in adult and aged C57BL/6J mice. *American Journal of Physiology - Regulatory, Integrative and Comparative Physiology*, **273**(5): 1631–1637.

Demas GE, Zysling DA, Beechler BR, Muehlenbein MP, French SS. 2011. Beyond phytohaemagglutinin: assessing vertebrate immune function across ecological contexts. *Journal of Animal Ecology*, **80**(4): 710–730.

Dhanabalan S, Dćruz SC, Mathur PP. 2010. Effects of corticosterone and 2, 3, 7, 8-tetrachloro-dibenzo-p-dioxin on epididymal antioxidant system in adult rats. *Journal of Biochemical and Molecular Toxicology*, **24**(4): 242–249.

Dickinson BC, Chang CJ. 2011. Chemistry and biology of reactive oxygen species in signaling or stress responses. *Nature Chemical Biology*, **7**(8): 504–511.

Dowling DK, Simmons LW. 2009. Reactive oxygen species as universal constraints in life-history evolution. *Proceedings of the Royal Society B*, **276**(1663): 1737–1745.

Fantuzzi G. 2005. Adipose tissue, adipokines, and inflammation. *Journal of Allergy and Clinical Immunology*, **115**(5): 911–919.

Finkel T, Holbrook NJ. 2000. Oxidants, oxidative stress and the biology of ageing. *Nature*, **408**: 239–247.

Grodzinski W, Wunder BA. 1975. Ecological energetics of small mammals. In: Golley FB, Petrusewicz K, Ryszkowski L (eds). Small Mammals: Their Productivity and Population Dynamics. Cambridge: Cambridge University

Press, 173–204.
Hall ME, Blount JD, Forbes S, Royle NJ. 2010. Does oxidative stress mediate the trade-off between growth and self-maintenance in structured families? *Functional Ecology*, **24**(2): 365–373.
Hammond KA, Wunder BA. 1995. Effect of cold temperatures on the morphology of gastrointestinal tracts of two microtine rodents. *Journal of Mammalogy*, **76**(1): 232–239.
Harman D. 1956. Aging: a theory based on free radical and radiation chemistry. *Journal of Gerontology*, **11**(3): 298–300.
Houston AI, McNamara JM, Barta Z, Klasing KC. 2007. The effect of energy reserves and food availability on optimal immune defence. *Proceedings of the Royal Society B*, **274**(1627): 2835–2842.
Hulbert AJ, Pamplona R, Buffenstein R, Buttemer WA. 2007. Life and death: metabolic rate, membrane composition, and life span of animals. *Physiological Reviews*, **87**(4): 1175–1213.
Kanter M, Aktas C, Erboga M. 2013. Heat stress decreases testicular germ cell proliferation and increases apoptosis in short term: an immunohistochemical and ultrastructural study. *Toxicology and Industrial Health*, **29**(2): 99–113.
Kim HG, Lee JS, Han JM, Lee JS, Choi MK, Son SW, Son CG. 2013. Myelophil attenuates brain oxidative damage by modulating the hypothalamus-pituitary-adrenal (HPA) axis in a chronic cold-stress mouse model. *Journal of Ethnopharmacology*, **148**(2): 505–514.
King DA. 2004. Climate change science: adapt, mitigate, or ignore?. *Science*, **303**(5655): 176–177.
Konarzewski M, Diamond J. 1995. Evolution of basal metabolic rate and organ masses in laboratory mice. *Evolution*, **49**(6): 1239–1248.
Kozyreva TV, Eliseeva LS. 2000. Immune response in cold exposures of different types. *Journal of Thermal Biology*, **25**(5): 401–404.
Kozyreva TV, Eliseeva LS. 2004. The immune system response to antigen in cold- and warm-adapted rats. *Journal of Thermal Biology*, **29**(7 – 8): 865–869.
Li YG, Yan ZC, Wang DH. 2010. Physiological and biochemical basis of basal metabolic rates in Brandt's voles (*Lasiopodomys brandtii*) and Mongolian gerbils (*Meriones unguiculatus*). *Comparative Biochemistry and Physiology Part A*, **157**(3): 204–211.
Li QF, Sun RY, Huang CX, Wang ZK, Liu XT, Hou JJ, Liu JS, Cai LQ, Li N, Zhang SZ, Wang Y. 2001. Cold adaptive thermogenesis in small mammals from different geographical zones of China. *Comparative Biochemistry and Physiology Part A*, **129**(4): 949–961.
Lin H, Decuypere E, Buyse J. 2004. Oxidative stress induced by corticosterone administration in broiler chickens (*Gallus gallus domesticus*). *Comparative Biochemistry and Physiology Part B*, **139**(4): 745–751.
Liu H, Wang DH, Wang ZW. 2003. Energy requirements during reproduction in female Brandt's voles (*Microtus brandtii*). *Journal of Mammalogy*, **84**(4): 1410–1416.
Liu JS, Yang M, Sun RY, Wang DH. 2009. Adaptive thermogenesis in Brandt's vole (*Lasiopodomys brandtii*) during cold and warm acclimation. *Journal of Thermal Biology*, **34**(2): 60–69.
Lomakina LV. 1980. Effects of low temperature on lipid peroxidation and intensity of proteolysis in rat brain and liver. *Ukrainskii Biokhimicheskii Zhurnal*, **52**(3): 305–308.
Marketon JIW, Glaser R. 2008. Stress hormones and immune function. *Cellular Immunology*, **252**(1–2): 16–26.
Marnila P, Lilius E. 2015. Thermal acclimation in the perch (*Perca fluviatilis L.) immunity. Journal of Thermal Biology*, **54**: 47–55.
Marri V, Richner H. 2015. Immune response, oxidative stress and dietary antioxidants in great tit nestlings. *Comparative Biochemistry and Physiology Part A*, **179**: 192–196.
Martin LB, Scheuerlein A, Wikelski M. 2003. Immune activity elevates energy expenditure of house sparrows: *a link between direct and indirect costs? Proceedings of the Royal Society B*, **270**(1511): 153–158.
Martin LB, Weil ZM, Nelson RJ. 2007. Seasonal changes in vertebrate immune activity: mediation by physiological trade-offs. *Philosophical Transactions of the Royal Society B*, **363**(1490): 1–19.
Metcalfe NB, Alonso-Alvarez C. 2010. Oxidative stress as a life-history constraint: the role of reactive oxygen species (ROS) in shaping phenotypes from conception to death. *Functional Ecology*, **24**(5): 984–996.
Monaghan P, Metcalfe NB, Torres R. 2009. Oxidative stress as a mediator of life history trade-offs: mechanisms, measurements and interpretation. *Ecology Letters*, **12**(1): 75–92.
Moret Y, Schmid-Hempel P. 2000. Survival for immunity: the price of immune system activation for bumblebee workers. *Science*, **290**(5494): 1166–1168.
Owens IPF, Wilson K. 1999. Immunocompetence: *a neglected life history trait or conspicuous red herring? Trends in Ecology & Evolution*, **14**(5): 170–172.
Pearl R. 1928. The Rate of Living. London, UK: University of London Press.
Pei YX, Wang DH, Hume ID. 2001. Effects of dietary fibre on digesta passage, nutrient digestibility, and gastrointestinal tract morphology in the granivorous Mongolian gerbil (*Meriones unguiculatus*). *Physiological and Biochemical Zoology*, **74**(5): 742–749.
Raut AM, Suryakar AN, Mhaisekar D. 2012. Study of oxidative stress in relation with antioxidant status in chronic bronchitis. *International Journal of Public Health Science*, **1**(1): 7–10.
Sapolsky RM, Romero LM, Munck AU. 2000. How do glucocorticoids influence stress responses? Integrating permissive, suppressive, stimulatory, and preparative actions. *Endocrine Reviews*, **21**(1): 55–89.
Selman C, McLaren JS, Himanka MJ, Speakman JR. 2000. Effect of long-term cold exposure on antioxidant enzyme activities in a small mammal. *Free Radical Biology and Medicine*, **28**(8): 1279–1285.
Selman C, McLaren JS, Collins AR, Duthie GG, Speakman JR. 2008. The impact of experimentally elevated energy expenditure on oxidative stress and lifespan in the short-tailed field vole *Microtus agrestis*. *Proceedings of the Royal Society B*, **275**(1645): 1907–1916.
Selman C, McLaren JS, Collins AR, Duthie GG, Speakman JR. 2013. Deleterious consequences of antioxidant supplementation on lifespan in a wild-derived mammal. *Biology Letters*, **9**(4): 1–4.
Selman C, Grune T, Stolzing A, Jakstadt M, Mclaren JS, Speakman JR. 2002. The consequences of acute cold exposure on protein oxidation and proteasome activity in short-tailed field voles, *Microtus agrestis*. *Free Radical Biology and Medicine*, **33**(2): 259–265.
Sheldon BC, Verhulst S. 1996. Ecological immunology: costly parasite defences and trade-offs in evolutionary ecology. *Trends Ecology & Evolution*, **11**(8): 317–321.
Shu J, Stevenson JR, Zhou X. 1993. Modulation of cellular immune responses by cold water swim stress in the rat. *Developmental & Comparative Immunology*, **17**(4): 357–371.

Smith KG, Hunt JL. 2004. On the use of spleen mass as a measure of avian immune system strength. *Oecologia*, **138**(1): 28–31.

Sordillo LM, Aitken SL. 2009. Impact of oxidative stress on the health and immune function of dairy cattle. *Veterinary Immunology and Immunopathology*, **128**(1–3): 104–109.

Speakman JR, Talbot DA, Selman C, Snart S, McLaren JS, Redman P, Krol E, Jackson DM, Johnson MS, Brand MD. 2004. Uncoupled and surviving: individual mice with high metabolism have greater mitochondrial uncoupling and live longer. *Aging Cell*, **3**(3): 87–95.

Stier A, Bize P, Habold C, Bouillaud F, Massemin S, Criscuolo F. 2014. Mitochondrial uncoupling prevents cold-induced oxidative stress: a case study using UCP1 knockout mice. *Journal of Experimental Biology*, **217**: 624–630.

Taff CC, Freeman-Gallant CR. 2014. An experimental test of the testosterone mediated oxidation handicap hypothesis in a wild bird. *Hormones and Behavior*, **66**(2): 276–282.

Tan GY, Yang L, Fu YQ, Feng JH, Zhang MH. 2010. Effects of different acute high ambient temperatures on function of hepatic mitochondrial respiration, antioxidative enzymes, and oxidative injury in broiler chickens. *Poultry Science*, **89**(1): 115–122.

Tieleman BI, Williams JB, Ricklefs RE, Klasing KC. 2005. Constitutive innate immunity is a component of the pace-of-life syndrome in tropical birds. *Proceedings of the Royal Society B*, **272**(1573): 1715–1720.

Trayhurn P. 2005. Endocrine and signalling role of adipose tissue: new perspectives on fat. *Acta Physiologica*, **184**(4): 285–293.

Trigunaite A, Dimo J, Jørgensen TN. 2015. Suppressive effects of androgens on the immune system. *Cellular Immunology*, **294**(2): 87–94.

Vasilijević A, Buzadžić B, Korać A, Petrović V, Janković A, Mićunović K, Korać B. 2007. The effects of cold acclimation and nitric oxide on antioxidative enzymes in rat pancreas. *Comparative Biochemistry and Physiology Part C*, **145**(4): 641–647.

Walker EP. 1968. Mammals of the World. 2nd ed. Baltimore: Johns Hopkins Press.

Wang DH. 2007. Advances in Animal Ecology. 1st ed. Beijing: Higher Education Press, 29–46.

Wang DH, Wang YS, Wang ZW. 2000. Metabolism and thermoregulation in the Mongolian gerbil *Meriones unguiculatus*. *Acta Theriologica*, **45**(2): 183–192.

Wang DH, Wang ZW, Wang YS, Yang JC. 2003. Seasonal changes of thermogenesis in Mongolian gerbils (*Meriones unguiculatus*) and Brandt's voles (*Microtus brandtii*). *Comparative Biochemistry and Physiology Part A*, **134**: S96.

Xu DL, Wang DH. 2010. Fasting suppresses T cell-mediated immunity in female Mongolian gerbils (*Meriones unguiculatus*). *Comparative Biochemistry and Physiology Part A*, **155**(1): 25–33.

Xu DL, Wang DH. 2011. Glucose supplement reverses the fasting-induced suppression of cellular immunity in Mongolian gerbils (*Meriones unguiculatus*). *Zoology*, **114**(5): 306–312.

Xu Y, Yang Z, Su C. 1992. Enhancement of cellular immune function during cold adaptation of BALBc inbred mice. *Cryobiology*, **29**(3): 422–427.

Xu DL, Liu XY, Wang DH. 2011. Food restriction and refeeding have no effect on cellular and humoral immunity in Mongolian gerbils (*Meriones unguiculatus*). *Physiological and Biochemical Zoology*, **84**(1): 87–98.

Yang XP. 2004. Laboratory Manual in Animal Physiology. 1st ed. Beijing: Higher Education Press, 91–94.

Yang DB, Xu YC, Wang DH, Speakman JR. 2013. Effects of reproduction on immuno-suppression and oxidative damage, and hence support or otherwise for their roles as mechanisms underpinning life history trade-offs, are tissue and assay dependent. *Journal of Experimental Biology*, **216**: 4242–4250.

Yuksel S, Dilek A, Ozfer Y. 2008. Antioxidative and metabolic responses to extended cold exposure in rats. *Acta Biologica Hungarica*, **59**(1): 57–66.

Zhang XY, Wang DH. 2006. Energy metabolism, thermogenesis and body mass regulation in Brandt's voles (*Lasiopodomys brandtii*) during cold acclimation and rewarming. *Hormones and Behavior*, **50**(1): 61–69.

Zhang ZB, Wang ZW. 1998. Ecology and Management of Rodent Pests in Agriculture. Beijing: Ocean Publishing House.

Zhao ZJ, Wang DH. 2006. Short photoperiod influences energy intake and serum leptin level in Brandt's voles (*Microtus brandtii*). *Hormones and Behavior*, **49**(4): 463–469.

Zhou SS, Cao LL, Xu WD, Cao J, Zhao ZJ. 2015. Effect of temperature on oxidative stress, antioxidant levels and uncoupling protein expression in striped hamsters. *Comparative Biochemistry and Physiology Part A*, **189**: 84–90.

Leukocyte cell-derived chemotaxin 2 inhibits development of atherosclerosis in mice

Wen-Ming He[1,2], Ting Dai[2], Jiong Chen[3,*], Jian-An Wang[1,*]

[1] *Department of Cardiology of the Second Affiliated Hospital*, *Zhejiang University School of Medicine*, *Hangzhou Zhejiang* 310009, *China*

[2] *Department of Cardiology*, *the Affiliated Hospital of Medical School of Ningbo University*, *Ningbo Zhejiang* 315010, *China*

[3] *Laboratory of Biochemistry and Molecular Biology*, *School of Marine Sciences*, *Meishan Campus*, *Ningbo University*, *Ningbo Zhejiang* 315832, *China*

ABSTRACT

Leukocyte cell-derived chemotaxin 2 (LECT2), a multifunctional hepatokine, is involved in many pathological conditions. However, its role in atherosclerosis remains undefined. In this study, we administered vehicle or LECT2 to male *Apoe*$^{-/-}$ mice fed a Western diet for 15 weeks. Atherosclerotic lesions were visualized and quantified with Oil-red O and hematoxylin staining. The mRNA expression levels of MCP-1, MMP-1, IL-8, IL-1β, and TNF-α were analyzed by quantitative real-time polymerase chain reaction. Serum TNF-α, IL-1β, IL-8, MCP-1, and MMP-1 concentrations were measured by enzyme-linked immunosorbent assay. CD68, CD31, and α-SMA, markers of macrophages, endothelial cells, and smooth muscle cells, respectively, were detected by immunostaining. Results showed that LECT2 reduced total cholesterol and low-density lipoprotein concentrations in serum and inhibited the development of atherosclerotic lesions, accompanied by reductions in inflammatory cytokines and lower MCP-1, MMP-1, TNF-α, IL-8, and IL-1β mRNA abundance. Furthermore, LECT2 decreased CD68, but increased α-SMA in atherosclerotic lesions, suggesting an increase in smooth muscle cells and reduction in macrophages. In summary, LECT2 inhibited the development of atherosclerosis in mice, accompanied by reduced serum total cholesterol concentration and lower inflammatory responses.

Keywords: Leukocyte cell-derived chemotaxin 2 (LECT2); Atherosclerosis; Inflammation; Lipid metabolism

INTRODUCTION

Cardiovascular diseases are the leading cause of mortality worldwide. With ageing populations and increasing exposure to metabolic risks, deaths due to cardiovascular diseases will increase to approximately 23 million by 2030 (GBD 2017 Risk Factor Collaborators, 2018). Atherosclerosis is an important underlying cause of many clinical cardiovascular events, and is a systemic disease characterized by fatty deposits, inflammation, cell death, fibrosis, and scar tissue build up within the walls of arteries (Mozaffarian et al., 2016). In the early stages of atherosclerosis, a large amount of lipids and proinflammatory mediators accumulate in macrophages within the arterial wall, which become foam cells (Lim & Park, 2014). As the disease advances, vascular smooth muscle cells (VSMCs) migrate from the media to intima, and then proliferate and produce extracellular matrix to form a fibrous cap that covers atherosclerotic plaque (Allahverdian et al., 2018). During this stage, the secretion of many proinflammatory cytokines is increased, including interleukin (IL)-8, IL-1β, monocyte chemoattractant protein-1 (MCP-1), and tumor necrosis factor (TNF)-α (Chistiakov et al., 2015). In the advanced stage, macrophages induce VSMC apoptosis via the TNF-α/NO signaling pathway (Boyle et al., 2003) and reduce collagen synthesis by secretion of matrix metalloproteinases (MMP) (Müller et al., 2014). Although the precise pathogenesis of atherosclerosis has not been clarified, it is now widely accepted that inflammation and lipid disorder both play crucial roles (Ference et al., 2017; Hansson &

Received: 01 April 2019; Accepted: 27 May 2019; Online: 4 June 2019

Foundation items: This project was supported by the Program for the National Natural Science Foundation of China (31772876), Ningbo Municipal Bureau of Science and Technology (2018A610389), Scientific Innovation Team Project of Ningbo (2015C110018), and K.C. Wong Magna Fund in Ningbo University

*Corresponding authors, E-mail: wangjianan111@ zju. edu. cn; jchen1975@163.com

DOI: 10.24272/j.issn.2095-8137.2019.030

Libby, 2006).

Recent studies have demonstrated that a set of predominantly liver-derived proteins can directly affect the progression of atherosclerosis (Yoo & Choi, 2015). Leukocyte cell-derived chemotaxin 2 (LECT2) is a 16 kDa secretory protein first isolated from cultured supernatants of phytohemagglutinin-activated human T-cell leukemia SKW-3 cells. It is predominantly secreted by hepatocytes (Yamagoe et al., 1998) and is generally expressed in vascular cells, endothelial cells, and VSMCs (Slowik & Apte, 2017). Previous studies have reported that LECT2 has an inhibitory effect on inflammation. In mice, LECT2 deficiency can cause severe arthritis, with reductions in the production of cytokines and chemokines, e.g., IL-1β, IL-6, TNF-α, and MCP-1, after exogenous LECT2 injection (Okumura et al., 2008). We recently reported that LECT2 can protect mice against bacterial sepsis by enhancing phagocytosis and bacterial killing of macrophages via CD209a (Lu et al., 2013) and can also induce hematopoietic stem cell expansion and mobilization (Lu et al., 2016). In human hepatocellular carcinoma, low LECT2 expression is correlated with advanced histological grade and inflammatory infiltrates. L'Hermitte et al. (2019) showed that LECT2-deficient hepatocellular carcinoma cells can secrete chemotactic signals, resulting in amplification of inflammatory monocytes, which harbor an immature phenotype with immunosuppressive capacities and tumor-promoting potential. In addition, Zhang et al. (2018) discovered that circulating LECT2 concentrations are significantly higher in newly diagnosed type-2 diabetic patients, especially those that are obese, and that concentrations of LECT2 are negatively associated with high-density lipoprotein-cholesterol levels. Researchers have also found that LECT2 is involved in many other pathological conditions, such as obesity (Sargeant et al., 2018), skeletal muscle insulin resistance (Jung et al., 2018), non-alcoholic fatty liver disease, and metabolic syndrome (Yoo et al., 2017), thus suggesting the potential role of LECT2 in atherosclerosis. However, such roles remain undefined. The purpose of this study was to investigate the effects of LECT2 on atherosclerosis in *Apoe*$^{-/-}$ mice.

MATERIALS AND METHODS

Animals

Male *Apoe*$^{-/-}$ and C57BL/6 wild-type mice (6 weeks old, 20±2 g) were purchased from Beijing Vital River Laboratory Animal Technology (China). The C57BL/6 mice were fed a normal laboratory diet and used as blank controls, whereas the *Apoe*$^{-/-}$ mice were fed a Western diet (0.15% w/w cholesterol, 40 kcal% butter fat, Beijing Biotech-HD) for 15 weeks as an atherosclerosis model. All mice were housed in a constant temperature (21±2 °C) room, under a 12 h dark/12 h light cycle in a pathogen-free environment in the Animal Care Facility of Ningbo University Medical School according to the institutional guidelines.

In vivo application of LECT2

Mice were randomly divided into three groups: i.e., (1) control group (C57BL/6 mice, PBS 100 μL, subcutaneous (sc), *n*=8), (2) atherosclerosis (AS) group (*Apoe*$^{-/-}$ mice, PBS 100 μL, sc, *n*=8), and (3) LECT2 group (*Apoe*$^{-/-}$ mice, LECT2 0.2 mg/kg, sc, *n*=8). Each mouse received a sc injection every 2 d from 6 to 21 weeks of age. LECT2 was dissolved in PBS and kept at 4 °C for 2 d. Two days after the last injection, mice were euthanized to analyze and characterize atherosclerosis.

Recombinant LECT2 protein

Recombinant mouse LECT2 proteins (purity: 96.20%) were produced from CHO cells, as described in our previous research (Lu et al., 2013, 2016).

Measurement of lipid parameters

Two days after final administration, all mice were sacrificed after retro-orbital bleeding. All blood samples were centrifuged at 3 000 r/min for 15 min at room temperature to collect serum. Commercially available kits were then used to measure total cholesterol (TC), total triglyceride (TG), high-density lipoprotein cholesterol (HDL-c), and low-density lipoprotein cholesterol (LDL-c) concentrations according to the manufacturer's protocols.

LECT2 detection

The ELISA system used one antibody as the capture antibody (rabbit anti-LECT2, C-terminal; Santa Cruz, CA, USA.) and another for detection (goat anti-LECT2, N-terminal; Santa Cruz, CA, USA.).

ELISA for cytokines

Serum concentrations of inflammatory cytokines, TNF-α (MTA00B, R&D Systems , Minneapolis, MN, USA), IL-1β (MLB00C, R&D Systems , Minneapolis, MN, USA), IL-8 (SBJ-M0010, Senbeijia Bio. Co, Nanjing, China), MMP-1 (CSB-E07417m, CUSABIO, China), and MCP-1 (CSB-E07430m, CUSABIO, China) were measured with commercial ELISA kits according to the manufacturer's instructions. Absorbance was measured using a Multiskan Ascent plate reader (Thermo Electron Corporation, Waltham, Massachusetts, USA).

Histological evaluation

After termination, the periaortic tissue around the aorta was cleaned, and the whole aorta from the heart to the abdominal aorta was dissected. Atherosclerotic plaque in the aortas was stained with 0.5% Oil-red O (Sigma-Aldrich) for 15 min at room temperature. After staining, the aortas were washed with 70% ethanol and then distilled water. Subsequently, the whole aorta was cut open and flattened on a black plate to take pictures. Aortic roots were embedded in optimal cutting temperature compound (Sakura, Torrance, CA, USA) and frozen in ultra-cold isopentane on dry ice. Serial cryosections (8 μm) were cut along the aortic root specimens at −20 °C using a cryotome (HM550, Thermo Scientific, Rockford, IL, USA). At least three transverse sections (spaced around 60 μm) from each aortic root were stained with hematoxylin/eosin for histology analyses. Oil-red O staining was performed

to evaluate the lipid content in the plaque area. Image Pro-Plus 6.0 (Media Cybernetics, USA) was used to analyze aorta images, following the recent AHA Statement (Daugherty et al., 2017).

Immunohistochemistry (IHC)

IHC staining was performed on 8 μm frozen sections of the aortic root to detect the proportion of macrophages, endothelial cells, and SMCs. Frozen sections were air-dried, fixed with cold acetone, and incubated in anti-CD31 antibody (1:50 dilution; ab28364, Abcam, USA), anti-CD68 antibody (1:50 dilution; ab125212, Abcam, USA), and anti-alpha smooth muscle actin antibody (1:200 dilution; ab5694, Abcam, USA), respectively, at 4 °C overnight. Substitution of PBS for the specific primary antibody was performed as a negative control. All steps were operated following the instruction manual of the SABC (rabbit IgG)-POD kit (Solarbio, Beijing, China). Finally, slides were stained with DAB, counterstained with hematoxylin, dehydrated, and mounted. Images were detected using a Nikon A1R confocal laser scanning microscope (Nikon, Tokyo, Japan). Image Pro-Plus 6.0 software (Media Cybernetics, Rockville, USA) was used to analyze the positively stained areas. At least three sections were analyzed per aortic root.

Total RNA isolation and quantitative real-time polymerase chain reaction (qRT-PCR)

Aorta total RNA (five mice from control, AS, and LECT2 groups) was extracted by Trizol reagent (Invitrogen, Carlsbad, CA, USA) following the manufacturer's protocols. Complementary DNA (cDNA) was synthesized using a HiFiScript first-strand cDNA synthesis kit (ComWin Biotech, Beijing, China) according to the manufacturer's instructions. PCR amplification was accomplished using 1×FastStart Essential DNA Green Master (Roche, Mannheim, Germany) with a LightCycler 480 II instrument (Roche, Switzerland). The primer sequences used included (forward and reverse): MCP-1, 5'-TTAAAAACCTGGATCGGAACCAA-3' and 5'-GCATTAG CTTCAGATTTACGGGT-3'; MMP-1, 5'-TGTTTGCAGAGCAC TACTTGAA-3' and 5'-CAGTCACCTCTAAGCCAAAGAAA-3'; IL-8, 5'-TCGAGACCATTTACTGCAACAG-3' and 5'-CATTGCC GGTGGAAATTCCTT-3'; IL-1β, 5'-AGAAGCTGTGGCAGCTA-3' and 5'-TGAGGTGCTGATGTACCA-3'; TNF-α, 5'-GAACTGG CAGAAGAGGCACT-3' and 5'-GGTCTGGGCCATAGAACTG A-3'; and 18S rRNA, 5'-TTTGTTGGTTTTCGGAACTGA-3' and 5'-CGTTTATGGTCGGAACTACGA-3'. Data were normalized to 18S rRNA and the dosage of the target fragments was calculated using the $2^{-\Delta\Delta CT}$ method. Sequences were confirmed using NCBI BLAST software.

Statistical analysis

Results were presented as means±standard deviation (*SD*). Statistical analysis was performed using GraphPad Prism 7.0 (GraphPad Software, San Diego, CA, USA). The Shapiro-Wilk test was used to check the normality of the data. If data displayed normal distribution, an unpaired Student's *t*-test was used to compare two groups. If the data did not display normal distribution, the Mann-Whitney U test was performed.

RESULTS

LECT2 inhibited development of atherosclerotic lesions in *Apoe*$^{-/-}$ mice

We analyzed the levels of LECT2 in the AS and control groups to examine the relationship between serum LECT2 levels and atherosclerosis. Results showed that the LECT2 levels in the AS group (33.37±2.85 ng/mL, n=6) were significantly lower than that in the control group (43.62±2.20 ng/mL, n=6; P<0.05). Oil-red O staining showed no obvious atherosclerotic plaque in the control group aortas, but apparent plaque in the aortas of the AS group. The LECT2 group had less atherosclerotic plaque in the ascending aortic arch and thoracic regions compared with the AS group (P<0.001) (Figure 1A). Consistently, hematoxylin and Oil-red O staining of the aortic sinus for atherosclerotic lesions also showed reduced lipid accumulation in the LECT2 group compared with the AS group (P<0.001) (Figure 1B).

LECT2 reduced serum lipids in *Apoe*$^{-/-}$ mice

There is a close connection between dyslipidemia and atherosclerosis (Wang et al., 2018). Compared with the AS group, LCET2 administration reduced the serum total cholesterol (927±160 mg/dL, 768±79 mg/dL, P<0.05), TG (57±16 mg/dL, 33±11 mg/dL, P<0.01), HDL-c (123±10 mg/dL, 111±7 mg/dL, P<0.05), and LDL-c concentrations (452±81 mg/dL, 374±37 mg/dL, P<0.05) (Figure 2).

LECT2 reduced mRNA abundance of inflammatory cytokines and chemokines

We performed qRT-PCR to confirm the effect of LECT2 on MCP-1, MMP-1, TNF-α, IL-1β, and IL-8 mRNA expression. Consistent with the systemic inflammation findings, the mRNA expression levels of these inflammatory cytokines and chemokines in the whole aorta were lower in the LECT2 group than that in the AS group (Figure 3A–E). Furthermore, results showed a dose-dependent relationship, whereby the inflammatory cytokines and chemokines decreased with the increase in LECT2 concentration (data not shown).

LECT2 led to lower serum inflammatory cytokine concentrations in *Apoe*$^{-/-}$ mice

Inflammation is a critical biological process in atherosclerosis (Wolf & Ley, 2019). Compared with the control group, serum concentrations of inflammatory cytokines and chemokines, including TNF-α (P<0.05), IL-1β (P<0.01), IL-8 (P<0.01), MCP-1 (P<0.001), and MMP-1 (P<0.001), were higher in the AS group. Administration of LCET2 led to reductions of these inflammatory cytokines (Figure 3F–J).

LECT2 changed atherosclerotic plaque composition

We assessed the proportion of smooth muscle cells, macrophages, and endothelial cells by IHC staining to determine whether LECT2 affected the composition of atherosclerotic plaque. Compared with the AS group, LECT2

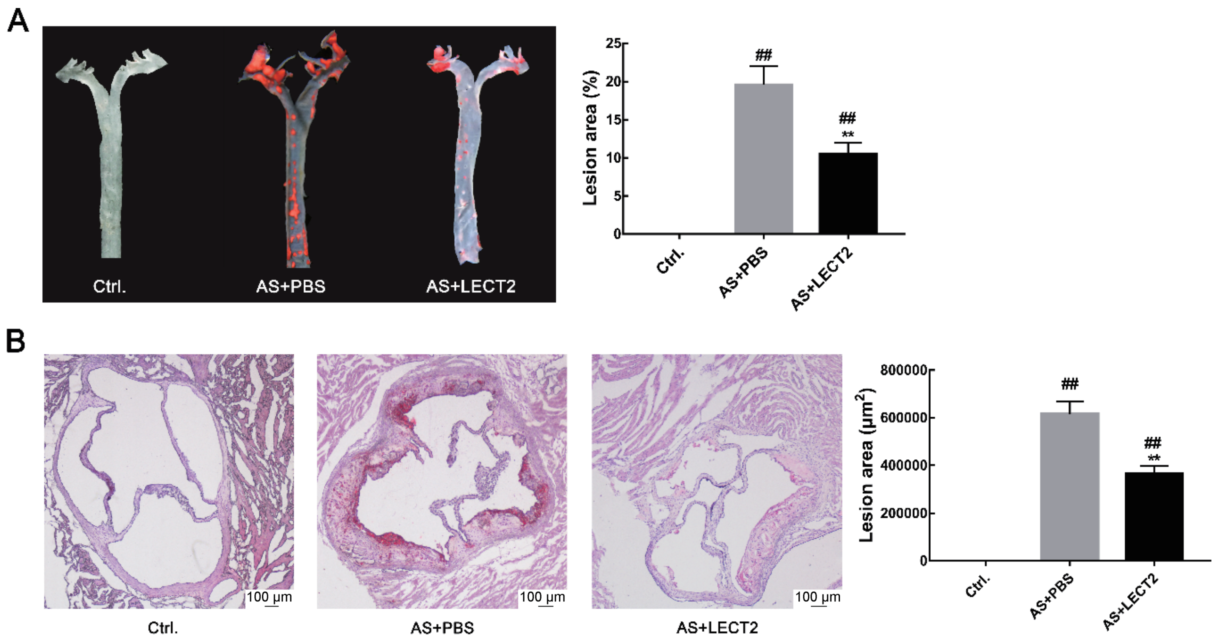

Figure 1 LECT2 attenuated development of atherosclerotic lesions in *Apoe*$^{-/-}$ mice

A: Representative en-face images of Oil-red O-stained aortas from control, AS, and LECT2 groups (*n*=3 per group). The percentage of atherosclerotic plaque area to total aortic surface area was measured using an en-face method. B: Oil-red O staining of aortic sinus sections (*n*=8 per group). Data are means±*SD*. ##: *P*<0.01, vs. control; **: *P*<0.01, vs. AS group. Scale bars: 100 μm.

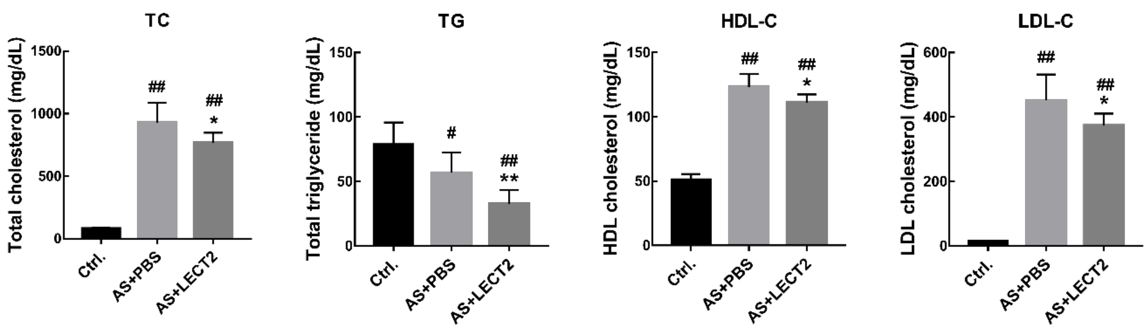

Figure 2 Effects of LECT2 on lipid profile in serum

Apoe$^{-/-}$ mice were fed a Western diet from 6 weeks of age and were treated with 0.2 mg/kg LECT2 every 2 d. A–C: Plasma total cholesterol (TC), triglyceride (TG), and low-density lipoprotein cholesterol (LDL-c) concentrations at 21 weeks of age (*n*=8 per group). Data are means±*SD*. #: *P*< 0.05, ##: *P*<0.01 vs. control; *: *P*<0.05, **: *P*<0.01, vs. AS group.

administration increased the number of smooth muscle cells (Figure 4A) and reduced the proportion of CD68 macrophages (Figure 4B) but had no influence on the proportion of CD31 endothelial cells in the lesions (Figure 4C).

DISCUSSION

In the present study, we investigated the effects of LECT2 on the development of atherosclerosis in mice. Results demonstrated that LECT2 exhibited an anti-atherosclerotic function, accompanied by a reduction in serum total cholesterol concentration and lower inflammatory responses.

We first measured atherosclerotic lesions in the aortas of *Apoe*$^{-/-}$ mice and found that LECT2 inhibited atherosclerosis, resulting in a 46% reduction in total plaque size. In addition to the observed reduction in plaque, LECT2 also had an effect on the serum lipid profile. The liver plays a central role in regulating whole body cholesterol homeostasis. Hepatocytes maintain cellular cholesterol homeostasis by controlling several cholesterol input and elimination pathways. These

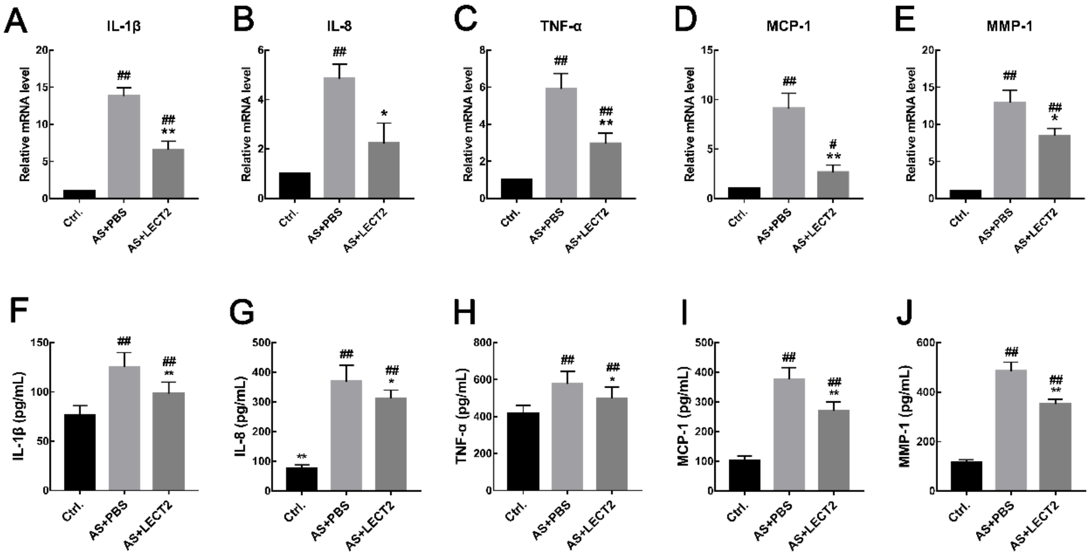

Figure 3 LECT2 reduced mRNA expression and serum concentrations of inflammatory cytokines and chemokines in *Apoe*$^{-/-}$ mice

mRNA expression of IL-1β (A), IL-8(B), TNF-α(C), MCP-1(D), and MMP-1(E) was quantified by qRT-PCR (*n*=5 per group). And the serum concentrations were determined using enzyme-linked immunosorbent assay (*n*=8 per group). Data are means±*SD*. #: *P*<0.05, ##: *P*<0.01, vs. control; *: *P*<0.05, **: *P*<0.01, vs. AS group.

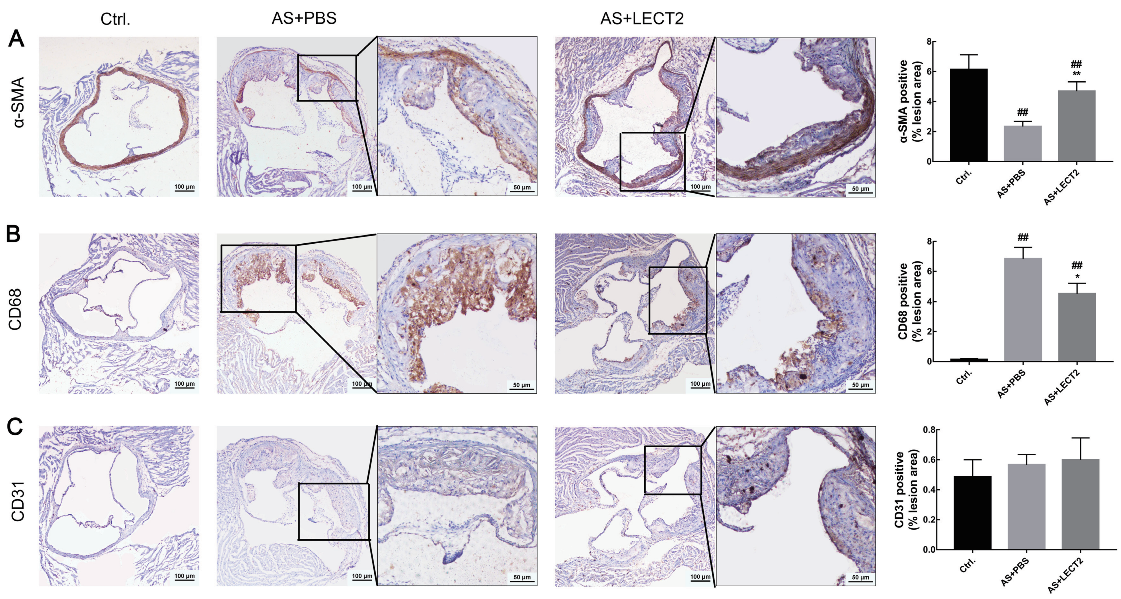

Figure 4 LECT2 changed atherosclerotic plaque composition

Sections of aortic root from control, AS, and LECT2 groups (*n*=8 per group) immunostained for smooth muscle cells (A: α-SMA), macrophages (B: CD68), and endothelial cells (C: CD31). Positive signals are shown in brown. Sections were counterstained with hematoxylin. Data are means±*SD*. ##: *P*<0.01, vs. control; **: *P*<0.01, vs. AS group. Scale bars: 100 μm.

input pathways are primarily regulated by the sterol regulatory element-binding protein (SREBP)-2-mediated cholesterol sensing mechanism (Ye & DeBose-Boyd, 2011). In earlier studies, Hwang et al. (2015) showed that LECT2 increases mTOR phosphorylation and SREBP-1 cleavage in hepatocytes, leading to hepatic lipid accumulation; however, the study did not show serum lipid levels or SREBP-2 expression. Mammalian cells produce three SREBP isoforms, which control the anabolic pathways of cholesterol, free fat acids, and triglycerides (Engelking et al., 2018). SREBP-1a and SREBP-1c are active in driving the transcription of genes involved in fatty acid synthesis, whereas SREBP-2 is more

active in stimulating transcription of genes involved in cholesterol biosynthesis (Ye & DeBose-Boyd, 2011). Based on our results, we hypothesize that LECT2 may reduce serum TG, TC, and LDL-c concentrations and contribute to its anti-atherosclerotic effects by impacting the SREBP pathways. However, this needs to be corroborated by subsequent studies.

In addition to lipid accumulation, the inflammatory mechanism is another important factor in the pathogenesis and clinical manifestation of atherosclerosis. In the process of atherosclerosis, proinflammatory factors, including IL-1β and IL-8, are expressed by ox-LDL-stimulated endothelial cells and VSMCs, which, in turn, activate macrophages, resulting in amplification of the inflammatory response (Chistiakov et al., 2015; Wolf & Ley, 2019). The MCP-1 chemokine, also known as CC-chemokine ligand 2, plays an important role in the recruitment of monocytes to atherosclerotic lesions, and also contributes to thrombin generation and thrombus formation by generating tissue factor (Charo & Taubman, 2004). Han et al. (1998) reported that elevated plasma LDL concentrations can enhance C-C chemokine receptor type 2 (CCR2, receptor for MCP-1) expression and chemotactic response. Thus, LECT2 may reduce MCP-1 expression by decreasing LDL-c concentrations. On the other hand, inflammation can increase cellular cholesterol uptake and synthesis via up-regulation of low-density lipoprotein receptor and 3-hydroxy-3-methylglutaryl-coenzyme A reductase, but can decrease cholesterol efflux via down-regulation of liver X receptor alpha and ATP-binding cassette transporter A1 (Zhong et al., 2015), implying that inflammation promotes lipid accumulation and foam cell formation by disrupting cellular cholesterol homeostasis. Previous research has also shown that LECT2 is a direct target gene of the Wnt/β-catenin signaling pathway, and β-catenin negatively regulates nuclear transcription factor (NF- κB) signaling, which plays an important role in the regulation of inflammation responses (Ovejero et al., 2004). The results of our study are consistent with the above theory. We proved that circulating LECT2 levels were significantly lower in atherosclerotic mice, suggesting that LECT2 has an inhibitory effect on atherosclerosis. LECT2 mitigated the expression and secretion of IL-1β, IL-8, TNF-α, and IL-1β (Figure 3) dose-dependently in *Apoe*$^{-/-}$ mice fed with a Western diet, suggesting that LECT2 may inhibit atherosclerosis by alleviating inflammatory responses via Wnt/β-catenin signaling. In addition, macrophage-derived MMPs, which play a potential role in fibrous cap thinning, are thought to promote vascular smooth muscle cell growth and extracellular matrix and atherosclerotic plaque homeostasis (Johnson, 2007) via degradation of various extracellular matrix proteins, including collagens (Moore & Tabas, 2011). We found that LECT2 also increased the content of SMCs but reduced the proportion of macrophages (Figure 4), likely reflecting the role of LECT2 in regulating the composition of atherosclerotic plaque.

In conclusion, we showed, for the first time, that LECT2 inhibits the development of atherosclerosis in a hypercholesterolemic mouse model, accompanied by reduced serum total cholesterol concentration and lower inflammatory responses. Our future studies will aim to define the mechanisms involved in LECT2 prevention of atherosclerosis development.

COMPETING INTERESTS

The authors declare that they have no competing interests.

AUTHORS' CONTRIBUTIONS

W.M.H., J.A.W., and J.C. conceived and designed the experiments. W.M.H. and T. D. performed the experiments, analyzed the data, and wrote the manuscript. J. A. W. and J. C. reviewed and corrected the manuscript. All authors read and approved the final version of the manuscript.

REFERENCES

Allahverdian S, Chaabane C, Boukais K, Francis GA, Bochaton-Piallat ML. 2018. Smooth muscle cell fate and plasticity in atherosclerosis. *Cardiovascular Research*, **114**(4): 540–550.

Boyle JJ, Weissberg PL, Bennett MR. 2003. Tumor necrosis factor-alpha promotes macrophage-induced vascular smooth muscle cell apoptosis by direct and autocrine mechanisms. *Arteriosclerosis, Thrombosis, and Vascular Biology*, **23**(9): 1553–1558.

Charo IF, Taubman MB. 2004. Chemokines in the pathogenesis of vascular disease. *Circulation Research*, **95**(9): 858–866.

Chistiakov DA, Orekhov AN, Bobryshev YV. 2015. Vascular smooth muscle cell in atherosclerosis. *Acta Physiologica*, **214**(1): 33–50.

Daugherty A, Tall AR, Daemen MJAP , Falk E, Fisher EA, Garcia-Cardena G, Lusis AJ, Owens P, III, Rosenfeld ME, Virmani R. 2017. Recommendation on design, execution, and reporting of animal atherosclerosis studies: A scientific statement from the american heart association. *Arteriosclerosis, Thrombosis, And Vascular Biology*, **37**(9): E131–E157.

Engelking LJ, Cantoria MJ, Xu Y, Liang G. 2018. Developmental and extrahepatic physiological functions of SREBP pathway genes in mice. *Seminars in Cell & Developmental Biology*, **81**: 98–109.

Ference BA, Ginsberg HN, Graham I, Ray KK, Packard CJ, Bruckert E, Hegele RA, Krauss RM, Raal FJ, Schunkert H, Watts GF, Borén J, Fazio S, Horton JD, Masana L, Nicholls SJ, Nordestgaard BG, van de Sluis B, Taskinen MR, Tokgözoğlu L, Landmesser U, Laufs U, Wiklund O, Stock JK, Chapman MJ, Catapano AL. 2017. Low-density lipoproteins cause atherosclerotic cardiovascular disease. 1. Evidence from genetic, epidemiologic, and clinical studies. A consensus statement from the European Atherosclerosis Society Consensus Panel. *European Heart Journal*, **38**(32): 2459–2472.

GBD 2017 Risk Factor Collaborators. 2018. Global, regional, and national comparative risk assessment of 84 behavioural, environmental and occupational, and metabolic risks or clusters of risks for 195 countries and territories, 1990-2017: a systematic analysis for the Global Burden of Disease Study 2017. *Lancet*, **392**(10159): 1923–1994.

Han KH, Tangirala RK, Green SR, Quehenberger O. 1998. Chemokine receptor CCR2 expression and monocyte chemoattractant protein-1-mediated chemotaxis in human monocytes. A regulatory role for plasma

LDL. *Arteriosclerosie, Thrombosis, and Vascular Biology*, **18**(12): 1983 – 1991.

Hansson GK, Libby P. 2006. The immune response in atherosclerosis: a double-edged sword. *Nature Reviews Immunology*, **6**(7): 508–519.

Hwang HJ, Jung TW, Kim BH, Hong HC, Seo JA, Kim SG, Kim NH, Choi KM, Choi DS, Baik SH, Yoo HJ. 2015. A dipeptidyl peptidase-IV inhibitor improves hepatic steatosis and insulin resistance by AMPK-dependent and JNK-dependent inhibition of LECT2 expression. *Biochemical Pharmacoloyg*, **98**(1): 157–166.

Johnson JL. 2007. Matrix metalloproteinases: influence on smooth muscle cells and atherosclerotic plaque stability. *Expert Review Cardiovascular Therapy*, **5**(2): 265–282.

Jung TW, Chung YH, Kim HC, Abd El-Aty AM, Jeong JH. 2018. LECT2 promotes inflammation and insulin resistance in adipocytes via P38 pathways. *Journal of Molecular Endocrinology*, **61**(1): 37–45.

L'Hermitte A, Pham S, Cadoux M, Couchy G, Caruso S, Anson M, Crain-Denoyelle AM, Celton-Morizur S, Yamagoe S, Zucman-Rossi J, Desdouets C, Couty JP. 2019. Lect2 controls inflammatory monocytes to constrain the growth and progression of hepatocellular carcinoma. *Hepatology*, **69**(1): 160–178.

Lim S, Park S. 2014. Role of vascular smooth muscle cell in the inflammation of atherosclerosis. *BMB Reports*, **47**(1): 1–7.

Lu XJ, Chen J, Yu CH, Shi YH, He YQ, Zhang RC, Huang ZA, Lv JN, Zhang S, Xu L. 2013. LECT2 protects mice against bacterial sepsis by activating macrophages via the CD209a receptor. *Journal of Experimental Medicine*, **210**(1): 5–13.

Lu XJ, Chen Q, Rong YJ, Yang GJ, Li CH, Xu NY, Yu CH, Wang HY, Zhang S, Shi YH, Chen J. 2016. LECT2 drives haematopoietic stem cell expansion and mobilization via regulating the macrophages and osteolineage cells. *Nature Communications*, **7**: 12719.

Moore KJ, Tabas I. 2011. Macrophages in the pathogenesis of atherosclerosis. *Cell*, **145**(3): 341–355.

Mozaffarian D, Benjamin EJ, Go AS, Arnett DK, Blaha MJ, Cushman M, Das SR, de Ferranti S, Despres JP, Fullerton HJ, Howard VJ, Huffman MD, Isasi CR, Jimenez MC, Judd SE, Kissela BM, Lichtman JH, Lisabeth LD, Liu S, Mackey RH, Magid DJ, McGuire DK, Mohler ER, 3rd, Moy CS, Muntner P, Mussolino ME, Nasir K, Neumar RW, Nichol G, Palaniappan L, Pandey DK, Reeves MJ, Rodriguez CJ, Rosamond W, Sorlie PD, Stein J, Towfighi A, Turan TN, Virani SS, Woo D, Yeh RW, Turner MB. 2016. Heart disease and stroke statistics-2016 update: A report from the American Heart Association. *Circulation*, **133**(4): e38–360.

Müller A, Krämer SD, Meletta R, Beck K, Selivanova SV, Rancic Z, Kaufmann PA, Vos B, Meding J, Stellfeld T, Heinrich TK, Bauser M, Hütter J, Dinkelborg LM, Schibli R, Ametamey SM. 2014. Gene expression levels of matrix metalloproteinases in human atherosclerotic plaques and evaluation of radiolabeled inhibitors as imaging agents for plaque vulnerability. *Nuclear Medicine and Biology*, **41**(7): 562–569.

Okumura A, Saito T, Otani I, Kojima K, Yamada Y, Ishida-Okawara A, Nakazato K, Asano M, Kanayama K, Iwakura Y, Suzuki K, Yamagoe S. 2008. Suppressive role of leukocyte cell-derived chemotaxin 2 in mouse anti-type II collagen antibody-induced arthritis. *Arthritis & Rheumatism*, **58**(2): 413–421.

Ovejero C, Cavard C, Périanin A, Hakvoort T, Vermeulen J, Godard C, Fabre M, Chafey P, Suzuki K, Romagnolo B, Yamagoe S, Perret C. 2004. Identification of the leukocyte cell-derived chemotaxin 2 as a direct target gene of β-catenin in the liver. *Hepatology*, **40**(1): 167–176.

Sargeant JA, Aithal GP, Takamura T, Misu H, Takayama H, Douglas JA, Turner MC, Stensel DJ, Nimmo MA, Webb DR, Yates T, King JA. 2018. The influence of adiposity and acute exercise on circulating hepatokines in normal-weight and overweight/obese men. *Applied Physiology, Nutrition, and Metabolism*, **43**(5): 482–490.

Slowik V, Apte U. 2017. Leukocyte Cell-Derived Chemotaxin-2: It's role in pathophysiology and future in clinical medicine. *Clinical and Translational Science*, **10**(4): 249–259.

Wang Y, Ding WX, Li T. 2018. Cholesterol and bile acid-mediated regulation of autophagy in fatty liver diseases and atherosclerosis. *Biochimica et Biophysica Acta. Molecular and Cell Biology of Lipids*, **1863**(7): 726–733.

Wolf D, Ley K. 2019. Immunity and inflammation in atherosclerosis. *Circulation Research*, **124**(2): 315–327.

Yamagoe S, Mizuno S, Suzuki K. 1998. Molecular cloning of human and bovine LECT2 having a neutrophil chemotactic activity and its specific expression in the liver. *Biochimica et Biophysica Acta*, **1396**(1): 105–113.

Ye J, DeBose-Boyd RA. 2011. Regulation of cholesterol and fatty acid synthesis. *Cold Spring Harbor Perspectives in Biology*, **3**(7): a004754.

Yoo HJ, Choi KM. 2015. Hepatokines as a link between obesity and cardiovascular diseases. *Diabetes & Metabolism Journal*, **39**(1): 10–15.

Yoo HJ, Hwang SY, Choi JH, Lee HJ, Chung HS, Seo JA, Kim SG, Kim NH, Baik SH, Choi DS, Choi KM. 2017. Association of leukocyte cell-derived chemotaxin 2 (LECT2) with NAFLD, metabolic syndrome, and atherosclerosis. *PLoS One*, **12**(4): e0174717.

Zhang Z, Zeng H, Lin J, Hu Y, Yang R, Sun J, Chen R, Chen H. 2018. Circulating LECT2 levels in newly diagnosed type 2 diabetes mellitus and their association with metabolic parameters: An observational study. *Medicine*, **97**(15): e0354.

Zhong S, Zhao L, Li Q, Yang P, Varghese Z, Moorhead JF, Chen Y, Ruan XZ. 2015. Inflammatory stress exacerbated mesangial foam cell formation and renal injury via disrupting cellular cholesterol homeostasis. *Inflammation*, **38**(3): 959–971.

Morphology-based intraspecific taxonomy of *Oreocryptophis porphyraceus* (Cantor, 1839) in mainland China (Serpentes: Colubridae)

DEAR EDITOR,

In this study, a total of 106 individuals of *Oreocryptophis porphyraceus* from mainland China were morphologically examined and recorded. Differences between populations were compared by combining data from this study and other published research. The skulls of three specimens representing three proposed subspecies (i.e., *O. p. pulchra*, *O. p. vaillanti*, and *O. p. hainana*) were examined by computed tomography (CT) scanning. Both external morphological characters and skull comparisons consistently showed significant differences between the studied populations. Based on these data, we suggest that at least four subspecies of *O. porphyraceus* should be recognized in mainland China: i. e., *O. p. porphyraceus*, *O. p. pulchra*, *O. p. vaillanti*, and *O. p. hainana*. However, the taxonomical arrangement of the central Chinese populations with intermediate morphology remain unresolved.

The red-bamboo rat snake *Oreocryptophis porphyraceus* (Cantor, 1839) (Figure 1) is a medium-sized colubrid widely distributed in southern and southeastern Asia, including India, Nepal, Bhutan, Myanmar, Thailand, Vietnam, Laos, Malaysia, Singapore, Indonesia, and China (Boundy et al., 2014). Within China, the species ranges from southern Xizang in the west to Taiwan in the east and from Gansu and Shaanxi in the north to Hainan in the south (Zhao, 2006).

The species was originally described as *Coluber porphyraceus* based on specimens from the Mishmee Hills (= Mishmii Hills) in Assam, India (Cantor, 1839), after which it was transferred into the genus *Elaphe* by Denburgh (1909). Finally, based on molecular phylogeny inferred from mitochondrial DNA, Utiger et al. (2002) erected the monotypic genus *Oreocryptophis* to accommodate the species.

The intraspecific taxonomy of *O. porphyraceus* has long been controversial. Nine subspecies have been proposed historically, with six originally described from China, though seven are thought to occur (Table 1).

Schulz & Entzeroth (1996) recognized seven of the nine subspecies mentioned in Table 1, except for *O. p. vaillanti* (Sauvage, 1877) and *O. p. sikiangensis* (Mell, 1931), based primarily on body patterns (Figure 2), and proposed that five subspecies, excluding *O. p. coxi* (Schulz & Entzeroth, 1996) and *O. p. laticincta* (Schulz & Entzeroth, 1996), could be found in China. Zhao (2006) suggested that *O. porphyraceus* should be identified as three subspecies in China: i.e., *O. p. porphyraceus* in southwest China, *O. p. nigrofasciata* (Cantor, 1839) in central and eastern China, and *O. p. hainana* (Mell, 1931) on Hainan Island. However, Das (2012) did not follow this taxonomical arrangement, instead advocating *O. p. pulchra* (Schmidt, 1925) in southern China, *O. p. vaillanti* in eastern China, and *O. p. kawakamii* (Oshima, 1910) on Taiwan Island. It should be noted, however, that all proposed taxonomical arrangements have been based on pholidosis, body patterns, and incomplete samples.

To explore the intraspecific diversity and clarify how many subspecies are present in mainland China, we examined the external morphology of *O. porphyraceus* specimens preserved in Chinese museums and also compared the skulls of several specimens from different populations.

In total, 47 characters related to scalation, coloration pattern, and body dimensions were examined and recorded for 106 specimens (49 males, 52 females, five juveniles; see Appendix I for details).

Measurements were taken with a digital slide-caliper to 0.1 mm except for snout-vent length (SVL), tail length (TL), and length of black flank stripes (BFS), which were measured by a measuring tape to 1 mm. The characters and their definitions are listed in Appendix II. Characters and their definitions followed Zhao (2006) and Zhong et al. (2017). For comparison, other data were obtained from previous literature (Pope, 1935; Schulz & Entzeroth, 1996; Zhao et al., 1998).

The skulls of three specimens from Yunnan (YBU 14076), Zhejiang (YBU 17246), and Hainan (YBU 12007), representing three proposed subspecies (i.e., *O. p. pulchra*, *O. p. vaillanti*, and *O. p. hainana*), were examined using CT scanning at the

Received: 17 October 2018; Accepted: 03 April 2019; Online: 10 April 2019

Foundation items: This study was supported by the Strategic Priority Research Program of the Chinese Academy of Sciences (XDA 20050201) and National Natural Science Foundation of China (NSFC31372152)

DOI: 10.24272/j.issn.2095-8137.2019.048

Figure 1 General view of *Oreocryptophis porphyraceus* from Yunnan (A: *O. p. pulchra*), Zhejiang (B: *O. p. vaillanti*), Hainan (C: *O. p. hainana*), and Sichuan (D: central China population)

Chengdu Institute of Biology (CIB), Chinese Academy of Sciences (CAS). Specimens were scanned at 70 KV with a flux of 114 μA, with other parameters set following Shi et al. (2017). A total of 720 transmission images were reconstructed into a 2 048×2 048 matrix of 802 slices using VGStudio max (a three-dimensional reconstruction program) developed by CIB, CAS. Based on the photos, 20 characters were recorded or measured by direct counting, Snake Measure Tool software, or digital slide-caliper. Measurements and descriptive methods for different bones and characters followed Cundall (1981) and Guo et al. (2010) and their abbreviations are listed in Appendix II.

Among the 106 specimens examined, the maximum total length was 1 096 (930+166) mm. The following characters were identified: 9–16 cross-bands on body, 2–5 on tail; each cross-band occupying 2–17 rows of vertebrae. Loreal 1 (absent in three individuals); preocular 1; postoculars 2; temporals 1+2 (rarely 1+1, 1+3); supralabials 8, 3-2-3 (rarely 7, 3-2-2, 2-2-3); infralabials 8–10, 3-2-3, 3-2-4, 4-2-3, or 4-2-4 (rarely 11, 4-2-5), with first 4–5 touching anterior chin-shields; dorsal scales in 19-19-17 rows (rarely 19-19-15), all smooth; ventrals 177–203 in males, 181–209 in females; subcaudals 53–76 pairs in males, 50–71 in females. Two black flank stripes extending from tip of tail through to whole body or interrupted at mid body. Black stripe present on middle of head, sometimes extending beyond posterior edge of parietal; on lateral head, two black stripes extending immediately behind eyes to first cross-band or to black flank stripes.

Several characters were significantly different between populations. For example, the specimens from southwestern China (Yunnan, Western Guizhou, and Southwestern Sichuan, same below) showed black head stripe exceeding posterior edge of parietal (vs. absent in other populations) and black flank stripes not exceeding half of total length (vs. exceeding half of total length in other populations); specimens from the Hainan population possessed more than 70 pairs of subcaudals (vs. less than 70 pairs in other populations). A detailed comparison of external morphology is listed in Supplementary Table S1.

The skulls of the three representative specimens were generally consistent with other colubrid snakes (Cundall, 1981; Zhang, 1988). The skulls were also phenotypically similar in some characters, including bulbiform parietal and post-orbits not touching frontals (Figure 3). However, the skulls also exhibited several differences; e. g., weak parietal ridge in southwestern China populations (vs. strong in other populations), posterior margin of frontal straight in Hainan population (vs. curved in other populations), supratemporals extending beyond posterior end of braincase in other populations (vs. not in southwestern China population), post-

Table 1 Subspecies proposed for *Oreocryptophis porphyraceus*

Subspecies	Original description	Type locality	Diagnostics	Distribution
O. p. porphyraceus	*Coluber porphyraceus* (Cantor, 1839)	Assam, India	Black flank stripe along posterior of body	India, Nepal, Bhutan, Myanmar, NW Thailand, W Yunnan China
O. p. nigrofasciata	*Psammophis nigrofascia-tus* (Cantor, 1839)	Singapore (doubted), E China was designated as type locality by Smith (1930)	Black flank stripe along entire of body	E China, N Vietnam
O. p. vaillanti	*Simotes vaillanti* (Sau-vage, 1877)	E China	Black head stripe not exceeding the posterior edge of parietal; black flank stripes along whole body	E China
O. p. kawakamii	*Liopeltis kawakamii* (Osi-ma, 1910)	Taiwan, China	6th supralabial touching parietal, cross-bands 4 scales wide	Taiwan Province of China
O. p. pulchra	*Elaphe porphyracea pul-chra* (Schmidt, 1925)	Kunming, Yunnan, China	Similar to *O. p. porphyracea*, but dis-tinguished by fewer ventrals (177–185) and subcaudals (51–56)	Yunnan, Sichuan, W Guizhou, Gansu, Shaanxi of China
O. p. hainana	*Elaphe porphyracea hain-ana* (Mell, 1931)	Hainan, China	Similar to *O. p. nigrofasciata*, distin-guished by more than 70 subcaudals	Hainan Province of China
O. p. sikiangensis	*Elaphe porphyracea sikian-gensis* (Mell, 1931)	Luofushan, Guang-dong, China	Similar to *O. p. nigrofasciata*, ven-trals 195, subcaudals 72	Guangdong and Fujian provinces of China
O. p. laticincta	*Elaphe porphyracea la-ticincta* (Schulz, 1996)	Malaysia and Sumatra	Much wider cross-bands, covering 9–15 rows of dorsal scales	Malaysia and Indonesia
O. p. coxi	*Elaphe porphyracea coxi* (Schulz, 1996)	NE Thailand	Distinctly broad flank stripes, lacking cross-bands in adults, which may be observed on necks of juveniles	NE Thailand

orbits triangular in southwestern China population (vs. broad T-shaped in eastern inland China population and arc-shaped in Hainan population). Detailed descriptions and comparisons of the three skulls are listed in Supplementary Table S2.

Based on comparison of external morphology and skull characteristics, we suggest that at least four subspecies of *O. porphyraceus* should be recognized in mainland China: i. e., *O. p. porphyraceus*, *O. p. pulchra*, *O. p. vaillanti*, and *O. p. hainana*. The diagnostic characters and approximate geographical distribution of each subspecies are discussed below and shown in Supplementary Table S3.

Oreocryptophis p. porphyraceus (Figure 2 A) was originally diagnosed by "bright porphyry-red, with black transverse lines edged with white, posterior portion of body with two black parallel dorsal lines; beneath light yellow; ventral scales 213; subcaudals 64" (Cantor, 1839). No topotype was available for morphological examination in this study. However, Prof. Jing Che from the Kunming Institute of Zoology, Chinese Academy of Sciences, recorded a juvenile (KIZ019349) from Motuo county, Xizang Autonomous Region, China, which is very close to the type locality of this subspecies (personal communication). The specimen possessed 206 ventrals, 58 pairs of subcaudals, and 23 cross-bands on its body, much more than that in other populations. Considering its proximity to the type locality, we regard the specimens from southeastern Xizang as *O. p. porphyraceus*.

Oreocryptophis p. pulchra was named based on specimens from Kunming, Yunnan Province. It was distinguished from *O. p. porphyraceus* by having fewer ventrals (177–185) and subcaudals (51–56 pairs) (Schmidt, 1925).

Morphological comparison indicated that specimens from the southwestern China population shared the following characters: ventrals less than 209, cross-bands on body 11–17, black head stripe extending beyond posterior edge of parietal, and black flank stripes visible only on posterior third of body (Figures 1A, 2B; Supplementary Table S1). Additionally, the skull from Yunnan was slender, with very weak parietal ridge, supratemporals did not exceed beyond posterior edge of braincase, and post process of prefrontal was not significant (Figure 3A; Supplementary Table S2). The numbers of ventrals and subcaudals fell within the range of those from the southern Yunnan, western Guizhou, and southwestern Sichuan populations (177–209 ventrals and 50–67 subcaudals, respectively. Supplementary Table S1).

Based on the above, we agree with Das (2012), Schmidt (1925), and Schulz & Entzeroth (1996) that the specimens from southwest China, including Yunnan, western Guizhou, and southwestern Sichuan should be identified as *O. p. pulchra*.

Three names have been proposed for the eastern inland China (Jiangsu, Anhui, Zhejiang, Jiangxi, Fujian, northeastern Guangdong, Hong Kong, eastern Hunan, eastern Hubei, and

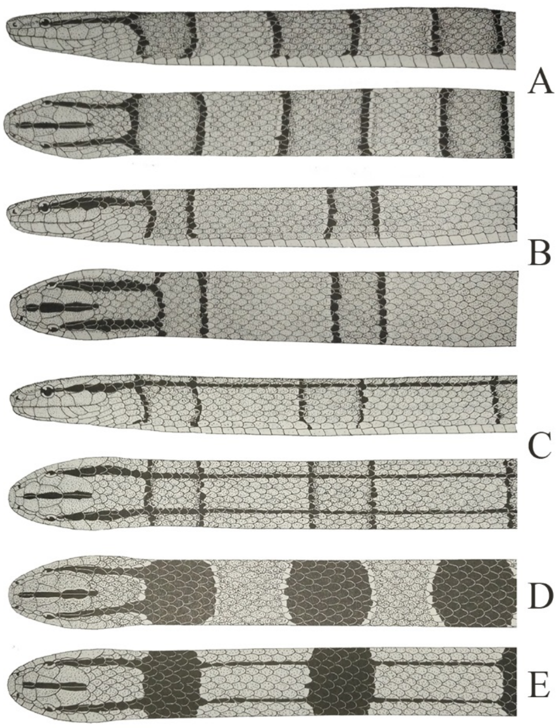

Figure 2 Body patterns of *Oreocryptophis porphyraceus* summarized by Schulz (1996)

A: Adult *O. p. porphyraceus*; B: Adult *O. p. pulchra*; C: Adults *O. p. vaillanti* and *O. p. hainana*; D: Juveniles *O. p. porphyraceus* and *O. p. pulchra*; E: Juveniles *O. p. vaillanti* and *O. p. hainana*.

southeastern Henan) population: i. e., *Psammophis nigrofasciatus* (*O. p. nigrofasciata*), *Simotes vaillanti* (*O. p. vaillanti*), and *Elaphe porphyracea sikiangensis* (*O. p. sikiangensis*). *Oreocryptophis p. nigrofasciata* was originally described based on specimens from Singapore and diagnosed by "light reddish-yellow above, with broad cross-bands and two barbed dorsal lines of the same color; the interval between these dorsal lines dotted with black; ventrals 245; subcaudals 75" (Cantor, 1839). Smith (1930), followed by several other authors (e.g., Pope, 1935; Schulz & Entzeroth, 1996; Zhao, 2006), suggested that the type locality of *O. p. nigrofasciata* was most likely incorrect, and thus eastern China was designated as the type locality of this subspecies. Within the specimens (40 individuals) we examined from eastern inland China, the maximum number of ventrals was 209 (214 in Zhao (2006)), much lower than that in the original description (Cantor, 1839); in addition, there were no more than 70 pairs of subcaudals. Obviously, the specimens from eastern inland China could not be identified as *O. p. nigrofasciata*.

The specimens from eastern inland China shared the following characters: cross-bands on body less than 11, black head stripe not exceeding posterior edge of parietal, black flank stripes extending along whole body, less than 70 pairs of subcaudals (Figures 1B, 2C; Supplementary Table S1). From the Zhejiang specimen skull, the anterior portion was short, ventral process of basioccipital was strong, and posterior edge of supraoccipital was strong (Figure 3B; Supplementary Table S2). These characters were distinct from the other populations but were congruent with the diagnostic characters of *O. p. vaillanti* proposed by Sauvage (1877): "The black head stripe does not exceed the posterior edge of the parietal, the black flank stripes extend from the back of the eyes and along the body to the end of the tail". *Oreocryptophis p. sikiangensis* was originally described from Guangdong Province, China, as by having 195 ventrals and 72 subcaudals (Mell, 1931). In fact, except for the subcaudals, its pholidosis and color pattern are in line with those of *O. p. vaillanti*. Thus, we suggest that the population from eastern inland China should be recognized as *O. p. vaillanti*.

The specimens from Hainan Island were originally described as *Elaphe porphyracea hainana* (*O. p. hainana*) and as having more than 70 pairs of subcaudals (vs. less than 70 in other subspecies). This arrangement was accepted by Schulz & Entzeroth (1996), but not by Das (2012); Zhao et al. (1998) proposed that some specimens from Guangdong and Guangxi have more than 70 pairs of subcaudals, and thus stated that this subspecies was likely invalid. However, Zhao (2006) subsequently recognized the validity of *O. p. hainana*.

Based on our examination and previously published data (Zhao et al., 1998), 17 out of 19 specimens from Hainan (89.5%) had more than 70 subcaudals, with only two females (10.5%) having fewer (Supplementary Table S1). The specimens from Hainan also exhibited the following unique skull characters: blunt, basioccipital process tall, posterior end of frontal straight, and post-orbit arc-shaped (Figure 3C; Supplementary Table S2).

Therefore, based on external and skull morphology, we suggest that *O. p. hainana* is valid, and maybe endemic to Hainan, China.

In addition to the populations mentioned above, the central China population (including northern Guangxi, eastern Guizhou, western Hunan, Chongqing, northern and eastern Sichuan, Gansu, Shaanxi, western Henan, and western Hubei) exhibited intermediate external morphology between the southwestern China and eastern inland China populations in body coloration and pholidosis. For example, the average numbers of ventrals, subcaudals, and cross-bands (189.83/58.8/10.68) of the central China population were between those of the southwestern China population (185.36/56.65/13.52) and eastern inland China population (196.06/64.61/9.8); the black flank stripes extended along the whole body or were only present in the posterior part of the body (Supplementary Table S1); and occasionally the black flank stripes were indistinct or intermittent anteriorly. However, based on current data, we cannot conclude to which subspecies it should be assigned, or whether the central China population represents a different subspecies altogether.

It should be noted that the above taxonomical arrangement was mainly based on morphological comparison. Subspecies boundaries and particularly subspecies geographical

Figure 3 CT scans of skulls of *Oreocryptophis porphyraceus* from Yunnan (A: *O. p. pulchra*), Zhejiang (B: *O. p. vaillanti*), and Hainan (C: *O. p. hainana*)

distributions were not clearly determined. Further study using genetic data and complete sampling could provide evidence to clarify these issues.

COMPETING INTERESTS

The authors declare that they have no competing interests.

AUTHORS' CONTRIBUTIONS

P. W. and P. G. designed the study. P. W. collected data, performed data analyses, and wrote the manuscript with input from all authors. P.G. and L. S. revised the manuscript. All authors read and approved the final version of the manuscript.

ACKNOWLEDGEMENTS

We are grateful to the following institutes, museums, and their curators for their help and permission to examine the preserved specimens under their care: Central China Normal University; Chengdu Institute of Biology, Chinese Academy of Sciences; Fujian Normal University; Guizhou Normal University; Hainan Normal University; Kunming Institute of Zoology, Chinese Academy of Sciences; Sun Yat-Sen University; and Zhejiang Forest Resources Monitoring Center.

Ping Wang[1,2], Lei Shi[1,*], Peng Guo[2,*]

[1] *College of Animal Science*, *Xinjiang Agricultural University*, *Urumqi Xinjiang* 830052, *China*

[2] *College of Life Science and Food Engineering*, *Yibin University*, *Yibin Sichuan* 644007, *China*

[*]Corresponding authors, E-mail: shileixj@126.com; ybguop@163.com

REFERENCES

Boundy J, Wallach V, Williams KL. 2014. Snakes of the World: A Catalogue of Living and Extinct Species. Boca Raton: Chemical Rubber Company Press.

Cantor TE. 1839. Picilegium Serpentium Indicorum. London: Proceedings of the Zoological Society of London.

Cundall D. 1981. Cranial osteology of the colubrid snake genus *Opheodrys*. *Copeia*, **1981**(2): 353–371.

Das I. 2012. A Naturalist's Guide to the Snakes of South-east Asia. Malaysia, Singapore, Thailand, Myanmar, Borneo, Sumatra, Java and Bali. Oxford, England: John Beaufoy Publishing.

Denburgh JV. 1909. New and previously unrecorded species of reptiles and amphibians from the island of Formosa. *San Francisco, California Academy of Sciences*, **3**(4): 49–56.

Guo P, Jadin RC, Malhotra A, Li C. 2010. An investigation of the cranial evolution of Asian pitvipers (Serpentes: Crotalinae), with comments on the phylogenetic position of *Peltopelor macrolepis*. *Acta Zoologica*, **91**(4): 402–407.

Mell R. 1931. List of Chinese snakes. *Lingnan Science Journal*, **8**: 199–219.

Oshima M. 1910. An annotated list of formosan snakes, with descriptions of four new species and one new subspecies. *Annotationes Zoologicae Japonenses*, **7**(3): 185–207.

Pope CH. 1935. The reptiles of China, natural history of central Asia. *American Museum of Natural History*, **10**: 303–304.

Sauvage HE. 1877. Sur quelques ophidiens d'espèces nouvelles ou peu connues de la collection du muséum. *Bulletin de la Société Philomathique de Paris*, **7**(1): 107–115.

Schmidt KP. 1925. New Chinese amphibians and reptiles. *American Museum Novitates***,** (175): 1890–1957.

Schulz KD, Entzeroth A. 1996. Monograph of the Colubrid Snakes of the Genus *Elaphe* Fitzinger. Königstein: Koeltz Scientific Books.

Shi JS, Wang G, Chen X, Fang YH, Ding L, Huang S, Hou M, Liu J, Li PP. 2017. A new moth-preying alpine pit viper species from Qinghai-Tibetan Plateau (Viperidae, Crotalinae). *Amphibia-Reptilia*, **38**(4): 517–532.

Smith MA. 1930. The Reptilia and Amphibia of the Malay Peninsula. Singapore: Bulletin of the Raffles Museum.

Utiger U, Helfenberger N, Schätti B, Schmidt C, Ruf M, Ziswiler V. 2002. Molecular systematics and phylogeny of Old and New World ratsnakes, Elaphe Auct., and related genera (Reptilia, Squamata, Colubridae). *Russian Journal of Herpetology*, **9**(2): 105–124.

Zhang FJ. 1988. A comparative study on the cranial morphology of Chinese *Zaocys*, *Ptyas*, *Elaphe* and *Entechinus*, with preliminary discussions on the function and phylogeny. *Acta Herpetologica Sinica*, **7**(1): 47–55.

Zhao EM. 2006. Snakes of China. Hefei: Anhui Science and Technology Publishing House.

Zhao EM, Huang MH, Zong Y. 1998. Fauna Sinica: Reptilia, Vol. 3, Squamata, Serpentes. Beijing: Science Press.

Zhong GH, Liu Q, Li C, Peng PH, Guo P. 2017. Sexual dimorphism and geographic variation in the Asian Lance-headed Pitviper *Protobothrops mucrosquamatus* in the Mainland China. *Asian Herpetological Research*, **8**(2): 11–122.

APPENDIX I

Information for specimens examined in this study.

CCNU: Central China Normal University; CIB: Chengdu Institute of Biology, Chinese Academy of Sciences; FJNU: Fujian Normal University; GZNU: Guizhou Normal University; HNNU: Hainan Normal University; KIZ: Kunming Institute of Zoology, Chinese Academy of Sciences; SYSU: Sun Yat-Sen University; YBU: Yibin University.

Chongan, Fujian: CIB9308−9310, CIB9312−9314, CIB9316−9318, CIB64I5354, FJNU3571008, FJNU3571011, FJNU3571012, FJNU3571014, FJNU3571015, FJNU3571018−3571020, FJNU3571023, FJNU3571024, FJNU3571026, FJNU3571028. Fuzhou, Fujian: FJNU3571022, FJNU3571030. Putian, Fujian: FJNU3571021, FJNU3571035, FJNU3571036. Nanping, Fujian: KIZ056354–056356. Dongyang, Zhejiang: YBU17273, YBU17246. Shangrao, Jiangxi: SYSU000646, SYSU000665. Shaoguan, Guangdong:

SYSU000821. Hainan: HNNUR0008, HNNUR0268, HNNUR1017, YBU12007, CIB9328. Chengzhou, Hunan: CIB9329 – 9331. Nanning, Guangxi: CIB9319. Guilin, Guangxi: SYSU000234, KIZ750003. Baise, Guangxi: YBU11202. Wuzhou, Guangxi: YBU17252. Fangchenggang, Guangxi: YBU15138. Suizhou, Hubei: CCNU0011753. Huanggang, Hubei: CCNU0000022. Yichang, Hubei: YBU13322A. Kunming, Yunnan: CIB78020, CIB9297, CIB9298, CIB9302, CIB94021, KIZ640015, KIZ640016, KIZ640008, KIZ83004, KIZ87001, KIZ87003. Pu'er, Yunnan: CIB78019, KIZ75II0202, KIZ75II0195, KIZ75II0840. Honghe, Yunnan: KIZ85I0069, YBU14076, KIZ85I0660. Baoshan, Yunnan: CIB9303–9306, CIB00358. Xishuangbanna, Yunnan: CIB9299, CIB9300, KIZ75008, KIZ75I360, KIZ75I411, KIZ75I430. Mianyang, Sichuan: CIB9294, CIB94011, CIB102877. Leshan, Sichuan: CIB9290, CIB9292, CIB9295. Pengzhou, Sichuan: CIB9296, CIB83610, CIB83611. Luzhou, Sichuan: YBU071076. Chongqing: CIB9293, CIB9307. Leishan, Guizhou: CIB03363, CIB9320 – 9322, CIB9324, CIB9325. Weining, Guizhou: CIB9327. Rongjiang, Guizhou: CIB99428, GZNUGS0056. Jiangkou, Guizhou: YBU13204. Liuan, Anhui: CIB9332.

APPENDIX II

Characters recorded and their abbreviations.

External morphology: SVL: Snout-vent length; TL: Tail length; Vs: Number of ventrals; Sc: Number of subcaudals; RBFSL: Ratio of black flank stripes to total body length; NCB: Number of cross-bands; BHS: Black head stripe exceeding posterior edge of parietal or not; CBCRD: Cross-band on body covering dorsal rows along body vertebrae; CTCRD: Cross-band on tail covering rows of dorsal tail scales along caudal vertebrae; CBBL: Length of cross-band on body along body vertebrae; CBTL: Length of cross-band on tail along caudal vertebrae; SIL: Length of sulcus between internasals; SPfL: Length of sulcus between prefrontals; FL: Length of frontal; HL: Length of head; ML: Length of mouth; SupOL: Length of supraoculars; PL: Length of parietal; NL: Length of nasals; LL: Length of loreals; BFSL: Length of black flank stripes; MWI: Maximum width between outside of internasals; MWPf: Maximum width between outside of prefrontals; FW: Maximum width of frontal; HW: Maximum width of head; PW: Maximum width of parietals; SupOW: Maximum width of supraoculars; NW: Width of nasals; LW: Width of loreals; EO: Diameter of eyes; BHSL: Length of black head stripe; CBW: Position where sides of cross-bands transversely extend; VS19 – 17: Ventral position corresponding to reduction from 19 to 17 scale rows of dorsal; Sc12 – 10: Subcaudal position corresponding to reduction of dorsal tail scales from 12 to 10 scale rows; Sc10–8: Subcaudal position corresponding to reduction of dorsal tail scales from 10 to 8 scale rows; Sc8 – 6: Subcaudal position corresponding to reduction of dorsal tail scales from 8 to 6 scale rows; Sc6 – 4: Subcaudal position corresponding to reduction of dorsal tail scales from 6 to 4 scale rows; Sc4 – 2: Subcaudal position corresponding to reduction of dorsal tail scales from 4 to 2 scale rows.

Skull bones: An: Angular; Bo: Basioccipital; Bs: Basisphenoid; Co: Columellar; Cp: Compound bone; Dt: Dentary; Ec: Ectopterygoid; Eo: Exoccipital; Fr: Frontal; Mx: Maxilla; Na: Nasal; Pa: Parietal; Pro: Pre-orbit; Pl: Palatine; Pm: Premaxilla; Po: Post-orbit; Pr: Prootic; Pt: Pterygoid; Qt: Quadrae; Sm: Septomaxilla; So: Supraoccipital; Sp: Splenial; St: Supratemporal; Vo: Vomer.

Skull characters: SL: Skull length; SW: Skull width; AP: Anterior portion; PL: Parietal length; FL: Frontal length; StL: Supratemporal length; PoL: Postfrontal length; SPLW: Skull proportion of SL (from front top of premaxilla to post end of exoccipital along mid line of head) to SW (widest parietal); RAPS: Relative length of anterior portion to HL; RLFr: Relative length of frontal to HL; RLP: Relative length of parietal to HL; RLS: Relative length of supratemporal to HL; RLQ: Relative length of quadrate to HL; RLM: Relative length of mandible to HL; RLPf: Relative length of postfrontal to HL; NPaT: Number of palatine teeth; NMT: Number of maxilla teeth; NDT: Number of dentary teeth; PR: Parietal ridge; SEBB: Supratemporal extending beyond posterior end of braincase; FSE: Fused (or not) supraoccipital and exoccipital; BoP: Basioccipital process; PP: Prefrontal process; BsP: Basisphenoid process; PeF: Posterior end of frontal; SdP: Supraoccipital dorsal process; SPo: Shape of post-orbit.

ZOOLOGICAL RESEARCH

A new cave-dwelling blind loach, *Triplophysa erythraea* sp. nov. (Cypriniformes: Nemacheilidae), from Hunan Province, China

DEAR EDITOR,

A new blind loach species, *Triplophysa erythraea* **sp. nov.**, from a karst cave in Hunan Province, central south China, is described based on morphology and cyt *b* gene sequencing. It can be distinguished from other species of *Triplophysa* by the following combination of characters: eyes absent; body scaleless and colorless; caudal-fin 17; maxillary barbel longest; fins transparent, compressed pectoral-fin reaching 2/3 distance between pectoral-fin and pelvic-fin origins; pelvic-fin and dorsal-fin origins relative; posterior chamber of airbladder well developed, long, oval, and dissociative.

Blindfish possess distinctly degenerated or completely lost eyes due to their cave or subterranean water system or deep ocean habitats (Zhao & Zhang, 2009). These specialized fish species are found within Cypriniformes, mostly belonging to *Sinocyclocheilus* or *Triplophysa*, and inhabit various inland river systems in China (Zhang & Dai, 2010). The genus *Triplophysa* (Nemacheilidae, Cypriniformes) is comprised of small fish living in streams and primarily distributed in the Tibetan Plateau and adjacent areas (He et al., 2011; Jacobsen et al., 2017; Xiao & Dai, 2011). A total of 202 species have been reported within the genus (Eschmeyer et al., 2018), including a number of cave-dwelling species (or populations) specialized for living in underground environments (Lan et al., 2013; Li et al., 2008; Yan, 2017). So far, a total of 30 cave-dwelling species of *Triplophysa* are known to occur in China (Li et al., 2017, 2018; Wu et al., 2018; Yan, 2017), of which 27 species have been identified from Yunnan, Guizhou, and Guangxi, and two from Chongqing (*T. rosa*) and Hunan (*T. xiangxiensis*) (Lan et al., 2013; Li et al., 2017; Wu et al., 2018; Yan, 2017; Zhang & Zhao, 2016; Figure 1).

In this paper, we describe a new species of cave-dwelling *Triplophysa* found during our exploration of cave animals in the Xiangxi Tujia and Miao Nationality Autonomous Prefecture, Hunan Province, central south China.

Specimens were collected in Dalong Cave (N28°16'25.11'', E109°28'57.18'', 563 m a. s. l.), Huayuan County, Hunan Province, central southern China. Morphometric measurements were made on fresh specimens with a digital caliper (0.01 mm) and a stereomicroscope (XTL-165VT) in accordance with the protocols described in the literature (Kottelat, 1984; Zhu, 1989). An abdominal muscle sample was removed and placed in ethanol (70%) for genome DNA extraction. The specimens were then preserved in formalin (10%) and deposited in the Zoological Collection Room, College of Biology and Environmental Sciences, Jishou University.

DNA extraction and mitochondrial cytochrome *b* (cyt *b*) gene sequencing were carried out as described previously (Yan, 2017). Samples were sequenced by Sangon Biotech (Shanghai, China) using the Sanger method on an ABI 3707 (ABI, USA) instrument. The sequencing results were uploaded to GenBank after the Blast program was run in the NCBI database for confirmation, and the cyt *b* sequences of several approximate species were downloaded for molecular analysis. Genetic distances were calculated by Mega 7.0 (Kumar et al., 2016) based on the Kimura 2-parameter (K2p) model (Kimura, 1980).

Taxonomy

Triplophysa erythraea **sp. nov.** Liu & Huang
Figures 2, 3; Table 1.

Etymology: The specific name “*erythraea*” is derived from the blood-red body color of the living fish. Although their body surface is colorless and transparent, the red blood vessels are visible.

Holotype: HY18022802, intact, undissected, 105.98 mm TL (total length), 88.22 mm SL (standard length); Dalong Cave, Huayuan County, Hunan, central southern China, 28 February 2018; coordinates N28°16'25.11'', E109°28'57.18'', 563 m a.s.l..

Paratypes: HY18011301, dissected, 81.53 mm TL, 68.49 mm SL, 13 January 2018; HY18022801, dissected, 109.34 mm

Received: 07 November 2018; Accepted: 02 April 2019; Online: 12 April 2019

Foundation items: This research was supported by the National Natural Science Foundation of China (31560130) and Learning Research & Innovative Experiment Project of Hunan Province (Xiangjiaotong [2018] No. 255-601)

DOI: 10.24272/j.issn.2095-8137.2019.049

Figure 1 Distribution of *Triplophysa erythraea* sp. nov. (★), *T. xiangxiensis* (●), and *T. rosa* (■)

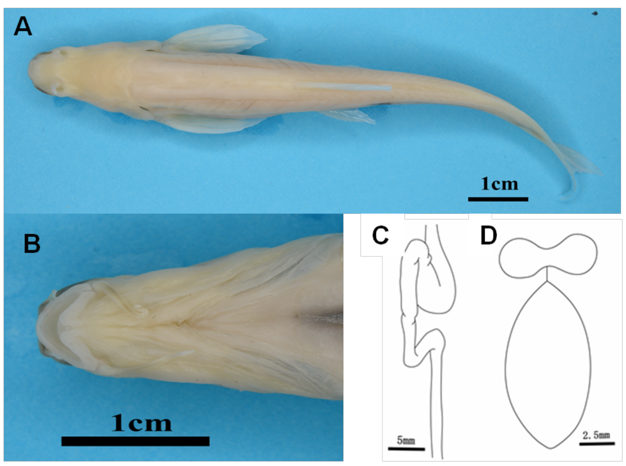

Figure 2 Morphology of *Triplophysa erythraea* sp. nov.

A: Dorsal view; B: Ventral view of head; C: Exterior view of digestive duct; D: Ventral view of bony capsule and rearward airbladder.

TL, 88.58 mm SL, 28 February 2018; two specimens collected with holotype.

Diagnosis: *Triplophysa erythraea* **sp. nov.** can be distinguished from all species of *Triplophysa* by the following combination of characters: eyes absent; body scaleless and colorless; pectoral-fin ii-10, dorsal-fin ii-8, pelvic-fin ii-5, anal-fin i-6, caudal-fin 17; maxillary barbel longest; fins transparent, compressed pectoral-fin reaching 2/3 of distance between pectoral-fin and pelvic-fin origin; pelvic-fin and dorsal-fin origin relative; edge of compressed pelvic-fin reaching anus; caudal-fin forked; posterior chamber of airbladder well developed, long, oval, and dissociative.

Description: External characteristics: Morphometric data of the new species specimens are given in Table 1. Dorsal-fin ii-8, anal-fin i-6, pectoral-fin ii-10, pelvic-fin ii-5, caudal-fin 17, 11 gill rakers in inner row on first gill arch. Cephalic lateral-line canals with 4 supratemporal, 7–9 supraorbital, 2+9–11 infraorbital, and 12 preoperculo-mandibular pores. Lateral line complete, with 63–67 pores.

Body elongated, scaleless, body side compressed posteriorly; abdominal organs and vessels of barbel, fins, and body side visible. Eyes absent. Ventral view of head fusiform, dorsum of head slightly concave in middle, posterior trunk becoming gradually smaller; trailing edge of gill covers widest and highest point of body. Snout dull, mouth inferior, upper and lower jaw arched. Edge of jaws leathery, upper jaw more developed, dentate process in center of maxilla. Lips developed, smooth, papillary process absent, lower lip with V-type median notch.

Naris circular, slanting down; anterior and posterior naris close, diameter of posterior naris larger; anterior naris in elongated nose flap without barbel-like tip, nose flap developed as triangular petal. Three pairs of developed barbels; one pair of inner rostral barbels, outer rostral barbel, and maxillary barbel, respectively; maxillary barbel longest, outer rostral barbel longer than inner rostral barbel.

Fins transparent, pterygiophore clearly visible. Pectoral-fin compressed reaching 2/3 of distance between pectoral-fin and pelvic-fin origin, first branched ray not extended; dorsal-fin distally truncate, dorsal-fin compressed slightly longer than pelvic-fin. Distance from dorsal-fin origin to caudal-fin origin closer than to snout. Pelvic-fin origin and dorsal-fin origin equal, edge of pelvic-fin reaching anus. Distance from pelvic-fin origin to anal-fin origin and caudal-fin origin to anal-fin origin equidistant. Caudal-fin forked, lobe tip; anus close to anal-fin origin.

Internal structure: Four pairs of gill arches, gill filaments intensive. Anterior chamber of airbladder wrapped in dumbbell-shaped bony capsule; posterior chamber expanded, dissociative, long, and oval. Stomach enlarged and U-shaped. Back of intestine bent in Z-shape. Length of intestine shorter than body length, indicating that new species is a possible demersal carnivorous fish.

Coloration: Live adults of the new species are bright red in color (Figure 3A, B), which is related to their visible blood vessels, not by skin pigmentation. Larvae are reddish white. Adults fixed in 10% formalin are pale (Figure 2A).

Sexual dimorphism: No sexual dimorphism was observed in the specimens examined.

Distribution and habitat: The new species is known only from Dalong Cave, Huayuan County, Hunan Province, China (Figure 1). At the cave entrance is a hydroelectric hub, from

Figure 3 Live specimens of *Triplophysa erythraea* sp. nov.

Table 1 Morphometric data of *Triplophysa erythraea* sp. nov. (all in mm)

Item	Holotype	Paratypes		Mean±*SD*
	HY18022802	HY18011301	HY18022801	
Total length (TL)	105.98	81.53	109.34	98.95±15.18
Standard length (SL)	88.22	68.49	88.58	81.76±11.50
Head length (HL)	23.44	18.49	23.44	21.79±2.86
Dorsal length	16.44	15.72	18.14	16.77±1.24
Pelvic length	13.40	10.74	13.4	12.51±1.54
Pectoral length	17.96	14.65	25.35	19.32±5.48
Anal length	13.72	9.67	14.73	12.71±2.68
Body depth/(SL) (%)	13.59	13.00	16.37	14.32±1.80
Predorsal length/(SL) (%)	53.63	52.62	55.14	53.80±1.27
Prepectoral length/(SL) (%)	28.71	26.19	28.71	27.87±1.45
Preanal length/(SL) (%)	76.91	75.61	76.91	76.48±0.75
Caudal-peduncle length/(SL) (%)	18.18	16.67	18.18	17.68±0.87
Caudal-peduncle depth/(SL) (%)	7.73	7.73	9.18	8.21±0.84
Length of dorsal-fin base/(SL) (%)	11.41	11.32	12.77	11.83±0.81
Length of anal-fin base/(SL) (%)	7.89	6.29	7.87	7.35±0.92
Length of pectoral-fin base/(SL) (%)	5.07	4.53	5.07	4.89±0.31
Length of pelvic-fin base/(SL) (%)	2.45	2.45	7.45	4.12±2.89
Upper jaw length/(SL) (%)	5.60	5.60	6.69	5.96±0.63
Lower jaw length/(SL) (%)	4.55	4.34	5.00	4.63±0.34
Mouth width/(SL) (%)	6.69	6.69	7.78	7.05±0.63
Nose width/(HL) (%)	17.36	17.36	18.39	17.70±0.59
Outer rostral barbell length/(HL) (%)	27.22	27.22	40.18	31.54±7.48
Inner Rostral barbell length/(HL) (%)	20.69	16.66	22.17	19.84±2.85
Maxillary barbell length/(HL) (%)	31.53	31.53	43.19	35.42±6.73

which rushes out a fast-flowing underground river (Figure 4). The new species was found 200−450 m into the cave tunnel from the entrance, with a mean water temperature and pH of 13.5 °C and 6.0, respectively. A total of 14 blind fish (including 12 adults and two larvae) were found in the resting shallow waters during our two surveys. We did not reach the end of the cave during the surveys due to the presence of an underground river. Additional research would be beneficial to understand the eco-biological characteristics of this new species in threatened conditions.

Molecular analysis: The length of the cyt *b* gene sequence was 1 140 bp (GenBank accession No.: MG967615), and the average content of the A, T, C, and G bases was 28.2%, 28.2%, 28.2%, and 15.4%, respectively. NCBI Blast analysis showed that the new species had highest similarity (90%) to *T. lewangensis*, although their genetic distances was 11.9%,

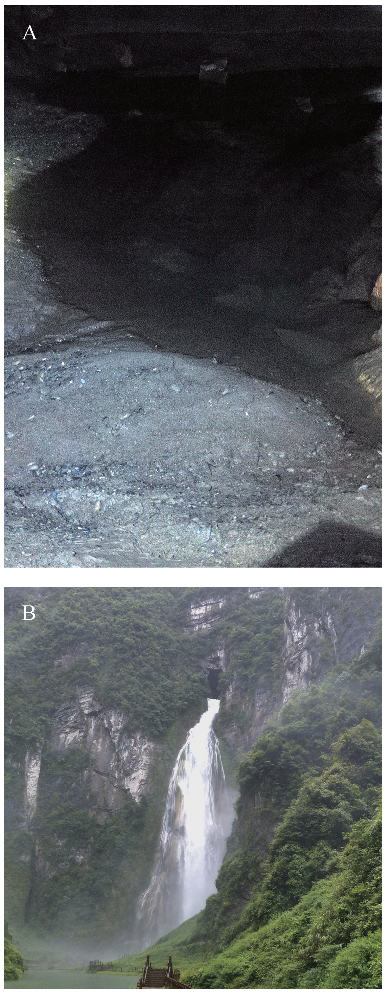

Figure 4 Habitat of *Triplophysa erythraea* sp. nov.

A: Dalong cave pool where specimens were collected; B: Waterfall at cave entrance during rainy season.

(Table 2), which surpassed the interspecies-averaged genetic distance (11.5%) of cave-dwelling *Triplophysa* based on the cyt *b* gene (Yan, 2017).

Table 2 K2p genetic distances based on the cyt *b* gene between *Triplophysa erythraea* sp. nov. and approximate species of *Triplophysa*

No.	Species (GenBank accession No.)	1	2	3
1	New species (MG967615)			
2	*T. lewangensis* (KU987438)	0.119		
3	*T. xiangxiensis* (KT751089)	0.127	0.089	
4	*T. rosa* (JF268621)	0.131	0.099	0.096

Although eyeless, with a scaleless and colorless body, the new species displayed a highly developed lateral line and barbel, indicating that it was a typical cavefish (Zhang & Dai, 2010; Zhao & Zhang 2006). Furthermore, it was easily distinguished from other species in the genus *Triplophysa* due to differences in eye normality or degeneration into a small black dot. Eyeless species in *Triplophysa* include *T. gejiuensis* (Chu & Chen, 1979), *T. xiangxiensis* (Yang et al., 1986), *T. shilinensis* (Chen et al., 1992), *T. longibarbatus* (Chen et al., 1998), *T. qiubeiensis* (Li et al., 2008), *T. huanjiangensis* (Yang et al., 2011), *T. jiarongensis* (Lin et al., 2012), *T. lihuensis* (Wu et al., 2012), *T. fengshanensis* (Lan et al., 2013), *T. dongganensis* (Lan et al., 2013), and *T. anshuiensis* (Wu et al., 2018).

The new species can be distinguished from *T. xiangxiensis*, *T. longibarbatus*, and *T. jiarongensis* by the following characters: compressed pectoral-fin reaching 2/3 of distance between pectoral-fin and pelvic-fin origin (vs. compressed pectoral-fin reaching or exceeding origin of pelvic-fin). It can be distinguished from *T. lihuensis*, *T. fengshanensis*, and *T. dongganensis* by the following characters: maxillary barbel longest, caudal-fin forked (vs. outer rostral barbel longest, caudal-fin shallow). The new species can be distinguished from *T. gejiuensis* by the following characters: distance from dorsal-fin origin to caudal-fin origin closer than to snout; maxillary barbel longest (vs. distance from dorsal-fin origin to snout closer than to caudal-fin origin; outer rostral barbel longest). It can be distinguished from *T. shilinensis* by the following characters: head tapered, front of dorsal-fin slightly compressed; posterior chamber of airbladder well developed; caudal-fin 17 (vs. head long and pointed, front of dorsal-fin slightly cylindrical; posterior chamber of airbladder degenerated; caudal-fin 14). It can be distinguished from *T. huanjiangensis* by the following characters: lip smooth, papillary process absent; pelvic-fin origin relative to vertical line of dorsal-fin origin; lateral line complete (lip papillary process present; pelvic-fin origin anterior to vertical line of dorsal-fin origin; lateral line absent). It can be distinguished from *T. qiubeiensis* by the following characters: lip developed, smooth, papillary process absent; dentate process in center of maxilla; dorsal-fin distally truncate; posterior chamber of airbladder well developed (vs. lip developed, smooth, papillary process present; no dentate process in center of maxilla; dorsal-fin distally truncate; posterior chamber of airbladder degenerated). It can be distinguished from *T. anshuiensis* by the following characters: maxillary barbel longest; pigments absent (vs. inner rostral barbel longest; black pigments irregularly present on dorsum of body).

The genetic distances indicated that the new species was most closely related to *T. lewangensis*, although the values surpassed the interspecies-averaged genetic distances (Yan, 2017) and *T. lewangensis* possess eyes (Liang & Zhou, 2019). In conclusion, based on morphology and cyt *b* gene sequencing, the blind loach collected from Dalong Cave (N28° 16'25.11'', E109° 28'57.18''), Hunan Province, central south China, was designated as a new species: *Triplophysa erythraea* **sp. nov.**

In particular, the live adult coloration (bright-red) of the new species was different from that of other cave-dwelling *Triplophysa* species (whitish, pink, or gill cover red). The

collected individuals of the new species were fed for one month in our laboratory and did not change body color during that time. This suggests that the new species should be formally designated as albino; however, further research is required to determine whether the pigment regulator genes were lost.

COMPETING INTERESTS

The authors declare that they have no competing interests.

AUTHORS' CONTRIBUTIONS

Z. X. L. designed the study. Q. Z. P., X. L. H., and P. L. Z. sequenced the mitochondrial DNA. T. W. and X. Y. G. contributed to the field work. Y. X. Z. took the specimen pictures. T. F. H. and P. L. Z. wrote the manuscript with assistance from Z. X. L. and X. L. H. All authors read and approved the final version of the manuscript.

NOMENCLATURAL ACTS REGISTRATION

The electronic version of this article in portable document format will represent a published work according to the International Commission on Zoological Nomenclature (ICZN), and hence the new names contained in the electronic version are effectively published under that Code from the electronic edition alone (see Articles 8.5–8.6 of the Code). This published work and the nomenclatural acts it contains have been registered in ZooBank, the online registration system for the ICZN. The ZooBank LSIDs (Life Science Identifiers) can be resolved and the associated information can be viewed through any standard web browser by appending the LSID to the prefixhttp: //zoobank.org/.

Publication LSID:

urn: lsid: zoobank.org: pub: 1F4D3CF7-3676-4EDC-B4F9-75F10FEA8F90.

Nomenclatural act LSID:

urn: lsid: zoobank.org: act: 8D92F37F-DB60-4395-95F1-09F0410ABAB1.

ACKNOWLEDGEMENTS

We are grateful to Dr. Zhi-Wei LIU (Eastern Illinois University) and Dr. William Harvey Reissig (Cornell University) for proofreading this manuscript, Dr. Hua-Mei Wen (Guizhou Normal University), Dr. Hai-Tao Zhao (Guizhou University of Engineering), and Dr. Zhuo-Gang Peng (Southwest University) for helping in specimen identification and offering related literature, Mr. Zhe-Yu Chen (Wuhan Polytechnic University) for advice on nomenclature, and Lu-Lu Zhou, Qiang Hu, and He-Xiang Wang (Jishou University) for assisting in the DNA experiments and field work.

Tai-Fu Huang[1,#], Pei-Ling Zhang[1,#], Xing-Long Huang[1], Tao Wu[1], Xiao-Yan Gong[1], You-Xiang Zhang[1], Qing-Zhong Peng[1], Zhi-Xiao Liu[1,*]

[1] *College of Biology and Environmental Sciences*, *Jishou University*, *Jishou Hunan* 416000, *China*

[#]Authors contributed equally to this work

[*]Corresponding author, E-mail: zxliu1965@163.com

REFERENCES

Chen YR, Yang JX, Sket B, Aljancic G. 1998. A new blind cave loach of *Paracobitis* with comment on its characters evolution. *Zoological Research*, **19**(1): 59–61. (in Chinese)

Chen YR, Yang JX, Xu GC. 1992. A new blind loach of *Triplophysa* from Yunnan stone forest with comments on its phylogenetic relationship. *Zoological Research*, **13**(1): 17–23. (in Chinese)

Chu XL, Chen YR. 1979. A new blind cobitid fish (Pisces, Cypriniformes) from subterranean waters in Yunnan, China. *Acta Zoologica Sinica*, **25**(3): 285–287. (in Chinese)

Eschmeyer WN, Fricke R, Laan R. (ed). 2018. [23 July 2018]. Catalog of fishes: genera, species, references. Electronic version, updated 2 July. Available from: (http: //researcharchive. calacademy. org/research/ichthyology/catalog/fishcatmain.asp).

Jacobsen D, Laursen SK, Hamerlik L, Hamerlik L, Moltesen K, Michelsen A, Christoffersen KS. 2017. Fish on the roof of the world: densities, habitats and trophic position of stone loaches (*Triplophysa*) in Tibetan streams. *Marine and Freshwater Research*, **68**(1): 53–64.

He CL, Song ZB, Zhang E. 2011. *Triplophysa* fishes in China and the status of its taxonomic studies. *Sichuan Journal of Zoology*, **30**(1): 150–155. (in Chinese)

Kimura M. 1980. A simple method for estimating evolutionary rates of base substitutions through comparative studies of nucleotide sequences. *Journal of Molecular Evolution*, **16**(2): 111–120.

Kottelat M. 1984. Revision of the indonesian and malaysian loaches of the subfamily Noemacheilinae. *Japanese Journal of Ichthyology*, **31**(3): 225–260.

Kumar S, Stecher G, Tamura K. 2016. MEGA7: Molecular evolutionary genetics analysis version 7.0 for bigger datasets. *Molecular Biology and Evolution*, **33**(7): 1870–1874.

Lan JH, Gan X, Wu TJ, Yang J. 2013. Cave Fishes of Guangxi, China. Beijing: Science Press, 103–144. (in Chinese)

Li CQ, Liu T, Li R, Li WX. 2018. A new cave species of the genus *Triplophysa* from Guizhou Province, China. *Journal of Jishou University (Natural Science Edition)*, **39**(4): 60–63. (in Chinese)

Li J, Lan JH, Chen XY, Du LN. 2017. Description of *Triplophysa luochengensis* sp. nov. (Teleostei: Nemacheilidae) from a karst cave in Guangxi, China. *Journal of Fish Biology*, **91**(4): 1009–1017.

Li WX, Yang HF, Chong H, Tao CP, Qi SQ, Han F. 2008. A new blind underground species of the genus *Triplophysa* (Balitoridae) from Yunnan, China. *Zoological Research*, **29**(6): 674–678. (in Chinese)

Liang J, Zhou J. 2019. The disappearance of male secondary sexual characteristics in the typical cave species in *Triplophysa*. *Transylvanian Review of Systematical & Ecological Research*, **21**(1): 57–68.

Lin Y, Chao LI, Song JK. 2012. A new species of troglobitic loach (Cypriniformes, Balitoridae), *Triplophysa jiarongensis*, from Guizhou, China. *Acta Zootaxonomica Sinica*, **37**(3): 640–647. (in Chinese)

Wu TJ, Wei ML, Lan JH, Du LN. 2018. *Triplophysa anshuiensis*, a new species of blind loach from the Xijiang River, China (Teleostei, Nemacheilidae). *ZooKeys*, **744**: 67–77.

Wu TJ, Yang J, Lan JH. 2012. A new blind loach *Triplophysa lihuensis* sp. nov. (Teleostei: Balitoridae) from Guangxi, China. *Zoological Studies*, **51**(6): 874–880.

Xiao H, Dai YG. 2011. A review of study on diversity of *Triplophysa* in China. *Fisheries Science*, **30**(1): 53–57. (in Chinese)

Yan YL. 2017. The Origin and Evolution of Cave-dwelling Group of *Triplophysa* Fishes (Teleostei, Cypriniformes, Nemacheilidae). Ph. D. Dissertation, Southwest University, Chongqing, China. (in Chinese)

Yang GY, Yuan FX, Liao YM. 1986. A new blind cobitidae fish from the subterranean water in Xiangxi, China. *Journal of Huazhong Agricultural University*, **5**(3): 219–223. (in Chinese)

Yang J, Wu TJ, Lan JH. 2011. A new blind loach species, *Triplophysa huanjiangensis* (Teleostei: Balitoridae), from Guangxi, China. *Zoological Research*, **32**(5): 566–571.

Zhang CG, Zhao YH. 2016. Species Diversity and Distribution of Inland Fishes in China. Beijing: Science Press, 135–146. (in Chinese)

Zhang XJ, Dai YG. 2010. Review for the studies on the karst cave fishes in China. *Journal of Shanghai Ocean University*, **19**(3): 364–371. (in Chinese)

Zhao YH, Zhang CG. 2006. Cavefishes: concept, diversity and research progress. *Biodiversity Science*, **14**(5): 451–460. (in Chinese)

Zhao YH, Zhang CG. 2009. Endemic Fishes of *Sinocyclocheilus* (Cypriniformes: Cyprinidae) in China-Species Diversity, Cave Adaptation, Systematics and Zoogeography. Beijing: China Science Press. (in Chinese)

Zhu SQ. 1989. The Loaches of the Subfamily Nemacheilinae in China (Cypriniformes: Cobitidae). Nanjing: Jiangsu Scientific Technology Press, 68–132. (in Chinese)

Transcription profiles of skin and head kidney from goldfish suffering hemorrhagic septicemia with an emphasis on the TLR signaling pathway

DEAR EDITOR,

Hemorrhagic septicemia is an acute, highly fatal disease that affects goldfish (*Carassius auratus*). To gain a better understanding of related immune genes, the transcriptomes of the skin and head kidney of goldfish suffering hemorrhagic septicemia were sequenced, assembled, and characterized. Based on functional annotation, an extensive and diverse catalog of expressed genes were identified in both the skin and head kidney. As two different organs, pair-wise comparison identified 122/77 unigenes up/down-regulated (two-fold change with $P<0.05$) in the skin and head kidney. Most genes of the immune pathways were expressed and isolated in both skin and head kidney, including interferon (IFN) transcription factors 1–10 and Toll-like receptors (TLRs). Interferon regulatory factor 3 (IRF3), a key IFN transcription factor, was up-regulated at the transcriptional level by polyriboinosinic: polyribocytidylic acid (poly I:C) challenge and regulated the IFN response by increasing the activity of IFN-β and IFN-stimulated response element (ISRE)-containing promoter. This study will benefit the identification and understanding of novel genes that play important roles in the immunological reactions of fish suffering from hemorrhagic septicemia.

The goldfish is not only an important ornamental and aquacultural fish in China, but also one of the most common aquarium fish worldwide (Shin & Choi, 2014). Rapid development of large-scale and highly intensive goldfish farming has increased outbreaks of disease, resulting in serious effects on aquaculture production (Choe et al., 2017). Hemorrhagic septicemia is often caused by stress and overcrowding. Both the innate and acquired immune pathways may be initiated in fish with hemorrhagic septicemia (Montero et al., 2009).

Teleosts possess both innate and adaptive immunity (Vasta et al., 2011). In addition, signal transduction in regard to immunity has been studied in mammals intensively. For example, in the Toll-like receptor signaling pathway, the innate immune system responds to pathogenic microorganism invasion using TLRs via recognition of specific molecular patterns present in microbial components. Therefore, distinct patterns of gene expression induced by the stimulation of different TLRs result not only in the activation of innate immunity but also the development of acquired specific antigen immunity (Akira & Takeda, 2004). Increased expression of immune genes such as IRF 3, IRF 7, IFN-stimulated genes (ISG)15, Type I IFN, and Interferon-induced GTP-binding protein Mx has been observed when viral copy numbers of the hemorrhagic septicemia virus (VHSV) are high, thus revealing their important roles in host defense against VHSV (Avunje et al., 2011). To the best of our knowledge, no related data have been reported regarding gene expression patterns related to hemorrhagic septicemia in goldfish. The identification of genes from infected fish could assist in the discovery of a cure for the disease. As a physical barrier in fish, the skin contains natural antibodies and protects against causative agent penetration (Bos & Kapsenberg, 1993; Hatten et al., 2001). Skin is considered the largest immunologically active organ in fish and differs from that of terrestrial vertebrates. A comprehensive understanding of fish skin is important for the development of new products such as mucosal vaccines aimed at improving the health of cultured fish (Beck & Peatman, 2015). The main cells found in the head kidney are macrophages, which aggregate into structures called melanomacrophage centers, and lymphoid cells, which are found at all developmental stages and exist mostly as B cells (Kobayashi et al., 2006).

In this study, one-year-old water-cultured goldfish were clinically diagnosed with hemorrhagic septicemia based on external reddening and hemorrhaging. Healthy fish, identified by their appearance and activity, were collected and randomly separated into two groups. The control-group was intraperitoneally injected with sterile phosphate buffer solution (PBS) and the treatment-group was injected with poly I:C (0.5 μg/g body weight; Sigma-Aldrich, USA) dissolved in

Received: 11 December 2018; Accepted: 11 April 2019; Online: 25 April 2019

Foundation items: This study was supported by a grant from the Key Project of Scientific and Technological Innovation of Blue Granary (2018YFD0901505)

DOI: 10.24272/j.issn.2095-8137.2019.028

sterile PBS. Organs, including skin, brain, liver, stomach, head kidney, ovary, and testes, were obtained from five individuals in each group 12 h after poly I:C treatment.

Trizol reagent (Invitrogen, USA) was used to extract total RNA as per the manufacturer's instructions. Genomic DNA of zebrafish was obtained from skeletal muscle tissue samples using the phenol/chloroform method.

An Illumina HiSeq library was constructed following the manufacturer's instructions. Multiplexed cDNA libraries mixed with a normalized concentration of 10 nmol/L were developed. The HiSeq 2000 platform (Illumina Inc., USA) was then used to sequence the library with the paired-end approach in a single run.

Stringent filtration and *de novo* assemble of the mixed raw sequencing reads from three samples were performed. The contigs assembled from all clean reads with Trinity software were then employed to estimate protein-coding regions through the GetORF module of the EMBOSS package (Itaya et al., 2013). Whether the read count for a given gene could be mapped depended on its sequence length and sequencing depth, with gene expression standardized by reads per kb per million reads (RPKM) (Mortazavi et al., 2008). The expression levels of all genes were compared (via RPKM) using MA plot-based DEGseq with random sampling (Wang et al., 2010). The threshold of the *q* value was determined by the Benjamini-Hochberg method with multiple tests. In the present study, "$q<10^{-3}$" and "|log2 (RPKM a/RPKM b)|⩾2" were used to judge organ-biased genes.

Quantitative polymerase chain reaction (qPCR) was carried out to measure *irf3* gene expression with the iTaq Universal SYBR Green Supermix (Bio-Rad, USA) package, as per our previous study (Wang et al., 2016). The qPCR primers are listed in Supplementary Table S1.

The full-length cDNA of goldish IRF3 was amplified with two pairs of primers, IRF3-ORF and IRF3-FLAG, using nested PCR, followed by cloning and insertion into the pCMV3-FLAG plasmid (Sigma) using double-enzyme restriction. In the same manner, the zebrafish IFN–β promoter was cloned and inserted into the luciferase reporter vector PGL3-Basic with the primer DrIFNβ-promoter. The primers used are listed in Supplementary Table S1. In the IRF3-pCMV3-FLAG plasmid, FLAG tag was merged with the N-terminal of IRF3.

Transfection of human 293T cells with plasmid and Lipofectamine 2000 was performed following the manufacturer's protocols. The 293T cells were seeded onto 24-well plates and cotransfected with different doses of pCMV3-FLAG-IRF3 together with 100 ng of zebrafish IFN–β promoter luciferase reporter plasmid and 10 ng of pRL-TK (Promega, USA).

After 24 h post-transfection and lysis of 293T cells with Reporter Lysis Buffer (Promega, USA), luciferase activity was evaluated with Dual-Luciferase Assay Reagent (Promega, USA). In addition, the human 293T cells were transfected with different doses of pCMV3-FLAG-IRF3 plasmid (0, 200, 400, and 600 ng) and an equal amount of internal reference pRL-TK plasmid (10 ng). Western blotting was performed as per our previous study (Gu et al., 2016).

Sequencing of the two libraries derived from the two organs generated 32 554 292 and 39 305 131 raw reads, encompassing 14.37 Gb of sequences, which is enough for quantitative analysis of gene expression profiles. After trimming for *de novo* assembly, we obtained 28 646 938 (87.99%) and 34 682 151 (88.24%) clean reads from the skin and head kidney, respectively. All reads were assembled into 30 119 unigenes ranging from 201 bp to 36 481 bp, with an average length of 2 004 bp and N50 length of 2 906 bp (Table 1). The raw sequence data from transcriptome shotgun assembly (TSA) were deposited in GenBank (accession No. GBZM00000000.1).

Results showed that 751 and 1 249 unigenes were unique to the skin and head kidney, respectively (Figure 1A). In addition, pair-wise comparisons revealed that 112/77 unigenes were up/down-regulated by at least a two-fold change between the skin and head kidney (Figure 1B). To characterize these differentially expressed genes (DEGs) between the skin and head kidney, we conducted GO annotation and KEGG pathway analyses. The GO annotation results showed that the DEGs could be assigned into 74, 17, and 15 categories of biological process, cellular component, and molecular function, and subsequently separated into 104 subcategories. Subcategories of "cytoskeleton organization", "transport", and "cellular component" were the main gene enrichment categories. The differentially expressed unigenes belonged to 51 KEGG subcategories (Figure 1C).

We identified 1 475 proteins associated with immune function. Furthermore, 221 proteins, accounting for 15% of total selected proteins, were identified in the transcriptome as belonging to the chemokine signaling pathway. As the result of the inflammatory response, chemokines are released from various cells after bacterial infection. Here, 57 genes from the Toll-like receptor signaling pathway were expressed in both skin and kidney (Supplementary Figure S1). In addition, as IFN transcription regulators, the IRF family (IRF1~10) and TLR1 were selected for reverse transcription PCR (RT-PCR), as those genes are expressed in different organs, including the skin and head kidney (Figure 2A). Based on RNA-seq and RT-PCR analyses, the goldfish skin and head kidney were both found to express important immune genes. Determination of differences in mRNA expression level in goldfish IRF3 was carried out using RT-PCR for the two organs in the diseased, poly I:C-treated, and control fish. After 12 h stimulation with poly I:C, mRNA expression was increased significantly in the skin and head kidney; however, the increase was not significantly different between the poly I:C-treated and diseased fish (Figure 2B).

The typical zebrafish interferon–β promoter dual luciferase reporter assay was carried out to evaluate the relationships among goldfish IRF3 (Figure 3A). As shown in Figure 3A, transfection of Irf3 expression plasmid was demonstrated in a dose-dependent manner (Figure 3B). Interferon–β promoter activity was significantly activated by the over-expression of goldfish IRF3 in the 293T cells compared with the empty vector ($P<0.05$) (Figure 3C). This indicated that goldfish IRF3 likely participates in IFN signaling in innate immunity.

Table 1 Summary statistics of RNA-seq data

	Total	
	Skin	Head kidney
Obtained from sequencing		
Reads	32 5542 92	39 305 131
Nucleotides (bp)	6 510 858 400	7 861 026 200
After trimming for de novo assembly		
Reads	28 646 938	34 682 151
Nucleotides (bp)	5 529 141 837	6 692 024 669
De novo assembly		
Contigs		
Total length (bp)	157 725 712	
Sequence number	488 213	
Longest sequence length (bp)	36 468	
Average length (bp)	323	
N50	467	
Transcripts		
Total length (bp)	341 412 899	
Sequence number	256 284	
Longest sequence length (bp)	36 481	
Average length (bp)	1 332	
N50	2 603	
Unigene		
Total length (bp)	60 368 848	
Sequence number	30 119	
Longest sequence length (bp)	36 481	
Average length (bp)	2 004	
N50	2 906	

Skin is the first immune barrier and effectively eliminates risk from outside pathogenic organisms. As an active immunological microenvironment, it is quite different from other barrier tissues between the body and exterior environment (Bos & Kapsenberg, 1993).

The skin mucus consists of several defensive systems, including antibody (Palaksha et al., 2008) and innate and acquired immune systems (Alvarez-Pellitero, 2008). Human skin transcriptome reveals many immune genes associated with epidermal wound healing, such as up-regulated IRF1, IRF7, IRF8, and interferon receptors (Nuutila et al., 2012). Next-generation sequencing identified over 600 000 reads assembled into 34 696 transcripts from the skin of Atlantic salmon (*Salmo salar*), representing a wide variety of genes, including immune-related ones (e. g., cytokines, chemokines, lectins, and interleukins) (Micallef et al., 2012).

The head kidney forms the front part of the fish kidney and undertakes immune functions much like mammalian bone marrow, e. g., hematopoiesis (Press & Evensen, 1999). The head kidney in fish is a basic organ forming blood elements, thus it is potentially useful for identifying new immune-related genes (Gerdol et al., 2015). Moreover, it is a fundamental organ of the fish immune system, and a source of diverse cell effector types and of hematopoietic stem cells in teleosts (Kobayashi et al., 2006). It has been reported that many unigenes from the head kidney in grass carp are involved in the Toll-like, RIG-I-like, and RIG-I-like receptor signaling pathways (Chen et al., 2012). Furthermore, gene expression of pro-inflammatory cytokines, including TNF−α, TNF−β, IL-6, IL-17A/F3, and IFN-γ, and other cytokines, including IL-4/13A, IL-4 / 13B, and Type I-IFN, is increased in particulate silica-stimulated head kidney cells in Japanese pufferfish (*Takifugu rubripes*) (Morimoto et al., 2016).

Between the two organs, we identified 750 (2.53%) and 1 248 (4.34%) genes showing organ-specific expression, with 112 and 77 genes highly and lowly expressed in the skin and head kidney, respectively. The main reason for this variance may be their different cell compositions, thus indicating possibly different reaction mechanisms to the same pathogen from different organs.

In this study, a set of genes associated with the immune response were expressed in both organs. Similar findings have been presented in previous human studies (Gerdol et al., 2015; Nuutila et al., 2012). As an important innate immune

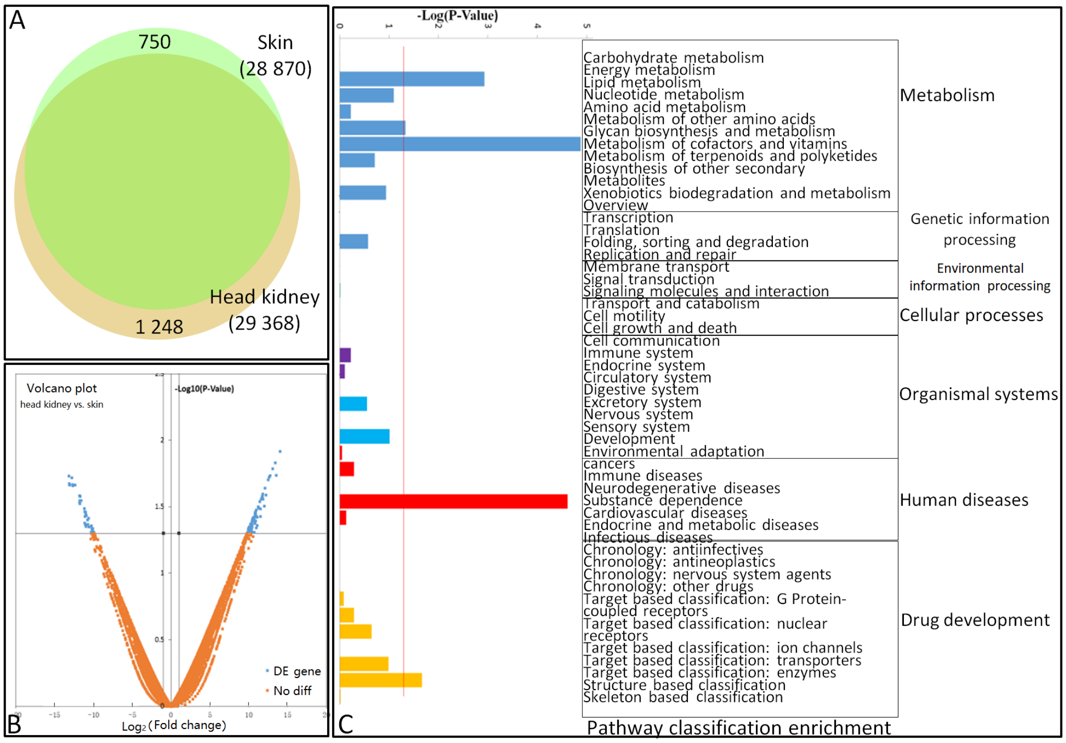

Figure 1 Differential gene expression profiles of goldfish skin and head kidney

A: Venn diagram showing number of total genes expressed in skin and head kidney. B: Volcano plot of differentially expressed genes. Scatter-plot of $-\log_{10}{}^{(\text{P-Value})}$ against $\log_2{}^{(\text{Fold Change})}$ expression in head kidney/skin. In total, 77 genes up-regulated on left (blue) and 112 genes down-regulated on right (blue) (FDR<0.001). C: KEGG pathway classification of DEGs.

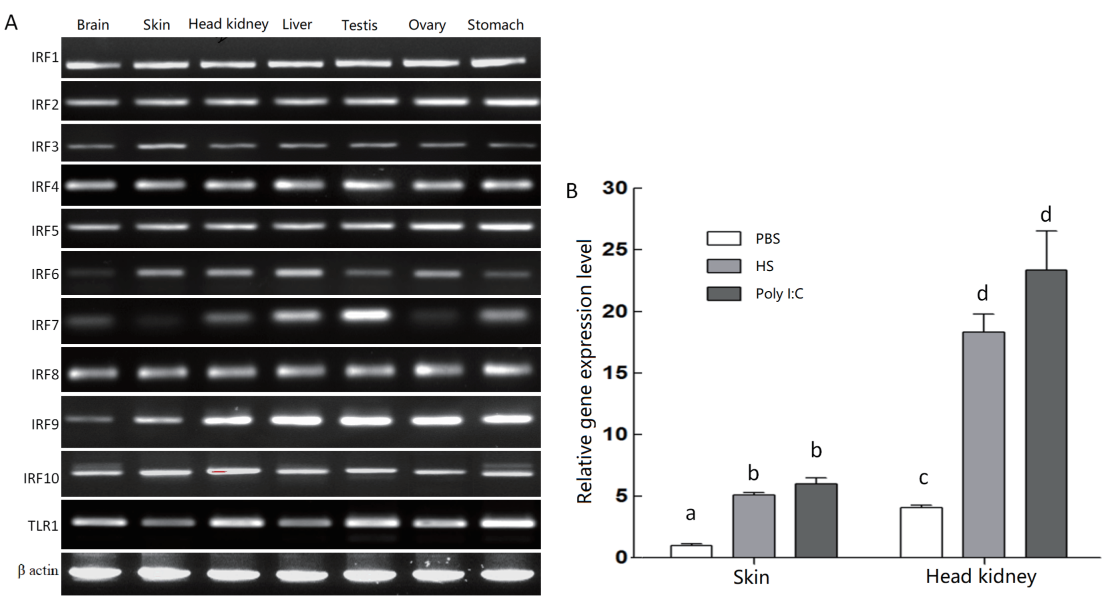

Figure 2 mRNA expression analysis of several genes from TLR signaling pathway

A: Reverse transcription-polymerase chain reaction analysis of 11 genes from interferon synthesis-related pathways in different organs, *β*-actin was constitutively expressed and used as a control to evaluate integrity of RNA and efficiency of RT-PCR. B: qPCR analysis of IRF3 expression in skin and head kidney from different groups. *β*-actin was used as a control to evaluate amount and quality of RNA. Densitometry values are means±*SD*. Different lowercase letters indicate significant differences (P<0.05). HS: Hemorrhagic septicemia-infected fish group.

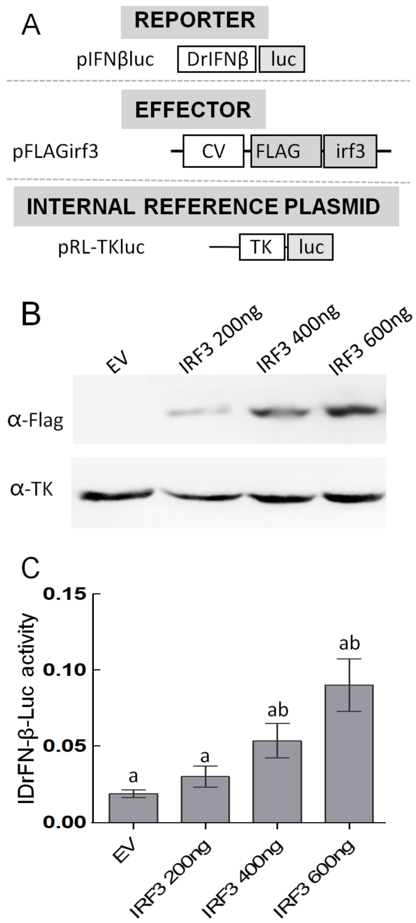

Figure 3 Luciferase reporter assay

A: Reporter and effector plasmids. CV: Human cytomegalovirus immediate early enhancer/promoter; DrINFβ: Zebrafish interferon β promoter (first letter of initiation codon ATG is defined as +1, nucleotides from −2 000 to +1 were cloned into the luciferase reporter plasmid); TK: Human herpes simplex virus thymidine kinase promoter; FLAG: FLAG tag; irf3: medaka irf3 cDNA; luc: firefly luciferase. B: Western blotting analysis of Irf3 expression in cells at different plasmid concentrations. C: Goldfish IRF3 activation of IFNβluc. pFLAG empty plasmid (EV; negative control) and luciferase reporter plasmids pIFNβluc or pISREluc plus pRL-TK (internal control reporter) were co-transfected into 293T cells. At 24 h post-transfection, cells were lysed for luciferase assay. Different lowercase letters indicate significant difference at *P*<0.05.

pathway, the Toll-like receptor signaling pathway was selected here for further study. All IRF family members and TLRs were expressed extensively in the two organs. To some degree, these results indicate that the goldfish skin and head kidney react to external stimuli by expressing immune genes and other cytokines to participate in the immune response.

In mammals, an IFN response is triggered by the activation of IRF3, a downstream adaptor of the TLR3 signaling pathway, following stimulation with poly I:C (Taniguchi et al., 2001). In this study, similar to IRF3 in other fish species (Gu et al., 2016; Holland et al.; Sun et al., 2010), the significant induction of IRF3 in goldfish by poly I:C stimulation indicated that IRF3 might play an important role in virus infection. It has been reported that mammalian IRF3 is a key transcriptional factor in the mediation of the type I IFN-dependent immune response against DNA or RNA-virus infection (Honda & Taniguchi, 2006). Mammalian IRF3 activates the mRNA transcription of type I IFN genes (IFN−α and −β) and ISG by binding to the ISRE on their promoters (Honda & Taniguchi, 2006; Paun & Pitha, 2007). Recently, it has been confirmed that IRF3 in fish plays a potential role in the IFN response as IFN-β and ISRE-containing activities can be induced by the over-expression of IRF3 (Holland et al., 2008; Sun et al., 2010). The characterization of the IRF3 function domain and positive relationship between IFN-β and IRF3 revealed by the luciferase reporter assay in this study suggests that goldfish IRF3 functions as a key regulator in the IFN response signaling pathway.

COMPETING INTERESTS

The authors declare that they have no competing interests.

AUTHORS' CONTRIBUTIONS

X.W.C. and Y.H.B. drafted the experiments; J.P.C., Z.W.Z., and W.P. performed the experiments; J.P.C. analyzed the data; X.W.C. and Y.H.B. wrote the paper. All authors read and approved the final version of the manuscript.

Jian-Peng Chen[1], Wei Pang[2], Zi-Wei Zhao[2],
Yan-Hui Bi[1], Xiao-Wu Chen[1,2,3,*]

[1] *National Demonstration Center for Experimental Fisheries Science Education*, *Shanghai Ocean University*, *Shanghai* 201306, *China*
[2] *Shanghai Engineering Research Center of Aquaculture*, *Shanghai* 201306, *China*
[3] *Shanghai Collaborative Innovation for Aquatic Animal Genetics and Breeding*, *Shanghai* 201306, *China*
[*] Corresponding author, E-mail: xwchen@shou.edu.cn

REFERENCES

Akira S, Takeda K. 2004. Toll-like receptor signalling. *Nature Reviews Immunology*, **4**(7): 499–511.

Alvarez-Pellitero P. 2008. Fish immunity and parasite infections: from innate immunity to immunoprophylactic prospects. *Veterinary Immunology and Immunopathology*, **126**(3–4): 171–198.

Avunje S, Kim WS, Park CS, Oh MJ, Jung SJ. 2011. Toll-like receptors and interferon associated immune factors in viral haemorrhagic septicaemia virus-infected olive flounder (*Paralichthys olivaceus*). *Fish & Shellfish Immunology*, **31**(3): 407–414.

Beck BH, Peatman E. 2015. Mucosal Health in Aquaculture. Amsterdam, New York: Elsevier/AP, Academic Press.

Bos JD, Kapsenberg ML. 1993. The skin immune system: progress in

cutaneous biology. *Immunology Today*, **14**(2): 75–78.

Chen J, Li C, Huang R, Du F, Liao L, Zhu Z, Wang Y. 2012. Transcriptome analysis of head kidney in grass carp and discovery of immune-related genes. *BMC Beterinary Research*, **8**: 108.

Choe Y, Yu JE, Park J, Park D, Oh JI, Kim S, Moon KH, Kang HY. 2017. Goldfish, *Carassius auratus*, as an infection model for studying the pathogenesis of *Edwardsiella piscicida*. *Veterinary Research Communications*, **41**(4): 289–297.

Gerdol M, Buonocore F, Scapigliati G, Pallavicini A. 2015. Analysis and characterization of the head kidney transcriptome from the Antarctic fish *Trematomus bernacchii* (Teleostea, Notothenioidea): a source for immune relevant genes. *Marine Genomics*, **20**: 13–15.

Gu YF, Wei Q, Tang SJ, Chen XW, Zhao JL. 2016. Molecular characterization and functional analysis of IRF3 in tilapia (*Oreochromis niloticus*). *Developmental and Comparative Immunology*, **55**: 130–137.

Hatten F, Fredriksen A, Hordvik I, Endresen C. 2001. Presence of IgM in cutaneous mucus, but not in gut mucus of Atlantic salmon, *Salmo salar*. Serum IgM is rapidly degraded when added to gut mucus. *Fish & Shellfish Immunology*, **11**(3): 257–268.

Holland JW, Bird S, Williamson B, Woudstra C, Mustafa A, Wang T, Zou J, Blaney SC, Collet B, Secombes CJ. 2008. Molecular characterization of IRF3 and IRF7 in rainbow trout, *Oncorhynchus mykiss*: functional analysis and transcriptional modulation. *Molecular Immunology*, **46**(2): 269–285.

Honda K, Taniguchi T. 2006. IRFs: master regulators of signalling by Toll-like receptors and cytosolic pattern-recognition receptors. *Nature Reviews Immunology*, **6**(9): 644–658.

Itaya H, Oshita K, Arakawa K, Tomita M. 2013. GEMBASSY: an EMBOSS associated software package for comprehensive genome analyses. *Source Code for Biology and Medicine*, **8**(1): 17.

Kobayashi I, Sekiya M, Moritomo T, Ototake M, Nakanishi T. 2006. Demonstration of hematopoietic stem cells in ginbuna carp (*Carassius auratus langsdorfii*) kidney. *Developmental and Comparative Immunology*, **30**(11): 1034–1046.

Micallef G, Bickerdike R, Reiff C, Fernandes JM, Bowman AS, Martin SA. 2012. Exploring the transcriptome of Atlantic salmon (*Salmo salar*) skin, a major defense organ. *Marine Biotechnology (New York, N.Y.)*, **14**(5): 559 – 569.

Montero J, Chaves-Pozo E, Cuesta A, Tafalla C. 2009. Chemokine transcription in rainbow trout (*Oncorhynchus mykiss*) is differently modulated in response to viral hemorrhagic septicaemia virus (VHSV) or infectious pancreatic necrosis virus (IPNV). *Fish & Shellfish Immunology*, **27**(6): 661–669.

Morimoto T, Biswas G, Kono T, Sakai M, Hikima J. 2016. Immune responses in the Japanese pufferfish (*Takifugu rubripes*) head kidney cells stimulated with particulate silica. *Fish & Shellfish Immunology*, **49**: 84–90.

Mortazavi A, Williams BA, Mccue K, Schaeffer L, Wold B. 2008. Mapping and quantifying mammalian transcriptomes by RNA-Seq. *Nature Methods*, **5**(7): 621–628.

Nuutila K, Siltanen A, Peura M, Bizik J, Kaartinen I, Kuokkanen H, Nieminen T, Harjula A, Aarnio P, Vuola J, Kankuri E. 2012. Human skin transcriptome during superficial cutaneous wound healing. *Wound Repair and Regeneration*, **20**(6): 830–839.

Palaksha KJ, Shin GW, Kim YR, Jung TS. 2008. Evaluation of non-specific immune components from the skin mucus of olive flounder (*Paralichthys olivaceus*). *Fish & Shellfish Immunology*, **24**(4): 479–488.

Paun A, Pitha PM. 2007. The IRF family, revisited. *Biochimie*, **89**(6−7): 744–753.

Press CM, Evensen Ø . 1999. The morphology of the immune system in teleost fishes. *Fish & Shellfish Immunology*, **9**(4): 309–318.

Shin HS, Choi CY. 2014. The stimulatory effect of LED light spectra on genes related to photoreceptors and skin pigmentation in goldfish (*Carassius auratus*). *Fish Physiology and Biochemistry*, **40**(4): 1229–1238.

Sun F, Zhang YB, Liu TK, Gan L, Yu FF, Liu Y, Gui JF. 2010. Characterization of fish IRF3 as an IFN-inducible protein reveals evolving regulation of IFN response in vertebrates. *The Journal of Immunology*, **185**(12): 7573–7582.

Taniguchi T, Ogasawara K, Takaoka A, Tanaka N. 2001. IRF family of transcription factors as regulators of host defense. *Annual Review of Immunology*, **19**: 623–655.

Vasta GR, Nita-Lazar M, Giomarelli B, Ahmed H, Du S, Cammarata M, Parrinello N, Bianchet MA, Amzel LM. 2011. Structural and functional diversity of the lectin repertoire in teleost fish: relevance to innate and adaptive immunity. *Developmental and Comparative immunology*, **35**(12): 1388–1399.

Wang L, Feng Z, Wang X, Wang X, Zhang X. 2010. DEGseq: an R package for identifying differentially expressed genes from RNA-seq data. *Bioinformatics*, **26**(1): 136–138.

Wang CL, Wang ZP, Wang JQ, Li MY, Chen XW. 2016. Identification of candidate piRNAs in the gonads of *Paralichthys olivaceus* (Japanese flounder). *Zoological Research*, **37**(5): 301–306.

ZOOLOGICAL RESEARCH
动物学研究
Bimonthly, Since 1980

Project for Enhancing International Impact of China STM Journals

2017 中国精品科技期刊 OUTSTANDING S&T JOURNALS OF CHINA

中国精品科技期刊 中国科技核心期刊 中国百强报刊

Editor-in-Chief: Yong-Gang Yao

Executive Editor-in-Chief: Yun Zhang

Editors: Su-Qing Liu Long Nie

Edited by Editorial Office of Zoological Research

(Kunming Institute of Zoology, Chinese Academy of Sciences, 32 Jiaochang Donglu, Kunming, Yunnan, Post Code: 650223 Tel: +86 871 65199026 E-mail: zoores@mail.kiz.ac.cn)

Sponsored by Kunming Institute of Zoology, Chinese Academy of Sciences; China Zoological Society©

Supervised by Chinese Academy of Sciences

Published by Science Press (16 Donghuangchenggen Beijie, Beijing 100717, China)

Printed by Kunming Xiaosong Plate Making & Printing Co, Ltd

Domestic distribution by Yunnan Post and all local post offices in China

International distribution by China International Book Trading Corporation (Guoji Shudian) P.O.BOX 399, Beijing 100044, China

Advertising Business License 广告经营许可证：滇工商广字66号

淘宝购买 微店购买

Domestic Postal Issue No.: 64-20

Price: 15.0 USD/80.0 CNY

ISSN 2095-8137